

The author(s) shown below used Federal funds provided by the U.S. Department of Justice and prepared the following final report:

Document Title: Microfluidic System for Automated Dye Molecule Extraction and Detection for Forensic Fiber Identification

Author(s): Thomas Dow, David Hinks, Kenneth Garrard, Alexander Sohn, Stephen Furst, Min Li, Sean Gunning, Nelson Vinueza

Document No.: 249891

Date Received: May 2016

Award Number: 2011-DN-BX-K561

This report has not been published by the U.S. Department of Justice. To provide better customer service, NCJRS has made this federally funded grant report available electronically.

<p>Opinions or points of view expressed are those of the author(s) and do not necessarily reflect the official position or policies of the U.S. Department of Justice.</p>

FINAL REPORT

Microfluidic System for Automated Dye Molecule Extraction and Detection for Forensic Fiber Identification

2011-DN-BX-K561

Over the period

October 1, 2011 to November 30, 2014

Authors

Thomas A. Dow, PI – Faculty, Precision Engineering Center
David Hinks, Co-PI – Textile Chemistry

Kenneth Garrard – Staff, Precision Engineering Center
Alexander Sohn - Staff, Precision Engineering Center
Stephen Furst - Consultant

Min Li – Textile Chemistry Graduate Student
Sean Gunning – Mechanical Engineering Graduate Student
Nelson Vinueza – Textile Chemistry

November 26, 2014

**Precision Engineering Center
North Carolina State University
Box 7918
Raleigh, NC 27695-7918
Tel (919) 515-3976
FAX (919) 515-3964
<http://www.pec.ncsu.edu>**

ABSTRACT

Due to the quantity of textile materials in the environment, there is a high probability of fiber transfer during the commission of a crime. A wide variety of techniques are available to test this hypothesis beginning with non-destructive visual comparison of characteristics such as material, color, diameter, cross-sectional shape, birefringence, refractive index and fluorescence.

One way to add additional specificity is to identify the dyes used to color the fabric. Such an analysis is more sensitive but, because it destroys the evidence, must be efficient and use a small sample. The time-of-flight mass spectrometry is a sensitive technique for identifying the dyes in a fiber with a high degree of molecular specificity. It can identify multiple dyes in a sample plus any contaminants extracted from the sample and is also capable of resolving isomers.

The research effort during this project was split between chemists in Textile Chemistry and engineers and computer scientists in the Precision Engineering Center. The Textile focus was to find the optimum extraction conditions for hundreds of fabrics and dye combinations. The PEC developed an automated device that used these conditions to extract the dye from a minute (10 ng) fabric sample. The dye solution (10 μ l) was extracted and measured in a time-of-flight mass spectrometer in less than 10 minutes.

The 2009 NAS Report on forensic sciences highlighted the need for improved scientific support for forensic analysis. One of the main points was the need for objective analytical methods as opposed to subjective examinations to reduce the potential for errors. Increasing repeatability and traceability in virtually all fields of forensic evidence processing was deemed necessary. Automating processes such as fiber analysis and making them more repeatable and reliable has the potential to pay dividends in the search for a more equitable and thorough justice system with fewer false convictions and more successful prosecutions.

EXECUTIVE SUMMARY

SYNOPSIS OF PROBLEM

Due to the quantity of textile materials in the environment, there is a high probability of fiber transfer during the commission of a crime. As a result, identification of fiber samples often plays a critical role in criminal investigations. In a typical case, a sample of known origin must be compared to an evidence sample to determine if both could have the same origin. A wide variety of techniques are available to test this hypothesis and each provides a different type of information. Forensic fiber examinations begin with non-destructive visual comparison of characteristics such as color, diameter, cross-sectional shape, birefringence, refractive index and fluorescence. These techniques include light microscope, UV-visible spectrometry and Fourier Transform Infrared spectrometry.

One way to add additional specificity is to identify the dyes used to color the fabric. Such analysis are more sensitive but destroy the evidence sample. Among the quantitative techniques available are high performance liquid chromatography, capillary electrophoresis, pyrolysis-gas chromatography /mass spectrometry and time-of-flight mass spectrometry. The latter technique is becoming increasingly popular for identifying the dye material from a fabric with a high degree of molecular specificity. It can measure the mass of a distribution of different dye molecules extracted from the fiber sample.

However, to use these analytic techniques, dye molecules must be separated from the fiber sample. While useful and pertinent research has been conducted to optimize macroscopic extraction conditions, what is needed is a microfluidic device that can quickly and automatically extract the dye from the fabric. The resulting dye solution could then be loaded into an LC column for separation and subsequent detection by mass spectrometry. Such a system would make it feasible for the forensic examiner to apply the quantitative methods to a larger number of samples while minimizing the risk of human error and sample contamination. Microfluidic systems have been developed for a variety of applications from chemical analysis to DNA amplification. The differences in the dye extraction problem are 1) the requirement to insert a macroscopic solid object into the device and 2) aggressive extraction solvents such as pyridine that limit the compatible materials.

The 2009 NAS Report on forensic sciences highlighted the need for improved scientific support for forensic analysis. One of the main points was the need for objective analytical methods as opposed to subjective examinations to reduce the potential for errors. Increasing repeatability and traceability in virtually all fields of forensic evidence processing was deemed necessary. Automating processes such as fiber analysis and making them more repeatable and reliable has the potential to pay dividends in the search for a more equitable and thorough justice system with fewer false convictions and more successful prosecutions.

PURPOSE OF THE PROJECT

The purpose of the project is two-fold:

- 1. Produce a novel, reliable and useful microfluidic system for dye extraction**
 - a. Goal 1 – Develop dye database and optimum extraction parameters
 - i. Develop protocols to optimize extraction condition for different combinations of dyes and fiber types using Design of Experiment methods (DOE)

- ii. Perform statistical analysis to evaluate repeatability of extraction process
 - iii. Make database available to other researchers through the Forensic Sciences Institute at NC State
- b. Goal 2 – Develop microfluidic device to automatically extract dye from fabric
 - i. Design and automate a microfluidic device for dye extraction
 - ii. Integrate this device as a front end for mass spectrometer to automatically deliver extracted dye molecules for identification
 - iii. Reduce total volume of extraction to 10 μ L, decrease total extraction time to less than 10 minutes and length of fiber to less than 1 mm
 - iv. Collaborate with North Carolina State Crime Laboratory (T. Suggs and J. Remy) to ensure that final product fulfills the needs of forensic scientists (ergonomics, ease of use, speed, chain of custody, etc.)

2. Increase knowledge and understanding necessary to guide criminal justice policy and practice related to forensic analysis of dyed fabric

- a. Minimize the risk of evidence loss and contamination by reducing sample handling
- b. Automate and accelerate analysis cycle to eventually help reduce backlog of forensic laboratories
- c. Improve probative¹ value of millimeter-size trace evidence
- d. Engage more scientists/engineers in the field of forensic science
- e. Train graduate students with pertinent experience in microfluidics, precision engineering and chemical analysis of trace evidence and introduce them to the field of forensic science

Goal 1(a) – Develop Dye Database

To develop the optimal dye extraction procedure, fabric samples were produced on different fabrics using 80 direct dyes, 84 acid dyes and 92 disperse dyes. The resulting fibers were then used to study the most efficient conditions to extract those dyes from fabrics and to extend the growing dye database that includes extraction conditions, liquid chromatography and mass spectrometry analysis. The manufacturer's information on each dye type was available and compared to the results of the molecular analysis. The database is available at the Forensic Sciences Institute at NC State.

The procedure for macro-level dye extraction tests followed standard protocol using the dye and fabric combinations discussed above. A fiber sample was placed in a 500 μ L laboratory vial, an extraction solvent was added, the sample was heated (sealed or unsealed) for some period of time. Then the solvent was evaporated, a buffer solution was added to the vial to dissolve the dye and the buffer/dye solution was removed for analysis. The volume of the solvent used was 200 μ L and the fabric was 5 mm square.

Optimization of macro-level extraction conditions at the Textile Chemistry Lab were performed by statistic D-Optimal screening design, full factorial design and Response Surface Methodology (RSM). D-Optimal screening design acts as a screening tool to find the statistically significant factors affecting extraction. Factors including extraction solvent, temperature, evaporation time, sample weight and dye concentration were investigated. Full factorial design and RSM are a collection of mathematical and statistical techniques based on the fit of a polynomial equation to the experimental data. Statistic models were built to predict the outcome (response) from the

¹ The ability of a piece of evidence to make a relevant disputed point more or less true

multivariate quadratic equation to further optimize the extraction conditions. Extraction effectiveness was evaluated through HPLC-Diode-Array Detection signal areas or the peak intensity of expected m/z peaks integrated from extracted ion current in the spectrum that corresponds to the concentration of dye extracts.

Goal 1(B) - Dye Extractor Design

A photograph of the microfluidic dye extraction system *XTract-iT* (with the cover removed to see the fluidic and electronic components) is shown in Figure 1. It is an automated system that only requires the forensic examiner to place the fiber sample in the extraction chamber, close the lid, slide it into the system and set the extraction parameters on the user interface. The rest is automated. The box is 9" wide, 10" deep, 7" high and weighs 10 lbs. The extraction process is controlled by a single board micro-processor in the box with analog and digital I/O and a user interface that is running on the PC shown the background.

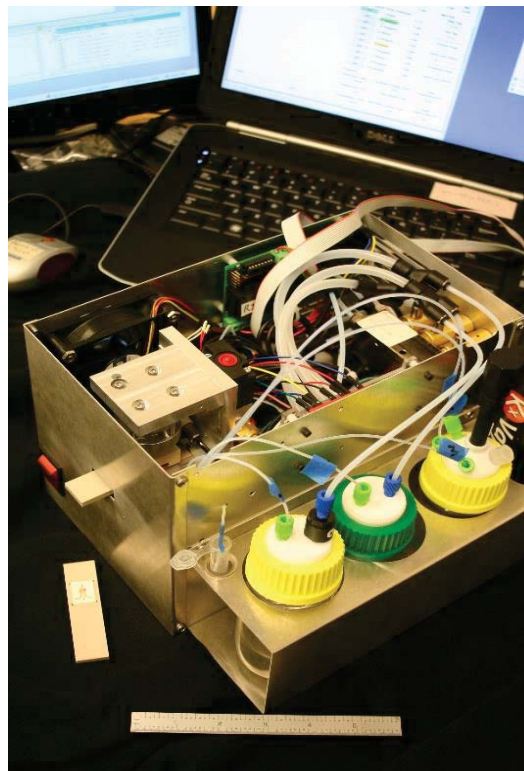


Figure 1. Dye extraction system (*Xtract iT*) with cover removed

Figure 2(A) shows the removable elastomeric extraction chamber (FFKM) being loaded into the plastic (PEEK) microfluidic chip. The fiber is placed on a holding feature (B) by the inspector using a microscope. The glass cover is put into place (C) to seal the extraction chamber and fiber location is verified (D) using the microscope.

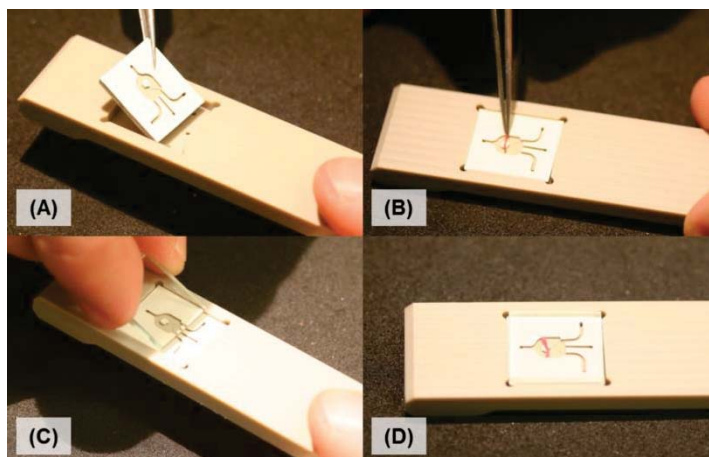


Figure 2. Microfluidic chip and elastomeric FFKM extraction chamber

When the system recognizes the chip being inserted into the slot in Figure 3, a pneumatic piston seals the extraction chamber and couples it to the fluid/air lines. The rest of the steps are briefly described in Table 1 with Figures 3-8 adding additional details.

Table 1. Steps in the dye extraction process

Figure	Extraction step	Done by	Components/Report Section
2	1. Place fiber in chamber on extraction chip	Forensic examiner	Microscope/forceps, microfluidic cavity and extraction chip
2	2. Place glass lid on cavity and check fiber location	“	Microscope
3	3. Insert chip into system	“	Chip breaks beam and piston presses down glass cover to seal
1	4. Input extraction parameters on user interface	“	Tern controller and Windows PC
	5. Start automated extraction process	<i>Xtract iT</i>	Timed steps to extract dye and produce sample

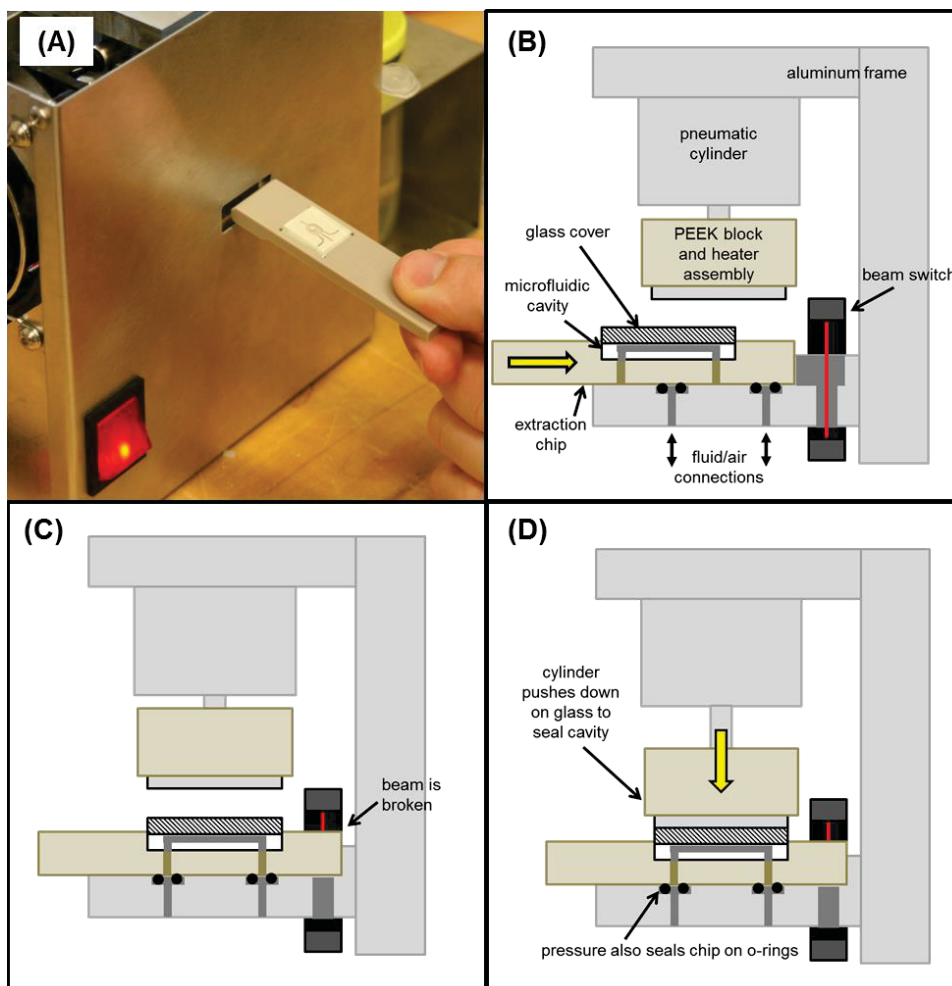


Figure 3. Insert chip into system and seal cavity with pneumatic cylinder

Table 1 (continued) - Steps in the dye extraction process

Figure	Extraction step	Done by	Components/Report Section
4	6. Extraction solvent pumped into microfluidic cavity, covering fiber	<i>Xtract iT</i>	Flow - Solvent-material compatibility –Air pressure, bottles, valves
5	7. Cavity and solvent are heated to facilitate dye extraction	“	Heaters and heater assemblies
6	8. Compressed air and heat evaporate solvent. Dye molecules is left on cavity surface.	“	FFKM cavity design, convective evaporation
7	9. Buffer solution is introduced to dissolve dye.	“	Valves
8	10. Buffer solution is ejected to container or mass spectrometer.	“	Sample container, HPLC-MS system

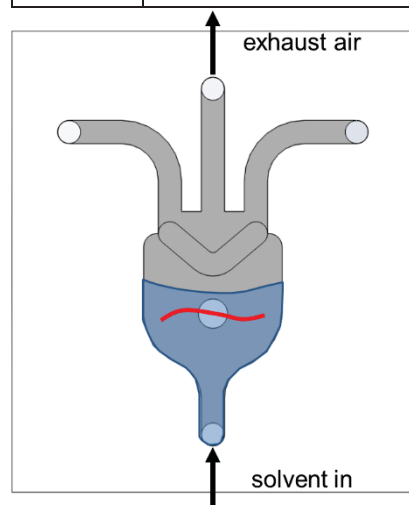


Figure 4. Solvent injection

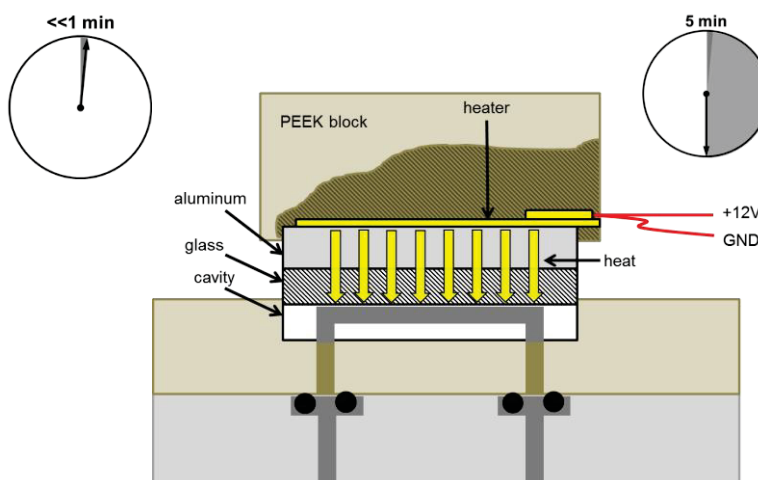


Figure 5. Cavity heating

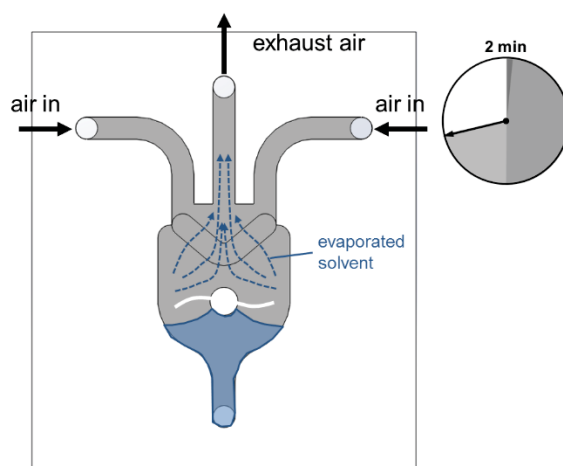


Figure 6. Solvent heating/dye extraction

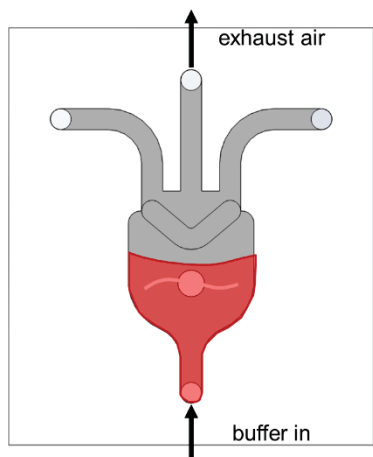


Figure 7. Buffer filling/dye pick up

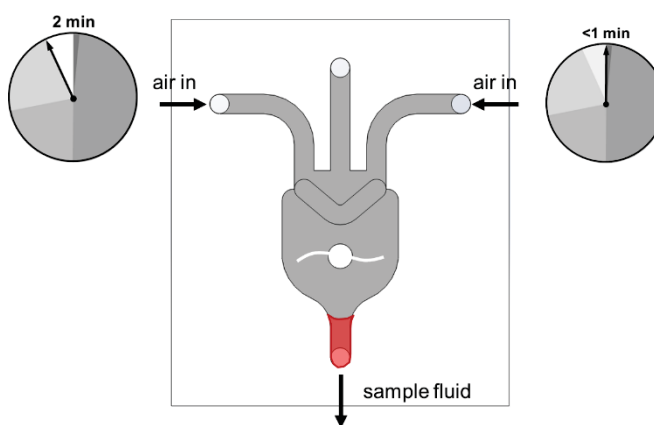


Figure 8. Sample ejection

The **Xtract-iT** system has been used to automatically extract a variety of dyes and dyes mixtures from cotton and nylon fabrics. The buffered dye solution was sent directly from the system into a LC-MS and the results of the dye analysis was visible on the MS screen in about 10 minutes from when the fabric was installed inserted.

Goal 2 – Emphasize Forensic Sciences

Textile Chemistry at NC State has a long history in the area of Forensic Science but the involvement of mechanical engineers and computer scientists from the Precision Engineering Center added a new viewpoint to the dye extraction problem. The proposed project brought together

1. David Hinks – Professor, Textile Chemistry, Chemistry and Forensic Science
2. Thomas Dow, Professor, Mechanical Engineering, Design, Fluids and Heat Transfer
3. Kenneth Garrard – Staff Member, PEC, Computer Science and Control
4. Alexander Sohn – Staff Member, PEC, Optics and Mechanical Design
5. Stephen Furst – Contractor, PEC, Mechanical Design and Actuation
6. Sean Gunning – Graduate student in Mechanical Engineering, MS, July 2014
7. Min Li – Graduate student in Textile Chemistry, PhD expected, December 2014

The background of the participants in chemistry, textiles, mechanical design, fluid flow, heat transfer, instrumentation and computer science proved to be an ideal team for the project. A number of different problem areas such as optimization of the extraction process, chemical compatibility of the materials and solvents, chamber sealing, internal valve volume, heating and cooling time, ergonomics and size were addressed and solved. The resulting instrument satisfies the goals of the project. In addressing these problem areas, the team became more aware of the issues in evaluating trace evidence and the challenges that forensic examiners deal with on a daily basis. The team feels confident that the **Xtract-iT** design will speed the implementation of quantitative dye assessment that improves the probative effect of trace fiber evidence.

FINDINGS

The objectives of the project – elucidating the optimum extraction conditions for different dyes and fabrics and developing an automated micro-fluidic dye extraction system - were successfully completed. Specific findings included:

1. Extraction solvent – Based on the macroscopic extraction experiments, the best solvent for the dyes/fabrics of interest was a pyridine/water mixture of 4:3. This was effective for all of the dyes/fabrics except acetate which was melted by this solvent. However, the change to a more diluted mixture of 2:1 solved the problem for acetate and extraction was successful.
2. Extraction chamber material – The need to insert a solid fabric sample into the extraction chamber coupled with the need to view the fiber required a sealable, transparent extraction chamber. Unfortunately the selection of pyridine as the extraction solvent eliminated most of the flexible materials except FFKM, also known as elastomeric Teflon. This material is soft but resistant to pyridine and can be machined or molded. The only drawback is the high cost - \$1000/lb.
3. Cavity shape – The shape of the extraction cavity was refined over several iterations to produce consistent fill and extraction times as well as avoiding aerodynamic forces pushing the fluid out of the cavity before the dye was extracted.
4. Valve configurations – The single cavity design requires a series of valves to send in the extraction solvent, air for evaporation, buffer to dissolve the extracted dye and finally sending the dye solution to a storage vial or directly to the mass spectrometer. Early implementations had a series of on/off and directional valves to route the fluid and air. A major breakthrough discovery was a rotary valve that had a single output tube into the extraction chamber but 10 input channels that either introduce another material or seal the chamber.
5. Extraction temperature – A range of temperatures from 60 °C to 120 °C were studied to optimize the extraction process. The conclusion was higher temperature was better as long as the extraction solvent did not boil – leading to nearly instantaneous evaporation and an end to the dye extraction. An interesting side note is that the boiling point of the water/pyridine mixture is 93° C which is lower than either fluid alone.
6. Microfluidic extraction and analysis – A series of extractions using the microfluidic system where the sample went directly into the mass spectrometer were very successful. In less than 10 minutes the MS screen showed the dye molecules from the sample. The signal intensity was higher than the macro-extraction and multiple fibers could be analyzed at the same time.

CONCLUSIONS

Optimized Extraction Conditions

Statistics-based methodologies were employed to optimize the extraction processes of three major dye classes (Acid, Disperse and Direct Dyes) at macro-level at analytical chemistry lab, and the optimized conditions were modified according to the microfluidic apparatus. Pyridine/water 4:3 was selected as a universal extraction solvent for different dye classes, except for disperse dyes in acetate fibers. A modification to pyridine/water 1:2 can effectively extract dyes to prevent fibers from melting.

Statistical studies of direct dye extraction demonstrated: for direct dye 50 °C, 8 min can be a sufficient to extraction more than 90% dye from fibers. Acid dyes needs much higher extraction temperature up to around 90 °C for in 160 second to achieve the best extraction performance. Disperse dyes requires much higher temperature, a temperature of 90 °C in 20 min is required in the study.

Chemical Separation via High Performance Liquid Chromatography (HPLC)

A fast separation methodology using high performance liquid chromatography (HPLC) has been developed for different dye classes. HPLC mobile phase composition, column temperature and ion-pairing agents were optimized for a better analysis of different dye classes. The methodology developed can analyze commercial dyes in less than 10 min.

Mass Spectrometry via Liquid Chromatography, Direct Inject and Microfluidics.

Three different solution inlets, liquid chromatography (LC), direct injection and Microfluidics, were used for mass spectrometry (MS) analysis. The three inlets methodologies were studied and compared to evaluated the best path for dye analysis.

1. Method 1: Microfluidic extractions of the dye follow by LC/MS analysis. The experiments for this study were focus on the extraction of the dye from the fiber by the microfluidic device follow by the analysis of LC/MS. The LC/MS results showed that most of the acids dyes can be separated by the HPLC and analyzed by MS. However, it was observed that the amount of dye collected influence the sensitivity of this method, due to the further dilution on the HPLC.

2. Method 2: Microfluidic extractions of the dye follow by direct injection of the dye extracted solution to the mass spectrometer. The experiments for this study were focus on the extraction of the dye by device follow by the injection of these extracted solutions to the mass spectrometer via electrospray ionization (ESI). Sensitivity was increased, and the set of these experiments were the base for the creation of the interface of the microfluidic device and the mass spectrometer.

3. Method 3: Microfluidic extractions of the dye follow online analysis by the mass spectrometer. Based on results on method 2, it was successfully attach the microfluidic device to the mass spectrometer. This methodology has the advantage that prevents sample lost and increase the sensitivity of the analysis. Results showed the method is highly reproducible. Furthermore, this proves that the device can be attached to any mass spectrometer that has an ambient ionization source like ESI.

Automated System

The microfluidic device connected directly to a high resolution mass analyzer (or any other mass spectrometer) allows automatic setting for the analysis of extracted dyes from fibers or a single fiber (~50 ng). The volume of solvent used to achieve the extraction and analysis is very low (10 μ L). The analysis of a sample can be done in 10 minutes. A great advantage of this process is the lack of sample manipulation for the extraction of the dye, which prevents possible scenarios of contamination.

Implications for Policy

One of the main themes in the 2009 NAS Report on Forensic Sciences was the need for improved the quantitative analysis of trace evidence. The microfluidic system used to extract dye molecules from a single fiber and the MS analysis can be a fast reliable method to add to the forensic field. The lack of manipulation of the sample minimizes any problems related to the Locard's principle of contamination. Also, give the lab personnel the ability to extract dyes in a faster and more reliable way.

One of the long-standing challenges of trace evidence analysis of dyed fibers is the paucity of statistical rigor in comparing a standard and unknown fiber. Statistical rigor can only be achieved via objective methods that are repeatable, reproducible and enable comparison to a comprehensive

database of dyes. Elimination of subjective assessment by the analyst is key. The methods developed in this project are a step towards identification of dyes within fibers and with minimal loss of fiber that could enable objective comparison of dyed fibers, and ultimately a statistical error calculation that could be meaningful in the courtroom. Future work is required to comprehensively ascertain the statistical rigor of the methods reported in this work.)

TABLE OF CONTENTS

Abstract	2
Executive Summary	3
LIST OF SYMBOLS	16
1 Introduction	18
1.1 Motivation	18
1.2 Background	18
1.2.1 Non-destructive and Minimally Destructive Analyses	18
1.2.2 Chemical Separation and Mass Spectrometry	19
1.2.3 Microfluidics	20
1.2.4 Manufacturing Methods for Microfluidic Devices	21
1.2.5 Extraction Process	21
1.2.6 Prior Work	21
1.3 Objectives	25
2 Automated Extraction System Design	26
2.1 Extraction System Overview	26
2.2 Material Selection	29
2.3 Components	30
2.3.1 Prototype 1 Layout	32
2.3.2 Prototype 2 Layout	33
2.3.3 Pneumatic Cylinders	35
2.3.4 Valves	37
2.3.5 Tubing, Fittings, Extractor Manifold	41
2.3.6 PTC Heaters and Heater Assembly	42
2.3.7 Thin-film Heaters and Heater Assembly	43
2.3.8 Containers and Filters	44
2.3.9 FFKM Cavity and Cavity Chip	46
2.3.10 Cavity Fabrication	48
2.3.11 Pressure Regulators	49
2.3.12 Sensors	50
2.3.13 Enclosure and Cooling Fan	53

2.4	System Control.....	55
2.4.1	Controller and Relay Bank.....	55
2.4.2	User Interface.....	56
3	DYE EXTRACTION.....	58
3.1	System Diagram and Sequences	58
3.1.1	Extraction Sequence.....	59
3.1.2	Cleaning Sequence.....	60
3.2	Mixture Properties of Pyridine and Water	61
3.3	Fluid Flow	65
3.3.1	Flow Modelling.....	65
3.3.2	Flow Model Validation Testing.....	68
3.3.3	Rotary Valve Flow Testing.....	70
3.3.4	Rotary Valve Automated Test	72
3.4	Cavity Design Iterations and Fill Tests.....	76
3.5	Cavity Air Flow.....	86
3.5.1	Inlet Air Flow.....	86
3.5.2	Cavity CFD Air Flow Analysis.....	88
3.6	Evaporation	91
3.6.1	Convective Evaporation Model	91
3.6.2	Evaporation Parameters and Design Considerations	93
3.6.3	Evaporation Testing.....	97
3.7	Heat Transfer.....	105
3.7.1	Initial Heating System and Temperature Considerations	105
3.7.2	Heating Model	108
3.7.3	ANSYS Transient Thermal Analysis and Initial Heating Tests	110
3.7.4	Heater Selection.....	115
3.7.5	Cooling Models.....	116
3.7.6	Heater Cycling	121
3.8	Extraction Testing	122
3.8.1	Extractions with Prototype 1 – PTC Heaters	122
3.8.2	Extractions with Prototype 1 – Thin-film Heaters.....	128
3.8.3	Pyridine-Water Mixture Cavity Boiling Tests.....	131
3.8.4	Extractions with Prototype 2.....	134
4	Macro Extraction Study	137

4.1	Introduction	137
4.2	Experimental Procedures.....	140
4.2.1	Dyeing.....	140
4.2.2	Extraction Procedure.....	141
4.2.3	Dye Measurement	142
4.2.4	Statistic Optimization of Extraction.....	143
4.3	Optimized extraction at macro-level.....	146
4.3.1	Extraction performance of extracting solvent.....	146
4.3.2	Quantification of dye extracts in Macro Extraction.....	148
4.4	Optimization of evaporation at macro-level.....	149
4.4.1	Statistical Analysis of Macro-level Evaporation	149
4.4.2	The profiler trace of evaporation	150
5	Microfluidic extraction Study	151
5.1	Microfluidic Extraction Conditions	151
5.2	Analysis of dyes with High Performance Liquid Chromatography.....	152
5.2.1	Sample Preparations For Q-TOF LC/MS Analysis	152
5.2.2	Optimized Chromatography for HPLC.....	152
5.2.3	Mobile phase preparation.....	153
5.2.4	Optimized chromatography for different dye classes	153
5.2.5	HPLC coupled to Electro Spray Ionization Quadropole TOF-MS.....	154
5.2.6	Microfluidic extraction-ESI QTOF MS.....	155
5.2.7	LC/MS analysis of dye extract from microfluidic extraction	156
5.2.8	Detection Limit of standard solution by LC-QTOF-MS	158
5.3	Microfluidic extraction coupled to direct injection mass spectrometry (DIMS)	159
5.4	Quantification of extraction and test of limit of detection	159
5.4.1	Quantitative analysis of C.I. Direct Yellow 106 extract.....	159
5.4.2	Detection of limit test of LC/MS analysis of acid dye standards	160
5.4.3	Detection of limitation-LC/MS.....	160
5.5	analysis - microfluidic extraction Direct to the QTOF MS.....	161
5.5.1	Analysis of single fibers.....	161
5.5.2	Analysis of fibers containing mixed dyes.....	162
6	CONCLUSIONS.....	163
6.1	Device design objectives:.....	163
6.2	Modeling processes of interest:.....	164

6.3	Develop Database of Dye Information.....	165
7	FUTURE WORK.....	165
8	References.....	168
9	Dissemination of Research Findings	171

LIST OF SYMBOLS

<u>Symbol</u>	<u>Meaning</u>
A	area
AIV	air inlet valve
AOV	air outlet valve
B _t	bolt tension
c _p	heat capacity
D	diameter
D _{AB}	mass diffusivity
DCV	directional control valve
D _h	hydraulic diameter
f	frequency
g	acceleration due to gravity
H	height
h	heat transfer coefficient
h _m	average mass transfer coefficient
I	current
ID	inner diameter
k	thermal conductivity
L	length
m	mass
\dot{m}	mass transfer rate
m/z	mass to charge ratio
M _A	molecular weight
MFD	microfluidic device
NCSU	North Carolina State University
Nu	Nusselt number
OD	outer diameter
p	pressure
Pr	Prandtl number
P _v	vapor pressure
Q	flow rate
q	heat transfer rate
R	resistance
r	radius/radial direction
R	specific gas constant
\hat{R}	universal gas constant
Ra	Rayleigh number
Re	Reynolds number

RV	rotary valve
Sc	Schmidt number
Sh	Sherwood number
SOV	shut-off valve
T	temperature
t	time
U, v	velocity
V	volume
V, E	voltage
W	width
z	axial direction
α	thermal diffusivity
β	thermal expansion coefficient
δ	slip length
Δp	pressure drop
Δt	finite time step
ΔT	temperature difference
θ_a	approach angle
μ	dynamic viscosity
ρ	density
σ	surface tension
τ	torque
ν	kinematic viscosity
Φ	relative humidity

1 INTRODUCTION

1.1 MOTIVATION

Fibers are an important form of trace evidence in crime scene investigation. The variability and uniqueness of fibers in regards to physical and chemical properties allow investigators to associate suspects, victims, and/or crime scenes by comparison. Visual inspection and microscopic techniques can be used to initially compare trace fibers lifted at a crime scene, but these methods are generally used to eliminate the possibility of a match. When visual methods fail to reject a potential match, chemical analysis of the sample is needed. The dye used to color the fiber can be examined for chemical composition and comparison to similar fibers. Dye must first be separated from the fiber to be analyzed.

1.2 BACKGROUND

Fiber evidence from a crime scene is classified as “class” evidence. This classification means that any identification made using the evidence is based on probability. “Class” evidence can be associated with a group unlike “individual” evidence (i.e. evidence that can be associated with a singular source such as DNA or fingerprints). It follows then that the value of the evidence is dependent on its rarity and the quality of comparison to a known sample [1,2] . In general, fibers are first examined through non-destructive methods. Microscopic and spectroscopic methods allow investigators to first determine characteristics of the fiber. Figure 1-1 shows the fiber analysis techniques, their uses and specificity.

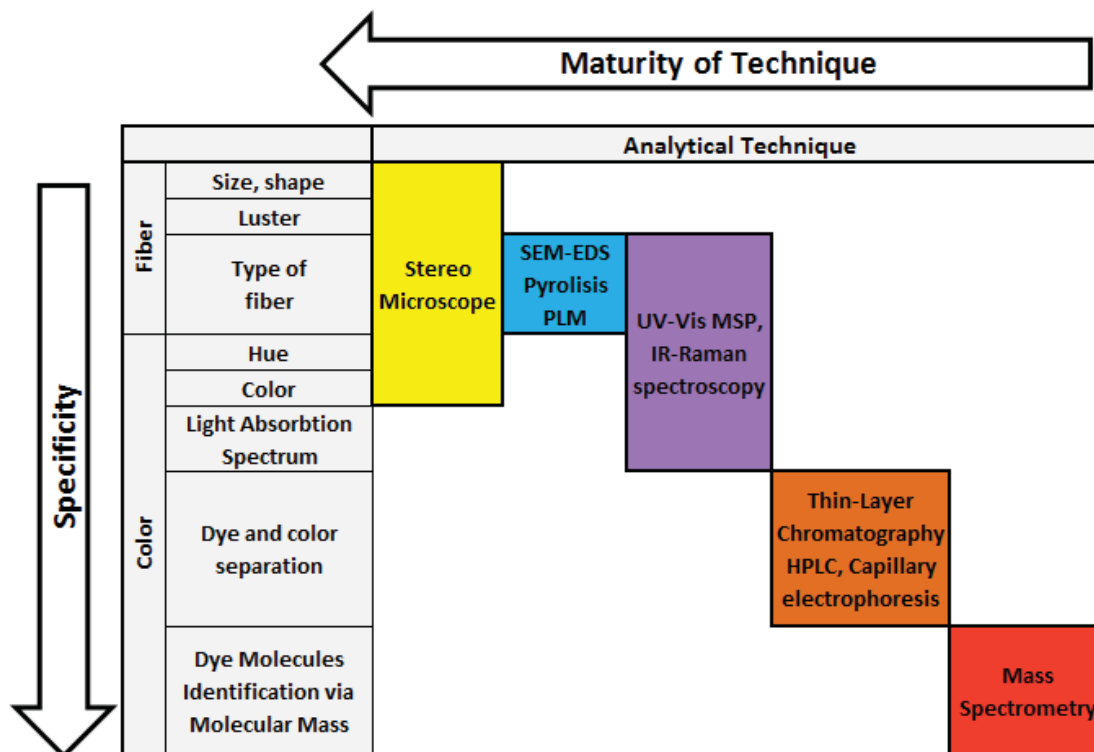


Figure 1-1. Different analytical techniques used to discriminate fiber samples [3]

1.2.1 NON-DESTRUCTIVE AND MINIMALLY DESTRUCTIVE ANALYSES

The techniques discussed in this section are used for initial fiber analysis and characterization. Each technique has certain advantages and can necessitate further analysis if a match between fibers of interest cannot be ruled out. Stereo microscopy is first used to identify fiber size, crimp, color, and luster. Techniques such as polarized light microscopy (PLM), Infrared (IR) and Raman spectroscopy, pyrolysis with gas chromatography, and scanning electron microscope with energy dispersive spectrometry (SEM-EDS) are used to provide higher levels of specificity.

Polarized light microscopy can be used to determine polymer type based on the rotation of polarized light incident upon the fiber. Infrared spectroscopy further distinguishes fiber type and can be used to compare two samples. It is particularly useful in identifying synthetic fibers that are visually indistinguishable. Raman spectroscopy is often used to complement IR spectroscopy analysis. Raman spectroscopy requires less preparation of the samples and may provide more specific details on its polymer structure and the main dye present in the sample. Multiple dyes are usually used to color fibers, however, and this method has difficulty identifying dyes present in smaller amounts (minor dyes). The dye can also interfere with readings from the polymer structure, requiring that IR spectroscopy also be used [4-6].

Pyrolysis with gas chromatography is a destructive technique that can be used if the polymeric structure of the fiber is known. The last method mentioned in this section, SEM-EDS, can provide information on the elemental make-up of the fiber [4]. There are a variety of other methods and variations of the ones mentioned here that are widely covered for other forensic analyses as well [2,4-9].

Each of these techniques provides added information about the evidence fiber(s) but cannot, in general, define a positive match to a known sample. To do so, more specific analyses must be performed. These are usually more destructive techniques that are used to identify the specific dye used on the fiber.

1.2.2 CHEMICAL SEPARATION AND MASS SPECTROMETRY

Chemical separation of fiber and dye is dependent on the class of dye used. Table 1-1 shows a list of dye classes and the typical fiber substances to which they are applied. By applying the non-destructive methods previously discussed, the class of fiber and dye can be determined. The best method of separation can then be defined.

Table 1-1. Summary of dye classes and typical fiber types to which they are applied [10]

Dye class	Description	Typical fiber substrates
Acid	Water-soluble anionic compounds; ionic bond between dye molecule and polymer	Wool, silk, polyamide, polypropylene
Basic	Water-soluble, applied in weakly acidic dye baths; very bright dyes; negatively charged fiber draws the dye cation	Polyacrylonitrile, acrylic, occasionally polyester and polypropylene
Direct	Water-soluble, anionic compounds; applied directly to fiber from aqueous medium that has an electrolyte; positively charged ion is attracted to negatively charged fiber surface and the dye is able to enter the fiber	Cotton, rayon, other cellulotics
Disperse	Not water-soluble; aqueous dispersion; hydrogen bonds and weak van der Waals forces hold dye molecule in fiber	Polyester, acetate
Reactive	Water-soluble; form covalent bond with functional groups of fiber; similar in structure to acid dyes and application similar to direct dyes	Cotton, wool, other cellulotics
Sulfur	Organic compounds containing sulfur or sodium sulfide; reduced using sodium sulfide or sodium hydrosulfite; dye enters fiber and is oxidized to original form	Cellulotics
Vat	Oldest dyes; more chemically complex; water-insoluble; good colorfastness	Cellulotics

Thin Layer Chromatography (TLC) and High Performance Liquid Chromatography (HPLC) are used to separate a dye from its fabric. Most textiles contain multiple dyes used to achieve a desired color. There is no one solvent system that works for all dye combinations. It is therefore necessary to first determine the physical characteristics of the fiber and dye to know which solvents to use. HPLC has advantages over TLC because it can provide greater resolution and requires smaller quantities of dye. A proper solvent must still be determined and the method must be coupled with an analysis technique such as mass spectrometry [4].

In mass spectrometry, the dye sample is sent to a high-vacuum chamber. There it is ionized by high speed electrons. The ion fragments are then passed through an electromagnetic field. The shapes of their parabolic trajectories are used to determine their mass-to-charge ratios, with each substance producing a unique pattern [1,11]. In this way a sample can be matched to a specific type (or sometimes a specific batch) of dye.

1.2.3 MICROFLUIDICS

Successful identification of the dye with a mass spectrometer requires a sufficient concentration of the extracted molecules. Given the small size of fibers found at a crime scene, this is not achievable using analyte volumes on the macro scale. To achieve useful sample concentrations, microfluidic technologies must be used.

Microfluidics is described as the research of fluid flows and interactions in micro-scale channels [12]. Microfluidic applications can be traced to the advent of ink-jet technologies in the 1950's. These were among the first to use fluid flows on the micro or nanoliter scale [13]. Another early application was in the field of molecular analysis. Analysis techniques such as gas-phase chromatography (GPC), high-pressure liquid chromatography (HPLC), and capillary electrophoresis (CE) were able to make use of micro-scale channels and flows [13,14].

The advent of genomics in the 1980's was another factor that promoted growth of the field. DNA amplification through polymerase chain reaction (PCR) could be achieved in significantly less time using microfluidic methods. The technology allowed greater efficiency and accuracy of DNA analysis. Another motivating factor was the use of microfluidics in biodefense applications in the 1990's. Government funding for research and development of microfluidic devices as chemical and biological threat detectors advanced the field.

A final factor in the growth of microfluidic technology was microelectronics production. It was originally thought that photolithography and similar techniques used in microelectronic production could be applied to the fabrication of microfluidic systems. Since then, the use of polymers has become the standard for microfluidic technology and other fabrication techniques have been prevalent [14].

The current use of the term microfluidics often refers to lab-on-a-chip technology. Lab-on-a-chip technologies are those that seek to miniaturize chemical and/or biological processes. Such technologies have the major advantage of requiring small sample quantities. Small sample quantities and high surface area to volume ratios produce higher resolution and sensitivity and shorter analysis times. In addition, the small size of such devices reduces manufacturing costs, consumption of reagents and analytes, and the production of harmful by-products [12,14,15]. The behavior of fluids on micro and nano scales introduces unique challenges as well. Phenomena such as capillary action, surface tension effects, and fluid interaction with hydrophobic surfaces become increasingly important at smaller scales.

1.2.4 MANUFACTURING METHODS FOR MICROFLUIDIC DEVICES

A variety of fabrication methods exist for the production of microfluidic devices. Earlier microfluidic technologies were produced through etching and photolithography of glass and silicon substrates. These processes are time-consuming, expensive, and require clean room facilities and equipment for production. Glass and silicon devices also present a challenge in sealing of the devices. In more recent years, polydimethylsiloxane (PDMS), among other polymers, has emerged as the substrate of choice for many applications. PDMS provides several advantages to the ceramic materials, especially in the reduction of cost and fabrication time. The polymeric material is machined using soft lithography techniques, providing features on the micron scale with high precision. PDMS has been used widely in bio-applications due to its non-toxic nature and availability for chemists and biologists [15-17].

The different micromachining processes use varying methods to physically shape the substrate material into microscale features. Material removal through melting and vaporization is used in methods such as electron beam machining (EBM) and laser beam machining (LBM). Ablation through the use of high energy lasers can also be used on work piece surfaces. Material forming with dies and molds is done through plastic deformation of solids and solidification of liquids. Photoetching and electrochemical etching remove material through chemical reactions at the work piece surface. Layer by layer construction processes such as stereolithography (SL) can be used to create complex internal features. Material removal methods through mechanical force have also been used to produce microscale holes and channels. These methods include cutting, sandblasting, grinding, ultrasonic machining (UM), and punching [15-18]. Other fabrication techniques are also used; however, this list mentions some of the more common ones. The method to be used is usually determined by the availability of proper equipment, cost, speed of production, geometric and dimensional capabilities, and the material substrate to be used [16]. For the microfluidic dye extraction device, a micromilling method was selected for production due to the availability of equipment, the capability to produce features on the desired scale with good accuracy, and the relative speed with which the microfluidic cavities could be produced. The machining of such a cavity is discussed further in Section 2.3.10.

1.2.5 EXTRACTION PROCESS

The general extraction chemistry and process operations were established and verified by the Textile Chemistry Department of North Carolina State University. The following is a list of extraction steps determined by the chemistry department:

1. A fiber is placed in a vial.
2. The fiber is immersed in solvent (~10 μ l).
3. The vial is heated to facilitate dye and fiber separation and to reduce the time needed to evaporate the solvent.
4. Air flows over the solvent to evaporate it, leaving only the fiber and dye residue.
5. The vial is then filled with a buffer substance to reconstitute the dye molecules on the glass surfaces.
6. The buffer solution containing the dye is injected into a HPLC-MS setup for analysis.

A lab technician generally takes 15 – 30 minutes of work to prepare one sample.

1.2.6 PRIOR WORK

The large majority of lab-on-a-chip technologies to date are those with biological and chemical identification applications [13,14]. Since the advent of genomics, DNA replication through polymerase chain reaction (PCR) and various DNA analyses have been a key focus of microfluidic technologies. The technologies are often coupled with electrophoretic separations methods for analysis [19,20]. Proteomics is another biological application of microfluidics (the study of proteins). Lab on a chip devices have been used to concentrate samples and for protein crystallization processes that are used to study molecular makeup [13,21,22]. Other applications have included drug identification, detection of toxins, and chemical syntheses (using microreactors) [12,23].

Research at the Precision Engineering Center (PEC) of North Carolina State University seeks to extend the application of such technology to dye extraction from fibers for forensic analysis. Prior to the development of an automated system, research focused on the capability of microfluidic technology in performing successful dye extractions.

Initial considerations for the research focused on fabrication capabilities and the shape of the microfluidic cavity. Polyetherether Keytone (PEEK) was initially chosen as the main structural component of the cavity due to its compatibility with the pyridine solvent and good machinability (see Section 2.2). The design included a glass cover for viewing of the fiber (for proper placement) and the extraction fluids. A simplified version of the microfluidic cavity was made to test machining and fluid filling capabilities as shown in Figure 1-2.

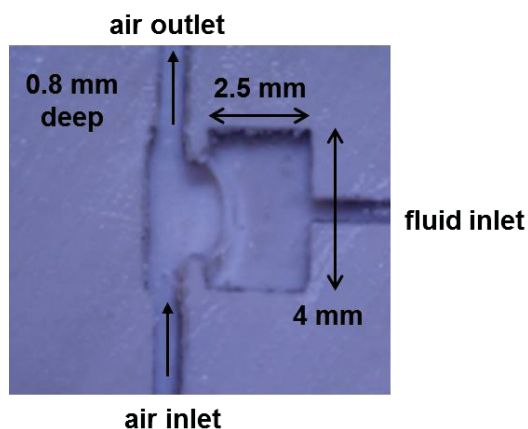


Figure 1-2. Simplified version of the device (8 μ l cavity)

The volume of the cavity shown is characteristic of later design iterations presented in this work. The early design was also used to evaluate the time required to evaporate solvent as shown in Figure 1-3.

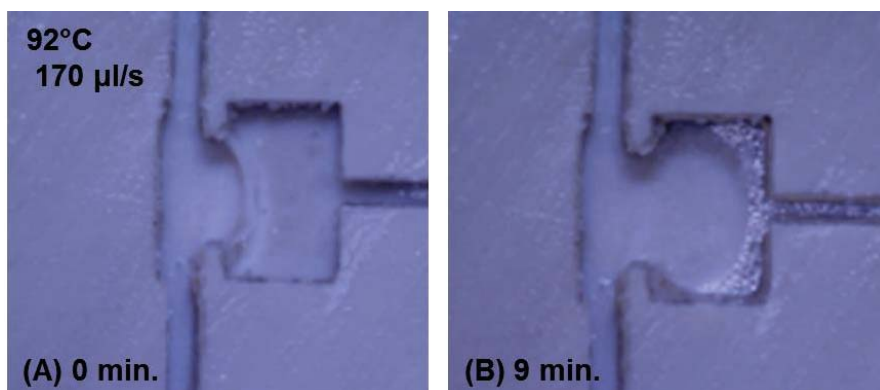


Figure 1-3. Early evaporation experiment for 170 µl/s air flow and 92°C fluid

Tests with the simple cavity design showed the ability to control fluid flow and to perform evaporation in a reasonable amount of time. Further design iterations of the PEEK fiber cavity were fabricated and tested, resulting in the design shown in Figure 1-4.

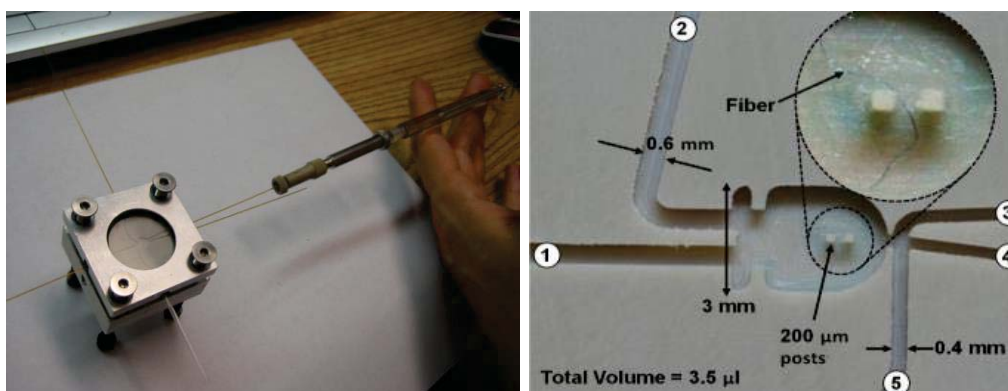


Figure 1-4. Fluid injection and PEEK cavity design with (1) gas exhaust, (2) gas inlet, (3) solvent inlet, (4) buffer inlet, and (5) sample ejection port [3]

The PEEK cavity makes use of five inlet/outlet legs for the injection of fluids, air flow, and ejection of the sample. An extraction was performed with the cavity on a 2 mm long polyester fiber colored with Disperse Blue 60 dye (also shown in Figure 1-4). The dye was successfully extracted and tested in a mass spectrometer, showing peaks at the characteristic mass to charge ratios of the two Blue 60 molecules ($m/z = 380.12$ and $m/z = 424.15$). The extraction is shown in Figure 1-5.

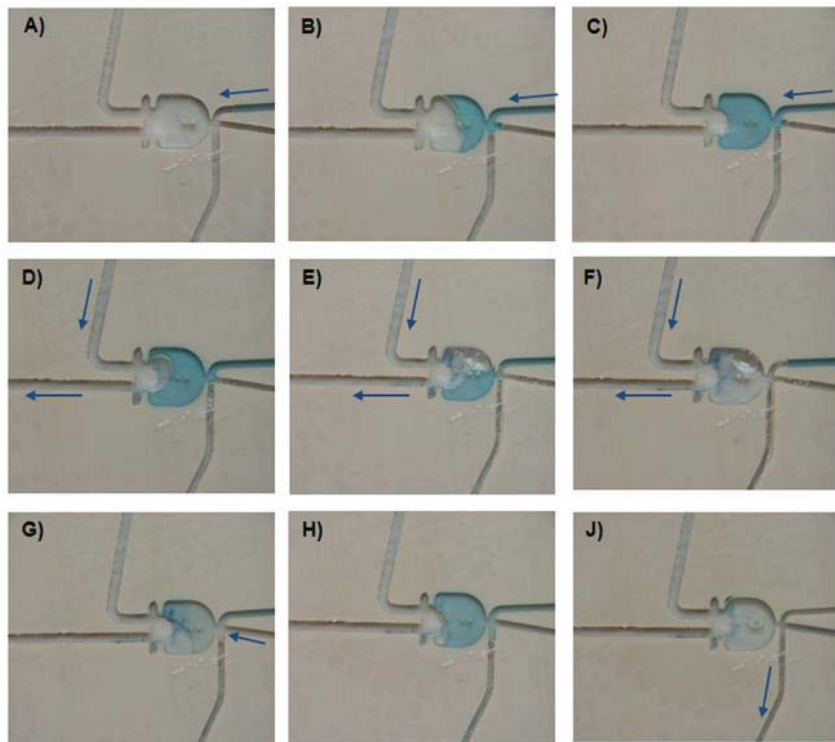


Figure 1-5. Disperse Blue 60 extraction in PEEK cavity

The solvent injection step is shown in (A)-(C), followed by evaporation in (D)-(F). Finally, the buffer injection and ejection of the sample are shown in (G)-(J). The success of the extraction indicated potential for further development of the technology. The following is a list of design challenges that were identified:

- **Sealing:** The PEEK cavity served as an impetus for further design iterations of the microfluidic cavity, however, the hard plastic material was a challenge to seal. In order to properly seal the cavity, Norland NOA65 epoxy was used between the glass and PEEK surface. A thin and even coating of epoxy was achieved through spin coating, but a better method of sealing was needed for use in a laboratory environment. This promoted the search for a polymer alternative that was compatible with the pyridine solvent.

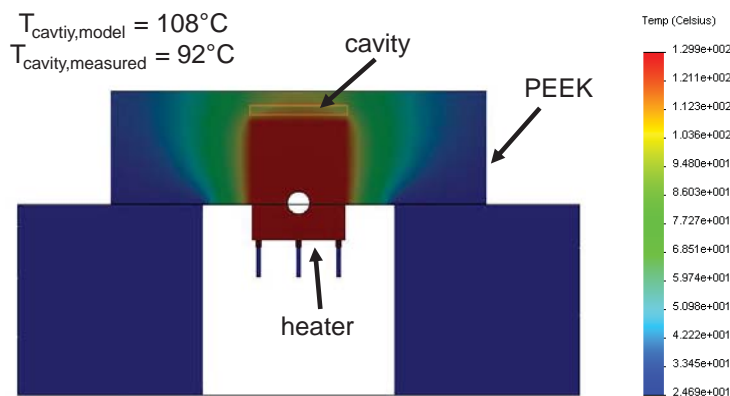


Figure 1-6. PEEK cavity heating from below

- Temperature control and measurement: The PEEK design was heated from beneath the cavity. PEEK is not a good thermal conductor, making it a challenge to achieve high temperatures within the cavity. Finite element models were used to predict temperatures as shown in Figure 1-6. A proper temperature control method was also identified as a need.
- Machining: Material selection for the cavity presents a tradeoff in machining and sealing performance. Softer polymer materials provide good sealing capability but are difficult to machine, particularly small features such as the fiber holding posts. In contrast, harder materials like the PEEK are more easily machined but require an adhesive layer to seal.
- Fluid loss through capillary action: Air flowing through the cavity removed fluid and dye from the chamber through capillary action in addition to evaporation during some tests. This phenomenon needed to be addressed in further design iterations.
- Material compatibility: The cavity and system components that contact the pyridine must be compatible with the solvent to prevent damage from occurring.

In addition to identifying design challenges, these early tests successfully established the dye extraction process in a microfluidic context.

1.3 OBJECTIVES

The purpose of this thesis research was to design and fabricate a device that separates dye from a small fiber sample and prepares it for analysis in a mass spectrometer. The goal was an automated extraction device that requires minimal interaction and monitoring from the user. The user would place a fiber in an extraction chip, insert the chip into the device, and initiate the extraction sequence. The device will prepare and store the dye sample for analysis upon completion of the sequence. The specific objectives of the project were as follows:

1. Design a microfluidic device capable of extracting dye from a trace fiber and preparing said dye for analysis via Time-of-Flight Mass Spectrometry (TOF MS).
 - a. Automation: The user will place a fiber in the device and initiate the extraction sequence.
 - b. Repeatability: The device must be able to extract dye from multiple samples of the same fabric in succession and produce the same results.
 - c. Reliability: Dye samples produced must be of useable quality, i.e. the dye must be detectable in the HPLC-MS system.
 - d. Fulfill the needs of forensic examiners: It should be ergonomic, easy to use, and reduce the amount of interaction and time required to extract dye samples.
 - e. Fabrication and testing: The prototype design must be fabricated and tested. Extraction of dyes from sample fibers must be performed and tested in the HPLC-MS system to show successful detection of dye molecules.
2. Model processes of interest in the microfluidic device.
 - a. Predict fluid flow, heating, and evaporation so that extraction sequence steps can be timed.
 - b. Verify process models with experimental data.
 - c. Use process modelling to calibrate the device.

2 AUTOMATED EXTRACTION SYSTEM DESIGN

The following sections outline the design of the microfluidic dye extraction system. Descriptions of the main components of the system are provided. The modelling and testing of system processes (fluid flow, heating, evaporation) and dye extraction results are provided in Section 3.

2.1 EXTRACTION SYSTEM OVERVIEW

The final step of the fiber identification process is the separation of dye for molecular analysis. Operation of the automated extraction system is presented in this section. The fiber is first prepared by the forensic examiner. The fiber preparation steps are given in Table 2-1.

Table 2-1. Fiber preparation steps

Time, (minutes)	Extraction step	Done by	Components/Section
<1	11. Place fiber in extraction chamber on extraction chip (Figure 2-1(A-B))	Forensic examiner	Microscope/forceps, microfluidic cavity and extraction chip – Section 2.3.9
0	12. Place glass lid on cavity and check fiber (Figure 2-1(C-D))	“	Microscope
0	13. Insert chip into system (Figure 2-2)	“	Chip breaks beam and piston presses down to hold and seal chip and microfluidic cavity – Sections 2.3.3 and 2.3.12
<1	14. Input extraction parameters on user interface (extraction time and temperature, evaporation time, buffer hold time, number of buffer fills)	“	Computer, Tern controller – Sections 2.4.1 and 2.4.2
0	15. Start automated extraction process	“	Timed steps to extract dye and produce sample – Section 3.1

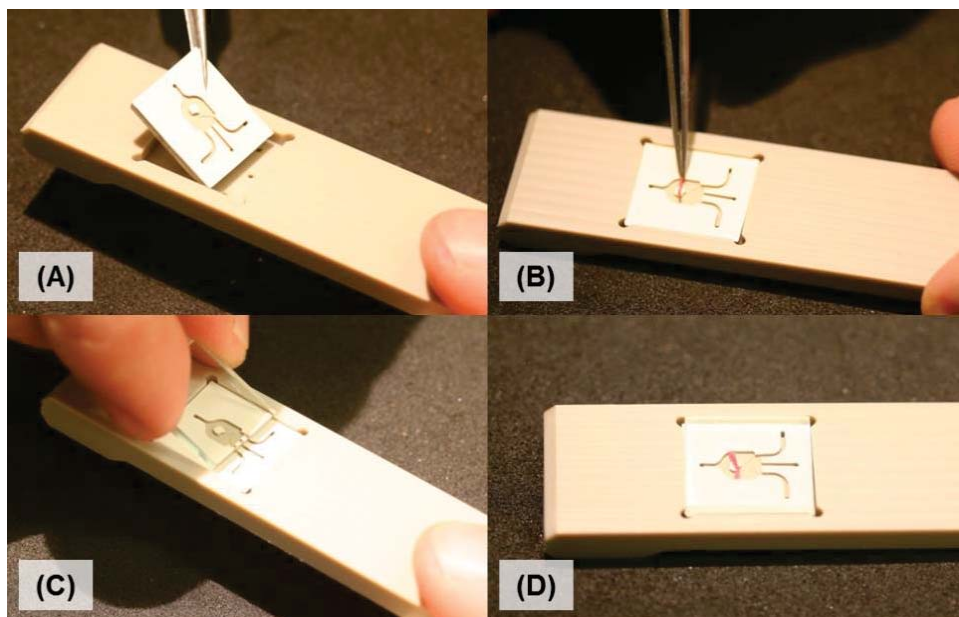


Figure 2-1. Placement of (A) cavity, (B) fiber, and (C) glass cover and (D) extraction chip before inserting into automated extraction device

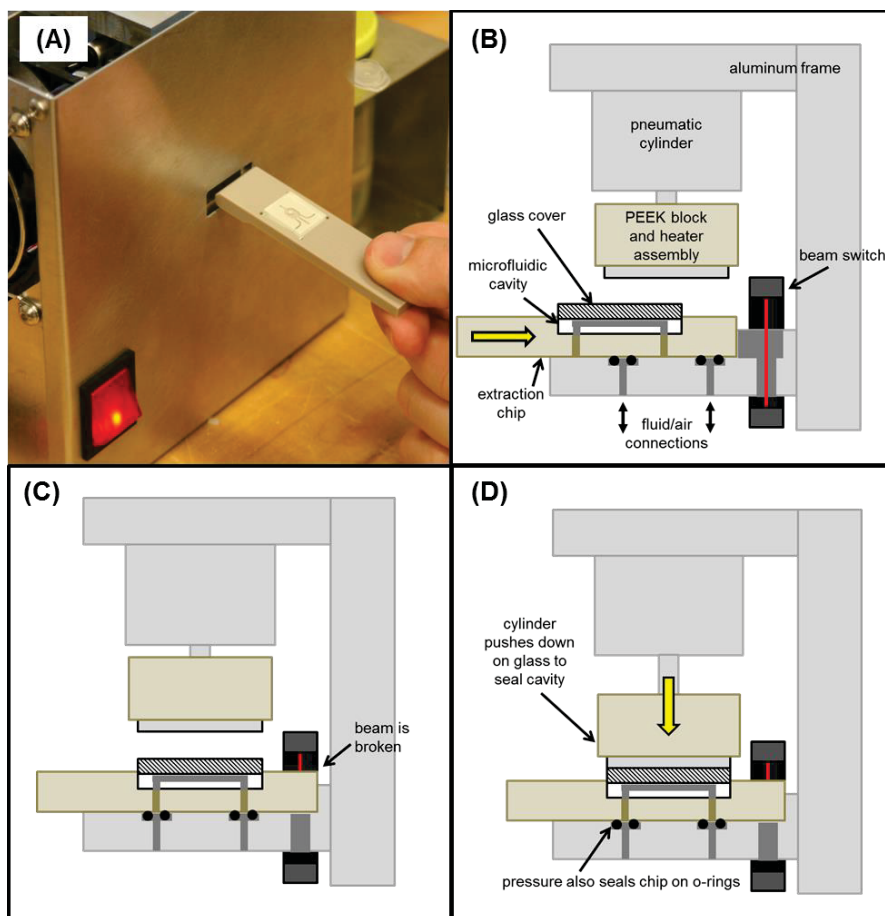


Figure 2-2. Securing chip and sealing cavity with pneumatic cylinder in device

After the process is initiated by the forensic examiner, the system extracts the dye and prepares the sample for analysis. The steps used by the system to do this are given in Table 2-2.

Table 2-2. Extraction steps

Time, (minutes)	Extraction step	Done by	Components/Section
<<1	16. Extraction solvent pumped into microfluidic cavity, covering fiber (Figure 2-3)	System	Flow - Section 3.3. Solvent-material compatibility – Section 2.2. Air pressure, bottles, valves – Sections 2.3.4, 2.3.5, 2.3.8, and 2.3.11
5	17. Cavity and solvent are heated to facilitate dye extraction (Figure 2-4)	“	Heaters and heater assemblies – Sections 2.3.6, 2.3.7, and 3.7
2	18. Compressed air is circulated through cavity to evaporate solvent, leaving dye molecules on cavity surfaces (Figure 2-5)	“	FFKM cavity design, convective evaporation – Sections 0, 3.4, 3.5, and 3.6
2	19. Buffer solution is pumped into the cavity to dissolve the dye molecules (Figure 2-6)	“	Valves – Section 2.3.4
<1	20. Sample fluid ejected to container or directly to mass spectrometer for analysis (Figure 2-7)	“	Sample container, HPLC-MS system

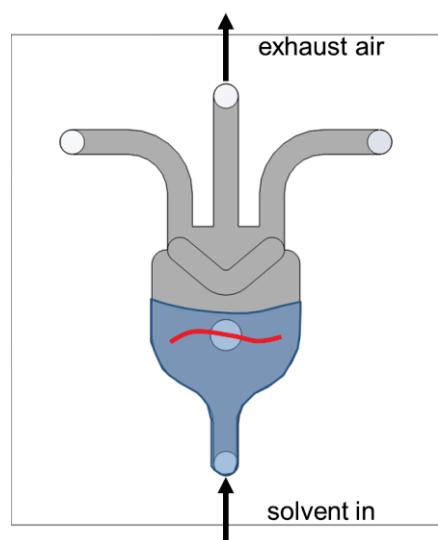


Figure 2-3. Solvent injection

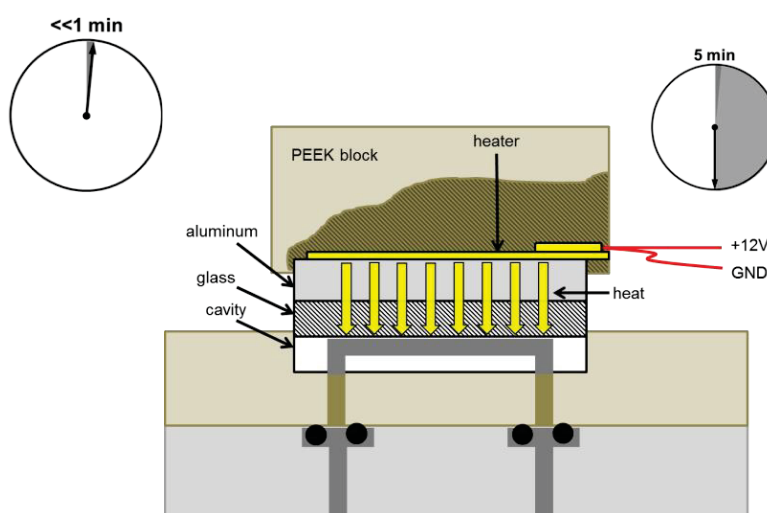


Figure 2-4. Solvent heating/dye extraction

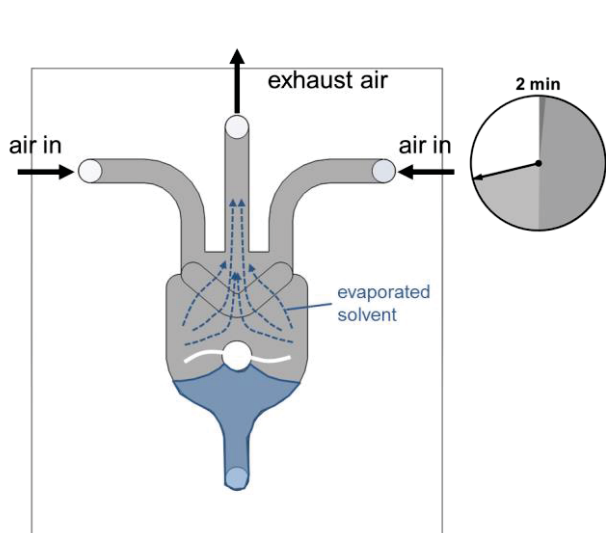


Figure 2-5. Solvent evaporation

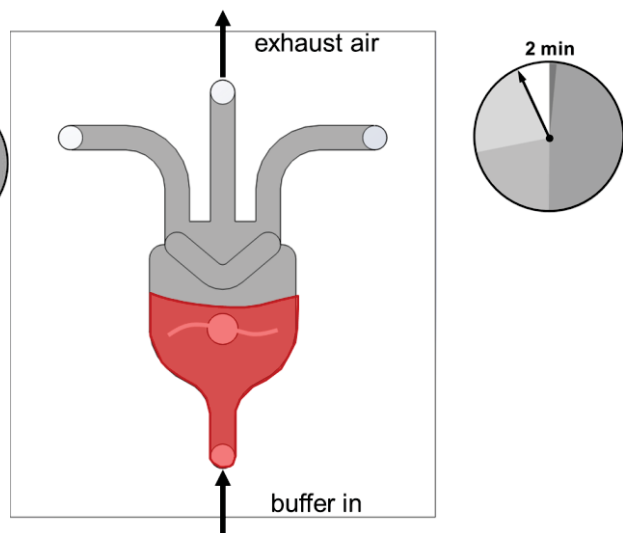


Figure 2-6. Buffer filling/dye pick up

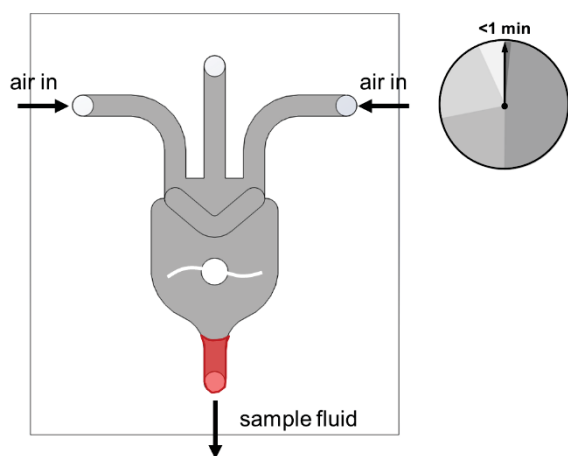


Figure 2-7. Sample ejection

2.2 MATERIAL SELECTION

Due to the negative effects of the pyridine solvent on many polymers, material selection for components in the extraction device was a significant consideration. The materials in the immediate vicinity of the extraction chamber must also be able to withstand temperatures in excess of 100°C to maintain integrity during the heating and evaporation processes. The microfluidic cavity requires an elastomeric material that provides sealing capabilities. A relatively high modulus is desirable, however, for ease of machining and minimal burr formation. Compatibility information is provided for a range of materials in Table 2-3.

Table 2-3. Material compatibility with pyridine [24]

Material	Compatibility w/ Pyridine	Modulus (GPa)	Max Temp (°C)	Comments
PDMS	D-Severe Effect	0.00087	200	
Acetal (Delrin)	B-Good	2.8	160	
Buna N (Nitrile)	D-Severe Effect			
Carbon graphite	A-Excellent			
Ceramic Al2O3	A-Excellent			
ChemRaz, Kalrez, Profluor (FFKM)	A-Excellent	0.0072	316	Low modulus high temperature
Copper	B-Good	117		
EPDM	B-Good			
Epoxy (high temp)	A-Excellent	1.5-10	120	Wide range of characteristics, available clear
Fluorocarbon (FKM, Viton)	D-Severe Effect			
Kel-F (PCTFE)	A ¹ -Excellent	1.4-1.7	132	High modulus, impact strength, high temperature, opaque
LDPE	B ¹ -Good	0.2-0.3	80	
Polyetherether Ketone (PEEK)	A-Excellent	3.6	143	
Polypropylene	A ² -Excellent	1.5-2	82	
Polyurethane (high temp)	D-Severe Effect	0.002	171	
PPS (Ryton®)	A-Excellent	14	200	High-temp high strength engineering plastic.
PTFE	A-Excellent	0.4-0.7	200	
PVC	D-Severe Effect			
Silicone	D-Severe Effect			
Titanium	B-Good			
Tygon	D-Severe			
Explanation of superscripts: 1 – satisfactory to 22°C, 2 – satisfactory to 48°C				

Upon comparison of compatibility, elastic modulus, and maximum temperature (in addition to cost considerations) PEEK and FFKM were selected as the main engineering materials. PEEK was selected for relevant structural materials and FFKM for the microfluidic cavity. EPDM was selected for the o-rings due to its availability in standard o-ring sizes and compatibility with pyridine.

2.3 COMPONENTS

The initial system used an array of directional-control valves (DCV's) and shut-off valves (SOV's) to select flow paths for buffer, solvent, and compressed air. The system layout is shown in Figure 2-8.

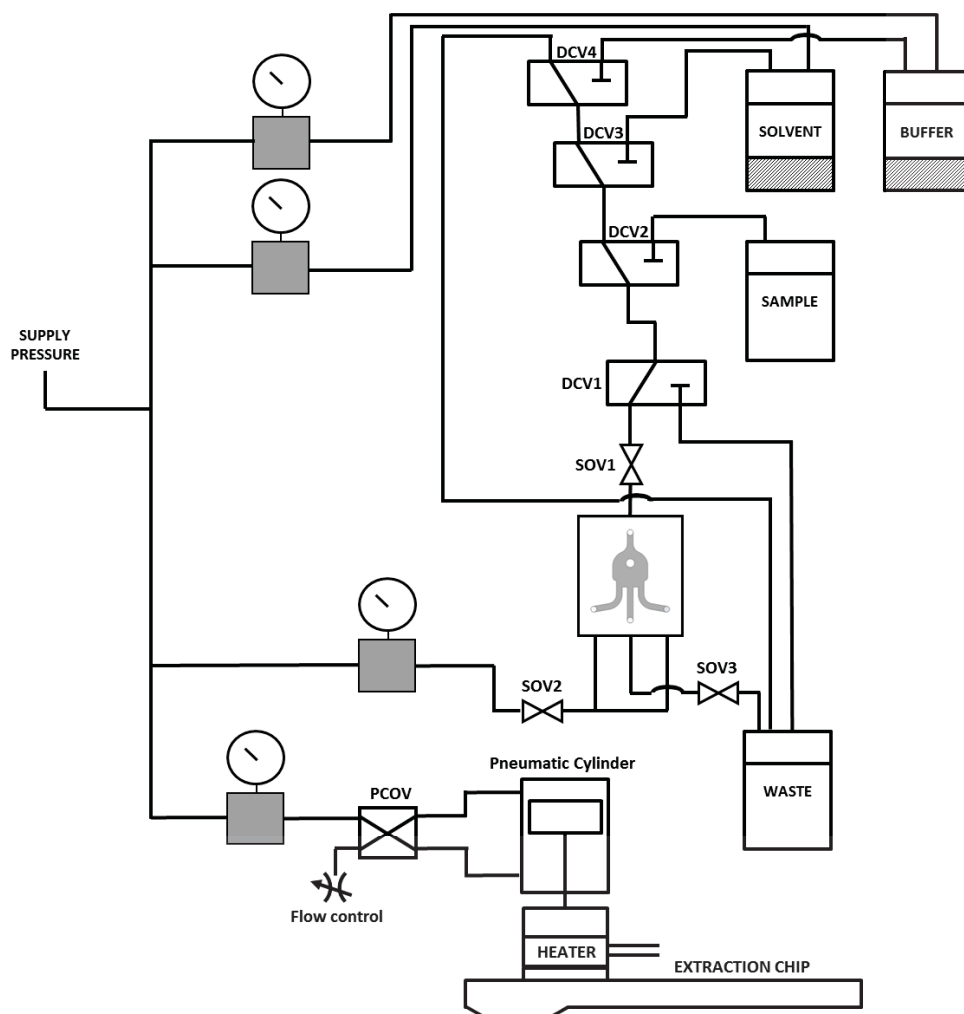


Figure 2-8. System layout diagram with directional-control valves (DCV's) and shut-off valves (SOV's)

A system concept using a rotary valve (RV) was developed to replace the array of directional-control and shut-off valves used for the fluid inlet. The general microfluidic system is shown in Figure 2-9. The system consists of pressurized solvent and buffer reservoirs, a rotary valve, two shut-off valves for air flow control, a microfluidic cavity, sample and waste containers, pressure regulators, and a pneumatic cylinder.

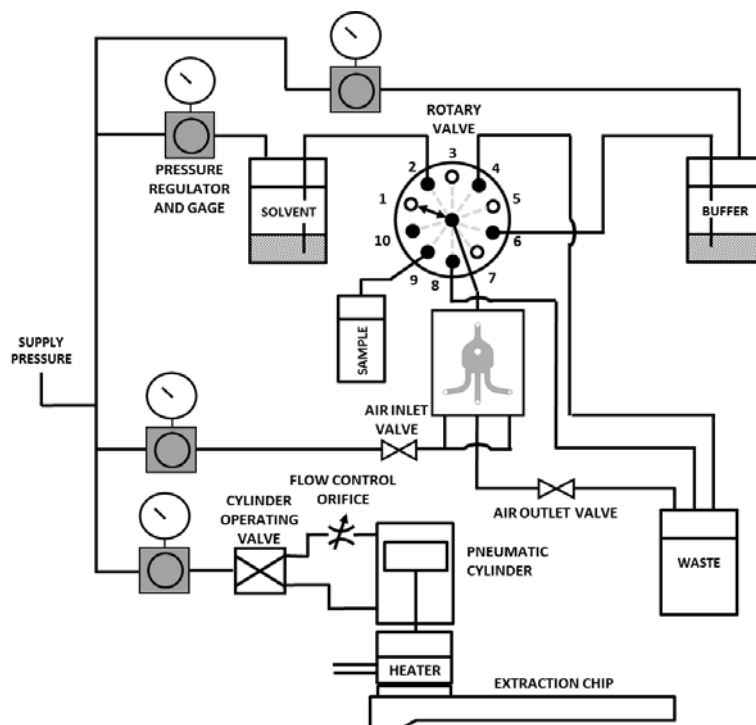


Figure 2-9. System layout diagram with rotary valve (RV) and shut-off valves (SOV's)

2.3.1 PROTOTYPE 1 LAYOUT

The first prototype is shown in Figure 2-10. The main components of the system are labelled.

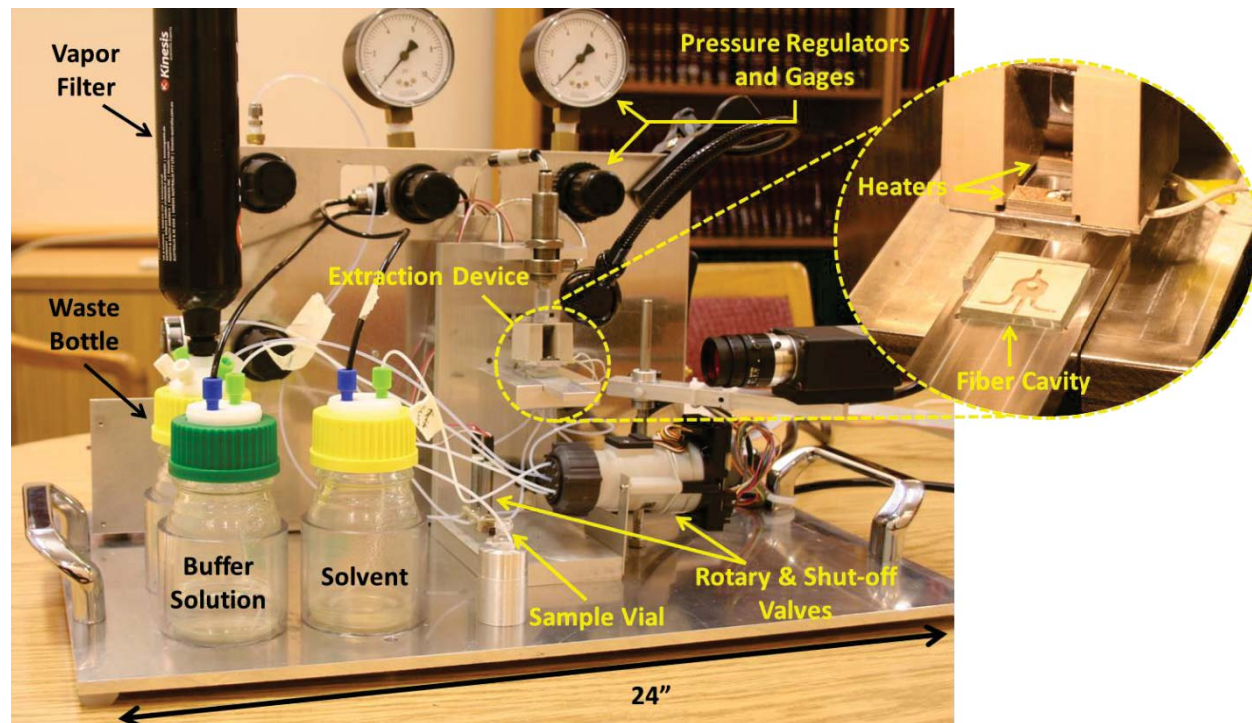


Figure 2-10. Prototype 1 front view

The size of the system is 24” wide by approximately 12” deep and tall. A view of the back side of the system shows the electronic components in Figure 2-11.

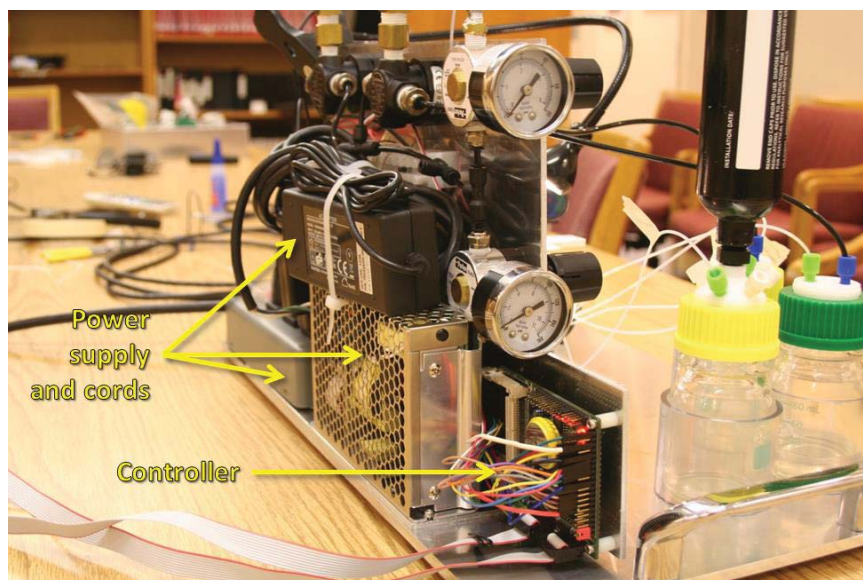


Figure 2-11. Prototype 1 rear view – electronic components

A 12 V supply provides power for a Tern controller, a Tern Relay7 relay bank, and electronic valves and heaters. The Tern board controls the operation of the electronic valves and heaters by sending signals to the relay bank and rotary valve controller. The relay bank provides +12 V to individual components when a signal is received. The rotary valve connects the fluid inlet of the system to fluid, waste, and storage container lines. The valve uses a 24V power supply brick as shown in the Figure 2-11.

Prototype 1 was used to test the automated dye extraction process and to finalize selection of system components. Results of testing showed that the system design could successfully extract and process dyed fiber samples. Extraction tests and results with the first prototype are provided in Sections 3.8.1 and 3.8.2.

2.3.2 PROTOTYPE 2 LAYOUT

The second prototype uses the same general system layout and components for the extraction process. The main additions to the system are sensors to monitor system pressures, an optical switch to detect the presence of an extraction chip, and a fan to cool the chip and electronics. Smaller pressure regulators reduced the size of the system. The overall size of the system has been reduced to approximately 10” x 6” x 6.5” (LxWxH). The general layout with the enclosure is shown in Figure 2-12.

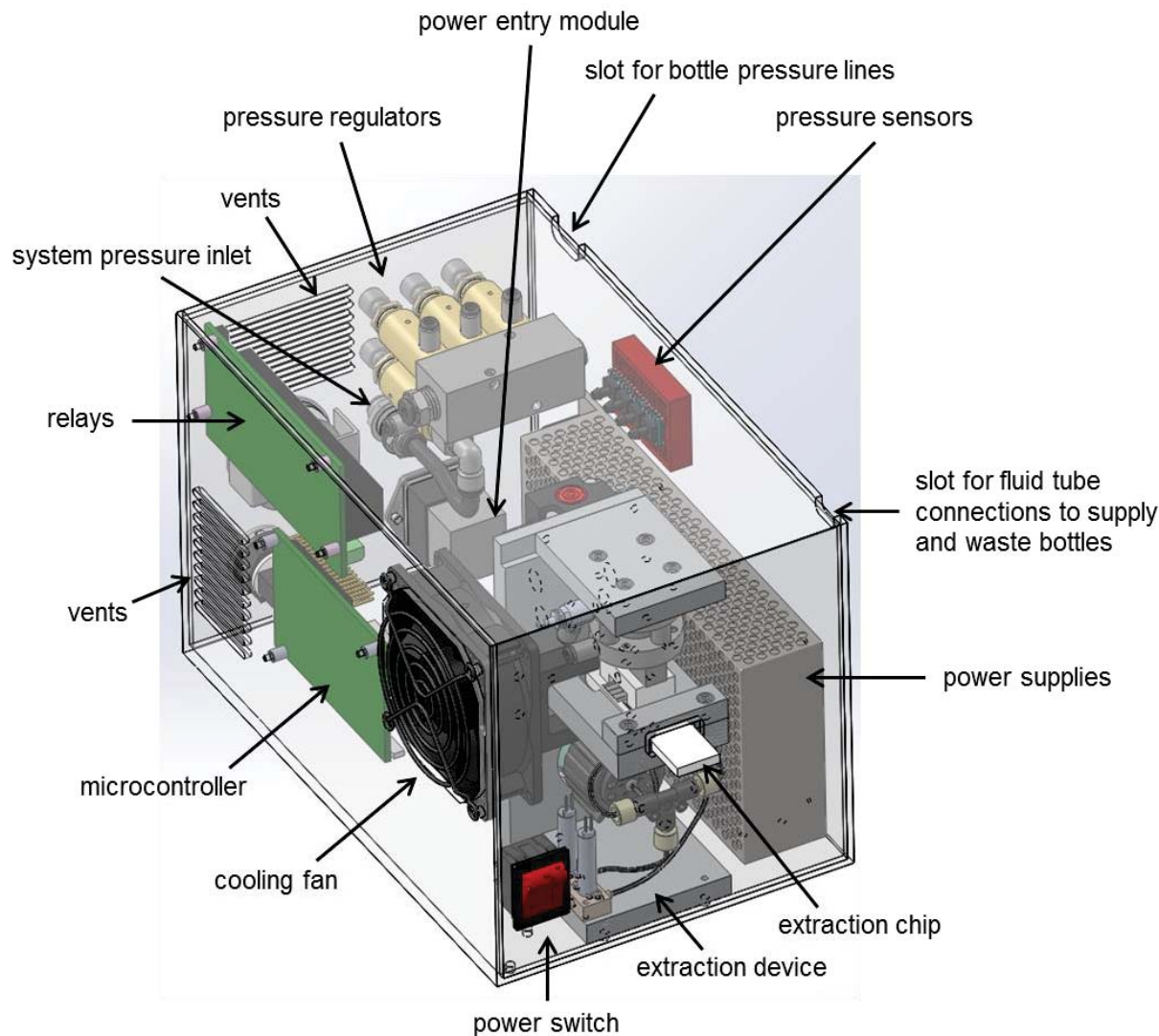


Figure 2-12. Prototype 2 Layout

External connections for the system are located at the rear panel as shown in Figure 2-13. Inputs to the system are AC power that is routed through the power entry module, a supply pressure line (minimum of 50 psi), and a USB connection that allows the user to operate the system with a computer. A bottle rack is attached to the side of the enclosure to hold solvent, buffer, and waste bottles as well as a sample vial.

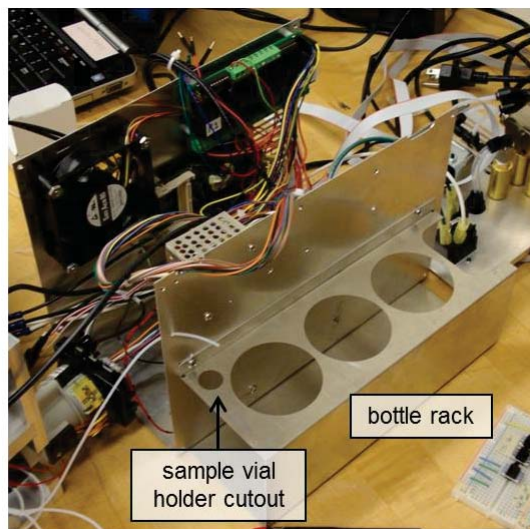
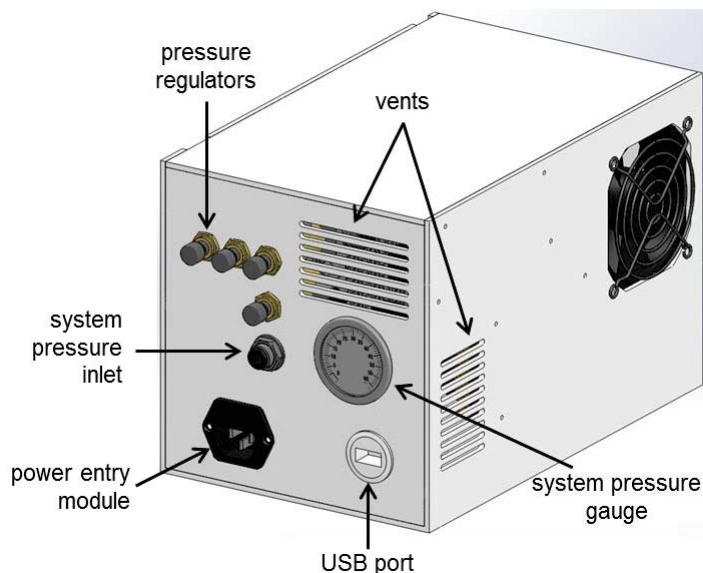


Figure 2-13. External connections and features of prototype 2

The extractor assembly is shown in Figure 2-14. The chip is inserted into the device as shown. The cylinder is pressurized and extends when the optical sensor detects the chip. The heater assembly then presses down on the chip to hold it in place and provide heat to the cavity. Fluids are routed to the extractor manifold through the valves and fluid lines located below.

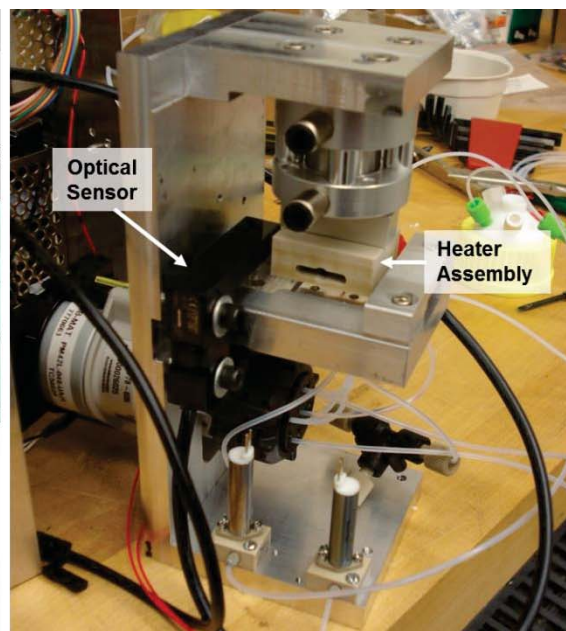
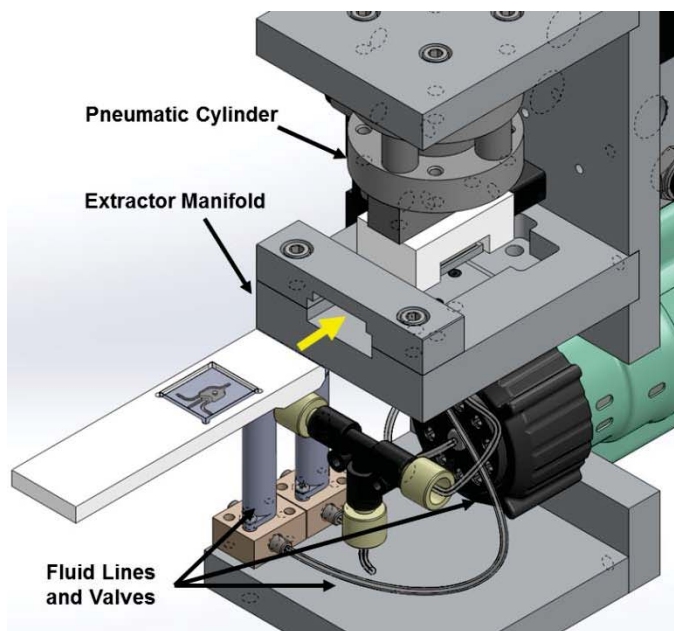


Figure 2-14. Extractor assembly

Detail is provided on the components of the system and their selection in the following sections.

2.3.3 PNEUMATIC CYLINDERS

A pneumatic cylinder produces the force required to seal the microfluidic cavity and the extraction chip. Previous sealing tests performed at the PEC with the FFKM material showed that a 7 lb force

was sufficient to seal a microfluidic cavity of characteristic size for a cavity pressure of 20 psi. A cylinder capable of producing 7 lb of force for standard wall pressure (usually around 80 psi max) was then required. The pneumatic cylinder used for the first prototype was a threaded-body, double-acting cylinder with a bore diameter of 0.5" and 1" stroke (McMaster-Carr part number 6604K25). Because the cylinder had a single rod connection to the heater assembly, a flexure was added to prevent rotation of the assembly. The flexure constrained motion of the rod and heater assembly to the vertical direction only. The cylinder and flexure are shown in Figure 2-15.

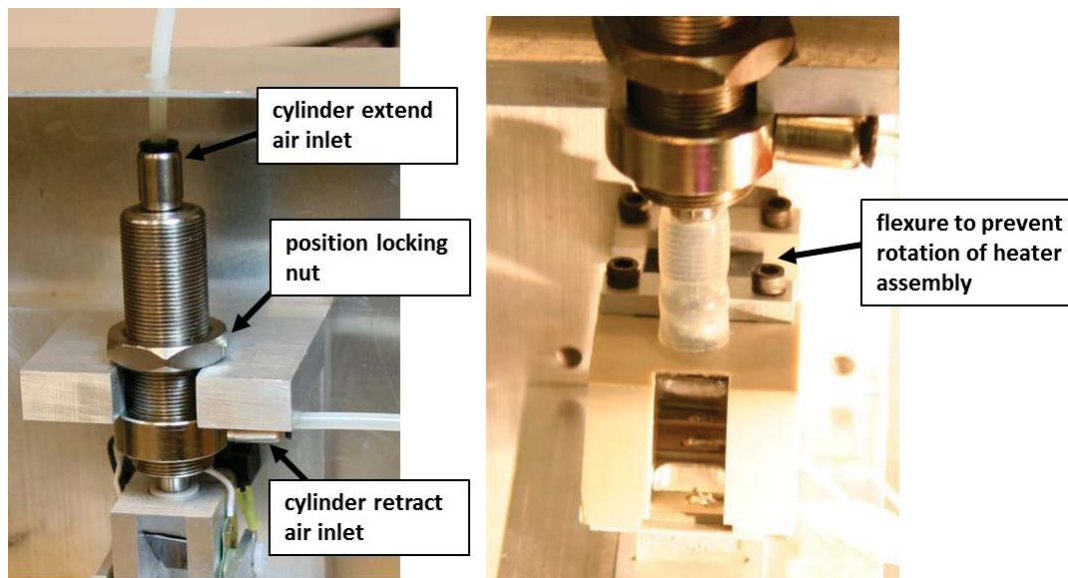


Figure 2-15. Prototype 1 pneumatic cylinder – 0.5" bore

In general, a pneumatic cylinder does not operate at its theoretical maximum force (where force output is equal to pressure times bore area) due to seal friction. To account for seal friction, the cylinder was calibrated using a Kistler Load Cell, Type 9011A, coupled with an Agilent Oscilloscope, model number 59624A (see Appendix A for load cell calibration). The calibration curve is shown in Figure 2-16 with the theoretical maximum force output of the cylinder (for the extend position).

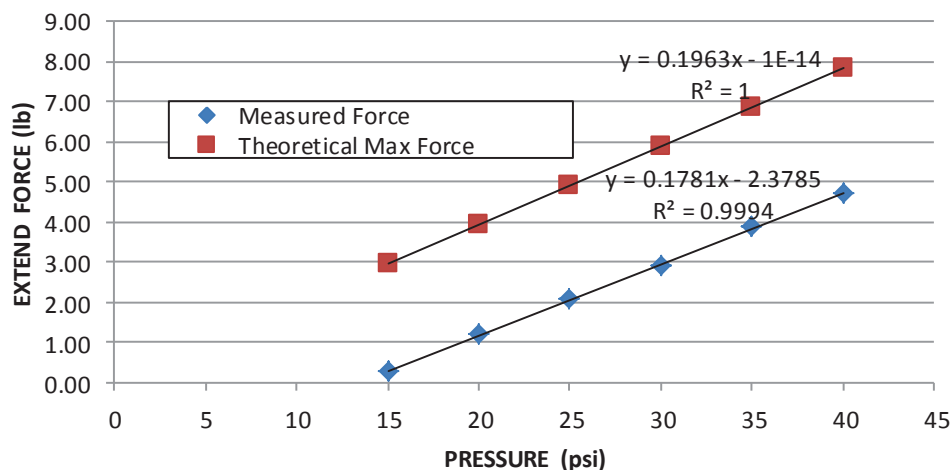


Figure 2-16. Pneumatic cylinder calibration – 0.5" bore

Another cylinder was obtained for the second prototype. The cylinder is also double-acting with a 0.75" bore and 0.25" stroke (Bimba Manufacturing Company part number FT-040.25-3R). Double rod extensions connected to a tooling plate, preventing rotation of the cylinder. It is mounted by four 6-32 threaded holes on the rear end cap. The cylinder is shown in Figure 2-17.

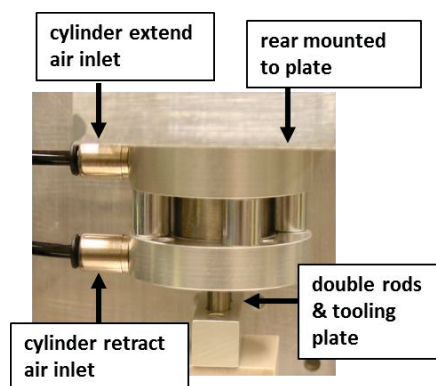


Figure 2-17. Prototype 2 pneumatic cylinder – 0.75" bore

The smaller profile of the cylinder is ideal for a more compact overall design of the extractor assembly. The larger 0.75" bore produces a higher force output per unit pressure as well. To determine the reduction in force due to seal friction, a test was performed to determine the pressure at which the cylinder moved. The extend port was connected to a pressure regulated line set to zero pressure initially. Starting in the retracted position, the pressure was slowly increased until the piston moved. Several repetitions of this test showed that the cylinder moved at approximately 4.5 psi. This corresponds to 2 lb of static friction from the piston seal. To achieve the 7 lb force, a minimum pressure of 20.3 psi is required.

2.3.4 VALVES

Selection of valves was an important consideration in the operation of the device. Valves can be used to start and stop fluid flow and to change its direction. An important consideration for valve selection is the body and seal material as well. Shut-off valves (SOVs) and directional-control valves (DCVs) designed for microfluidic systems were obtained from The Lee Company (part numbers: LFNA1250225H for SOVs and LHDA1221515H for DCVs). The DCV selected is a three-way, two-position valve with a common port, a normally open port, and a normally closed port. The valve is shown in Figure 2-18.

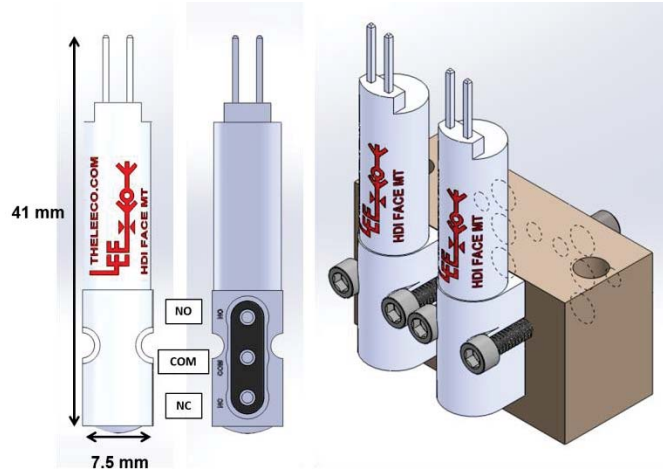


Figure 2-18. Lee Co. valve, 3-way 2-position directional control (LHDA1221515H)

Flow is able to move between the common port and the normally-open port by default. When the valve is powered, a solenoid actuates an internal plunger to open the normally-closed port and to seal the normally-open port. The body and sealing materials are FFKM, PPS, and PBT. The DCV was used in initial system configurations and tests. It was determined that possible sample contamination and inconsistencies in flow timing could be attributed to the valve. Its use was discontinued in later prototype configurations (see Appendix B for further detail on problems observed in directional control valve flow tests).

The shut-off valve is used to start and stop fluid flow. The valve has an inlet and an outlet port. The valve is normally closed. A plunger with a seal is loaded against the port openings by an internal spring. When the valve is powered on, a solenoid is actuated to retract the plunger and establish a flow path between the ports. The valve is shown in Figure 2-19.

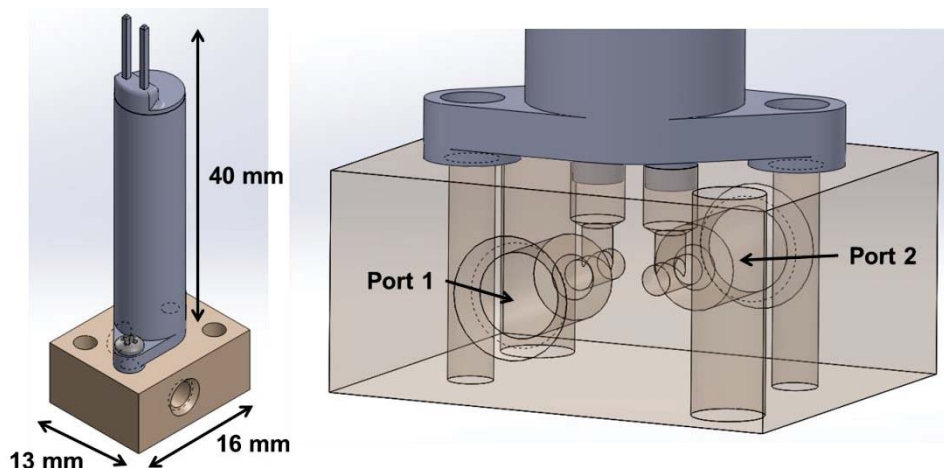


Figure 2-19. Lee Co. valve, 2-way 2-position shut-off (LFNA1250225H)

An array of four DCVs and one SOV at the fluid inlet of the system was replaced with a rotary selector valve (Rheodyne part number MLP778-605). The rotary valve has 10 positions and 11 ports with connections for 1/16" tube ODs. The center port is the common port and is connected to one of the adjacent ports (port 1 by default). The original array of valves only provided five separate flow path selections, whereas the rotary valve shown in Figure 2-20 provides ten.

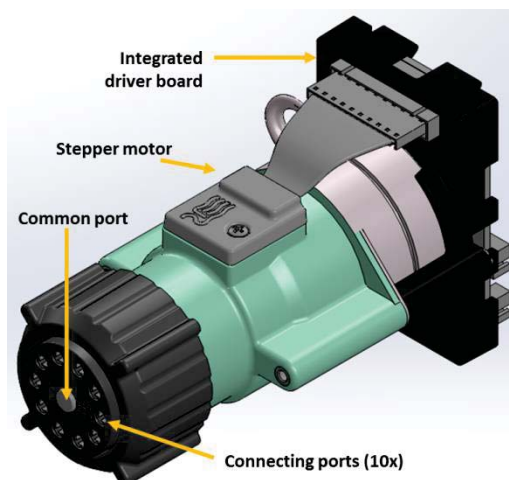
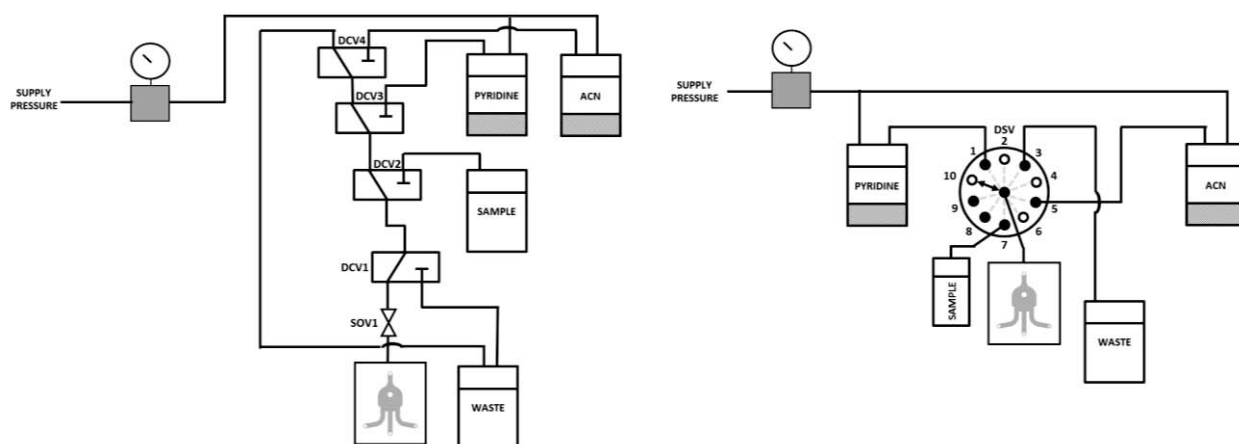


Figure 2-20. Rheodyne rotary valve, 11-port 10-position (MLP778-605)

The rotary valve has several advantages over the DCVs. The port-to-port internal volume of the valve is less than 6 μl (this compares to an internal volume of 75 μl for the DCVs and 13 μl for the SOVs). The rotary valve also eliminates the need for any other valves at the inlet as shown in Figure 2-21.



A) Cavity inlet valve configuration with DCV's and SOV's

B) Cavity inlet configuration with rotary valve

Figure 2-21. Valve configurations using (A) DCVs and SOVs and (B) a rotary valve

The valve position is controlled by a stepper motor and an integrated driver board. The driver board receives a 4 line BCD (binary coded decimal) signal from the system controller. The connections for the J4 chip on the driver board are listed in Table 2-4.

Table 2-4. J4 PIN assignments for rotary valve

<u>J4 Pin:</u>	<u>Function:</u>
1	FB0 (LSB*)
2	FB1
3	FB2
4	FB3 (MSB*)
5	Error FB
6	-
7	Done FB
8	CMD3 (MSB)
9	Ground
10	CMD2
11	CMD1
12	CMD0 (LSB)

* LSB - least significant bit

* MSB - most significant bit

CMD - command signal

FB - feedback signal

The value of each command signal can be determined as shown in Figure 2-22. For the Rheodyne valve and driver board, the numerical value represented in binary corresponds to the valve port number. For example, position 6 would be achieved by sending the signal: CMD3=0, CMD2=1, CMD1=1, CMD0=0. The four line BCD signal is sent to the integrated driver board by four digital output pins on the Tern controller.

CMD3	CMD2	CMD1	CMD0
↓	↓	↓	↓
<u>0</u>	<u>0</u>	<u>0</u>	<u>1</u>
↑	↑	↑	↑
2^3	2^2	2^1	2^0

Figure 2-22. 4 line BCD command values

The pneumatic cylinder is operated using a four-way, two-position directional control valve made by Ingersoll Rand. The valve is shown in Figure 2-23.

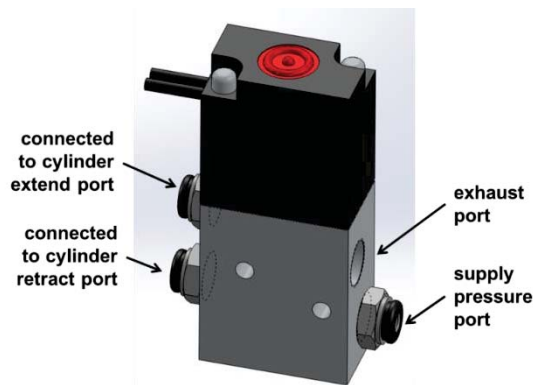


Figure 2-23. Ingersoll Rand valve, 4-way 2-position directional (Grainger part number 6JJ43)

The supply pressure port is normally connected to the cylinder extend port shown in the figure. Likewise, the exhaust port is normally connected to the cylinder retract port. When voltage is supplied, a solenoid actuates to alter the connections. When powered, the supply pressure port is connected to the cylinder retract port and the exhaust port is connected to the cylinder extend port. The simple operation allows the cylinder to be extended and retracted using the valve.

2.3.5 TUBING, FITTINGS, EXTRACTOR MANIFOLD

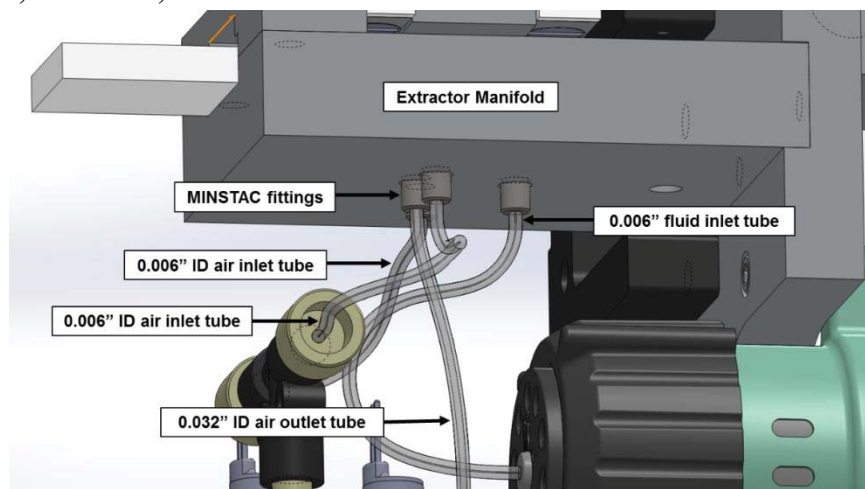


Figure 2-24. Extractor manifold connections

The selection of tubing was very important for proper operation of the device. The tubing must be compatible with pyridine. The inner diameter of the tubing is an important design consideration in regards to flow rate (for timing of flow) and total fluid volume in the system (see Section 3.3 for flow considerations). Tubing made from PTFE was obtained from Valco Instruments Co. Inc. (VICI). A tubing inner diameter (ID) of 0.032" was selected for the main fluid lines leading to and from the solvent, buffer, and waste bottles and main air supply. A tubing ID of 0.006" was selected for the main fluid inlet line and air inlet lines. The 0.006" is small enough to provide control over flow timing for the small lengths and volumes of the system. The smaller tube diameter also reduces the dead volume of the fluid system. For a given length, the volume of the 0.032" tube would be ~28 times that of the 0.006" tube. The extra fluid volume would greatly dilute the dye containing buffer sample. Both tubes have an outer diameter (OD) of 1/16". Tubing connections for the extractor manifold are shown in Figure 2-24.

To route the tubes to fluid manifolds within the system, MINSTAC fittings from The Lee Company were used. The fittings were selected because they create a seal at both the tube and manifold interfaces. A cutaway view of the manifold shows the fluid flow path into the chip in Figure 2-25. A diagram of the MINSTAC fitting is also provided [25].

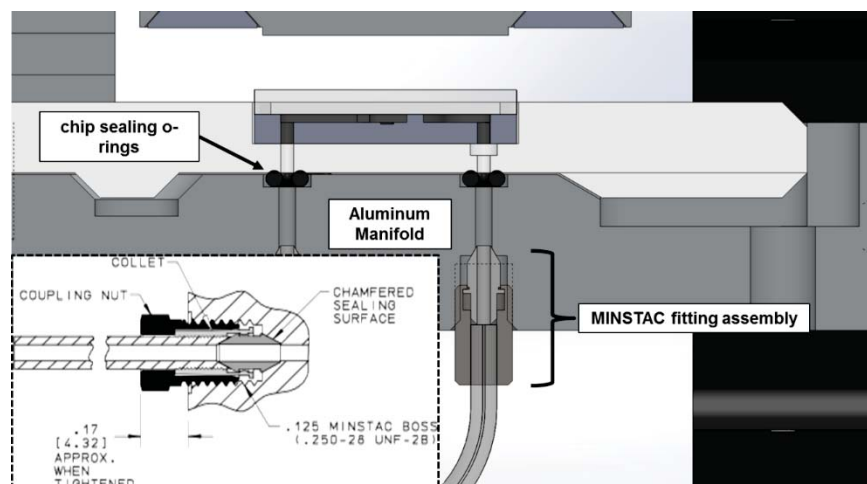


Figure 2-25. Extractor manifold cutaway – MINSTAC fitting sealing [25]

The air inlet and outlet tubes are routed to two shut-off valves as shown in Figure 2-26. A single 0.006" ID tube connects the air supply to the extractor manifold after splitting the flow path with a tee fitting. Three finger tight fittings connect the 0.006" ID tubing to the tee by sealing on the OD of the tube. The air inlet and outlet tubes connect to the shut-off valve manifolds through MINSTAC fittings.

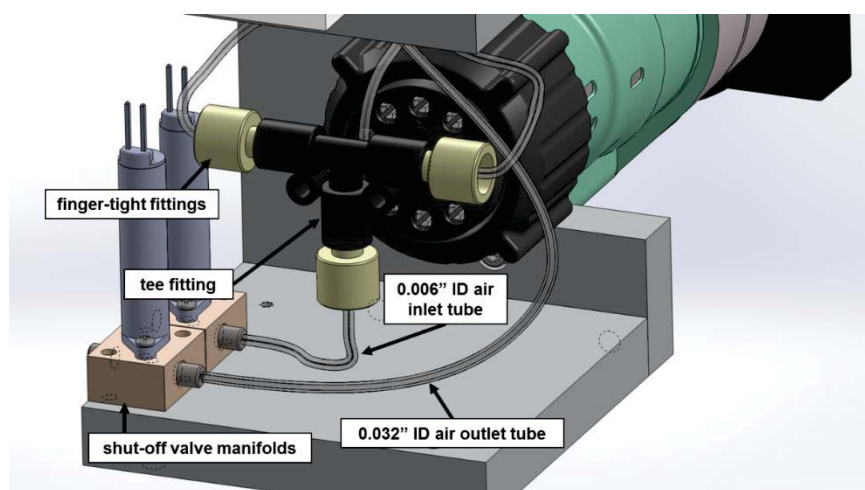


Figure 2-26. Air inlet and outlet tube connections

The length of the small ID (0.006") tubes is important for flow timing. The 0.006" singular air inlet tube is 5.5 cm long. The air inlet tubes connected to the extractor manifold and tee fitting are 9.2 cm long each. The fluid inlet tube is 20 cm long.

2.3.6 PTC HEATERS AND HEATER ASSEMBLY

Heating of the cavity is an important consideration for extraction conditions and evaporation time. Initial extractions with the PEEK microfluidic cavity were performed at approximately 92°C. The first heater assembly for the automated system used two positive temperature coefficient (PTC) heaters rated for 90°C set temperature (Spectrum Sensors and Controls Inc., part number PR425C090S101H). The heater assembly consisted of a 1" square PEEK block with a slot

machined at 45° and a reflective surface for viewing of the cavity. The PTC heaters and heater assembly are shown in Figure 2-27.

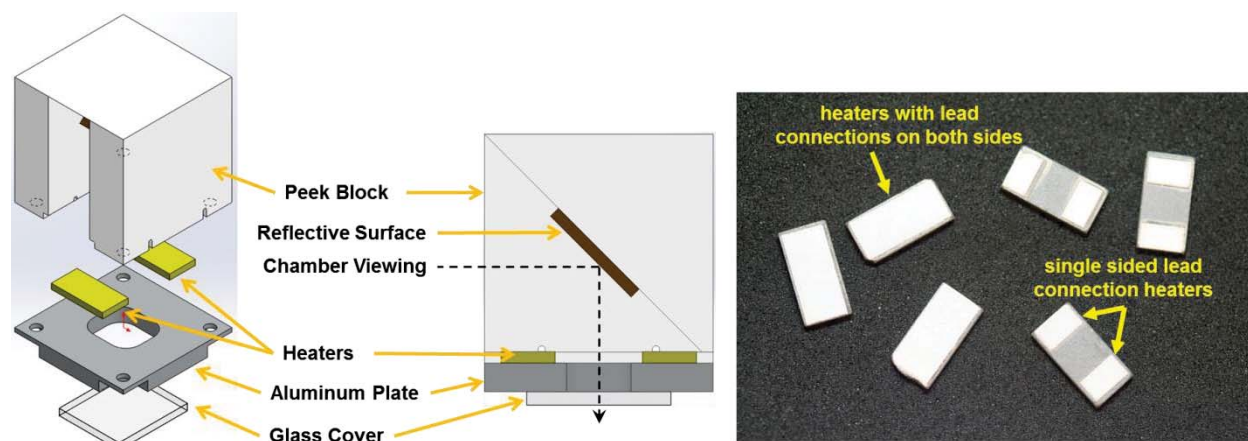


Figure 2-27. PTC heaters (PR425C090S101H) and heater assembly

The aluminum plate is heated and transfers heat to the glass and microfluidic cavity. A cavity temperature between 75 and 80°C was achieved with this setup after approximately 4 minutes. A discussion of how the PTC heater is presented in Section 3.7.

2.3.7 THIN-FILM HEATERS AND HEATER ASSEMBLY

The second heater assembly design uses a thin-film resistive heater from Birk Manufacturing, Inc. (part number BK3546-10.5-L24-01). The resistive heater was chosen to provide higher temperatures in less time and to allow for temperature control with the Tern controller. The heater is attached to a thin aluminum plate with a thermally conductive adhesive. The aluminum plate is attached to the PEEK heater assembly block using two PEEK screws. The screws and block act as insulators ($k_{\text{PEEK}} = 0.25 \text{ W/mK}$) to prevent the pneumatic cylinder from getting hot. The PEEK block is slotted and hollow above the heater for cooling purposes. The heater and heater assembly are shown in Figure 2-28. Description of the heater operation and control are presented in Section 3.7.

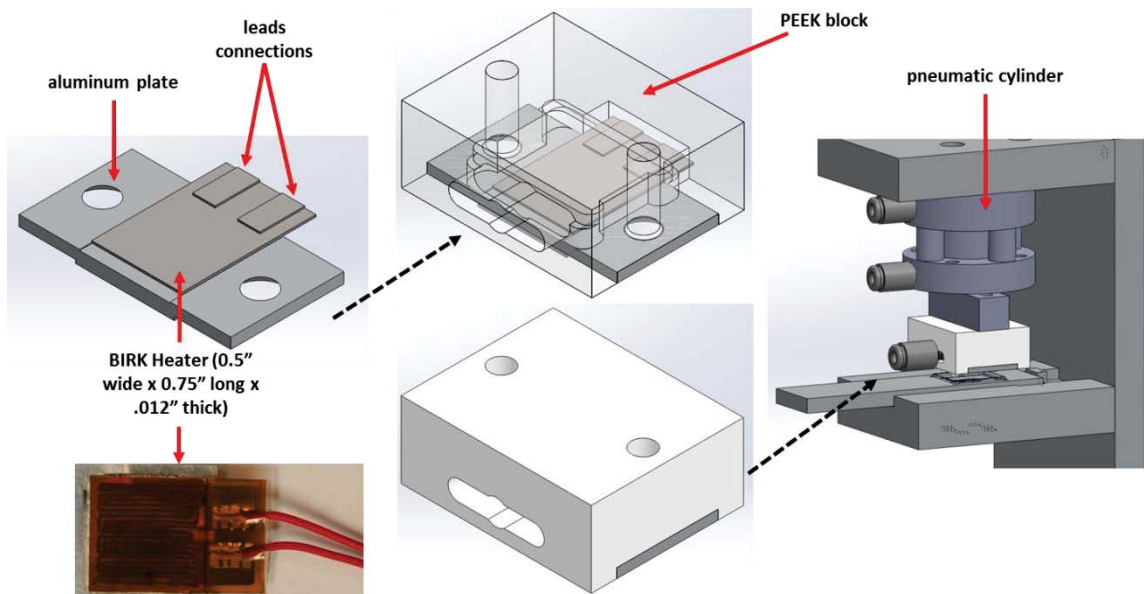


Figure 2-28. Birk thin-film heater and heater assembly (BK3546-10.5-L24-01)

2.3.8 CONTAINERS AND FILTERS

Good sealing and chemical compatibility were required for the solvent, buffer, and waste containers for the system. Sealing is important for maintaining constant regulated pressure during operation and chemical compatibility ensures that the seal does not degrade from pyridine vapors over time. Omnifit (a brand of Diba Industries) Q-series bottle caps with standard glass solvent containers were selected for the application. The materials of construction for the caps are PTFE and glass-filled polypropylene, which have excellent compatibility with the solvent (see

Table 2-3).

The OSHA standard for pyridine exposure is 5 parts per million (ppm) parts of air [26]. The waste filter cap includes a Kx VaporSafe activated-carbon vapor filter (a product of Kinesis Inc.) to filter waste vapors to acceptable limits as shown in Figure 2-29.

The solvent and buffer bottles use Omnifit caps with a port and fitting each for the 1/8" OD supply pressure tube and a port and fitting for the 1/16" fluid tube. Bottom-of-the-Bottle™ (BOB) filters (obtained from IDEX Health and Science LLC) connect to the 1/16" OD tube at the bottom of the solvent container. These filters have a porosity of 10 μ m and prevent any large particles or fabric remnants from entering the system and producing potential clogs. The solvent/buffer container line and filter configuration are shown in Figure 2-30.

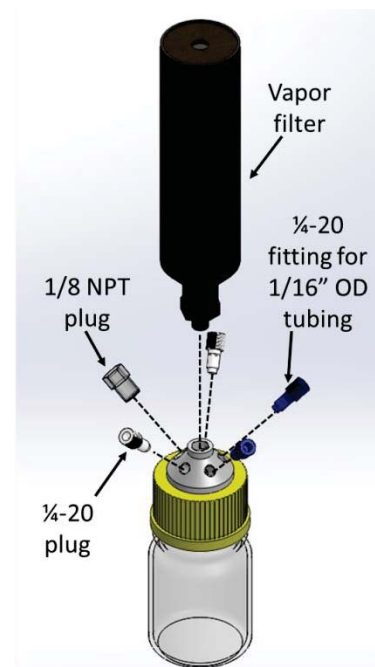


Figure 2-29. Waste container with vapor filter and fittings

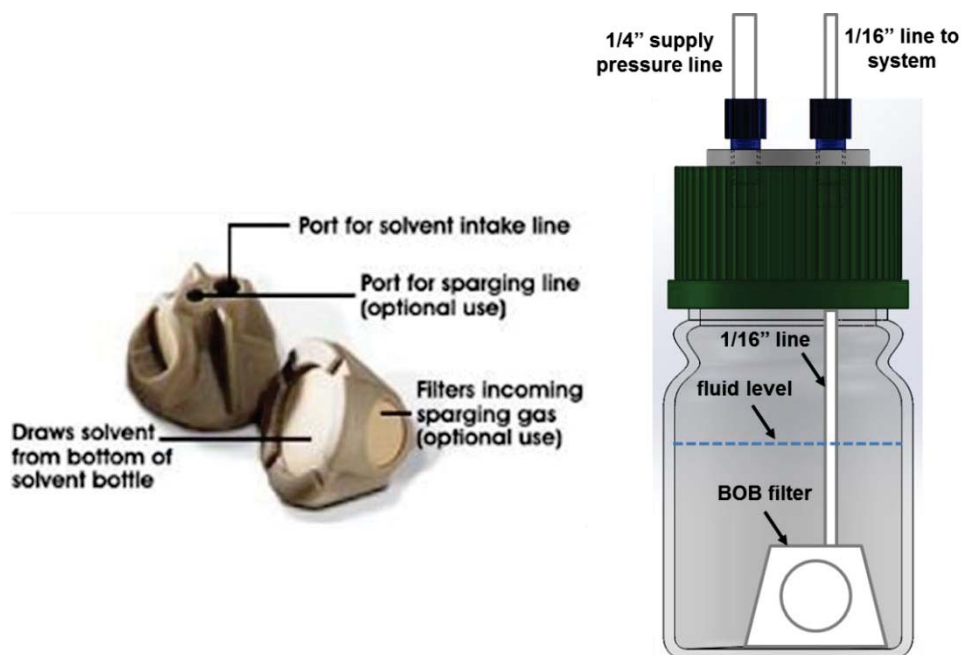


Figure 2-30. Bottom-of-the-Bottle™ filter [27] and bottle configuration

In addition to filtering fluid entering the system from supply reservoirs, filtering of fluid back-flowing to the system from the microfluidic cavity is critical. To accomplish this, a stainless steel filter frit (2 μm porosity, Idex part number C-407) was added to the inlet of the extraction chip. The filter frit is positioned beneath the fluid inlet of the cavity as shown in Figure 2-31, to filter dirt and fiber particles from the sample as it is pumped to the sample container.

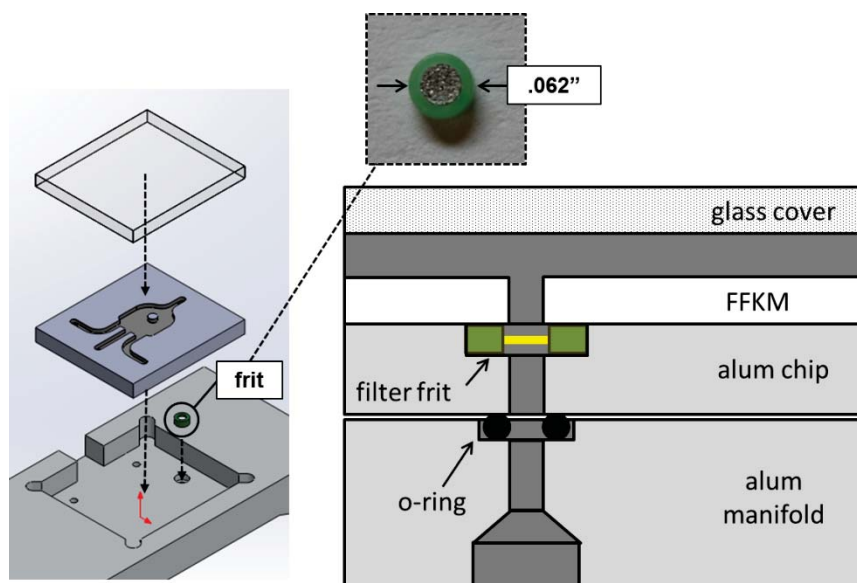


Figure 2-31. Filter frit (2 μm porosity) in microfluidic extraction chip

The HPLC column diameter is small and can be easily clogged by dirt or fiber particles so the sample must be filtered before testing with the HPLC system. A filter with a porosity of 0.2 μm is used to do this. Due to the small sample volume size, it is difficult to filter the sample after extraction without losing a significant volume of fluid. Filter vials from Thomson Instrument

Company were obtained and tested (0.2 μm porosity). The vials can filter a minimum sample size of 10 μl . The total volume of the system and cavity is approximately 20 μl . The fluid is pumped into the vial shown in Figure 2-32. The plunger is then pushed to the bottom of the vial, forcing the fluid through the filter in the base of the plunger.

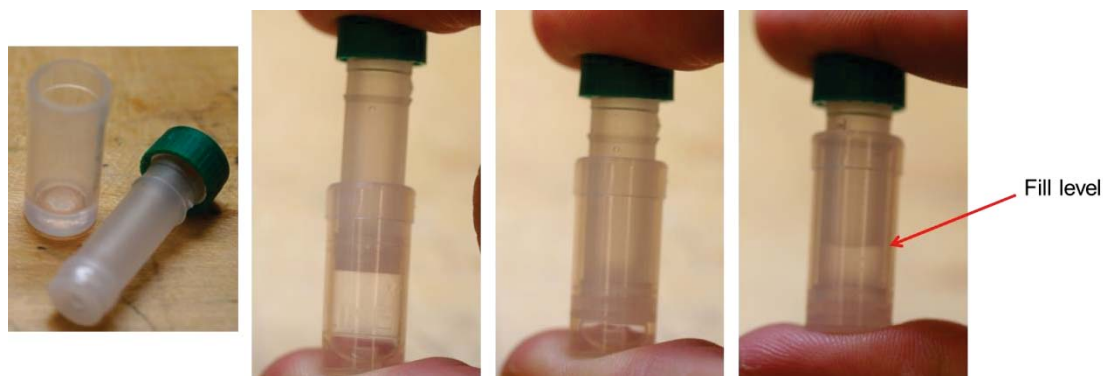


Figure 2-32. Thomson filter vial

This is one recommendation for post-extraction filtering, although other methods are available for appropriate sample volumes.

2.3.9 FFKM CAVITY AND CAVITY CHIP

The microfluidic cavity design is shown in Figure 2-33. The design of the cavity has a single fluid inlet, two air inlets for evaporation and fluid ejection, and an air outlet (see Section 3.4 for a discussion of the cavity design process).

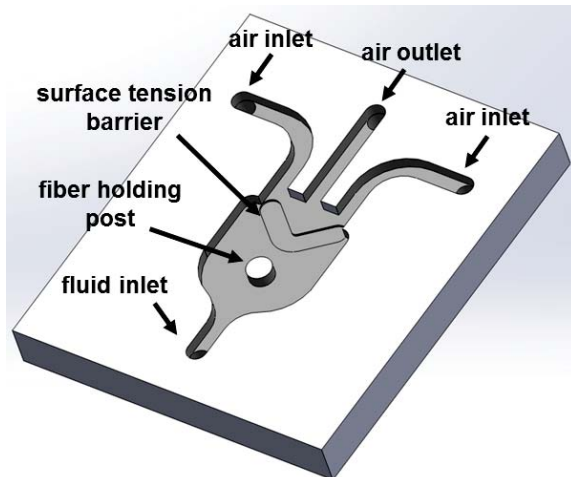


Figure 2-33. FFKM microfluidic cavity design

The cavity has a fiber holding post to retain the fiber by pressing it against the glass cover. The goal of fiber placement is to minimize the area of the fiber in contact with the post and glass where dye cannot be efficiently extracted. The microfluidic cavity is placed in the extraction chip with the fluid inlet in line with the filter frit as shown in Figure 2-34.

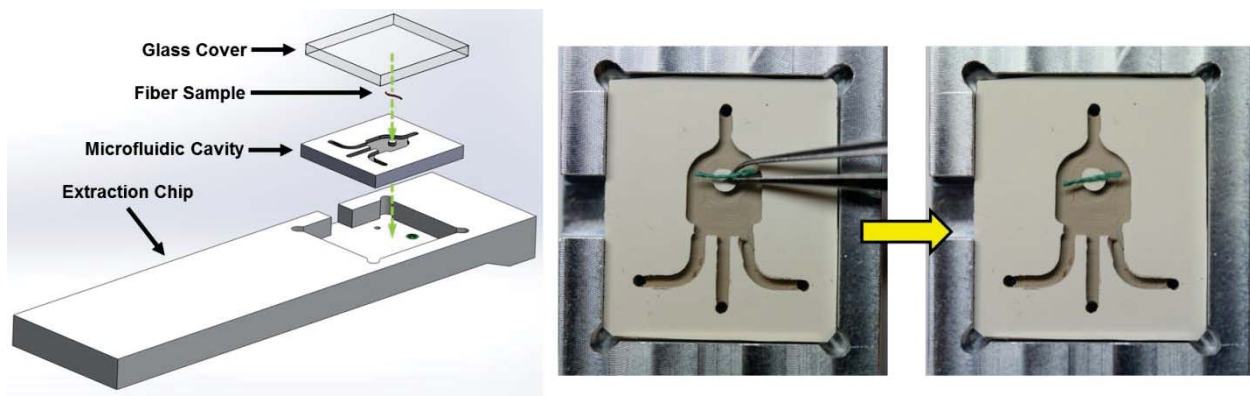


Figure 2-34. Fiber placement and assembly of extraction chip for testing

The fiber is then placed over the fiber holding post at the center of the cavity. Finally the glass cover is placed on top of the cavity and pressed down to ensure the fiber is secured. The final chip design is shown in Figure 2-35.

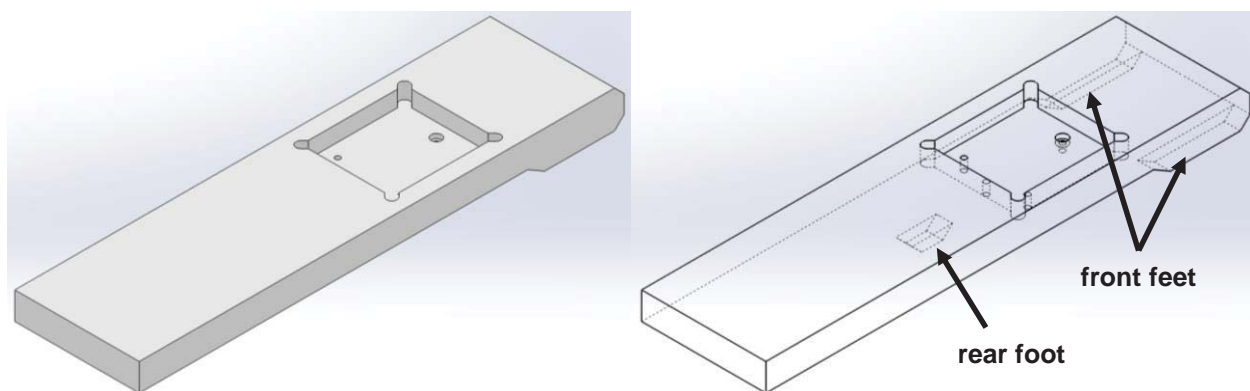


Figure 2-35. Extraction chip

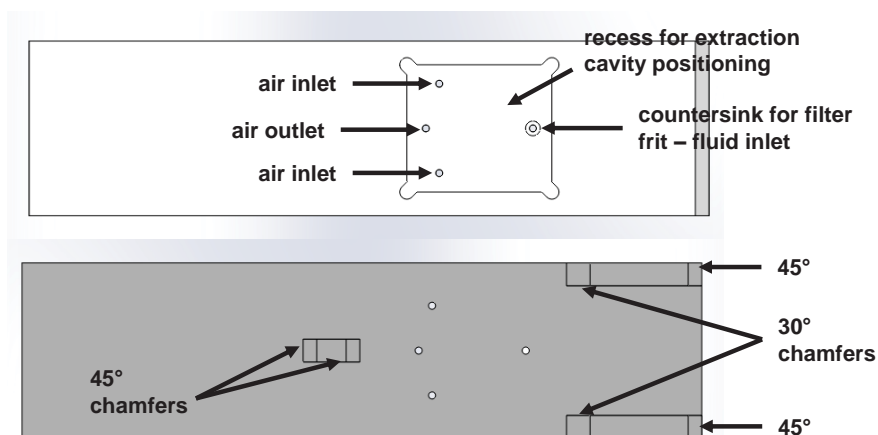


Figure 2-36. Extraction chip features

Chamfers are included on the front edge to help in guiding the chip during insertion into the system. The bottom of the chip has three feet. The front two provide clearance for the o-rings on the manifold so that the chip edge does not contact them. A third foot in the center and behind the extraction cavity keeps the chip level during insertion into the system. Forty-five degree chamfers

on this foot assist in inserting and removing the chip without catching. Thirty degree chamfers on the rear of the front feet provide the same function and help to properly position the chip over the fluid holes in the manifold. The chip features are shown in Figure 2-36.

2.3.10 CAVITY FABRICATION

The FFKM cavities were made using a micro-mill designed for machining small parts. An end mill with a 1/32" (794 μm) diameter was spun at 30,000 rpm to create the cavity and channels in the FFKM material. An example cavity machined from acrylic is shown in Figure 2-37.

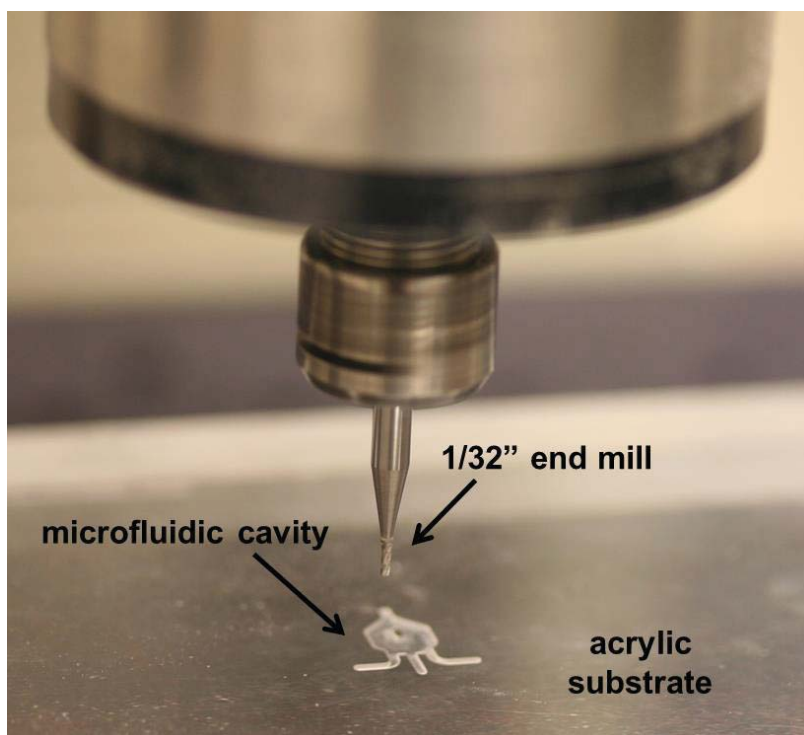


Figure 2-37. Example of microfluidic cavity machining capabilities in acrylic substrate

The acrylic shown in Figure 2-37 produced clean features; however, the material is not compatible with the pyridine solvent. FFKM has a much lower modulus (.007 GPa) in comparison to the acrylic (3.2 GPa), making it more difficult to produce clean features on the sub-millimeter scale. To reduce the formation of burs and deflection of the FFKM during the machining of sharp corners and small fiber holding features, the material was placed between two polycarbonate layers as shown in Figure 2-38.

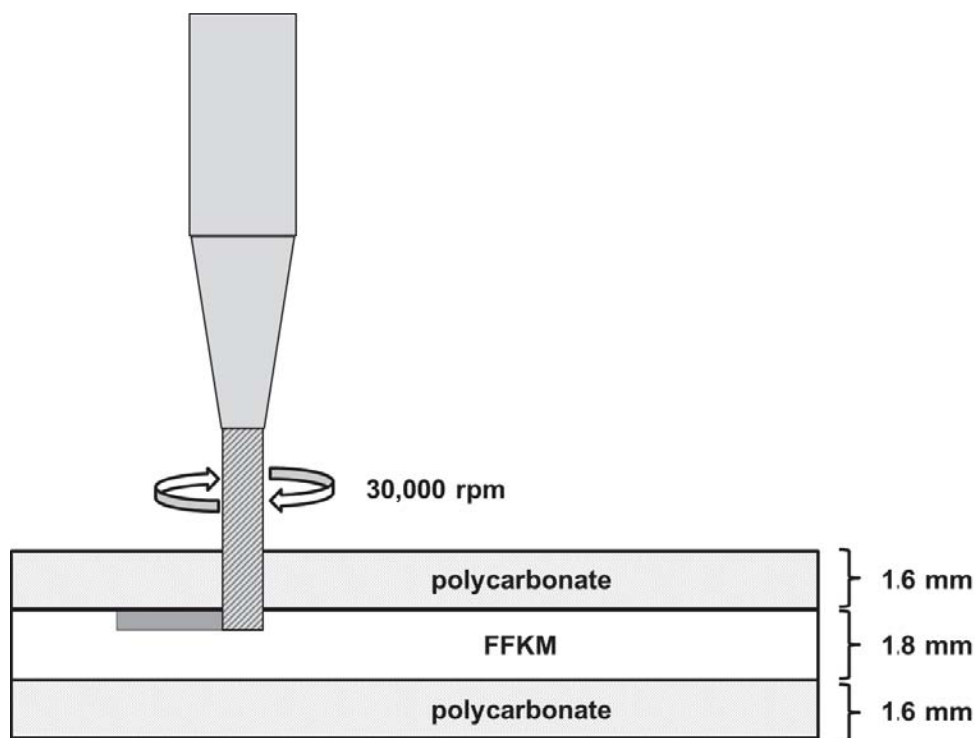


Figure 2-38. FFKM cavity machining

The top polycarbonate layer provided rigidity to reduce the formation of burs and deflection of the FFKM. Details on the machining setup and machine tool path generation are provided in Appendix H.

2.3.11 PRESSURE REGULATORS

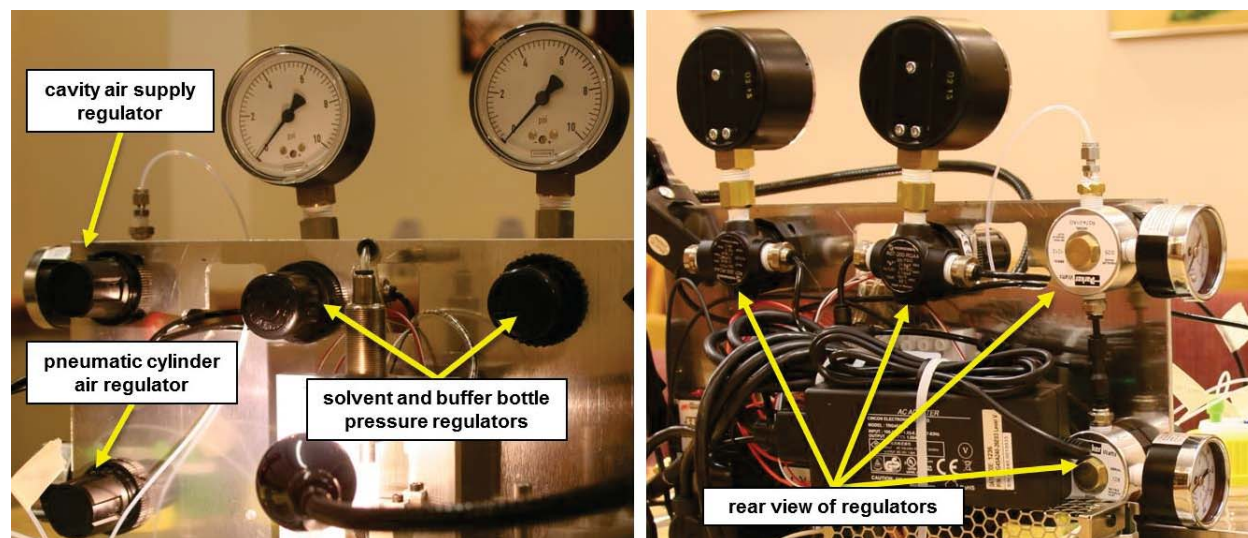


Figure 2-39. Prototype 1 pressure regulators

The first prototype used two miniature air regulators with a pressure range of 0-25 psi and two with a range of 0-60 psi (McMaster-Carr part number 676K811). The solvent and buffer bottles require a pressure < 10 psi to control fluid flow control. The lower pressure range of the 0-25 psi regulators allowed better accuracy in setting the bottle pressures. Pressure gages with a range of

0-10 psi were also used to improve accuracy of setting the bottle pressures. The higher pressure range regulators were used to regulate the pneumatic cylinder pressure and cavity air supply with standard 0-100 psi gages. The regulators are shown in Figure 2-39.

A more compact pressure regulator design was selected for the second prototype. Miniature, manifold mounting pressure regulators from Clippard Instrument Laboratory, Inc were incorporated into the design as shown in Figure 2-40. A pressure range of 0-30 psi was selected for the bottle and cavity air supply pressures (part number MAR-1P-3). A regulator with a range of 0-60 psi (MAR-1P-6) was selected to regulate wall pressure down to the air cylinder pressure. The output of this regulator is also routed to the manifold housing the other pressure regulators.

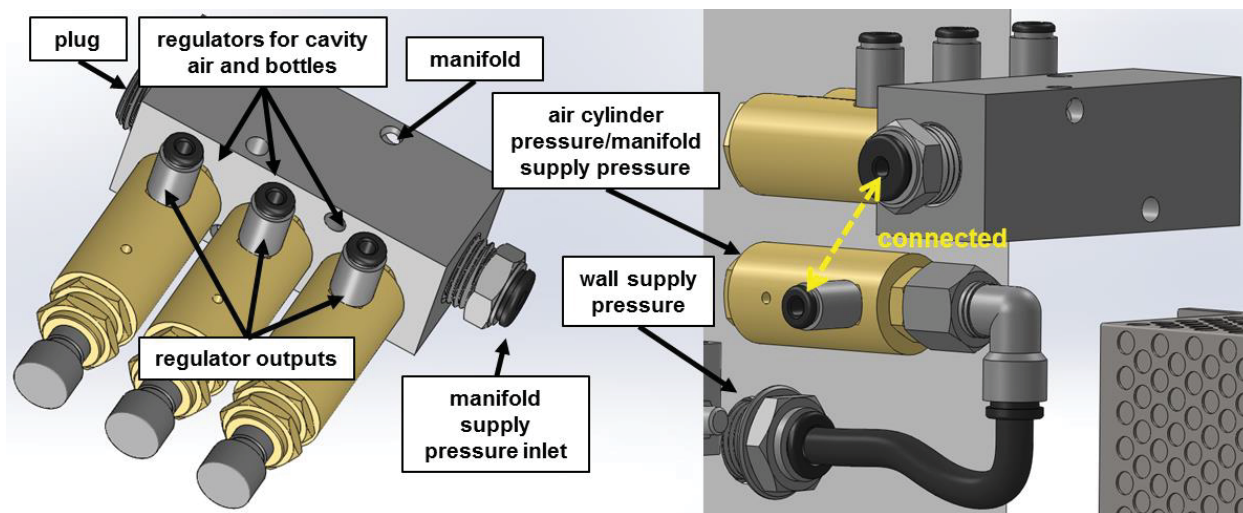


Figure 2-40. Prototype 2 pressure regulators

2.3.12 SENSORS

Four pressure sensors and an interrupted-beam (IB) sensor were added to the system to monitor pressures and to ensure the presence of the extraction chip in the device before allowing extraction to proceed. It is important to monitor the pressures of the fluid reservoirs and cavity air because the fluid filling and evaporation processes are dependent on timed operation of valves. If set pressures fall below a threshold value, the timed processes may not operate as expected, resulting in failed extraction.

The IB sensor is used to sense the extraction chip when it is inserted into the device. The sensor is an E3Z-G (part number E3Z-G61 2M) single optical axis sensor from Omron. A beam is transmitted from one end of the optical axis to a receptor on the other end. A hole was drilled through the manifold for the beam to transmit through. The setup was tested to determine the position of the chip required to trigger the sensor. The test setup is shown in Figure 2-41.

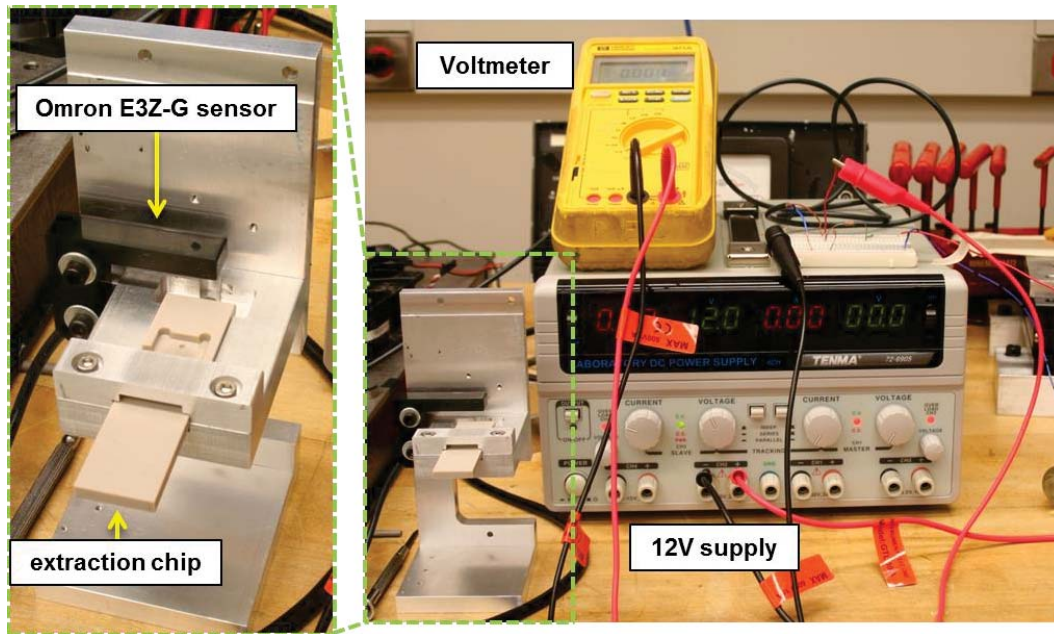


Figure 2-41. Optical beam sensor test setup

The sensor uses a 12 VDC power source and outputs a 12 V signal. A voltmeter was used to measure the output signal from the sensor to determine the chip position required to trigger the sensor. The chip was slowly adjusted until the beam was broken, producing a voltage reading on the voltmeter. The distance between the end of the chip and the back stop of the aluminum manifold was then measured to be approximately 0.03" when the beam was broken as shown in Figure 2-42.

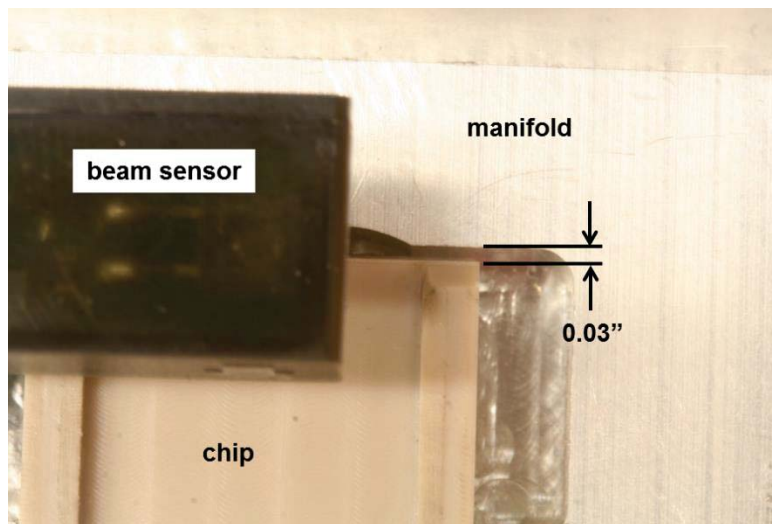


Figure 2-42. Chip position to break beam

The voltage limit of the digital input pins on the relay card is 5 V. To use the 12 V output signal from the sensor, a Panasonic TX2SA-12V relay was selected. The relay is shown in Figure 2-43. The coil pins of the relay are connected to the 12 V supply and signal wire of the beam sensor. When the beam is broken, the signal wire supplies ground and the relay coil is powered, making connection between the common (COM) pin and the normally open (NO) pin. The common pin is

connected to +5 V and the NO pin to a digital input on the controller. The controller can then receive a signal when the relay is triggered by the breaking of the beam.

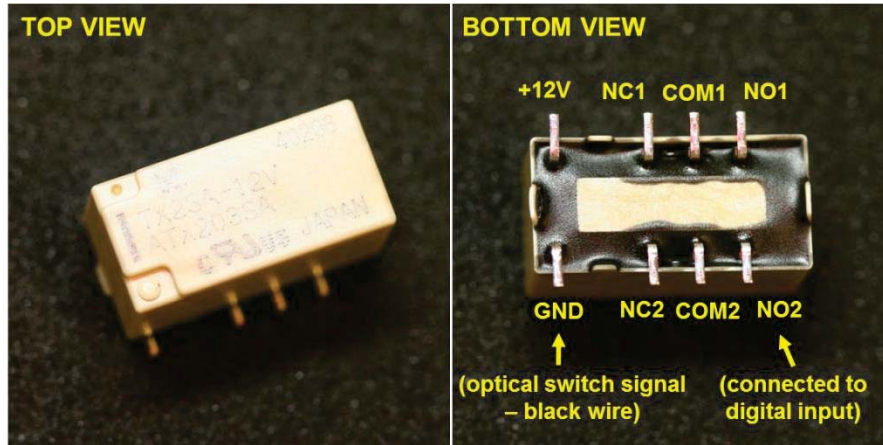


Figure 2-43. Panasonic TX2SA-12V relay

The first prototype used standard dial pressure gages to display the four regulated pressures: solvent bottle, buffer bottle, cavity air, and piston. To reduce the overall size of the device and to add the ability for the controller to monitor pressures, the gages were replaced with Honeywell pressure sensors for the second prototype design. The sensors are DIP (dual inline package) style for easy mounting to a breadboard as shown in Figure 2-44.

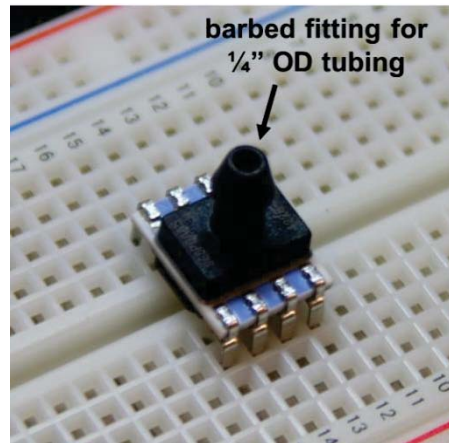


Figure 2-44. Honeywell pressure sensor

The sensors are analog output and are pre-calibrated. The pressure can be calculated from the output voltage of each sensor as shown in Equation (2.1).

$$P = P_{\min} + (V_{\text{out}} - 0.1 \times V_{\text{in}}) \left(\frac{P_{\max} - P_{\min}}{0.8 \times V_{\text{in}}} \right) \quad (2.1)$$

where P is the calculated pressure, P_{\min} (usually zero) is the minimum pressure rating of the sensor, V_{out} is the measured output voltage, V_{in} is the input voltage of the sensor, and P_{\max} is the maximum pressure rating of the cylinder. Three different sensors were selected for the device. The pressure range of each is 0-60 psi (SSCDANN060PGAA5) for the cavity air, 0-100 psi

(SSCDANN100PGAA5) for the piston, and 0-1 bar (0-14.5 psi, HSCDANN001BGAA3) for the solvent and buffer bottles. The calibration curves for each are given in Figure 2-45.

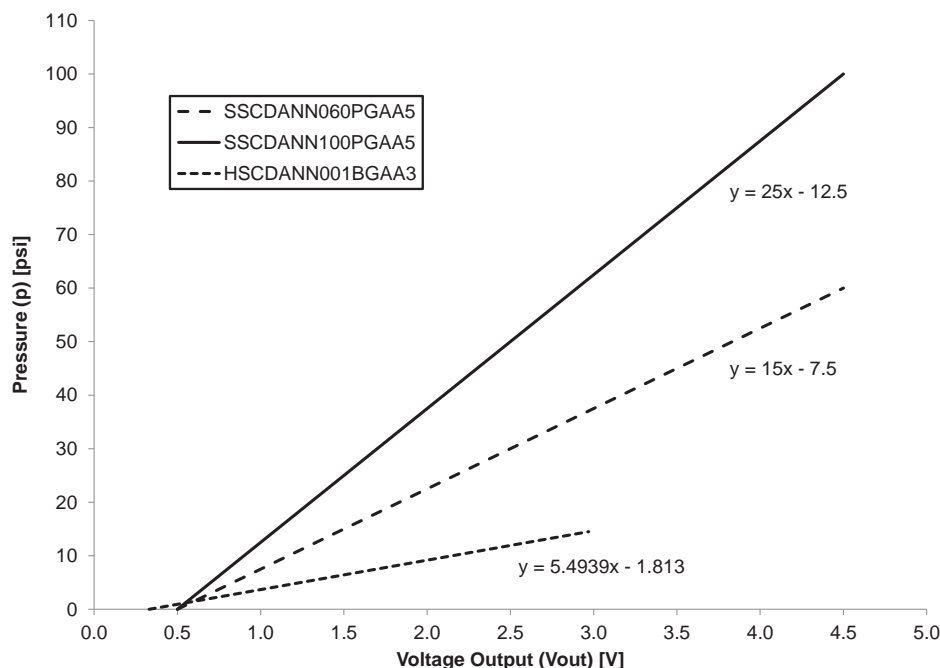


Figure 2-45. Calibration curves for Honeywell pressure sensors

The minimum voltage output for each is 10% of the input voltage. The maximum voltage output for each is 90% of the output voltage. The 0-60 psi and 0-100 psi sensors use a 5 VDC supply. The 0-1 bar sensors use a 3.3 VDC supply. Voltage was supplied to each using analog output pins on the Tern controller (see wiring diagram in Appendix J for details).

2.3.13 ENCLOSURE AND COOLING FAN

The goal of the enclosure design for the second prototype was to reduce the size of the system for efficient placement in a forensics lab and ease of use. The footprint of the system is reduced by 80% from the first footprint of the first prototype (288 in² → 60 in²). The height has also been reduced from 12" to 6.5". In addition, the components are protected by the case. The enclosure has internal dimensions of 6" x 10" x 6.5" (L x W x H). A model of the enclosure is shown in Figure 2-46.

A fan was selected to provide air flow for cooling of the power supplies, valves, and heater assembly components. A key function of the fan is to cool the heater assembly. This reduces the temperature of the microfluidic cavity for the buffer injection step and ensures the heater assembly components are cool for subsequent extractions. The assembly must be relatively close to room temperature for the calibrated timing to work properly. If the assembly is still hot, the heating system will raise the temperature of the cavity past the desired set point. Cooling of the system is covered in detail in Section 3.7.5.

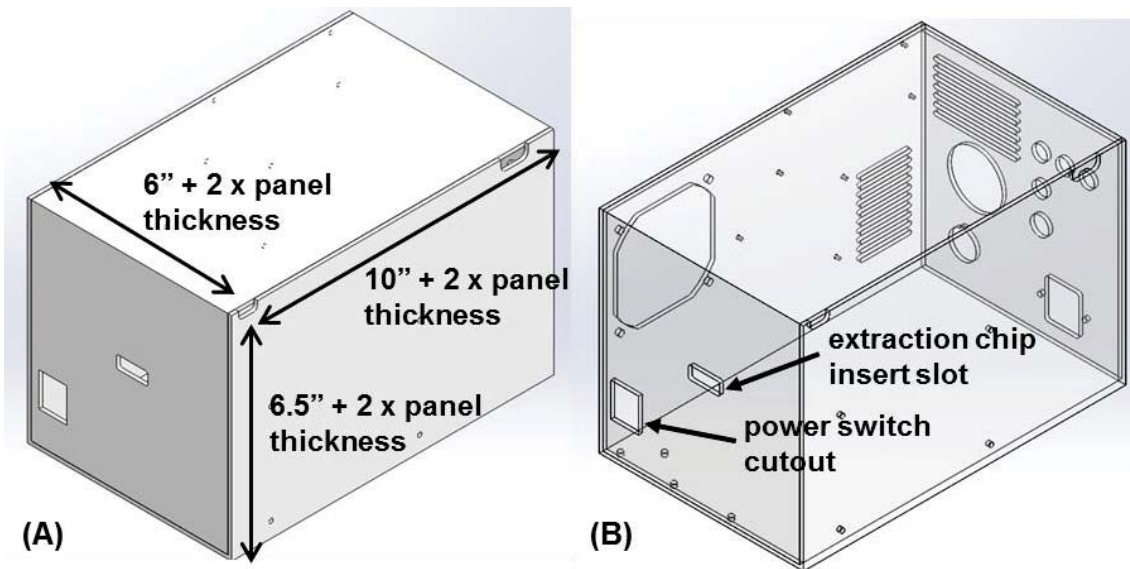


Figure 2-46. Prototype 2 enclosure design

A SUNON model number KD1208PTB1-6 fan was first used cool the device in open air (without an enclosure around it). The fan model is rated for 2.6 W and 42.5 cfm of air flow at zero static pressure. A Fluke 922 airflow meter was used to measure the airflow velocity near the heater assembly, which can be correlated to the cooling rate of the heated components. The velocity was measured to be approximately 1.5-2 m/s. The goal of selecting a fan for the enclosure was to produce at least the same amount of flow at the location of the extraction device within the enclosure. A box of approximately the same dimensions as the final enclosure design was modified to simulate air flow in the enclosure. A cutout was made for the placement of test fans and a side vent of 10 1/8" x 3.5" slits was placed in the rear of the enclosure (total area of ~4.4 in²). A flow meter was inserted into the box, and the inlet was positioned at the location of the extraction device. A diagram of the setup is shown in Figure 2-47.

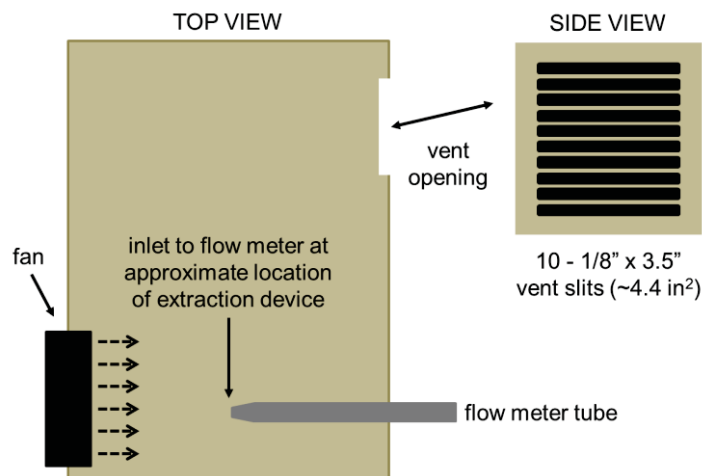


Figure 2-47. Enclosure fan flow mock setup

Using a Panaflo model FBH-08A12H fan, a flow velocity of approximately 2.3 m/s was measured with the flow meter at the indicated position. The fan is rated for 12 V, 0.34 A (4.08 W) and 40 cfm at zero static pressure. Static pressure within the box was measured at the corners where flow

was near zero and was found to be approximately 20 Pa (~.003 psi). Flow at the vents was also measured with the flow meter to be approximately 6 m/s giving a flow through the box of ~37 cfm. The test showed that the 4.4 in² vent produced minimal resistance for the fan and allowed sufficient flow. To further increase air flow a SanAce model 9GA0812P4J001 fan was selected for the second prototype design. The fan is rated for 12 V, 0.6 A (7.2 W) and 73 cfm. A flow simulation was performed with the enclosure design and an inlet flow rate of 70 cfm to ensure good flow over the electronic components within the enclosure as well. The total area of the vents in the enclosure is 4.3 in². Results from the simulation are shown in Figure 2-48.

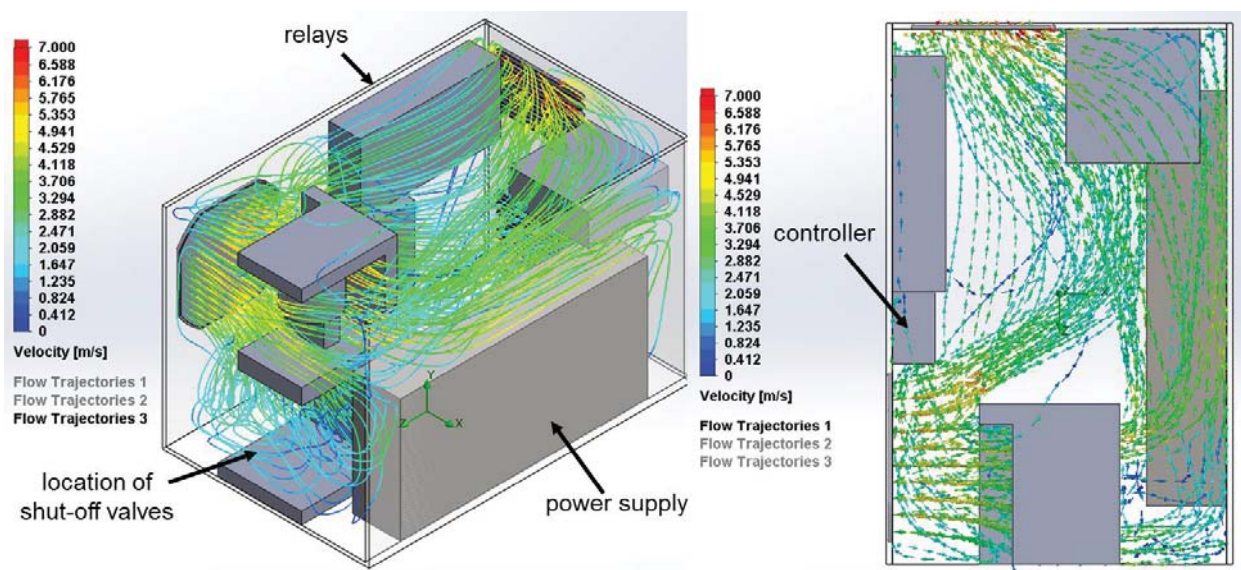


Figure 2-48. Enclosure air-flow simulation

The simulation shows good flow throughout the device. By placing the fan at the front of the enclosure in close proximity to the heater and extraction chip, high air flow velocities are achieved and the device can be cooled efficiently.

2.4 SYSTEM CONTROL

Automation of the microfluidic device requires a controller and user interface. The following sections provide a brief description of the selected controller and the user interface developed to operate the device. A detailed wiring diagram can be found in Appendix J.

2.4.1 CONTROLLER AND RELAY BANK

A Tern, Inc. 586-P Engine was selected as the controller for the microfluidic device. The controller has 4 16-bit analog inputs, 8 16-bit analog outputs, and 32 bits of configurable TTL digital I/O's. The board uses serial communication ports to communicate with the user's computer. The controller provides signal voltages at low current, so a Tern Relay7 board was obtained to operate the 12 and 24 V components of the system (the board provides 7 relays). Details on the power supplies used to power the devices within the system are provided in Appendix G. The controller and relay bank are shown in Figure 2-49.

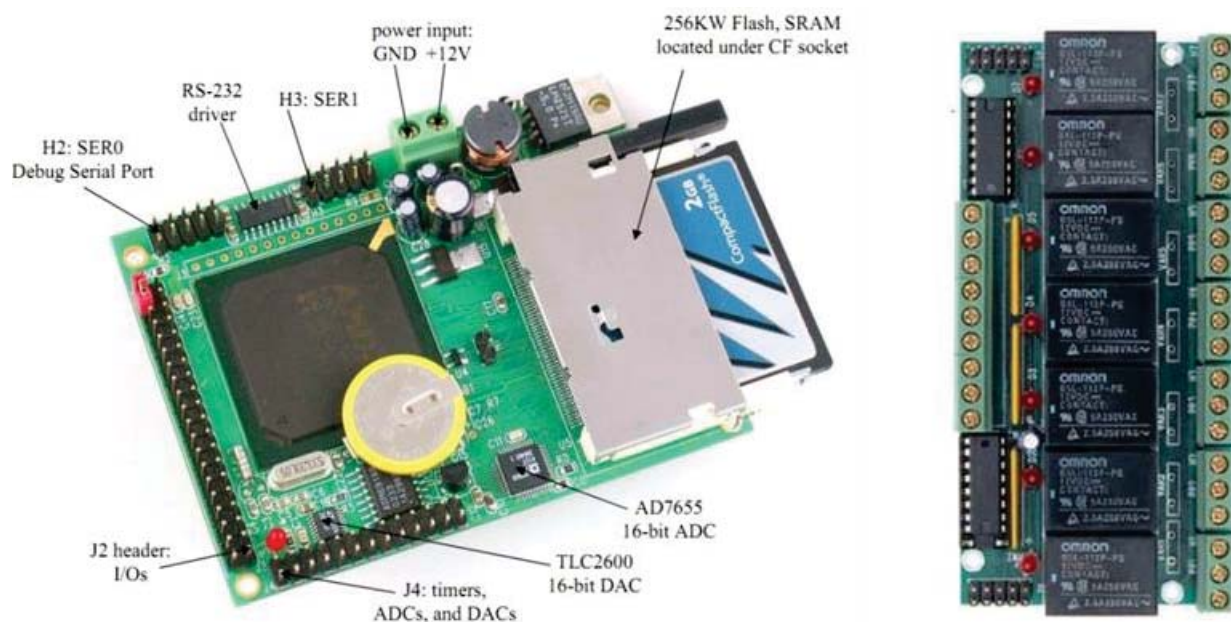


Figure 2-49. Tern 586-P controller (left) and Relay7 relay board (right) [28]

2.4.2 USER INTERFACE

The user interface for controlling the microfluidic device is shown in Figure 2-50. The user has the ability to define the dye extraction parameters (i.e. extraction time and temperature, evaporation time, cool temperature for the buffer steps, and the number of buffer fills and settle times for dye pickup). Air pressures can be read from the pressure transducers and used to manually set the pressures with the regulators. Limits can also be set for each pressure so that the extraction program will not run when a pressure is out of a specified range. Manual control of individual components is also available and is mainly used for troubleshooting with the system.

The user interface gives the user control over extraction conditions (these options are shown in the “Parameters” box). Due to the multitude of dye and fiber types, optimal extraction conditions may vary. By giving the user control over parameters such as temperature, extraction time, the number of buffer fills, and buffer settling times, optimization can be carried out with the device for each dye and fiber type. Parameter selection is shown in Figure 2-51.

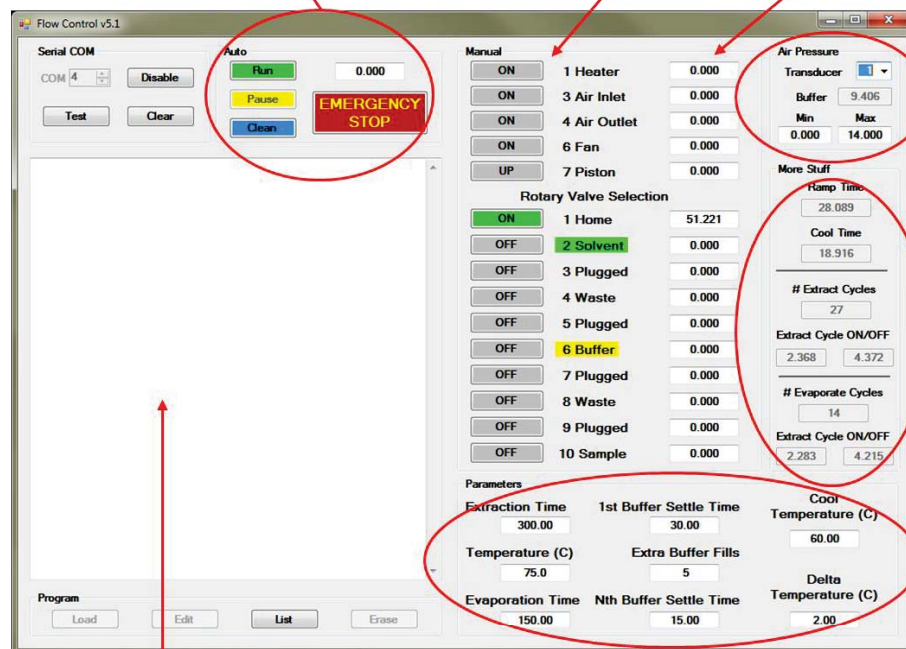
The automated programs are selected from the “Auto” box. The extraction sequence is initiated by clicking “Run”. A cleaning sequence is also available. The cleaning sequence is performed between extractions to cleanse the valves, tubing, and manifolds that come into contact with the extracted dye. The operation of valves and heaters for each sequence is described in detail in Sections 3.1.1 and 3.1.2.

automated process buttons:

- extraction program run
- system clean/flush program run
- emergency stop and pause for automated programs

manual device control buttons

manual device control clocks



read air pressures (psi):

- piston/system
- cavity air
- solvent bottle
- buffer bottle

program times and cycle #'s calculated from input parameters:

- heating ramp time
- cooling time (w/ fan)
- # heater cycles for extraction and evaporation
- cycle on and off times

extraction parameters:

- extraction temperature
- extraction time
- evaporation time
- cool temperature
- number of buffer fills and buffer settle times

control window

Figure 2-50. User interface

Parameters		
Extraction Time	1st Buffer Settle Time	Cool Temperature (C)
300.00	30.00	60.00
Temperature (C)	Extra Buffer Fills	
75.0	5	
Evaporation Time	Nth Buffer Settle Time	Delta Temperature (C)
150.00	15.00	2.00

Figure 2-51. Extraction parameter inputs

When the extraction and cleaning programs are run, the operation of components is listed with duration times (in seconds) in the control window as shown in Figure 2-52. The total duration of the process is also displayed in the “Auto” box.

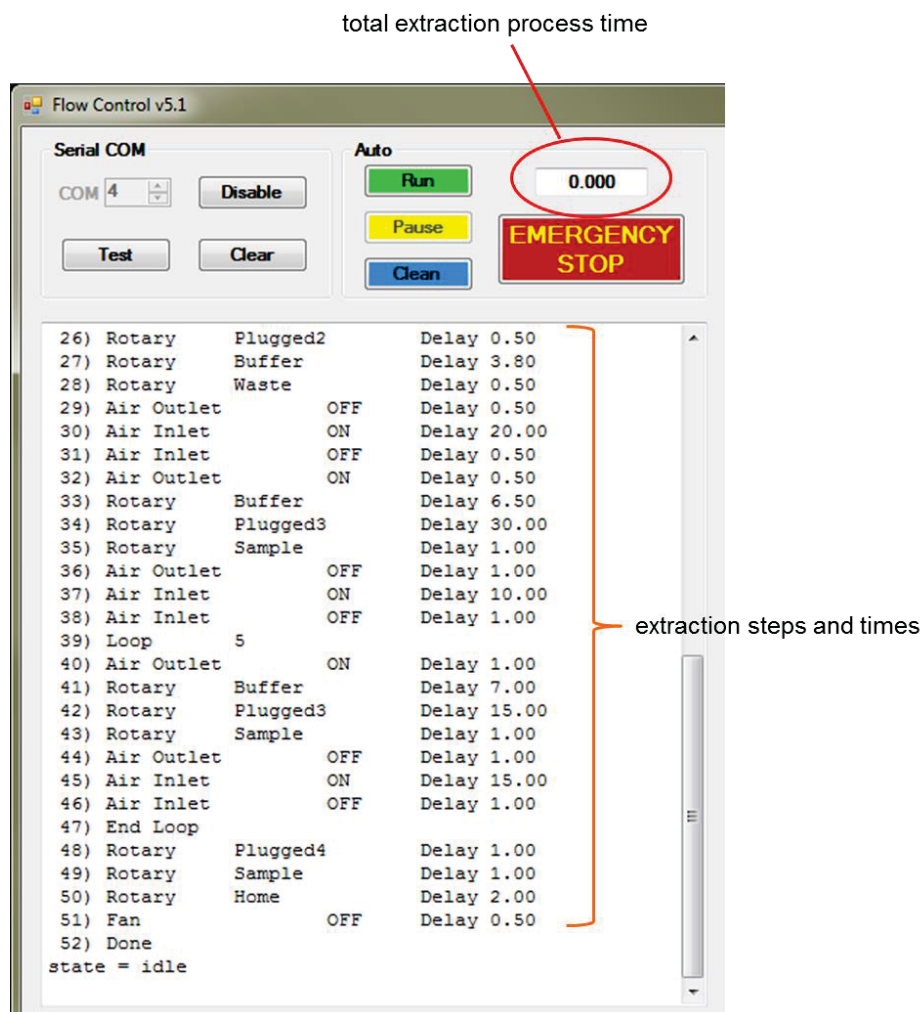


Figure 2-52. Control window displaying operation of components and times

3 DYE EXTRACTION

3.1 SYSTEM DIAGRAM AND SEQUENCES

The system diagram is provided again in Figure 3-1. The microfluidic device uses a sequence for the extraction of the dye and a sequence for flushing out the system between tests. This ensures that no residual dye or dye containing fluid remains in the system. The general sequence for the extraction process was given in Section 2.1. A detailed overview of the operation of valves and other components in each sequence is provided in this section.

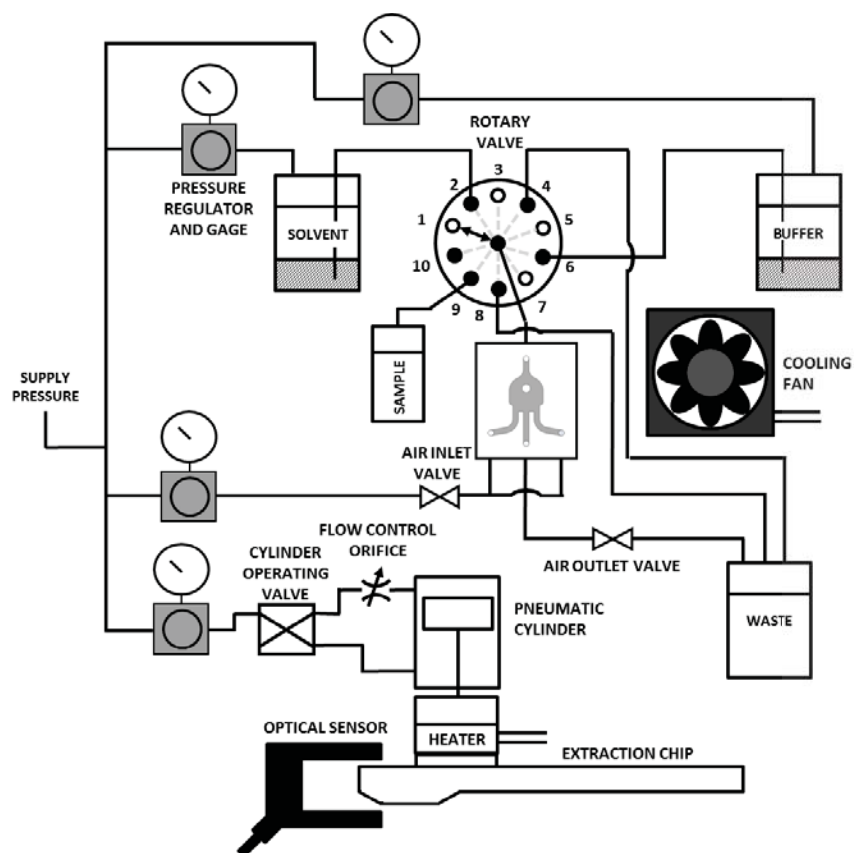


Figure 3-1. Microfluidic dye extraction system diagram

3.1.1 EXTRACTION SEQUENCE

After the extraction chip and fiber have been prepared and inserted into the system, the automated extraction sequence is initiated with the user interface. This section will refer to the system diagram shown in Figure 3-1 in describing the sequence of operations. The following is a list of operations:

- The chip breaks the beam of the optical sensor when it is inserted, triggering the cylinder operating valve to pressurize the extend port of the pneumatic cylinder. This presses the heater assembly onto the glass cover to seal the microfluidic cavity and to seal the extraction chip on the manifold o-rings below.
- When the extraction sequence is initiated, the air outlet valve (AOV) is opened.
- The rotary valve (RV) is set to port 1 by default. The RV actuates to port 2 after the AOV is opened. The pressurized solvent reservoir pushes solvent through the tubing and valve into the cavity.
- The solvent fill is timed, and after filling the cavity, the RV actuates to port 3.
- The heater is turned on for the ramp time (time to reach the set temperature).
- The heater is then cycled on and off to maintain the set temperature. Cycling is continued for the set extraction time.
- After cycling for the extraction time, the air inlet valve (AIV) is opened to allow pressurized air to flow through the cavity and into the air outlet. The heater continues to cycle for the evaporation time.

- After evaporation time ends, the heater is turned off. The cooling fan is then turned on to start cooling the heater assembly, glass cover, and microfluidic cavity.
- The AIV and AOV are closed and the RV actuated to port 4.
- The AIV is opened to push waste solvent in the extraction manifold, tubing, and rotary valve port into the waste container.
- After cooling, the AIV is closed and the RV actuated to port 5.
- Before performing the dye pick up step with the buffer, the RV, tubing, and extractor manifold are first flushed with buffer to remove residual solvent. The AOV is opened and the RV actuated to port 6. Buffer is pumped through the valve, tubing, and extractor manifold up to the cavity. Flow is stopped before the buffer enters the cavity (done by actuating the RV to port 7 after a set amount of time).
- The AOV is then closed and rotary valve actuated to port 8. The AIV is opened so that pressurized air pushes the buffer solution into the waste container.
- The AIV is then closed and the AOV opened.
- The RV is actuated to port 6 and buffer fills the cavity.
- After timed filling with the buffer, the RV is actuated to port 7. The system maintains this state for the buffer settle time set by the user.
- After the settle time the AOV is closed and the RV actuated to port 9 (sample ejection port).
- The AIV is opened so that the sample is then ejected through port 9 into a sample container or lab instrumentation (such as the mass spectrometer). The AIV is then closed.
- The total volume of the RV, tubing, manifold, and cavity is $\sim 20\ \mu\text{l}$. To increase the sample size and/or to pick up more dye, extra buffer fills are performed using the same sequence.
- After completion of the sample ejection, the RV is actuated to port 1 and all electronic components of the system are set to their default state. The extraction chip and sample can then be removed for storage and further analysis.

3.1.2 CLEANING SEQUENCE

The cleaning sequence is a key step because the system must be cleared of any residual solvent or dyes. This is done by performing a cleaning sequence between each test. A blank cavity and extraction chip are inserted into the device in the same manner as the extraction sequence. The operation is initiated by clicking “Clean” on the user interface. This initiates the following sequence of operations:

- The AOV opens and the RV is actuated to port 6. The program and RV controller do this by actuating in reverse so that the valve does not pass over the pressurized solvent port. Buffer fills the system and microfluidic cavity.
- The RV is then actuated to port 7 to stop flow.
- The AOV is closed and the RV actuated to port 8.
- The AIV is opened and the buffer is pushed to the waste container.
- The AIV is then turned off and RV returned to port 1.
- All components are returned to their default states.

3.2 MIXTURE PROPERTIES OF PYRIDINE AND WATER

Fluid properties are readily available for water and pyridine individually, however the mixture (4:3, pyridine to water by weight) used for extraction has unique properties dependent on the quantity of each component. Through literature review, various experimental properties were identified for use in flow and evaporation models. Useful charts and equations were produced for estimating properties under operating conditions.

Fluid viscosity plays an important role in flow rates in the system. The dynamic viscosity of pure water (9.61×10^{-4} Pa-s at 22°C) is close to that of pure pyridine (9.37×10^{-4} Pa-s at 22°C). As a mixture, however, the viscosity increases. The mixture viscosity as a function of the weight percentage of pyridine at 0°C and 25°C is shown in Figure 3-2. The target weight percentage is 56.7% and is shown on the plot as well. The solvent reservoir has been measured to be at 23°C , so the 25°C value at 56.7% is a good approximation of the viscosity of solvent flowing through the system.

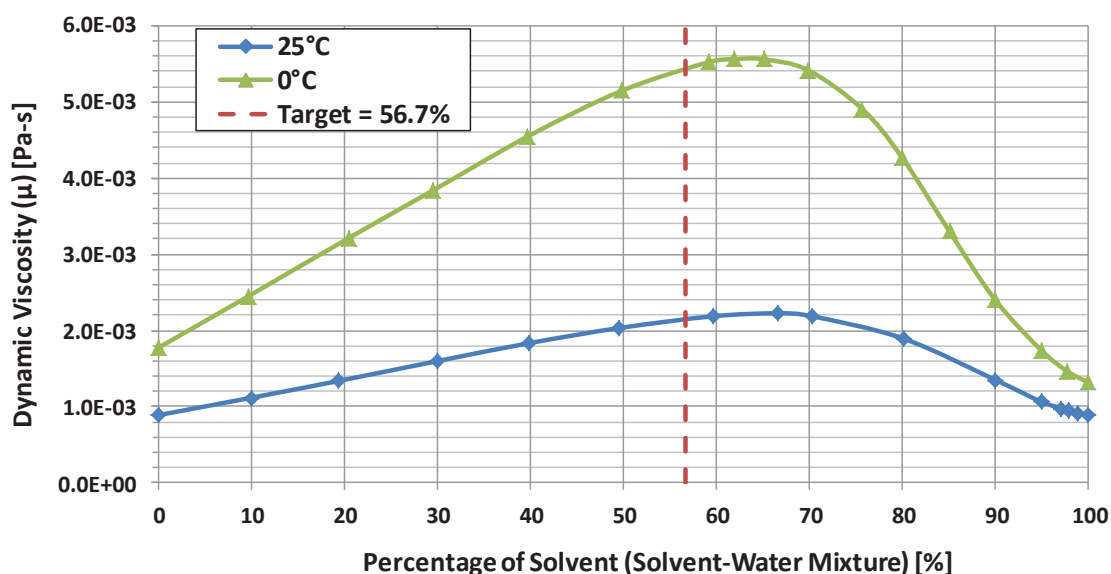


Figure 3-2. Dynamic viscosity of pyridine:water mixtures of varying weight percentage [29]

If it is desirable to estimate the viscosity values at other temperatures, the equation for the data fit in Figure 3-3 can be used. At 25°C the viscosity is 2.14×10^{-3} Pa-s. Interpolating and evaluating at 23°C the viscosity is approximately 2.33×10^{-3} Pa-s [29].

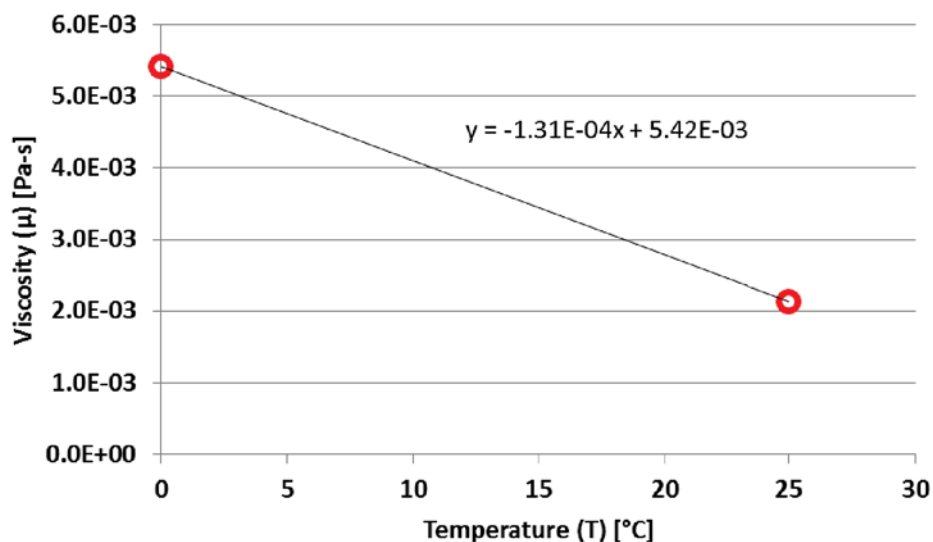


Figure 3-3. Viscosity values at 0 and 25°C. Because most of the experiments were done near room temperature of 20°C, a viscosity of 2.0E-3 was the starting point for the flow calibration described in the next section.

The density is also a value of interest in calculating the evaporation rate of the solvent. Values are plotted from literature for 0°C and 25°C in Figure 3-4, as well as several higher temperatures [29,30].

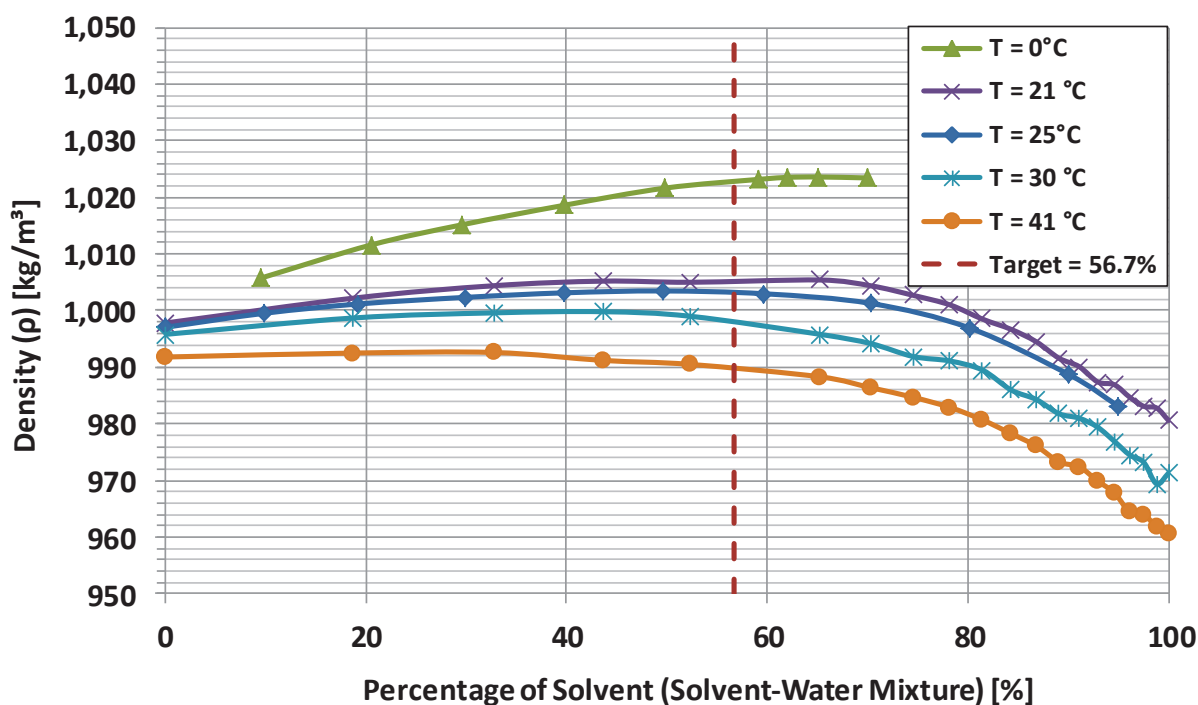


Figure 3-4. Density of pyridine:water mixtures at various temperatures and weight percentages [29,30]

The temperature dependence of the density of a fluid is given by Equation (3.1) [31].

$$\rho_1 = \frac{\rho_0}{1 + \beta(T_1 - T_0)} \quad (3.1)$$

where ρ_1 is the density of interest, β is the thermal expansion coefficient, T_1 is the temperature of interest, and T_0 and ρ_0 are a reference temperature and density. Using data [29,30,32] for the density of the pyridine:water mixture of interest at various temperatures, the thermal expansion coefficient was estimated as $\beta = 1.03 \times 10^{-3} \text{ m}^3/(\text{m}^3 \text{ } ^\circ\text{C})$.

Another variable of interest is the vapor pressure of the solvent-water mixture. The vapor pressure at the fluid temperature and the ambient temperature are needed to estimate the evaporation time (discussed in further detail in Section 3.6). Values obtained from literature review are shown in Figure 3-5 [33,34].

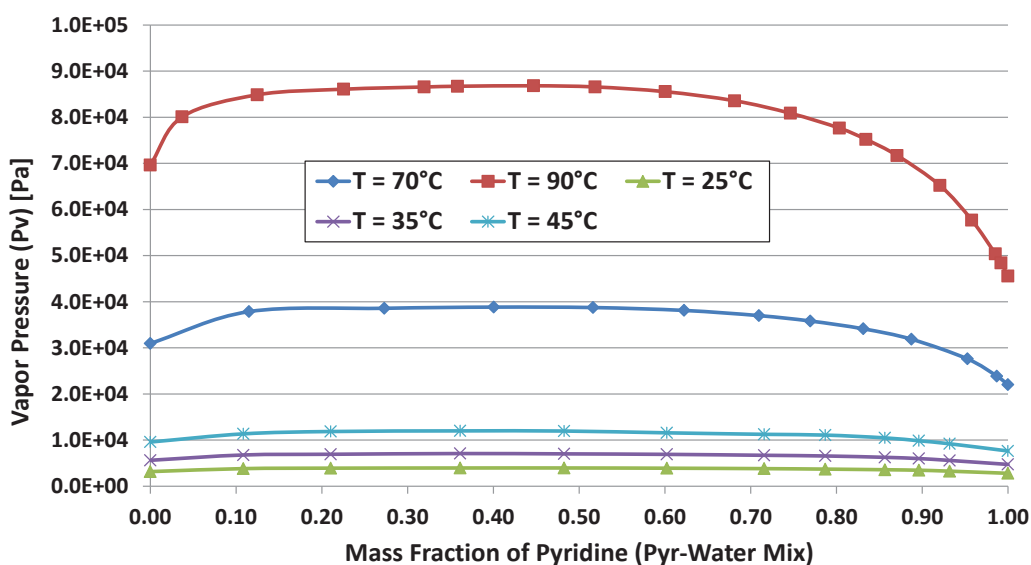


Figure 3-5. Vapor pressure of pyridine:water mixtures at various temperatures and mass fractions [33,34]

Interpolating each curve to find values for a target mass fraction of 0.567 (56.7%), the data was plotted and fit with an exponential curve as shown in Figure 3-6. Evaluating the curve at the ambient air temperature (assuming 25°C) and 75°C, P_v values of 4,256 Pa and 45,533 Pa were found, respectively.

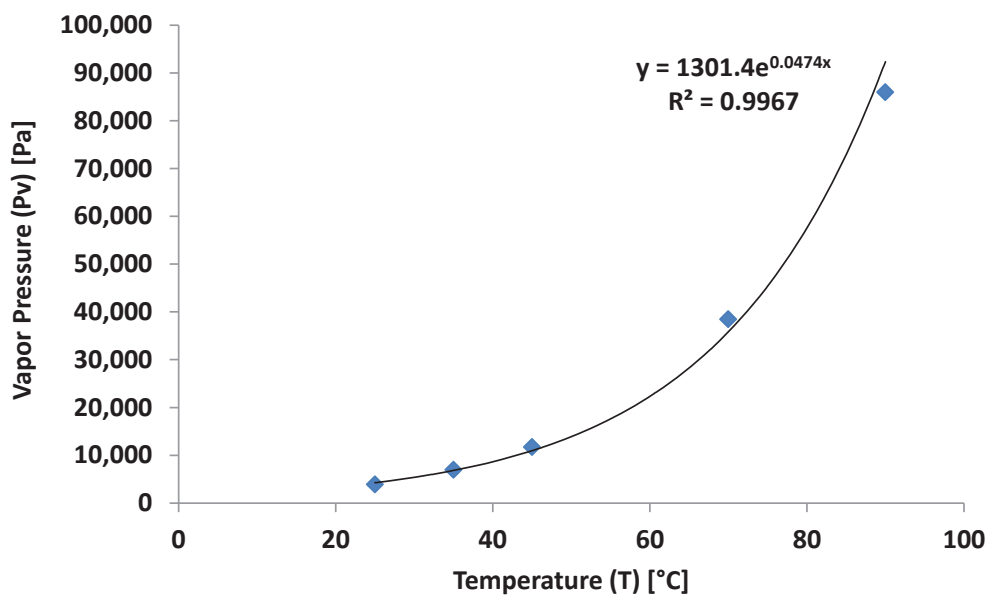


Figure 3-6. Vapor pressure of solvent mixture as a function of temperature

Another property of interest is the mass diffusivity of the pyridine-water vapor in air. No published data on the mass diffusivity of a pyridine water mixture for these conditions could be found. As an estimation, the diffusivity of the components was averaged based on their mass ratios. The diffusivity of pyridine in air at 25°C is $9.10 \times 10^{-6} \text{ m}^2/\text{s}$ [35]. For water in air at the same temperature the diffusivity is $2.60 \times 10^{-5} \text{ m}^2/\text{s}$. Averaging the two based on their mass ratio, the diffusivity of the mixture is estimated to be $D_{AB} \approx 1.64 \times 10^{-5} \text{ m}^2/\text{s}$. This value was used for evaporation estimations (see Section 3.6). Values for the parameters of interest under operating conditions are shown in Table 3-1.

Table 3-1. Pyridine:water mixture values and equations

<u>Variable</u>	<u>Value</u>	<u>Units</u>
Viscosity (μ) @ 23 °C:	2.33×10^{-3}	Pa-s
Viscosity (μ) @ 25 °C:	2.14×10^{-3}	Pa-s
Viscosity (μ) @ 75 °C:	3.37×10^{-4}	Pa-s
Density (ρ) @ 25 °C:	1,003	kg/m ³
Density (ρ) @ 75 °C:	954	kg/m ³
Vapor Pressure (P_v) @ 25 °C:	4,256	Pa
Vapor Pressure (P_v) @ 75 °C:	45,533	Pa
Mass Diffusivity (D_{AB}) @ 25 °C:	1.640×10^{-5}	m ² /s
<u>Variable</u>	<u>Equation</u>	
ρ	$\frac{1003.118}{1 + (1.0309 \times 10^{-3})(T_1 - 25)}$	
μ	$0.0054e^{-0.037T}$	
P_v	$1301.4e^{0.0474T}$	

3.3 FLUID FLOW

3.3.1 FLOW MODELLING

One of the goals of the device is to accomplish repeatable filling of the microfluidic cavity with timed operation of the fluid valve. Length scales in the cavity and tubing become important when determining the flow modelling approach. Macro-scale flow theory can be used for fluids in channels with a hydraulic diameter, $D_h \geq 10 \mu\text{m}$. The same flow theory can be applied to gas flows with $D_h \geq 100 \mu\text{m}$. The hydraulic diameter (D_h) for a rectangular channel can be calculated from the height (H) and width (W) as shown in Equation (3.2) [36].

$$D_h = \frac{2HW}{H + W} \quad (3.2)$$

The dimensions of the smallest channel in the cavity are shown in Figure 3-7.

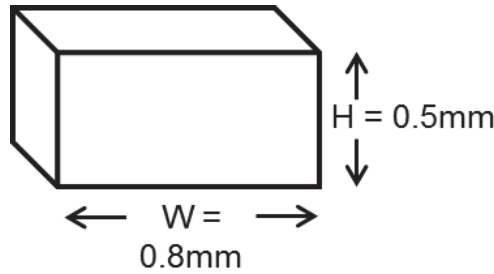


Figure 3-7. Minimum channel dimensions in microfluidic cavity

This gives a hydraulic diameter of $615 \mu\text{m}$. Similarly, the smallest tube diameter considered for the fluid system was $0.006'' = 152 \mu\text{m}$, so a standard approach can be utilized.

Fluid flow in a tube (Poiseuille flow) can be predicted with the Hagen-Poiseuille Equation [37]. The flow rate is given in Equation (3.3).

$$Q = \frac{\pi \Delta p D^4}{128 \mu L} \quad (3.3)$$

where,

Δp = pressure drop over the length of the tube

D = tube diameter

L = tube length

μ = fluid viscosity

In the case of a significant restriction to flow, the time to fill the tube must be taken into account as well. Flow rate in the tube is also represented as shown in Equation (3.4).

$$\begin{aligned} Q &= UA \\ &= \frac{dL}{dt} \frac{\pi}{4} D^4 \end{aligned} \quad (3.4)$$

In Equation (3.4), $U = dL/dt$ is the average fluid velocity in the tube and $A = \pi D^2/4$ is the cross-sectional area. Combining Equations (3.3) and (3.4) and solving for time, the fill time can be evaluated as shown in Equation (3.5).

$$\frac{\pi D^4 \Delta p}{128 \mu L} = \frac{\pi D^2}{4} \frac{dL}{dt}$$

$$\int_0^{t_{fill}} dt = \frac{32 \mu}{D^2 \Delta p} \int_0^L L dL$$

$$t_{fill} = \frac{16 \mu L^2}{D^2 \Delta p} \quad (3.5)$$

Using water as a test fluid ($\mu = 1 \text{ Pa}\cdot\text{s}$ @ 20°C), the equations are evaluated for various tube diameters at a characteristic system pressure of 10 psi. Expected flow rates are shown in Figure 3-8 (refer to Appendix C.1 for MATLAB code).

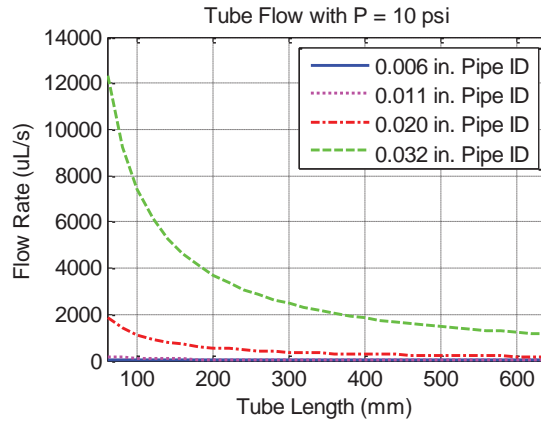


Figure 3-8. Flow rate for water in tubing of different diameters

The values cover a typical range of available tube sizes for the application. The total fill time for the tube and a 10 μL volume are shown in Figure 3-9.

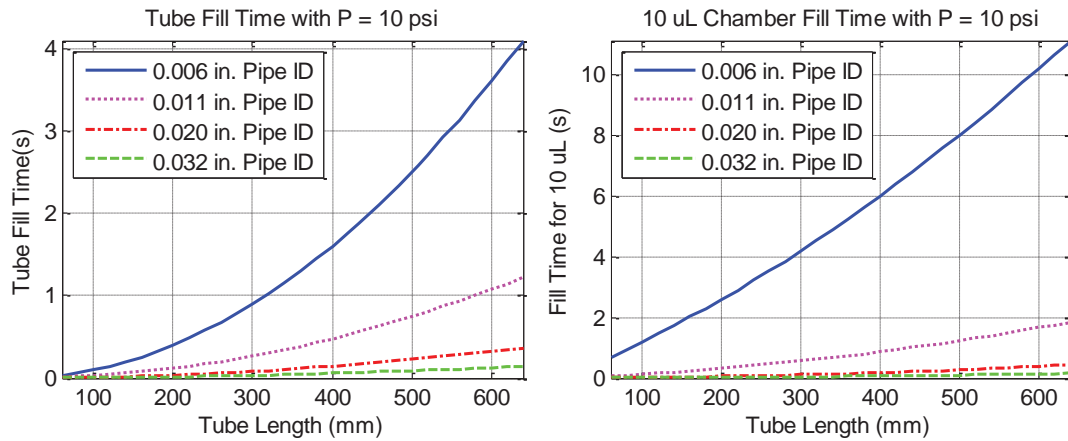


Figure 3-9. Tube fill time (left) and fill time for 10 μL volume + tube (right)

For the low volume of the fluid cavity and manifolds between the cavity and tubing (total volume $< 100 \mu\text{L}$), the larger tubing diameters do not provide adequate flow control. The smaller tube diameter of 0.006" was selected for the main inlet tube of the device for this reason.

The small diameter tubing selected is made from Teflon (PTFE). Because PTFE is a hydrophobic material, an adjustment to the flow calculation must be made. Poiseuille flow is derived with the assumption of a no-slip boundary condition (i.e. fluid velocity is zero at the tube's inner surface). For a hydrophobic surface, this assumption may not be valid. Slip flow can occur where the fluid velocity over the wall is non-zero [36,38]. One model that captures this effect was first suggested by Navier. Navier proposed that the velocity of a fluid at a solid surface is proportional to the shear rate at that surface [39]. A qualitative comparison of Poiseuille and slip flows is shown in Figure 3-10.

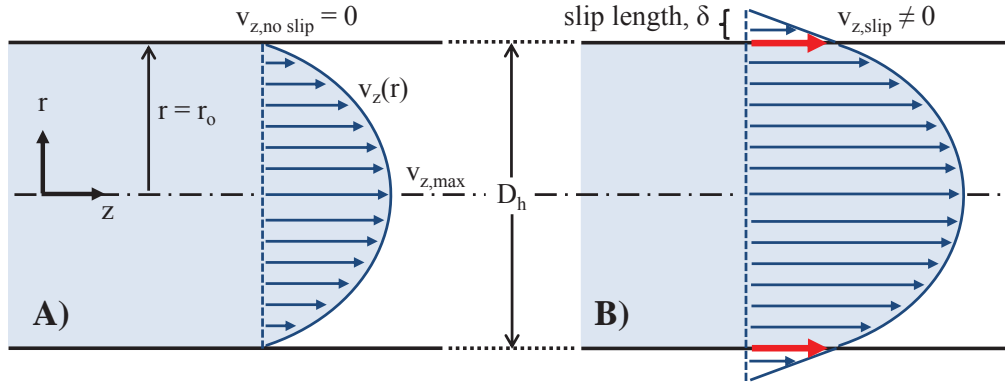


Figure 3-10. (A) Poiseuille-flow and (B) slip-flow profiles

The velocity boundary condition for slip-flow at the wall is given in Equation (3.6) [36].

$$v_{z, slip} = \delta \left. \frac{\partial v_z}{\partial r} \right|_{r=r_o} \quad (3.6)$$

Using the boundary condition, the velocity profile and flow rate can be determined as a function of the slip length, δ (see Appendix E for derivation). The flow rate for the slip condition is given in Equation (3.7).

$$Q = \frac{\pi \Delta p D_h^4}{128 \mu L} \left(1 + \frac{4\delta}{r_o} \right) = Q_{Poiseuille} + Q_{slip} \quad (3.7)$$

The total flow for Navier's model is the sum of Poiseuille flow and the flow given by the slip velocity. An example slip profile is shown in comparison to the equivalent Poiseuille profile in Figure 3-11. The profiles are given for water in a 200 mm long tube with a diameter of 0.006" and a pressure drop across the length of 4 psi. A slip length of 5.2 μm was used to compute the results. See Appendix C.2 for MATLAB code to calculate profiles and flow rates.

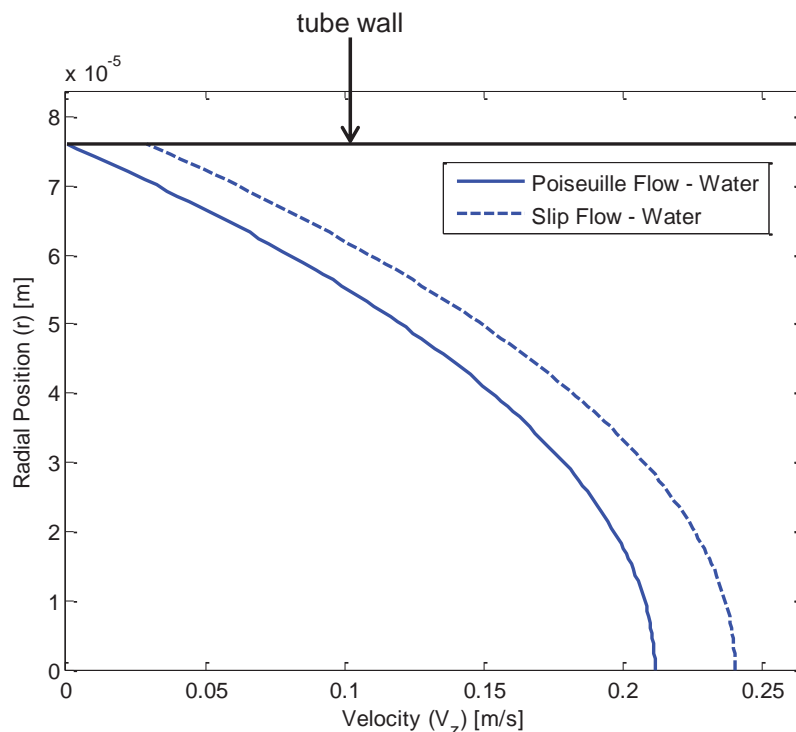


Figure 3-11. Comparison of axisymmetric Poiseuille and slip flow profiles

3.3.2 FLOW MODEL VALIDATION TESTING

Flow tests were performed to compare measured flow to predictions and to show that a consistent flow can be achieved. The first flow tests were performed with the setup shown in Figure 3-12. The test setup consisted of a pressure source and regulator, sealed fluid reservoir, shut-off valve, microbalance, and a container to receive the ejected fluid. The CAHN TA-4100 microbalance has a sensitivity of 0.1 mg (for water, this converts to approximately 0.1 μ l of volume at room temperature). Air currents in the fume hood caused the scale to float over a range of approximately 5 mg. To gather more accurate measurements, a cover was placed over the scale. This allowed for readings of 0.1 mg \pm 0.2 mg approximately. This resolution is sufficient to measure the fluid mass for desired flow rates and times. Flow tests were performed with the 0.006" inner diameter tubing. The tube going from the fluid reservoir to the shut-off valve was 390 mm long with an inner diameter of 0.032". The pressure drop from the larger tube is negligible in comparison to the 0.006" ID test tube. It was therefore assumed that the pressure drop across the small diameter tube was equal to the gage pressure of the bottle.

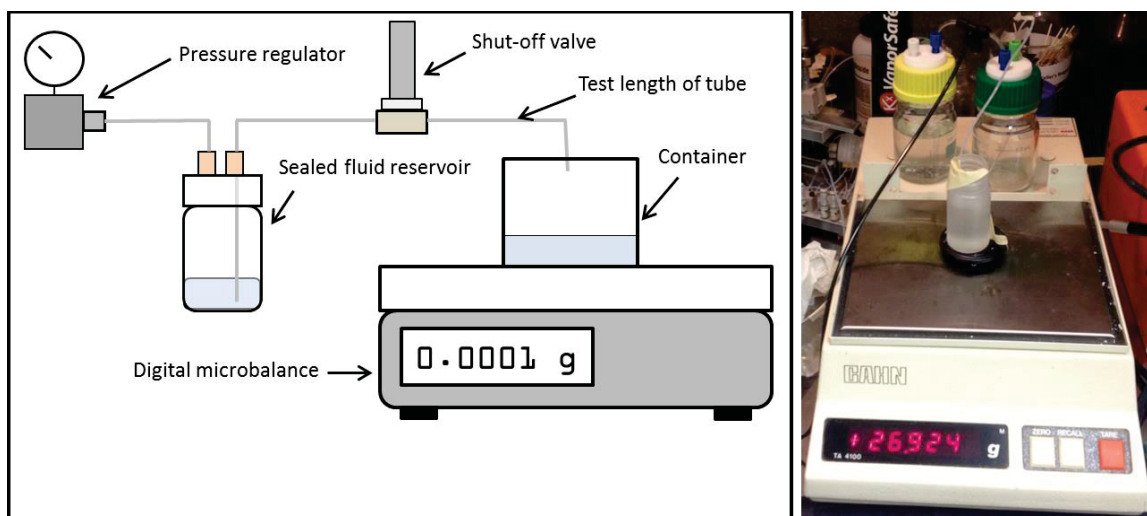


Figure 3-12. Flow test setup

The first set of flow tests were performed with water and the (4:3) pyridine:water mixture. The tests were performed by opening the shut-off valve for a set amount of time (valve times of 30s and 45s were set by the controller) and observing the mass added to the container on the microbalance. Given the density of the fluid (at room temperature, $\sim 23^\circ\text{C}$), the volume of fluid was calculated ($\rho = m/V$) and divided by the valve timing to obtain the flow rate. The parameters for the initial tests are shown in Table 3-2.

Table 3-2. Initial flow test parameters

Test Fluid	Tube Length (mm)	Tube ID (in)	Gage Pressure (psi)	# of Tests at 30s	# of Tests at 45s
Water	98	0.006	8.2	10	10
Pyridine:Water	98	0.006	8.4	10	10

The results of the tests with water showed an average flow rate of $10.2\ \mu\text{L/s}$ for the 30 s and 45 s valve timings (refer to Appendix D for flow test data tables). The Poiseuille solution predicts a flow rate of $8.0\ \mu\text{L/s}$ for the given conditions. By varying δ in the slip flow equation, an appropriate slip length could be determined for the measured flow rate. Using the results from the water tests, a slip length of $5.2\ \mu\text{m}$ gives a predicted flow of $10.2\ \mu\text{L/s}$. Using the same slip length for the pyridine:water mixture, a predicted flow rate of $4.6\ \mu\text{L/s}$ was obtained. This compares well to the measured average flow rates of $4.5\ \mu\text{L/s}$ (30 s valve timing) and $4.6\ \mu\text{L/s}$ (45 s valve timing).

A second set of flow tests were performed to validate the results and slip length used for different conditions. The parameters of the second set of flow tests are shown in Table 3-3.

Table 3-3. Second flow test parameters

Test Fluid	Tube Length (mm)	Tube ID (in)	Gage Pressure (psi)	# of Tests at 30s	# of Tests at 8s
Water	200	0.006	4.0	20	20
Pyridine:Water	200	0.006	4.4	10	10

The results of the flow tests are provided in Table 3-4. The results show good correlation to the slip model with the empirical slip length ($\delta = 5.2 \mu\text{m}$). The predicted flows for the Poiseuille equation are shown for comparison.

Table 3-4. Flow test results and comparison to models

Test Fluid	Tube Length (mm)	Tube ID (in)	Gage Pressure (psi)	Poiseuille Prediction ($\mu\text{l/s}$)	Slip Prediction ($\mu\text{l/s}$)	Avg. Measured Flow ($\mu\text{l/s}$)
Water	98	0.006	8.2	8.0	10.2	10.3
Water	200	0.006	4.0	1.9	2.5	2.5
Pyridine:Water	98	0.006	8.4	3.6	4.6	4.5
Pyridine:Water	200	0.006	4.4	0.9	1.2	1.0

Similar results can also be obtained using the Poiseuille equation and assuming a larger diameter. Adding 2δ to the diameter of the tube (7% increase), the Poiseuille equation predicts flows of 10.5, 2.5, 4.8, and 1.2 $\mu\text{l/s}$. These values are close to the total flow calculated with the slip flow model.

3.3.3 ROTARY VALVE FLOW TESTING

Flow tests were performed with the rotary valve to ensure that timed operation of the valve would provide consistent results. A test length of 200 mm of 0.006" tube was used for the test. The rotary valve flow test setup is shown in Figure 3-13.

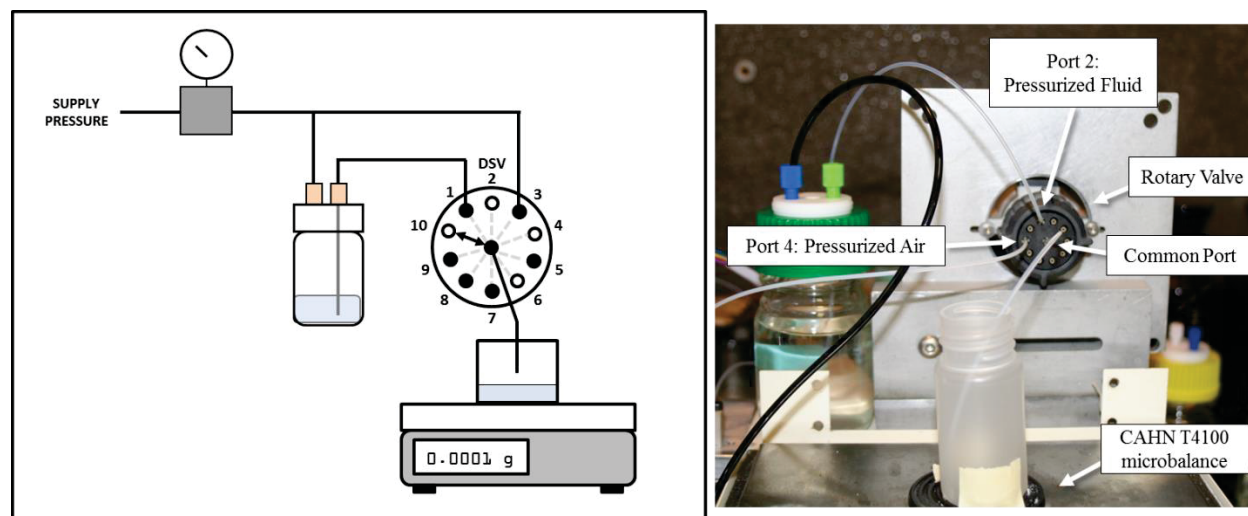


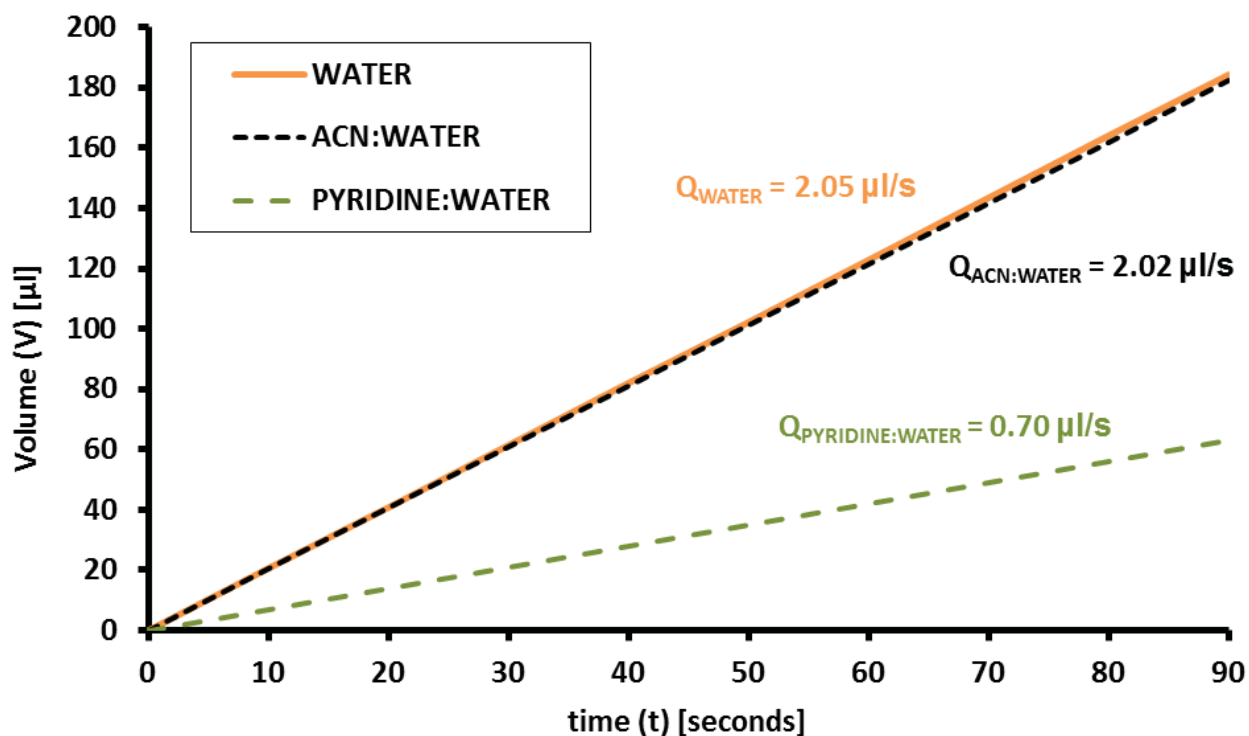
Figure 3-13. Rotary valve flow test setup

In Figure 3-13, the ten connecting ports of the rotary valve are shown on the outer perimeter of the valve. The common port is shown at the center with the test tube extending to the fluid container on the microbalance. The common port is shown, connected to port 10, for the start of each test. The valve was actuated to port 1 to start fluid flow. The valve was then actuated to port 2 to stop flow. The mass of fluid ejected from the tube was then recorded. The fluid remaining in the valve and test length of tube was then ejected by actuating the valve to port 3, which was connected to pressurized air. This was done for each test so that the fill step would include the internal volume of the system, simulating operation of the device. Tests were performed initially with water, followed by the buffer solution (97% water) and pyridine:water mixture. The rotary valve flow test parameters are given in Table 3-5.

Table 3-5. Rotary valve flow test parameters

Test Fluid	Tube Length (mm)	Tube ID (in)	Gage Pressure (psi)	Flow Timing (sec)	# of Tests
Water	200	0.006	3.9	10	10
ACN:Water	200	0.006	3.9	10	10
Pyridine:Water	200	0.006	3.9	15	10
Pyridine:Water	200	0.006	9.2	10	10

A pressure of 3.9 psi was used for each fluid initially. The results of the tests at constant pressure showed a much lower flow rate of the pyridine:water mixture due to the higher viscosity. The buffer solution and water had almost identical flow rates. The flow rates are shown in Figure 3-14.

**Figure 3-14.** Fluid flow rates from rotary valve and tube at 3.9 psi

Because of the higher viscosity of the pyridine:water mixture, the pressure was increased to 9.2 psi to achieve the same total mass for the 10 second flow time. The results of the rotary valve flow tests, shown in Figure 3-15, indicated that consistent flow can be achieved with timed valve operation.

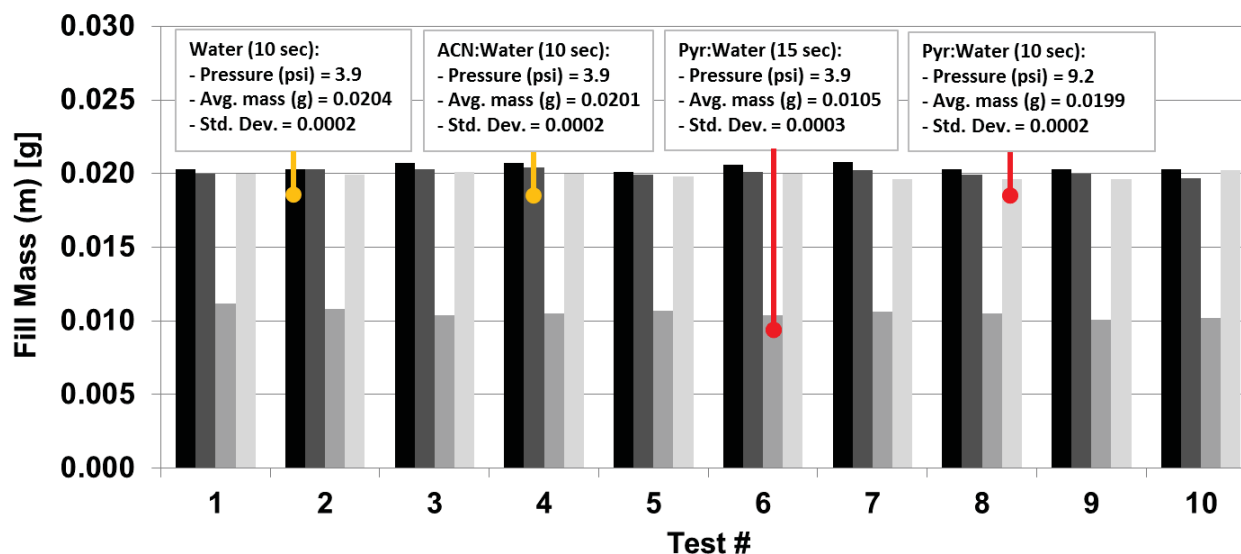


Figure 3-15. Rotary valve flow test results

3.3.4 ROTARY VALVE AUTOMATED TEST

Flow testing showed that consistent volumetric flow rates could be achieved under set conditions using the rotary valve. Full automation of the process was then performed to validate operation of the system without a fiber. The operating conditions used for testing with (4:3) pyridine:water solution and ACN:water buffer solution are shown in Table 3-6.

Table 3-6. Automation testing conditions with rotary valve

Solvent bottle pressure:	~9	psi
Buffer bottle pressure:	~4	psi
Air pressure:	~20	psi
Solvent fill time:	9.0	seconds
Buffer fill time:	9.0	seconds
Heating time:	300	seconds
Heating temperature:	~75	°C
Evaporation time (air-flow):	180	seconds

The pressure regulators for the fluid bottles were set to the pressures listed in Table 3-6. Solvent flow was then initiated by actuating the rotary valve. The solvent (pyridine:water) fill step is shown in Figure 3-16.

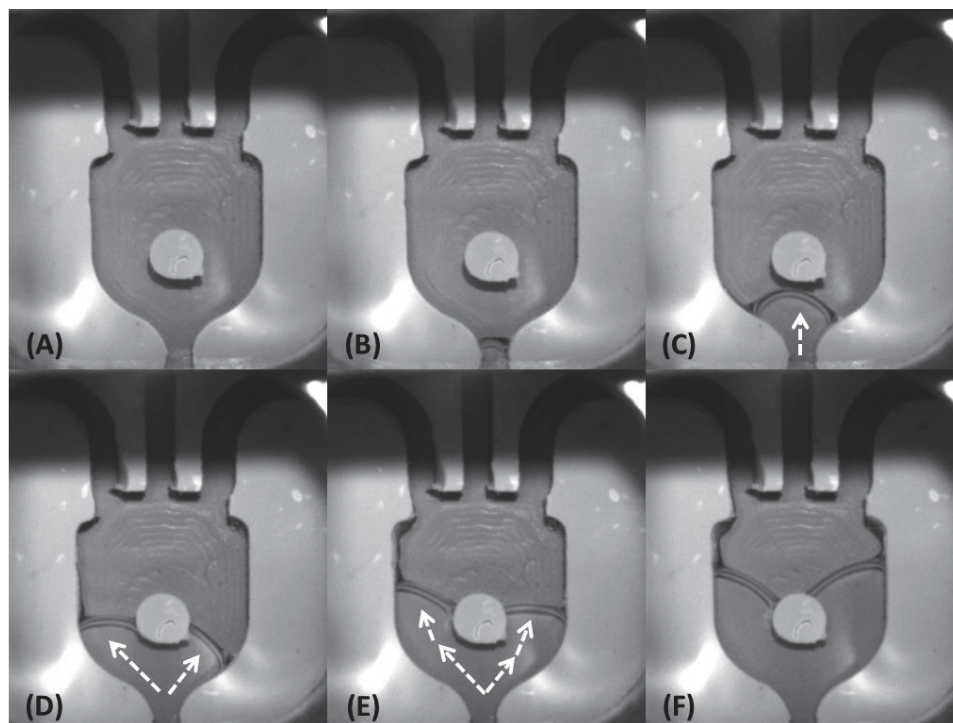


Figure 3-16. Automated test – solvent fill

In Figure 3-16(A)-(E), the solvent is flowing into the cavity and around the fiber holding post. The solvent fill stopped near the midpoint of the cavity as shown in Figure 3-16(F). The fiber holding post in the center splits flow. By symmetry of the design, flow on either side of the post should be symmetric. Surface defects from machining, small particles, or substances on the surface can create flow resistance that causes the fluid to flow around the post in an uneven manner. This was observed in multiple automated runs. This problem was addressed further with the design of the cavity as discussed in Section 3.4.

Following the solvent fill step, the solvent was heated for 300 seconds (5 min) with the PTC (positive temperature coefficient) heater to simulate the dye extraction step. During heating, condensation of fluid can be observed on the FFKM surface. Because the cavity is heated from above, the surface of the FFKM is cooler, accounting for the appearance of droplets on its surface as shown in Figure 3-17. Additionally, very small pockets of air trapped in the corners of the cavity by the solvent expand as they heat, forming small bubbles as seen in Figure 3-17(C). This phenomenon is commonly observed in microfluidic devices that use fluid heating processes (see ref. [40]). The observation of these phenomena is interesting; however, the small air bubbles should not have a negative impact on the extraction process.

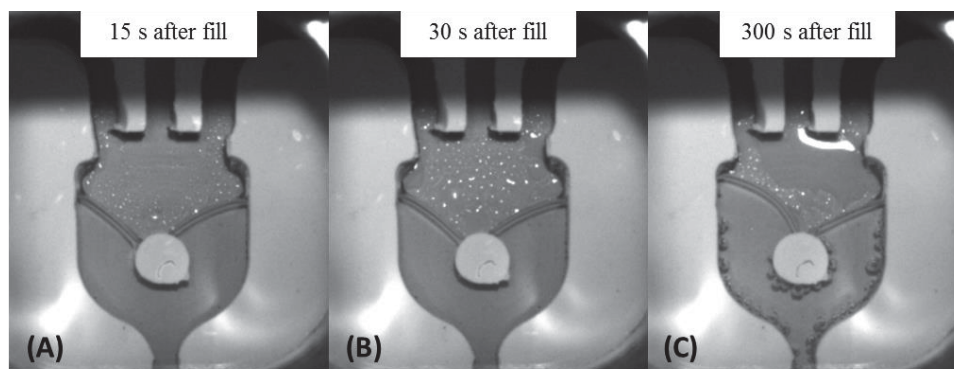


Figure 3-17. Automated test – solvent heating

After heating of the fluid, air flow through the cavity was initiated to facilitate evaporation of the solvent. The majority of fluid in the cavity was evaporated after 180 seconds (3 min) as shown in Figure 3-18.

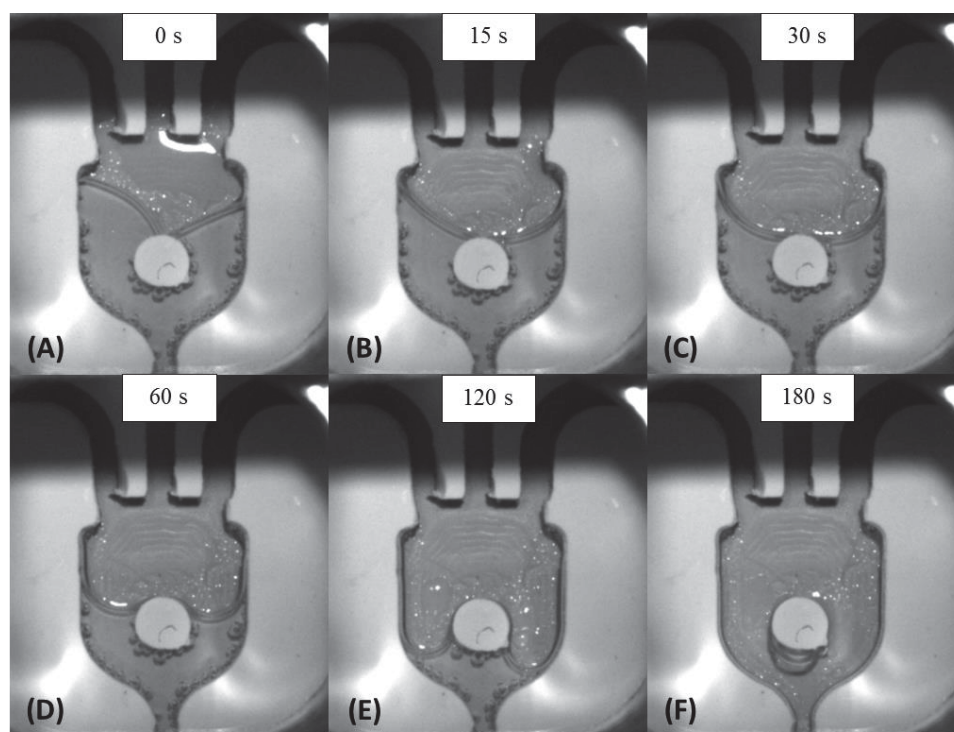


Figure 3-18. Automation test – solvent evaporation

The next step of the automation process was to push any excess solvent in the tube or valve to the waste bottle. Following waste ejection, the buffer was introduced to the cavity. The fill profile for the buffer is shown in Figure 3-19(A)-(E), with the final buffer fill shown in Figure 3-19(F). The automated timing produced the desired volumetric fill; however, the fill profile was uneven as shown in Figure 3-19(E)-(F). This would be a problem in an extraction procedure as dye deposited on the cavity surfaces to the right side of the post would not be reconstituted into the sample as desired. Losing dye in this manner reduces the probability of being able to successfully identify the dye in the mass spectrometer.

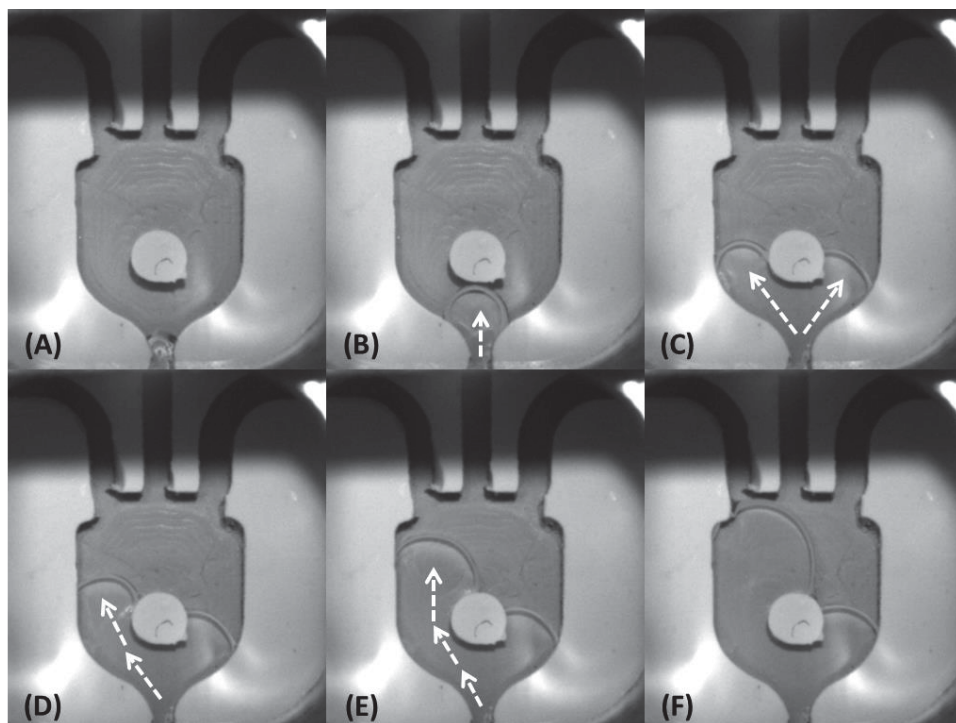


Figure 3-19. Automated test – buffer fill

In the final step, the buffer was ejected through the central fluid inlet leg to a sample container. The buffer volume in the cavity is shown in Figure 3-20(A). In Figure 3-20(B)-(E), pressurized air from the two air inlet legs pushes the fluid out of the cavity. The buffer sample is successfully pushed out of the cavity as seen in Figure 3-20(F). This step can be repeated several times to improve dye pick-up and/or increase sample size (a larger sample volume can be beneficial for filtering where fluid may be retained by the filter element). If the majority of dye is dissolved in the first buffer fill, the repetition of the buffer fill step should be minimized to prevent over-diluting the sample.

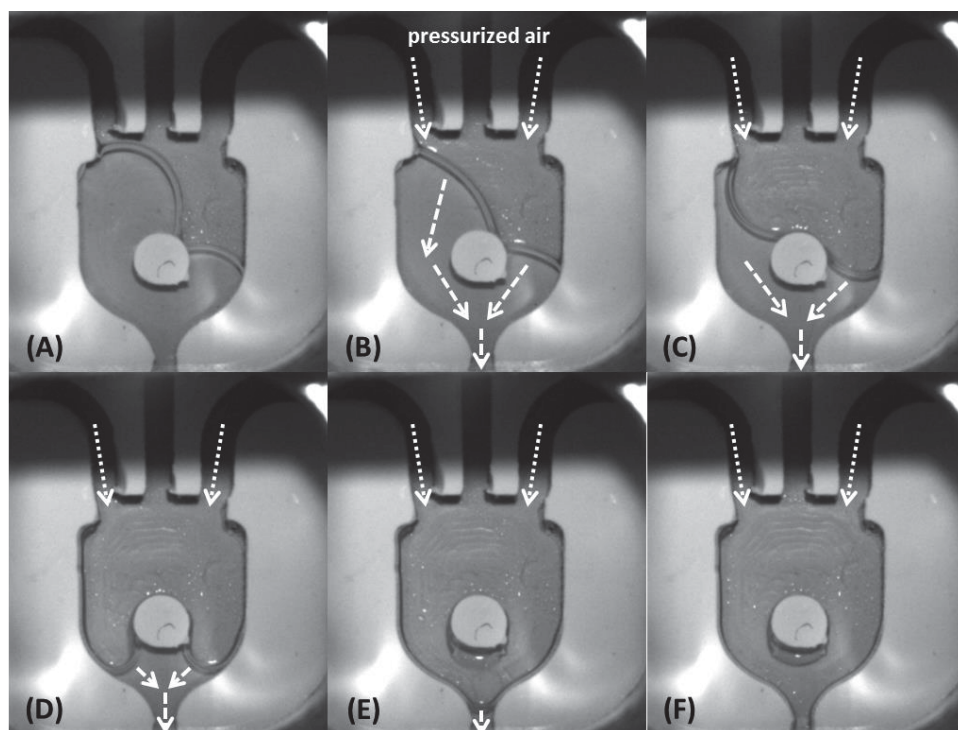


Figure 3-20. Automated test – buffer ejection

3.4 CAVITY DESIGN ITERATIONS AND FILL TESTS

The design of the microfluidic cavity was critical to controlling the extraction processes. For example, the evaporation process is partially dependent on the interface area between the compressed air flowing through the cavity and the heated fluid body shown in Figure 3-21. This dependence will be discussed in Section 3.6.2. Therefore it was desirable to design a cavity which maximized this area to reduce the time needed for evaporation.

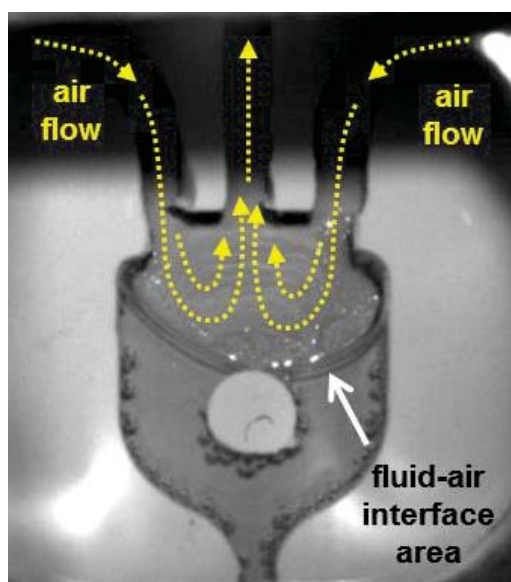


Figure 3-21. Fluid-air interface in microfluidic cavity

The process of approaching a final cavity design was an iterative one. The following factors were key considerations during the process:

- The number of inlet/outlet legs: At minimum, the cavity design requires an air inlet, air outlet, and fluid inlet leg (3 legs in total). The system valve and manifold configuration is dependent on the number of legs and use of each.
- Fluid flow within the cavity: The main cavity has a relatively large width in comparison to inlet and outlet legs (4-5 mm in comparison to 0.8mm as shown for the cavity design in Figure 3-22). It is therefore difficult to control the direction of fluid flow within the cavity. The goal is to completely immerse the fiber (location shown in Figure 3-22) in fluid and to prevent fluid from flowing into the other legs of the cavity. Without proper control of the flow, extraction solvent can enter the air inlet and/or exhaust leg(s). When air-flow is initiated during evaporation, this fluid is forced into the waste container along with any dye molecules in the lost volume.

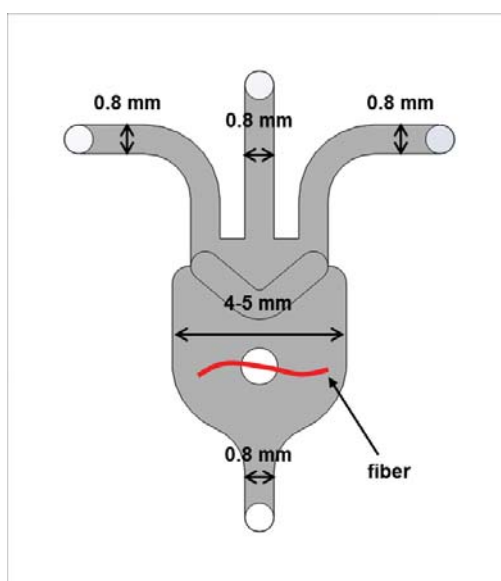


Figure 3-22. General dimensions of cavity body and inlet/outlet channels

- Machinability: Due to the unique requirements of the design material (i.e. sealing and solvent compatibility) a soft polymer material was required (FFKM). A micro-milling process provided the best method for rapid fabrication of cavity prototypes. The material and process limit the minimum width or diameter of machined features. The deflection of the material during machining increases as the characteristic feature size decreases. Burr formation at machined edges and surfaces was also an issue.
- Cavity volume: The extraction process developed by the Textile Chemistry department requires approximately 7-10 μl of solvent for extractions. This volume of fluid also ensures proper immersion of all fiber and yarn sizes that would be used for extraction.
- Fiber retention method: Placement of a fiber in the cavity is important in ensuring its complete coverage by the solvent and effective extraction of the dye. Depending on its size (3 mm long threads were used for test extractions), the fiber can also have an impact on the movement of fluid within the cavity. It is important then to be able to place the fiber in a central location and to prevent it from moving about the cavity during the extraction process.

- Evaporation of fluid: The design of the cavity should maximize the interfacial area between the fluid and flowing air during the evaporation process. The iteration of cavity designs was done with the original PTC heater setup (where $T_{\text{cavity}} \approx 75^{\circ}\text{C}$).

Using this key set of factors, several cavity versions were developed, fabricated, and tested. Cavity V1 is shown in Figure 3-23. The cavity contains a solvent inlet, buffer solution inlet, an air inlet and an air exhaust leg.

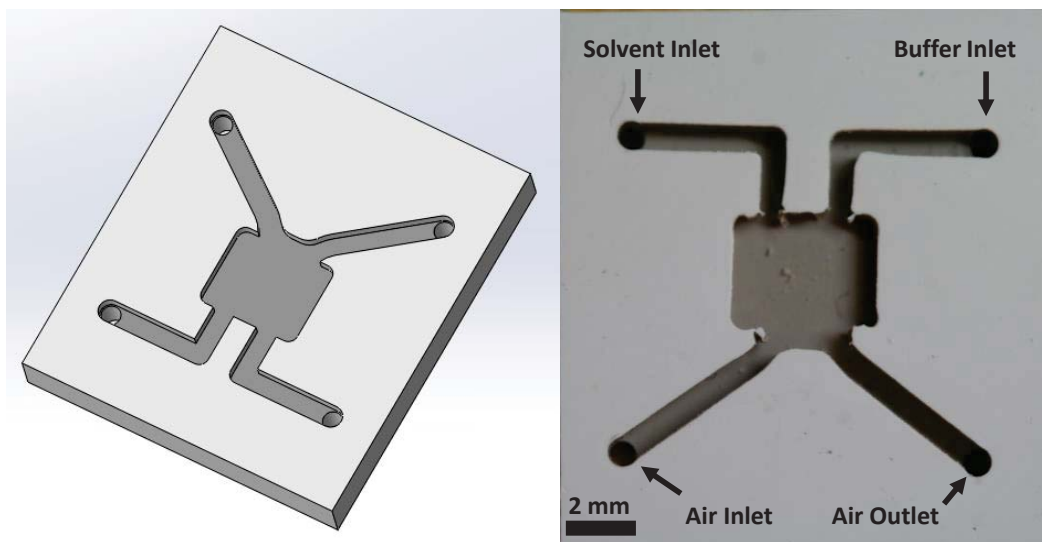


Figure 3-23. Cavity V1

Initial tests with water showed that the cavity fill was asymmetric and allowed fluid to flow into the air legs before completely filling the cavity. The fill sequence is shown in Figure 3-24.

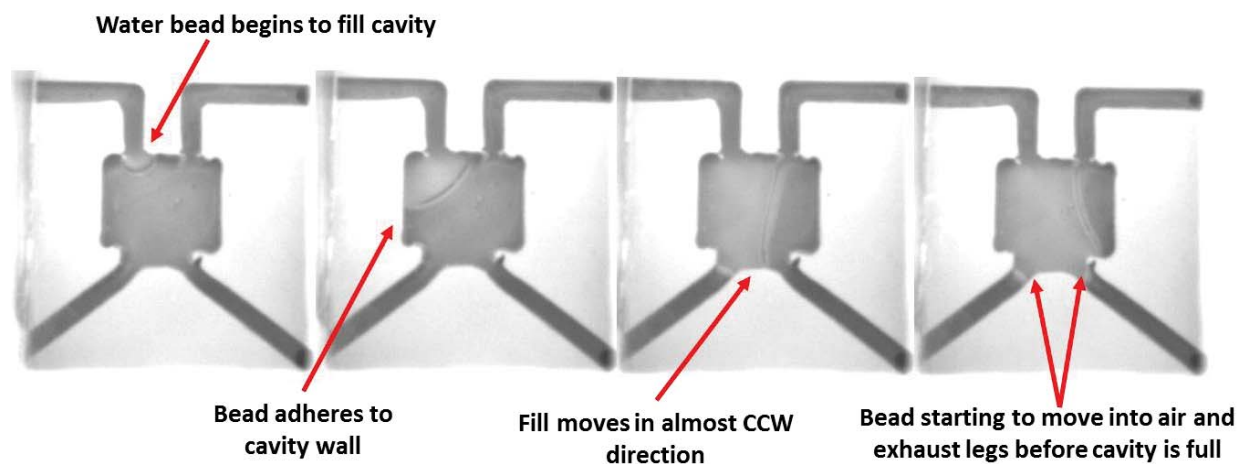


Figure 3-24. Cavity V1 fill sequence

For Cavity V2, a single inlet was machined for the solvent and buffer with the goal of a more symmetric fill profile. Cavity version 2 is shown in Figure 3-25.

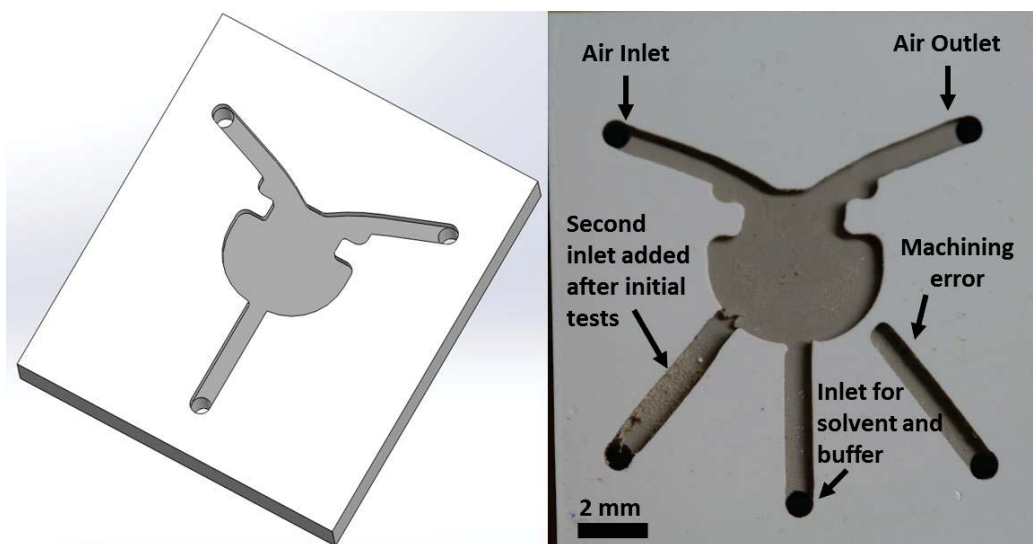


Figure 3-25. Cavity V2

The fill profile for the second cavity design is shown in Figure 3-26. The water fills in a symmetric manner, preventing it from prematurely entering the air inlet and exhaust legs.

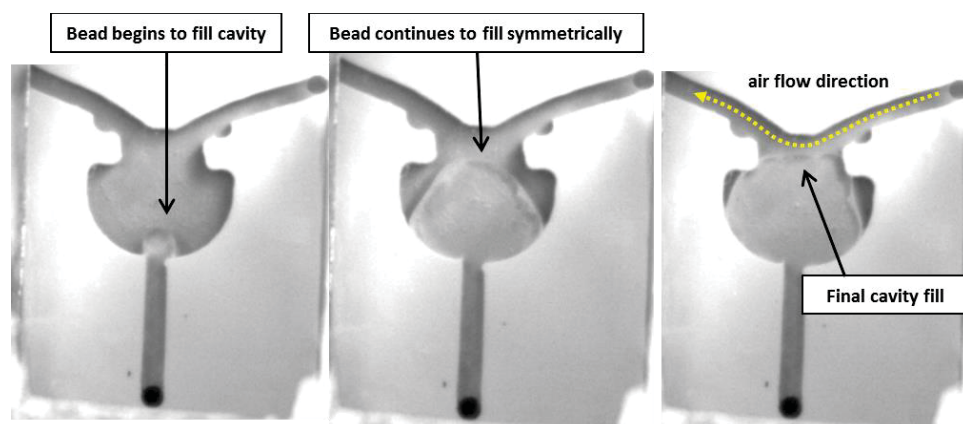


Figure 3-26. Cavity V2 fill sequence

The second cavity design promoted a better fill profile where the fluid stayed within the cavity instead of moving into the air legs. During the evaporation process, air flows through the air inlet across the fluid surface and into the air outlet. As a result of air flow, fluid was forced along the cavity walls and surfaces through pressure and capillary action taking the fluid into the air outlet. This gave the appearance of rapid evaporation (~30 seconds), even in circumstances where no heat was applied.

A third cavity design was developed with features added to help confine the fluid to the main cavity area and prevent the observed phenomenon. Cavity V3 is shown in Figure 3-27. In this design, notches and steps were added to the air inlet and outlet legs to act as a barrier to the fluid during the cavity fill and air flow steps. The solvent fills from the central fluid inlet. The buffer fills from the fluid inlet extending from the side of the cavity. The sample would then be ejected through the same inlet. A step was machined at the central inlet in addition to the air legs to prevent any of the sample fluid from becoming trapped in this leg during buffer ejection.

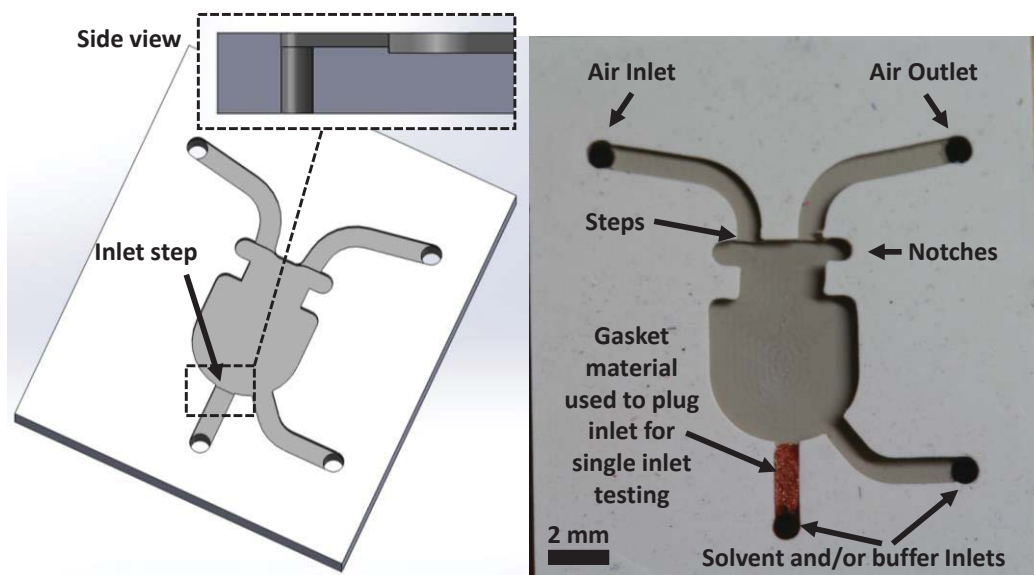


Figure 3-27. Cavity V3

The configuration of the air legs was developed with the aid of the Flow Simulation software in SolidWorks as will be discussed in Section 3.5.2. Although the addition of notch features reduced the effects of fluid loss through non-evaporative means, they did not prevent fluid from flowing into the air legs. Nor did the steps machined at the air legs and central fluid inlet leg create a noticeable barrier to flow.

The first three cavities provided useful insight into the movement of fluid within the cavity and potential issues with controlling that movement. The subsequent cavity designs also incorporated a feature to hold the fiber. A central fiber holder was determined as the best method for retaining fibers. Cavity V4, shown in Figure 3-28, incorporates a central feature that holds the fiber by squeezing it between the cavity and the glass cover. The fiber holder is approximately 1.3 mm wide.

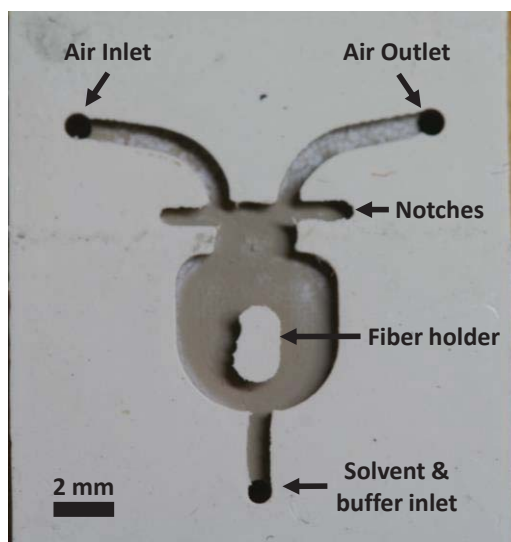


Figure 3-28. Cavity V4

The non-evaporative fluid loss phenomenon was still observed in Cavity V4. A second air inlet leg was added to the design, and the air outlet leg was moved to the center. The goal was to provide a barrier of flowing air to prevent fluid from entering the air legs. Cavity V5 and V6 are shown in Figure 3-29. These cavities employed the same air outlet configuration and fiber holding shape.

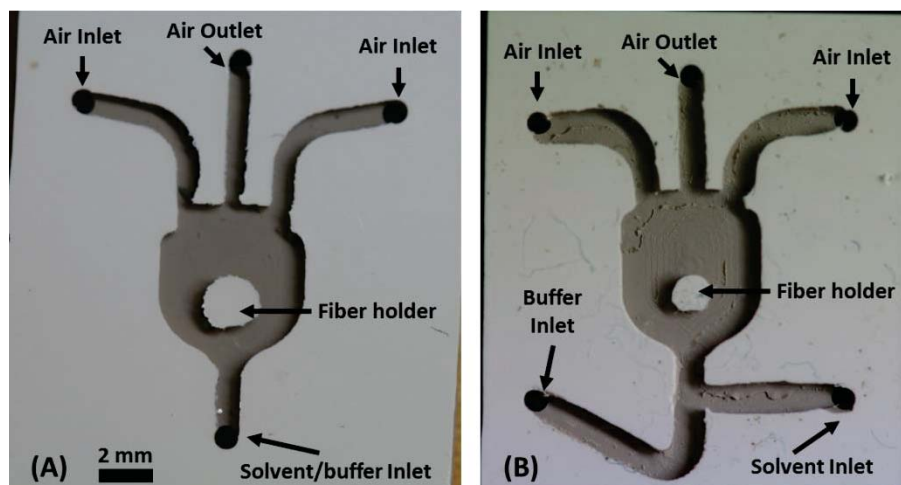


Figure 3-29. (A) Cavity V5 and (B) Cavity V6

Cavity V5 used a single inlet for the buffer and solvent. This required an array of four directional-control valves and one shut-off valve. By using two fluid inlets, Cavity V6 reduced the inlet valve array to two directional-control valves and one shut-off valve. The main advantage of the simplified valve system with Cavity V6 was that it reduced the dead volume of the valves from 313 μL to 176 μL (75 μL for each directional-control and 13 μL for each shut-off).

In addition to reducing the complexity of the valve array, Cavity V6 allowed both solvent and buffer to fill the cavity from a central point. As observed in Cavity V2, the cavity fill profile is better when filled from a central inlet. The added leg created problems during the extraction step of the process, however. During the heating of the cavity, air in the buffer leg began to expand. The expanding air forced the extraction solvent into the air legs as illustrated in Figure 3-30.

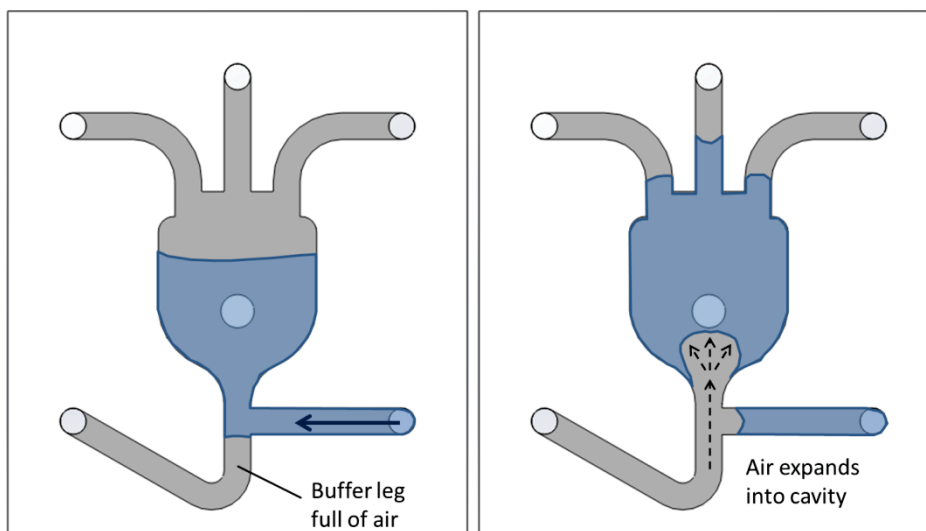


Figure 3-30. Air expansion in Cavity V6 during heating for extraction

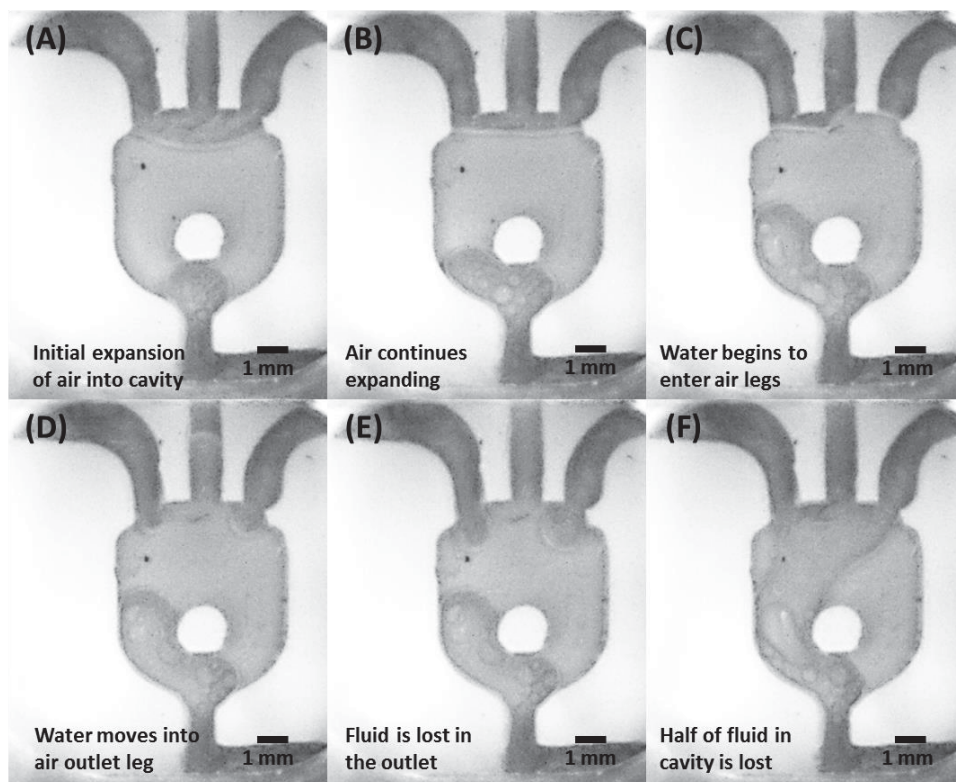


Figure 3-31. Air bubble expansion into cavity during heating

Water was pumped into the cavity and heated ($\sim 75^{\circ}\text{C}$) to demonstrate the expansion of an air bubble from the buffer inlet. The expansion of the air bubble is shown in Figure 3-31. The bubble expanded, forcing fluid into the outlet. At the end of heating (see Figure 3-31 image (E)), approximately half of the fluid that was originally in the cavity was pushed into the air outlet leg and lost.

The expansion of the air was reduced by preheating the cavity. The heater was turned on for 270 seconds to ensure that the system was up to temperature. Water was then pumped into the cavity and allowed to heat as before. The effects of preheating are shown in Figure 3-32 where the air bubble expansion was greatly reduced. Several extractions were performed with the system using the pre-heating method and Cavity V6 (see Section 3.8.1). Although the cavity produced some successful tests, it was not an ideal design. The preheating of the cavity was very time-consuming, and a portion of the sample fluid was trapped in the solvent leg during the sample ejection step. By replacing the inlet valve configuration with the rotary valve, the single inlet Cavity V5 could be used.

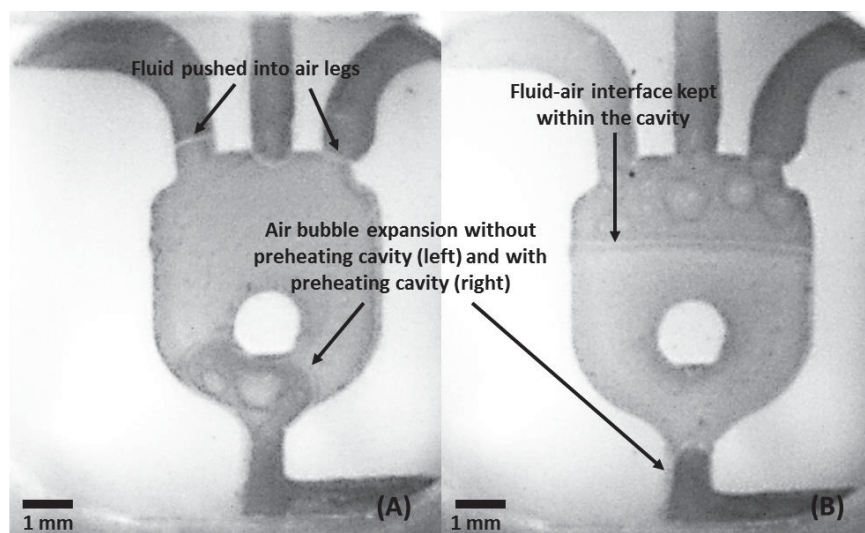


Figure 3-32. Cavity V6 air bubble expansion (A) without pre-heating and (B) with preheating

Problems controlling flow within the cavity persisted in Cavity V5. During the solvent and/or buffer fill steps of the process, fluid is able flow up one side of the cavity. This could be a result of the surface finish of the cavity, small particles on the cavity surfaces (burs formed during machining or dirt from the fiber), and the location of the fiber. When air flows through the cavity it then forces a large portion of the fluid into the air outlet and to the waste bottle. Extracted dye in the solvent and/or buffer can be lost. In addition, when the buffer only flows on one side of the cavity, it does not reconstitute dye residue on other side. An example of this is shown in Figure 3-33.

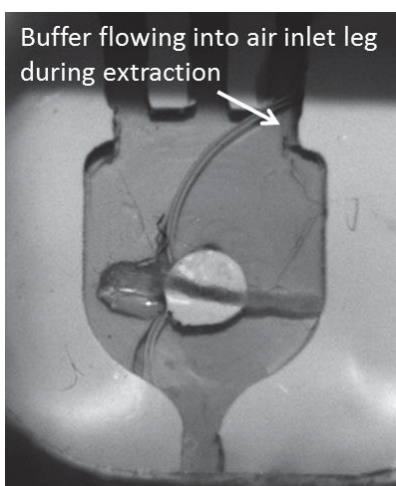


Figure 3-33. Buffer flowing through one side of the cavity into an air inlet

Further design iterations were examined to address the problem. Cavity V7 and V 8 are shown in Figure 3-34.

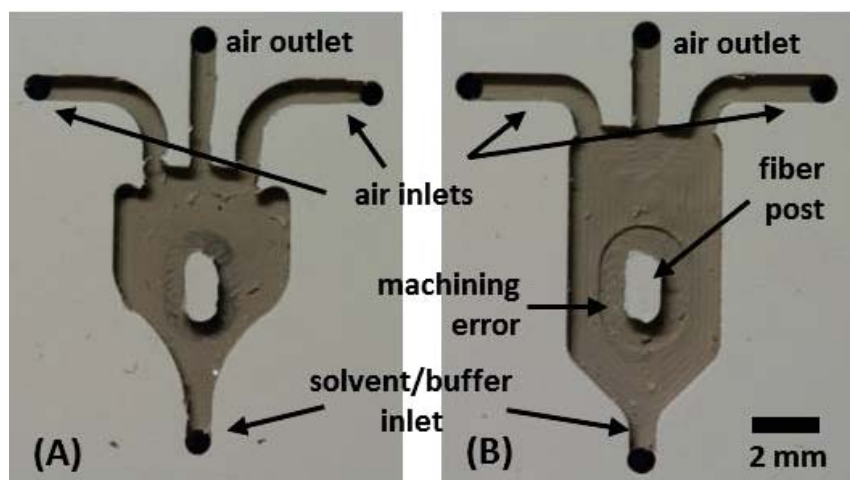


Figure 3-34. (A) Cavity V7 and (B) Cavity V8

For Cavity V7, the inlet was designed with a more gradual curve. Hook-like features were added near the air inlets to stop fluid flow. Cavity V8 was designed with straight walls and a larger volume. The goal of using straight walls was to reduce the resistance to flow. A machining error was made around the fiber holding post of V8 where the area around the fiber post was lower than the chamber floor around it. Flow tests were performed where fluid was pumped into the cavities. The change of features made for cavity version 7 did not prevent fluid from flowing into the air legs as shown in Figure 3-35.

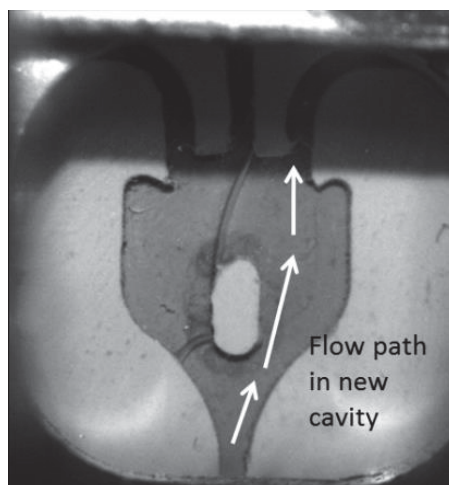


Figure 3-35. Flow test for cavity V7

A flow test was also performed for the straight-walled cavity. During the flow test, fluid was observed flowing around the offset area around the fiber holding post as shown in Figure 3-36. As can be seen in this figure, the fluid flowed farther up one side of the cavity than the other. The effects of the cavity surface on the flow were not mitigated as desired.

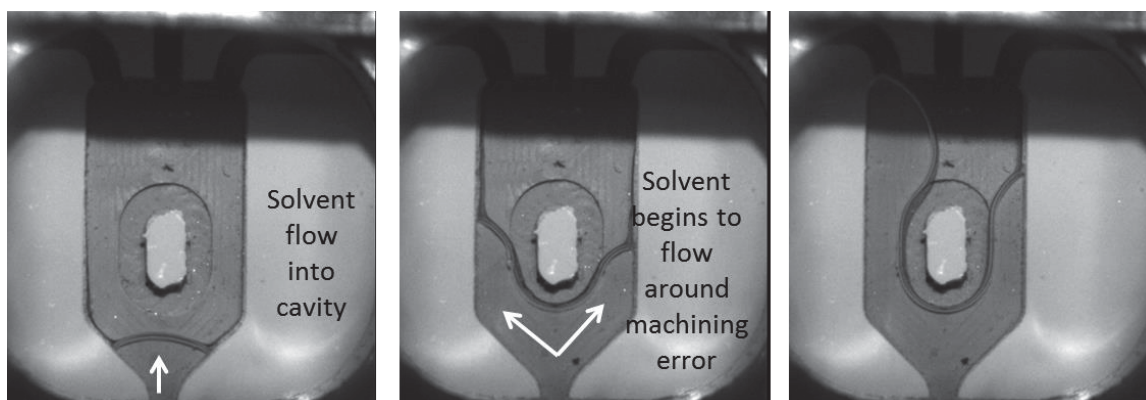


Figure 3-36. Flow tests for cavity V8

The fluid flow around the machining defect, however, indicated a potential method for controlling the cavity fill. The machining defect creates a flow resistance as the fluid meniscus reaches the edge. The surface tension of the fluid prevents it from initially flowing over the edge. The flow resistance increases as the angle of approach (θ_a) of the fluid increases as shown in Figure 3-37.

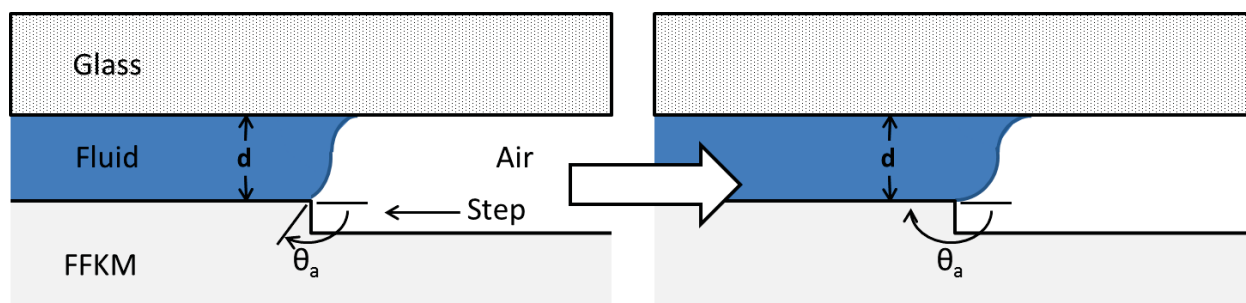


Figure 3-37. Effect of step in cavity on fluid approach angle

The surface tension force acting on the flow front is a function of the contact angle (θ_a) as $\sigma \cos \theta_a$ (where σ is the surface tension of the given fluid). For an approach angle greater than 90° , the surface tension produces resistance to flow [41]. At the step in the cavity, θ_a increases and the resistance therefore increases. Although the contact angle of the glass is negative and would act to pull the fluid as seen in surface-tension driven flows, the resistance at the step is higher. This produces the desired effect of halting flow while the rest of the cavity fills.

A “surface tension barrier” was incorporated into a new cavity design to guide fluid as it fills the cavity. Cavity V9 is shown in Figure 3-38. In cases where the fluid flows up one side of the cavity, the effect of the barrier should be to provide a higher resistance to the advancing fluid than surface defects or particles. This forces the fluid to flow up the other side of the cavity.

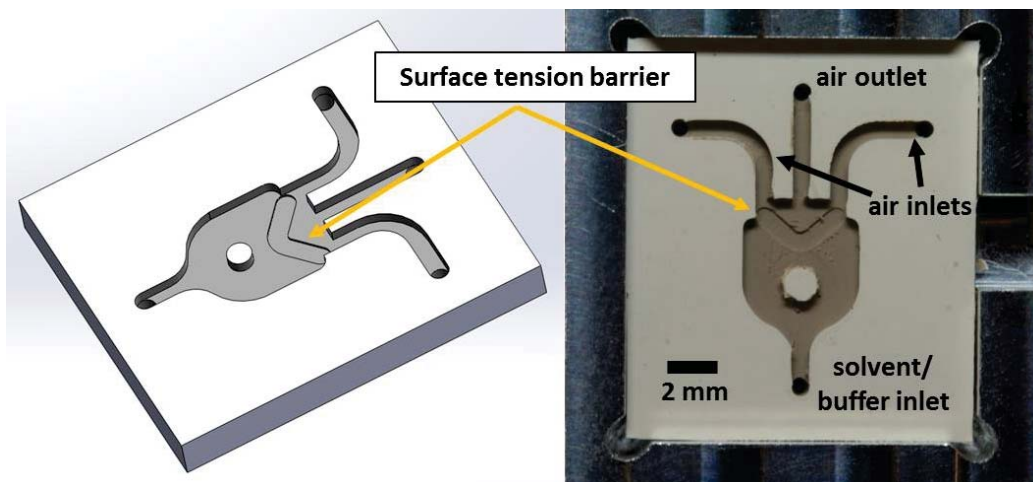


Figure 3-38. Cavity V9 – including “surface tension barrier”

The design works as intended for dry cavity surfaces as shown in Figure 3-39. Flow is controlled for the solvent fill step and the first buffer fill step where the surfaces are dry. For subsequent buffer fill steps the cavity surface is no longer dry and some buffer can potentially enter the air outlet. The majority of dye is picked up in the first buffer step, however, so the small volume lost in the air outlet in subsequent fills does not result in a failed extraction.

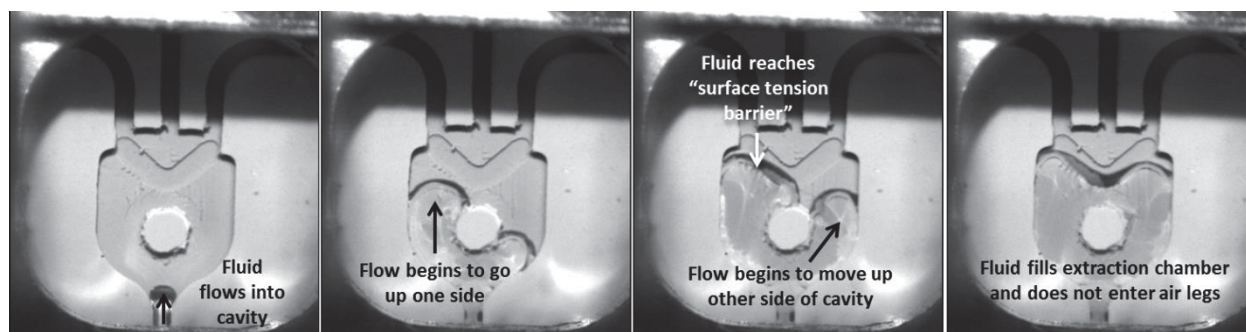


Figure 3-39. Flow test for Cavity V9 – effects of “surface tension barrier” on fill

3.5 CAVITY AIR FLOW

SolidWorks flow simulations were performed to determine cavity flow velocities for evaporation. The cavity flow simulations were also used to optimize the configuration of the air legs to promote better flow within the main cavity volume.

3.5.1 INLET AIR FLOW

To estimate the flow (Q) of air into the cavity, Equation (3.3) (Poiseuille flow equation) was used. Flow versus tube length for a 0.006” ID tube at several pressures is shown Figure 3-40.

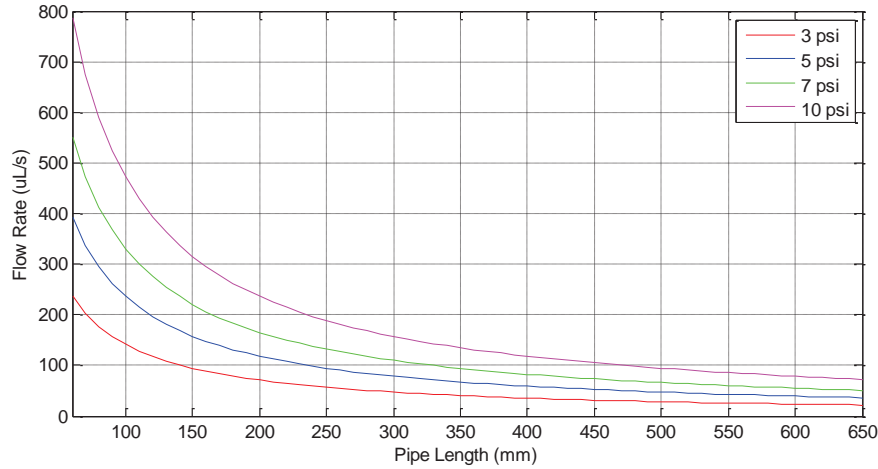


Figure 3-40. Volumetric flow of air in 0.006" ID tube

The flow equation is valid for laminar flow, where the Reynolds number is less than 2100. The Reynolds number for pipe flow is given by Equation (3.8) [42].

$$Re = \frac{QD_H}{\nu A} \quad (3.8)$$

A plot of Reynolds numbers for the given flow verifies flow is within the laminar regime as shown in Figure 3-41.

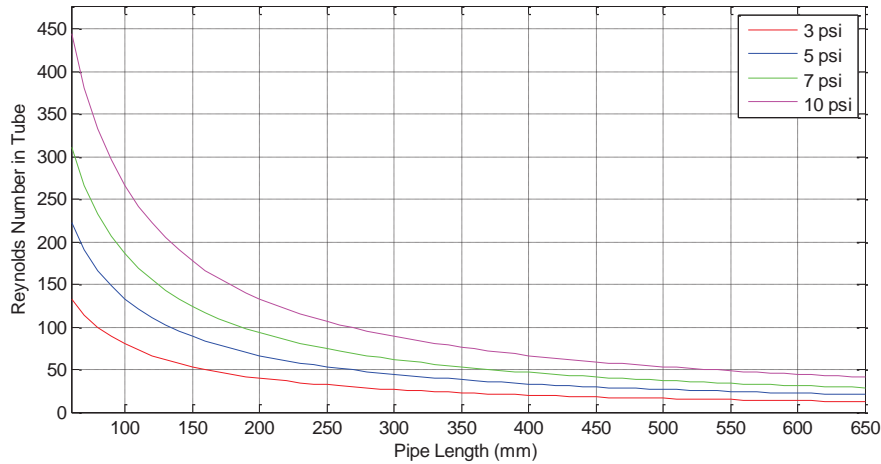


Figure 3-41. Reynolds numbers for air flow in 0.006" ID tube

In the cavity configurations where two air inlets were used, a different inlet tubing configuration was used. The configuration is shown in Figure 3-42.

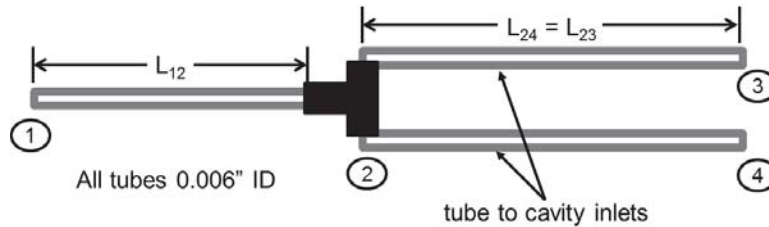


Figure 3-42. Inlet tube configuration for two-air-inlet cavity designs

The flow calculation is slightly more complicated in the new configuration. In this case it is more convenient to represent each tube as a resistance to flow as shown in Equation (3.9). The tubes leading to the cavity have the same length and pressure drop and therefore the same flow rates ($Q_{23}=Q_{24}$).

$$Q_{12} = \frac{\Delta p_{12}}{R_{12}} \dots Q_{23} = Q_{24} = \frac{\Delta p_{23}}{R_{23}} \quad (3.9)$$

$$R_{12} = \frac{128\mu L_{12}}{\pi D_h^4} \dots R_{23} = \frac{128\mu L_{23}}{\pi D_h^4}$$

Since flow in must equal flow out, $Q_{12}=2Q_{23}$. Using this fact and Equation (3.9), the flow through the system is determined as a function of the total pressure drop (p_1 = regulated air pressure, p_3 = atmospheric pressure). The flow is given by Equation (3.10).

$$Q = \frac{\Delta p_{13}}{R_{12} + \frac{R_{23}}{2}} \quad (3.10)$$

For both of the microfluidic system prototypes $L_{12} = 5.5$ cm and $L_{23} = L_{24} = 9.2$ cm. A plot of pressure versus flow rate for the prototype configuration is shown in Figure 3-43.

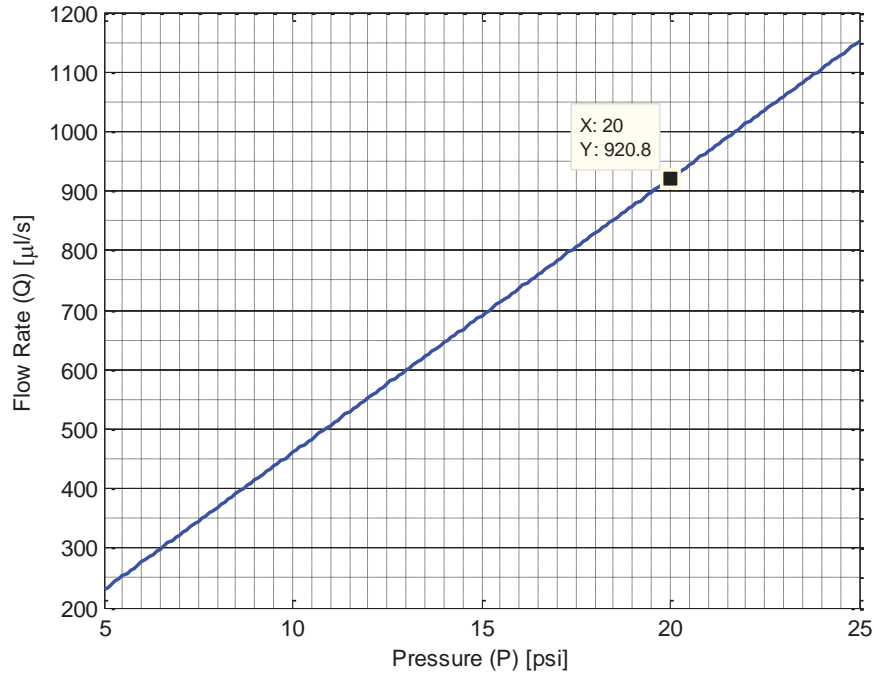


Figure 3-43. Split air inlet flow versus total pressure drop. The flow rate value of 921 $\mu\text{l/s}$ at 20 psi was noted on the graph because it was used in Figure 3-48 to model the evaporation rate.

3.5.2 CAVITY CFD AIR FLOW ANALYSIS

SolidWorks Flow Simulation software was first used in the design of the air legs for Cavity V3. The goal of the simulations was to determine a configuration of the legs that produced the best air-flow profile in the cavity body. Three configurations were simulated as shown in Figure 3-44 through Figure 3-46.

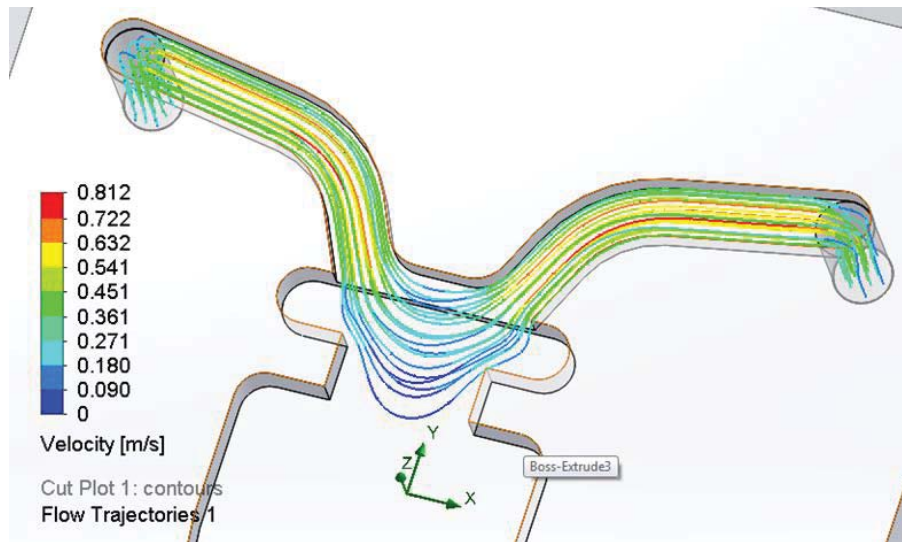


Figure 3-44. Cavity V3 – air inlet/outlet configuration 1

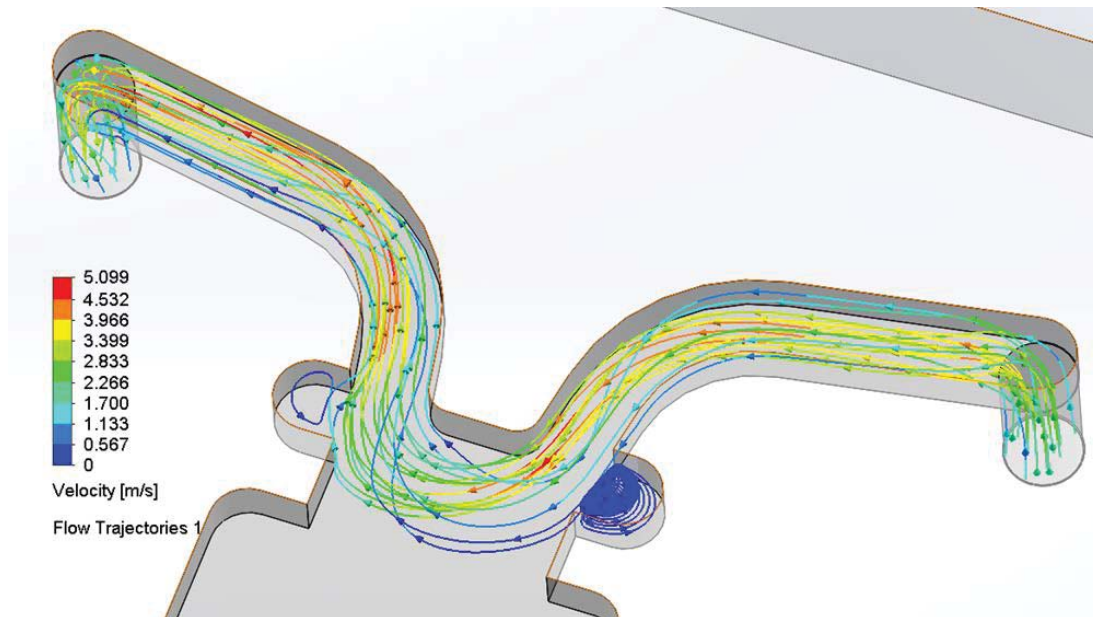


Figure 3-45. Cavity V3 – air inlet/outlet configuration 2

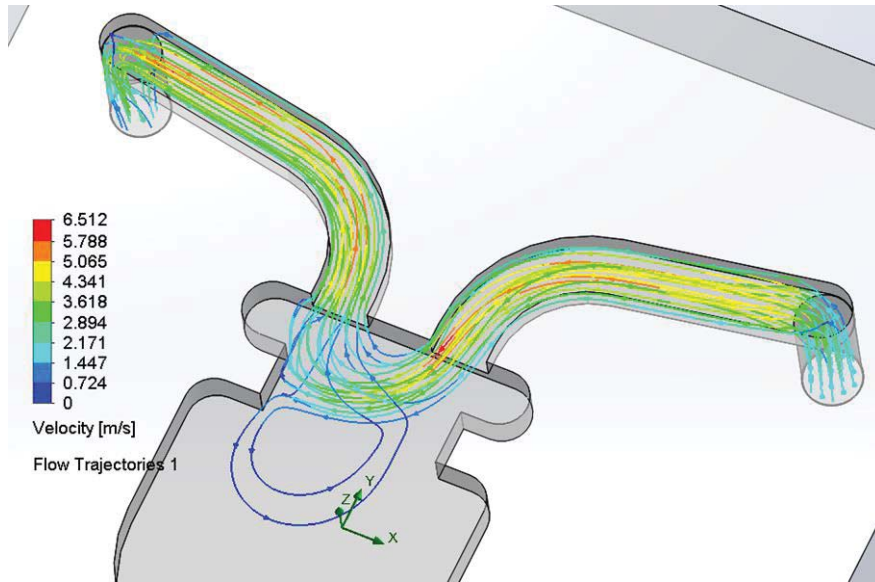


Figure 3-46. Cavity V3 – air inlet/outlet configuration 3

The simulation shown in Figure 3-44 assumed a pressure drop of 3 psi over a 50 mm long tube (10 psi for the other two), hence the lower velocity magnitudes. It is clear that air inlet/outlet configuration 1 (Figure 3-44) creates a slight bottleneck at the entrance to the cavity. In configuration 2 (Figure 3-45), the opening between the air legs and cavity was widened. The inlet and outlet were directed more toward the cavity. In configuration 3 (Figure 3-46), the air inlet and outlet enter the cavity perpendicular to the theoretical fluid air interface. Air inlet/outlet configuration 3 shows better flow within the cavity qualitatively and was used for fabrication of cavity V3.

Flow simulations were performed for Cavity V5 (see Figure 3-29) using 250 $\mu\text{l/s}$ (500 $\mu\text{l/s}$ total) and 660 $\mu\text{l/s}$ (1320 $\mu\text{l/s}$ total) of air flow at each air inlet as shown in Figure 3-47. The flow values correspond to pressure drops of 12 and 32 psi respectively. The simulations were used to show the effect of increasing the inlet volumetric flow on the flow velocities within the cavity.

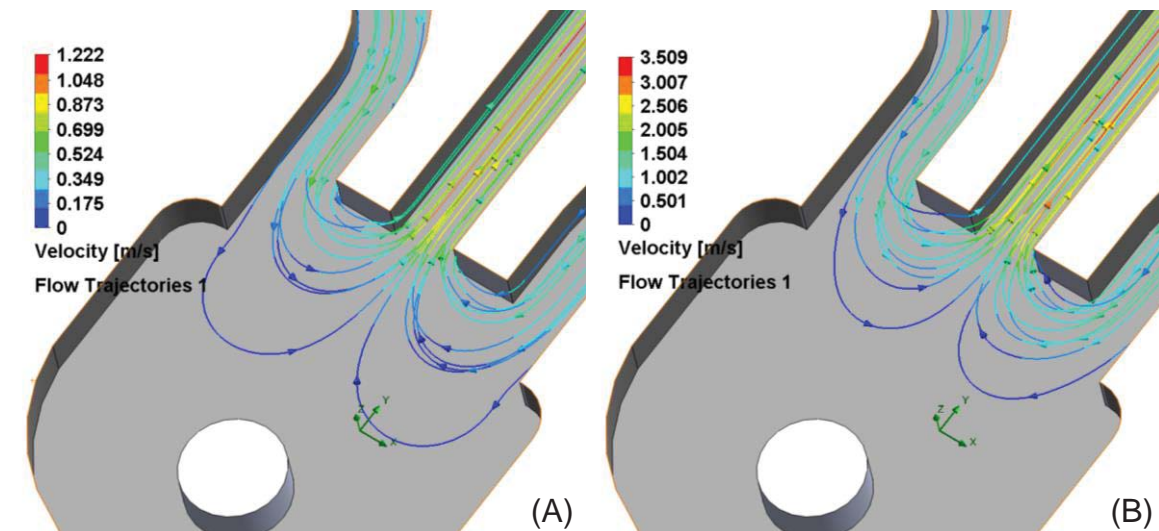


Figure 3-47. Cavity V5 air-flow profiles for (A) 250 $\mu\text{l/s}$ and (B) 660 $\mu\text{l/s}$ air flow at each inlet

Several air pressures were tried for the air inlets. A pressure of 20 psi was determined to give high flow for evaporation and pressure for ejection of waste and sample fluids through the fluid inlet. At higher pressures the initial flow of air into the cavity disrupted the fluid in cavity, blowing some fluid into the air outlet. At 20 psi the total flow in was calculated to be 920 $\mu\text{l/s}$ (460 $\mu\text{l/s}$ at each inlet). A simulation was performed under these conditions. The results are shown in Figure 3-48. An average flow velocity of ~ 0.5 m/s over the fluid surface was estimated from the flow simulations. This value was used for initial evaporation estimates as discussed in following sections.

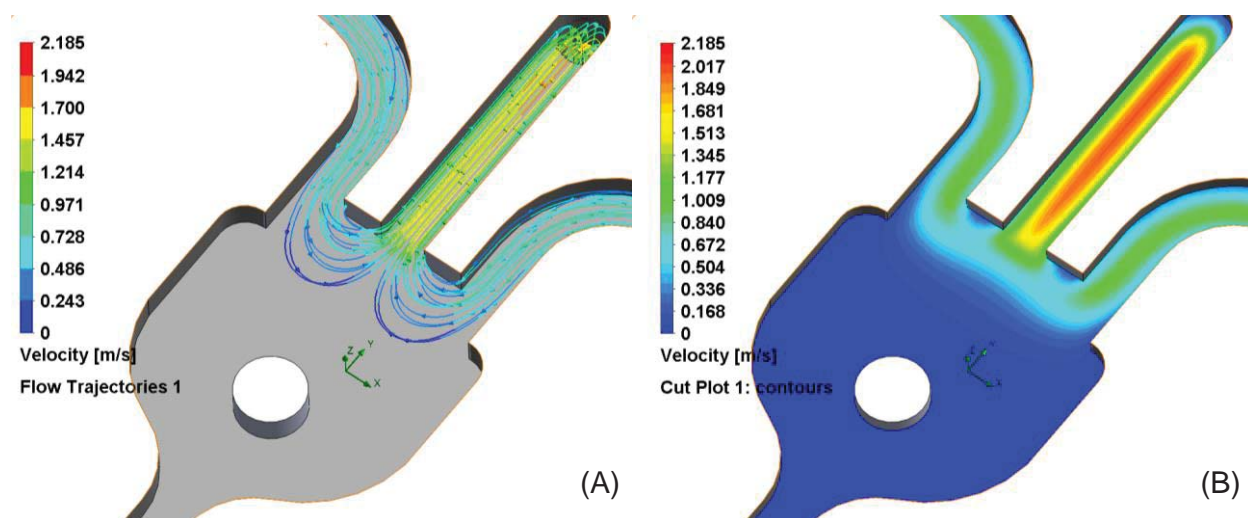


Figure 3-48. Cavity V5 air-flow for 460 $\mu\text{l/s}$ air flow at each inlet

3.6 EVAPORATION

The ability to model evaporation serves several purposes. The first and most obvious reason is in timing the process. The evaporation model was used to estimate the expected time for this step for given operating parameters. The model was also used to optimize the geometry of the cavity and device plumbing to minimize evaporation time. By examining the relationships and effects of various parameters on the rate of mass transfer from the fluid to the air, changes could be made to the design to improve the process.

3.6.1 CONVECTIVE EVAPORATION MODEL

Predicting evaporation in the device is not a simple exercise. The geometry of the fluid body and air flow paths is fairly complex and dynamic with time, indicating a varying rate of evaporation. The process was modelled as simple convective mass transfer over a body of fluid. The model is shown in Figure 3-49.

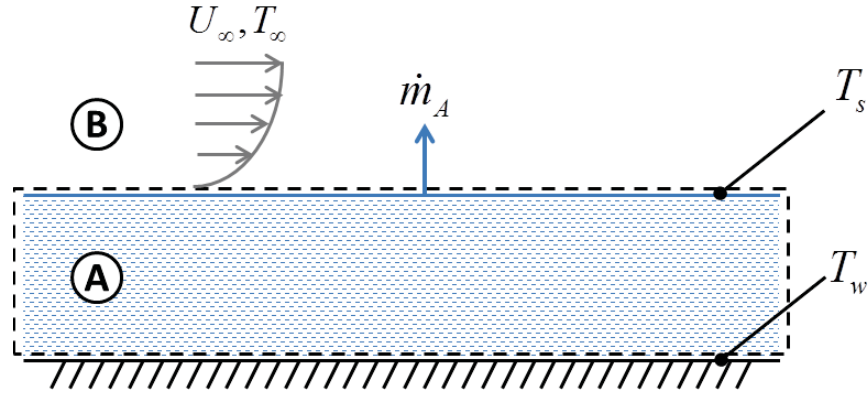


Figure 3-49. Convective mass transfer at a gas-liquid interface

In the model described here, several assumptions are made:

- The concentration of species A is constant at the surface.
- The temperature at the surface is the same as that at the wall ($T_s = T_w$).
- The mass transfer coefficient (h_m) used in the calculations is the average mass transfer coefficient over the surface.
- Thermodynamic equilibrium exists at the gas-liquid interface (T_s can be used to determine properties of A at the surface).
- The surface (effective length and area), gas velocity and mass transfer are constant.

Similar to convective heat transfer, convective mass transfer can be determined as a function of the liquid and gas properties and a convective mass transfer coefficient. The relationship is shown in Equation (3.11).

$$\dot{m}_A = h_m A_s (\rho_{A,s} - \rho_{A,\infty}) \quad (3.11)$$

The density of A ($\rho_{A,s}$) is the density associated with the saturated vapor pressure of A at T_s . Similarly, $\rho_{A,\infty}$ can be determined from the saturated vapor pressure of A at T_∞ (the temperature of air flowing over the surface). The densities can be accurately approximated from the ideal gas law as shown in Equations (3.12) and (3.13).

$$\rho_{A,s} = \frac{M_A P_{sat}(T_s)}{\hat{R} T_s} = \frac{P_{sat}(T_s)}{R T_s} \quad (3.12)$$

$$\rho_{A,\infty} = \frac{\phi P_{sat}(T_\infty)}{R T_\infty} \quad (3.13)$$

where,

M_A = molecular weight of the fluid

\hat{R} = universal gas constant

R = specific gas constant of A

ϕ = relative humidity of the air

P_{sat} = saturation pressure at the given temperature

Determining the convective mass transfer coefficient is more complex; however with the simplified geometry it is not unreasonable. The average mass transfer coefficient (h_m) can be determined from Equations (3.14)-(3.17) [43].

$$h_m = \frac{Sh \cdot D_{AB}}{L} \quad (3.14)$$

$$Sh = 0.664 Re^{1/2} Sc^{1/3} \quad (3.15)$$

$$Re = \frac{U_\infty L}{\nu} \quad (3.16)$$

$$Sc = \frac{\nu}{D_{AB}} \quad (3.17)$$

where,

Sh = Sherwood number

D_{AB} = mass diffusivity for species A and B

L = characteristic length of the surface

ν = kinematic viscosity of air at T_∞

The Sherwood number is defined as a function of the Reynolds number (Re) and the Schmidt number (Sc). The total evaporation time is estimated in Equation (3.18).

$$t_E = \frac{\rho_A V_A}{\dot{m}_A} \quad (3.18)$$

where,

ρ_A = density of the fluid

V_A = volume of the fluid

Combining Equations (3.11)-(3.17), the mass transfer rate is expressed in Equation (3.19) in terms of the process parameters.

$$\dot{m}_A = \frac{0.664 U_\infty^{1/2} D_{AB}^{2/3} A_s}{\nu^{1/6} L^{1/2}} \left(\frac{P_{sat}(T_s)}{RT_s} - \frac{\phi P_{sat}(T_\infty)}{RT_\infty} \right) \quad (3.19)$$

3.6.2 EVAPORATION PARAMETERS AND DESIGN CONSIDERATIONS

The evaporation of 10 μ l of water is considered in this section. The same conditions are used in each calculation while varying the parameter of interest; 0.1 m/s air velocity, 70°C water temperature, 25°C air temperature, 2.5 mm characteristic length, 0.5 mm cavity depth, and 50% relative humidity.

The humidity and temperature of the air flowing through the device are first examined. Ideally, the quality of the air would be controlled for consistent performance. Dry air (or another gas such as nitrogen) would produce the fastest evaporation. First, the effect of the relative humidity is evaluated. Solving Equation (3.19) and then Equation (3.18) it can be seen that the evaporation time should vary linearly with this humidity as shown in Figure 3-50

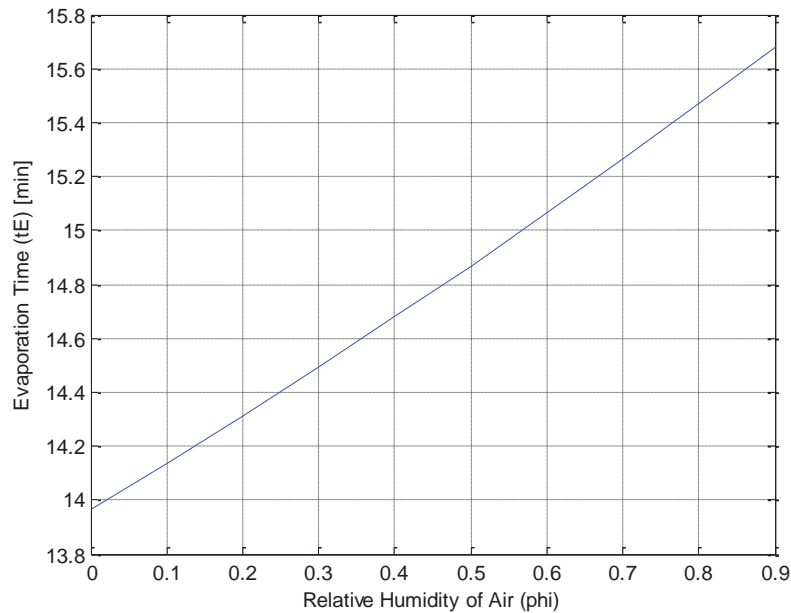


Figure 3-50. Change in evaporation time with relative humidity of air

The total evaporation time increases by approximately 12% (less than two minutes) from 0 to 90% relative humidity. The temperature of the air can also be controlled. Evaporation time over a range of air temperatures is shown in Figure 3-51.

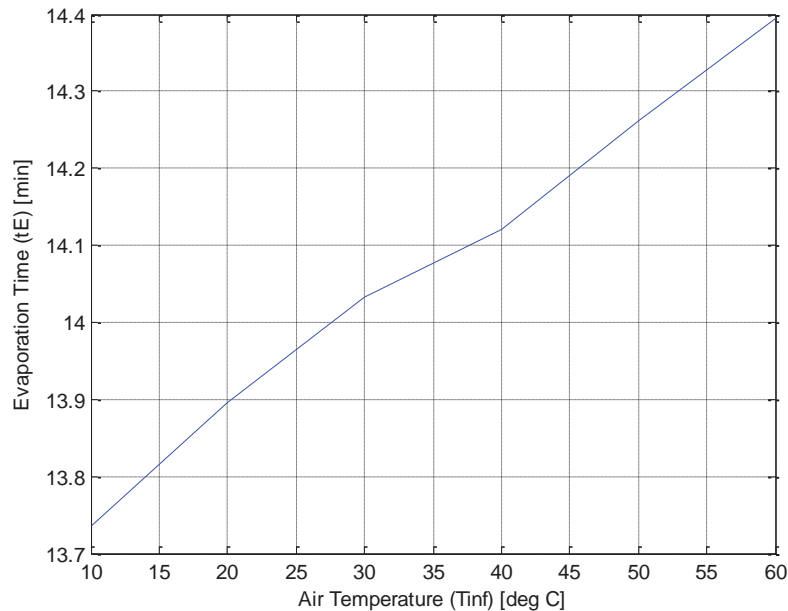


Figure 3-51. Change in evaporation time with air temperature

In addition to the temperature and humidity of air flowing into the device, the air velocity over the surface can be controlled as was discussed in Section 3.5. The effects of air velocity over the surface are shown in Figure 3-52.

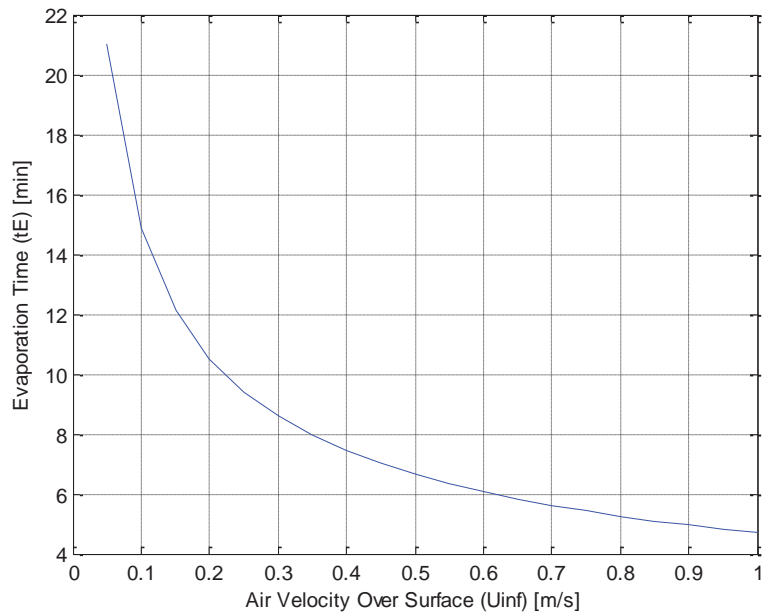


Figure 3-52. Change in evaporation time with air velocity over the fluid surface

The temperature of the fluid in the cavity is considered next. It is difficult to easily recognize the effects of fluid temperature from Equation (3.19). Evaluating at various temperatures and plotting gives a relationship as shown in Figure 3-53. The rapid decrease in the evaporation time as fluid temperature increases is due to the exponential increase in the vapor pressure of the fluid with temperature. For instance, the vapor pressure of water is 7,358 Pa at 40°C and 70,034 Pa at 90°C. Equation (3.19) shows that the evaporation rate increases directly with this pressure.

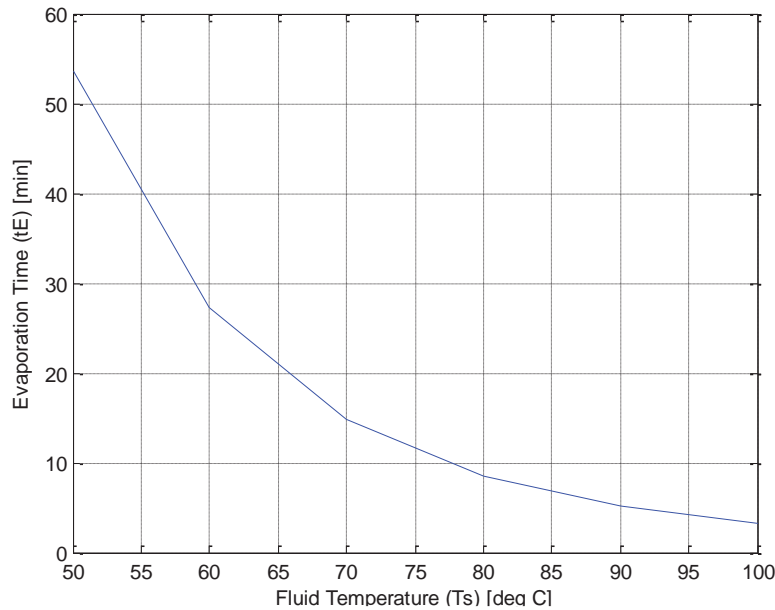


Figure 3-53. Change in evaporation time with water temperature

Cavity geometry also provides control over evaporation. The mass transfer rate increases with increasing area of the fluid-air interface. Assuming a constant cavity depth of 0.5 mm, the effects

of increasing the length of this interface are examined. Evaporation times for increasing characteristic length values are shown in Figure 3-54. Equation (3.19) is a function of $L^{1/2}$, resulting in the total evaporation time being a function of $L^{-1/2}$ as seen in Figure 3-54.

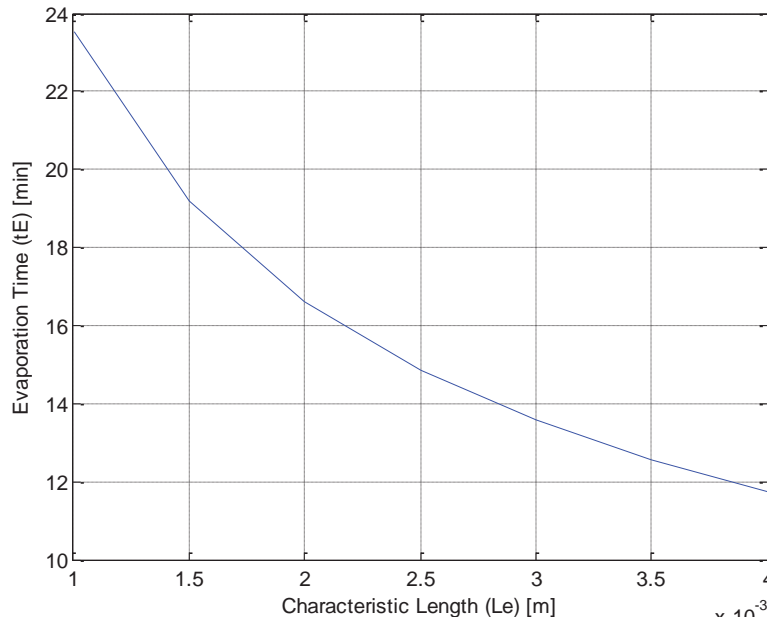


Figure 3-54. Change in evaporation time with characteristic length

The initial fluid-air interface location and flow direction is shown in Figure 3-55.

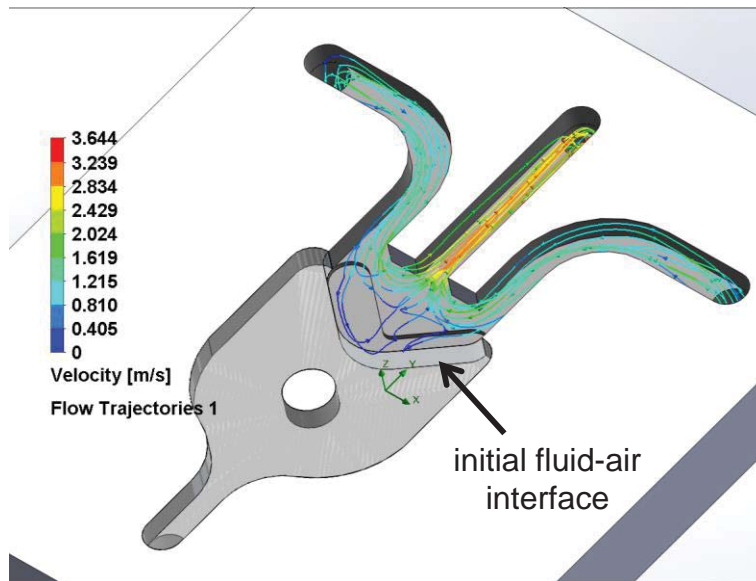


Figure 3-55. Air flow and interface location in microfluidic cavity

Conclusions drawn from the parameter analysis were used to create the final cavity design:

- The temperature of the fluid being evaporated has the greatest impact on the length of the process. Analysis showed that, as the water increased in temperature from 50°C and approached 100°C under the given conditions, evaporation time would be reduced by approximately 90% .

- Over the range of possible air velocities seen within the microfluidic device (over the fluid surface), predicted evaporation time was reduced by approximately 75% as velocity approached 1 m/s.
- The characteristic length and corresponding surface area have a significant impact on the mass transfer rate and overall evaporation time as well. For the given conditions, increasing the characteristic length by 3 mm reduces the total evaporation time by 50%.

The effects of varying air quality are less significant:

- Reducing the humidity of the air from 90% to 0% decreases total evaporation time by less than two minutes (only ~11%).
- Reducing the temperature of the air from 60°C to 10°C decreases total evaporation time by 5%. The small benefit from reducing the air temperature is far outweighed by the complication of adding air temperature control to the system.

From a design standpoint, the two easiest parameters to control were the fluid-air interface area and the air flow velocity. Higher flow velocities could be achieved by increasing inlet pressure and reducing tubing restrictions (small diameters and long tube lengths). The interface area could be increased through cavity geometry.

3.6.3 EVAPORATION TESTING

The convective evaporation model makes several assumptions and is a simplified analysis of the process. For instance, the complex shape of the cavity and changing surface characteristics of the fluid as it evaporates change the local velocities of the flowing air. The surface area of the fluid also changes as the fluid-air interface recedes to the fluid inlet. Realistically, the rate of evaporation would be expected to change with time. A more realistic modelling of the process could be achieved using multi-physics simulation software. Evaporation tests were performed to determine if Equations (3.18) and (3.19) could be used to accurately predict the total evaporation times.

Videos of the evaporation process with the PTC heater setup were analyzed to compare to the expected range of evaporation times (tests were performed at approximately 75 °C). Video of the cavity was recorded with a Basler A622f camera and a reflective surface as shown in Figure 3-56.

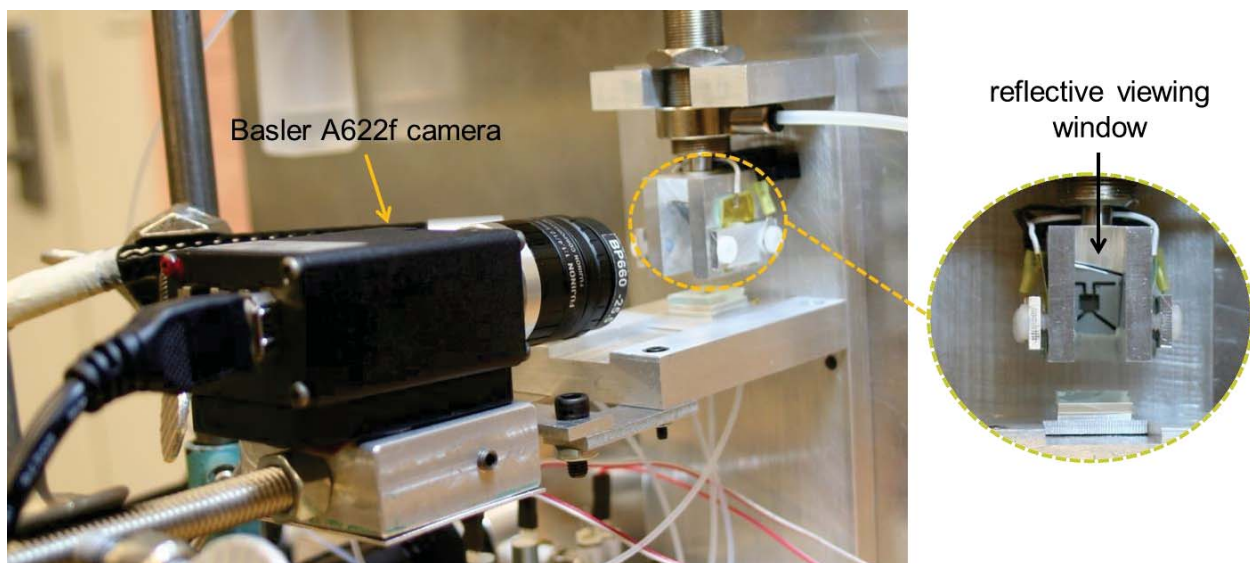


Figure 3-56. Cavity viewing and video recording setup

Images from four tests were taken at 5, 10, and 15 second intervals. The timed progress of solvent (4:3, pyridine:water) evaporation for each test is shown in Figure 3-57 - Figure 3-60. The individual frames show a very consistent profile for the fluid during evaporation at each time step.

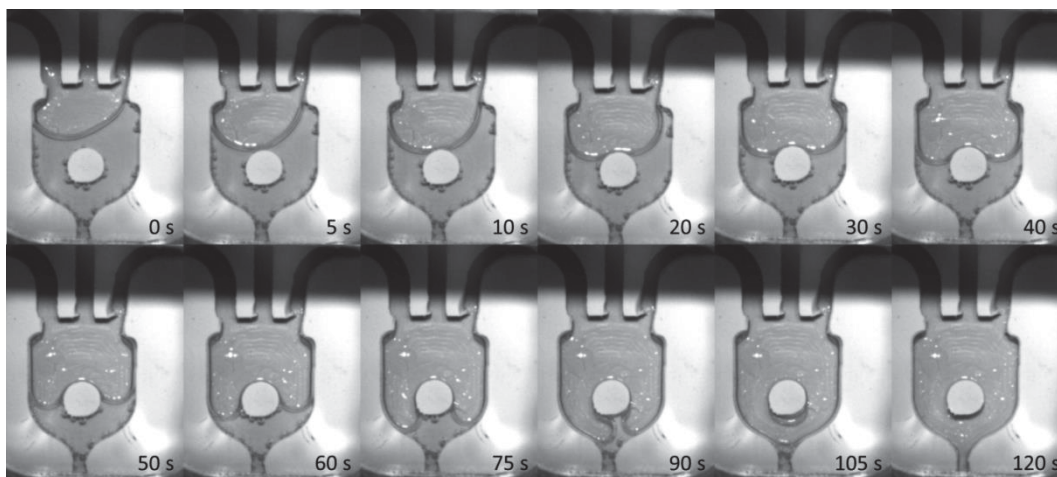


Figure 3-57. Solvent evaporation test #1

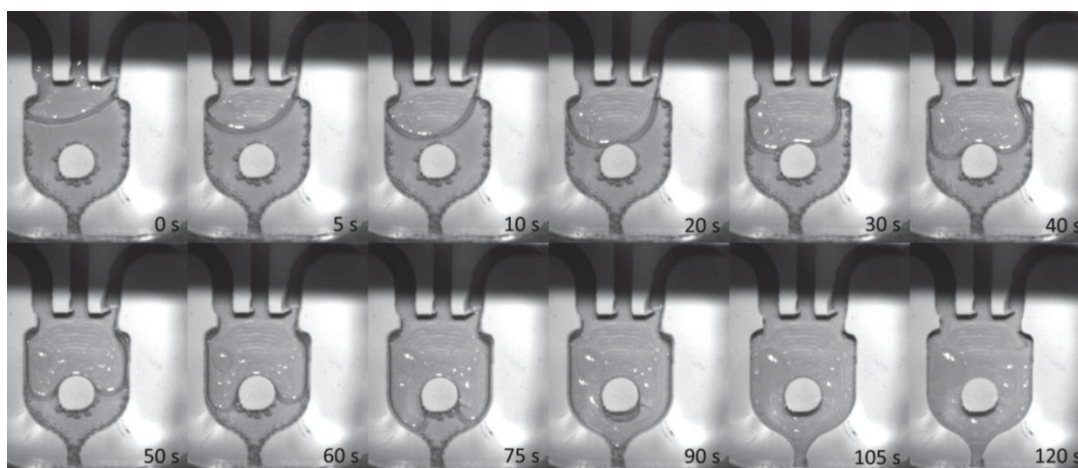


Figure 3-58. Solvent evaporation test #2

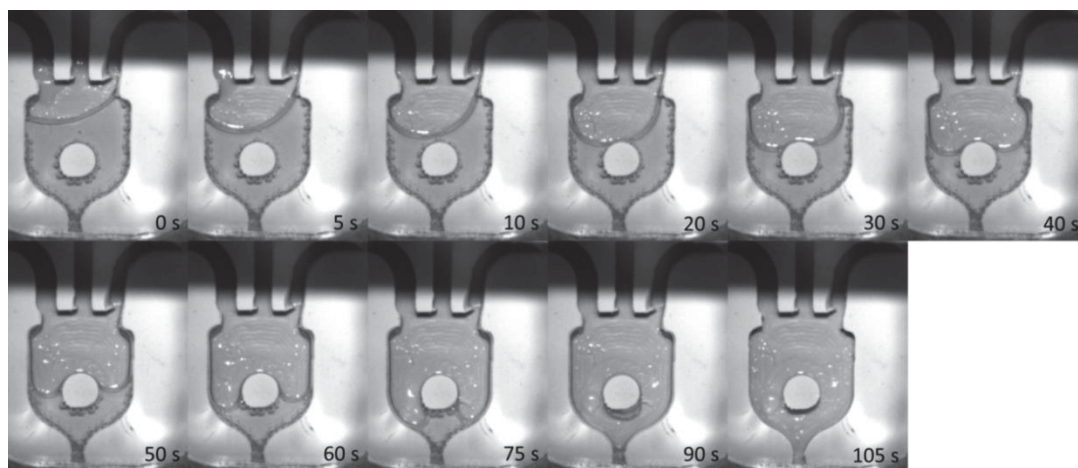


Figure 3-59. Solvent evaporation test #3

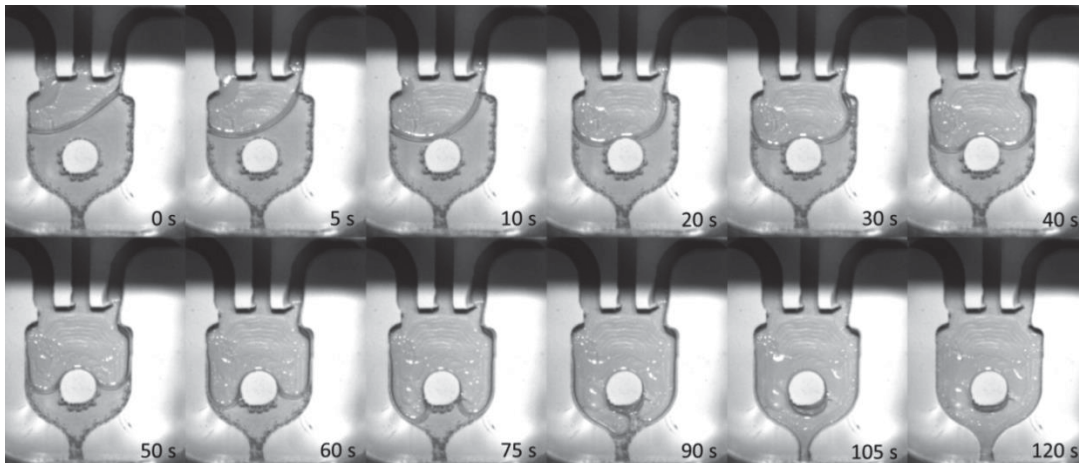


Figure 3-60. Solvent evaporation test #4

From the timed images, the MATLAB program digitize13² was then used to analyze the area of the fluid body. The program provides a calibration option so that the number of pixels in a known distance can be set. Once calibrated, an area can be determined by tracing out a surface with a finite number of points. This was done for each time step image as shown in Figure 3-61.

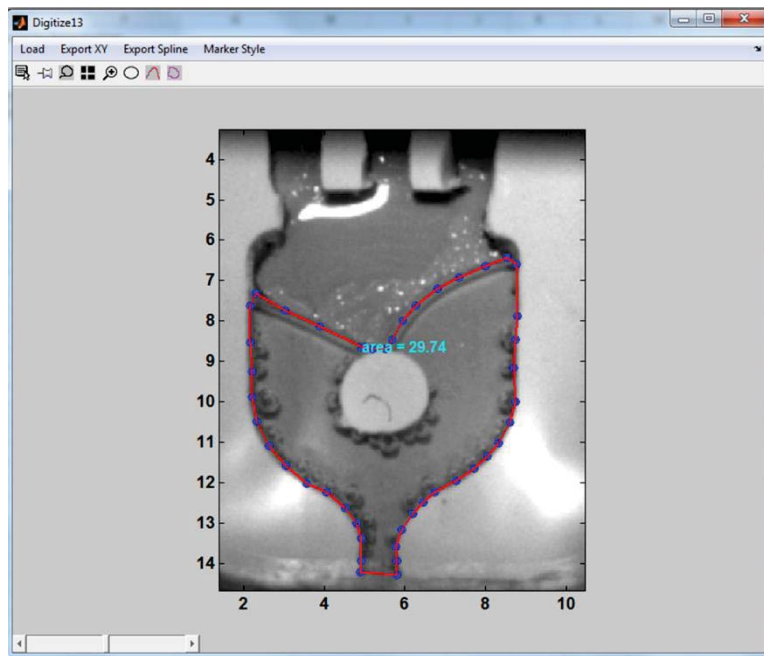


Figure 3-61. Area measurement using digitize13

The fluid volume of each step is calculated by subtracting the area of the fiber post in the center and multiplying by 0.5 mm (cavity depth). These volumes are shown over the duration of each evaporation test in Figure 3-62.

² Digitize13 is a program written by Ken Garrard of the Precision Engineering Center at North Carolina State University. The program is used to make two-dimensional measurements of image files.

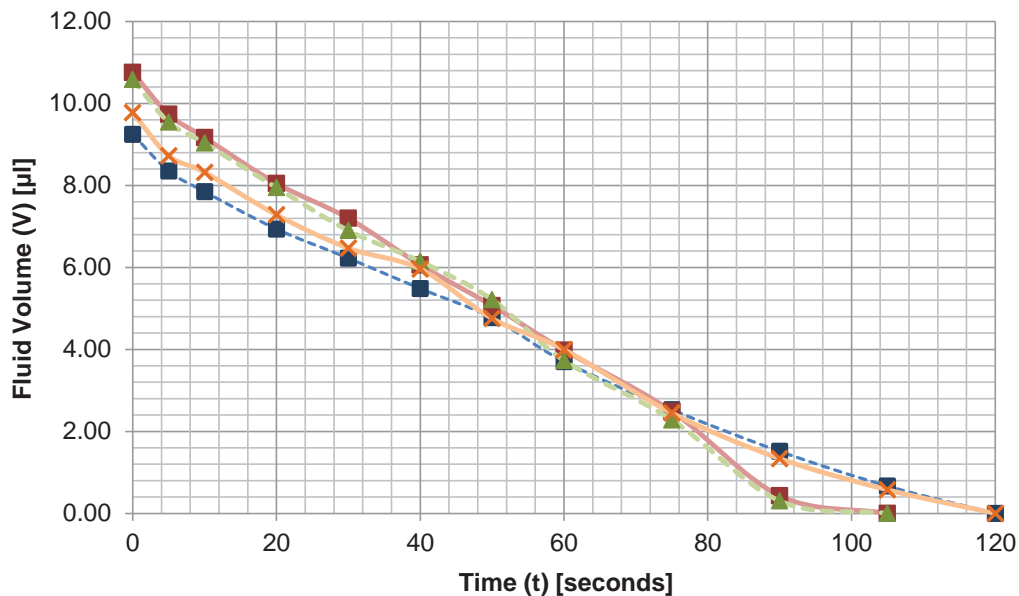


Figure 3-62. Fluid volume in cavity over duration of evaporation tests (~75°C)

The data is approximated accurately with a linear data fit as shown in Figure 3-63.

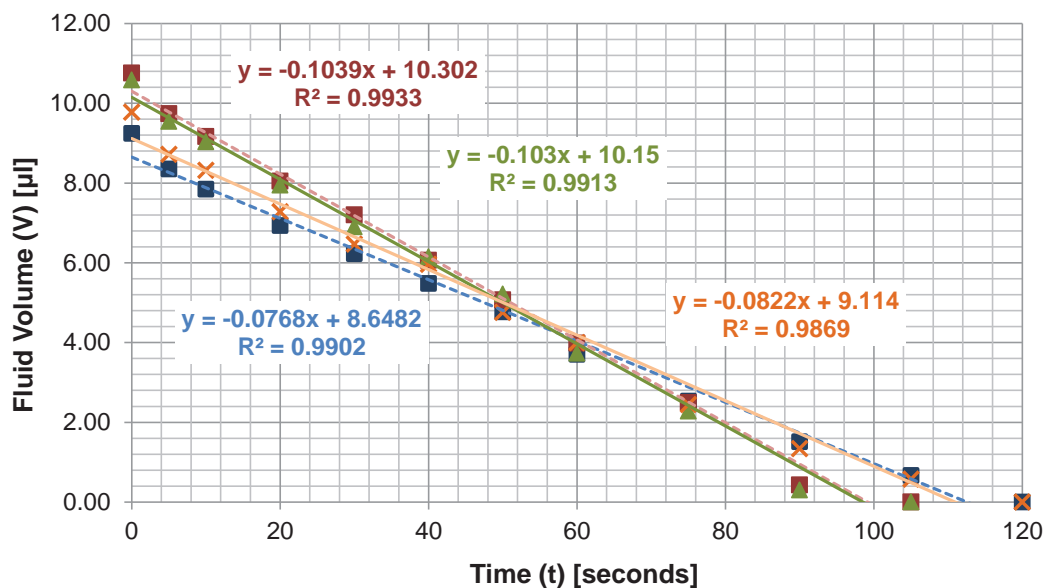


Figure 3-63. Linear data fits to evaporation data

Evaporation rates for time intervals were also calculated and compared to the linear data fits as shown in Figure 3-64.

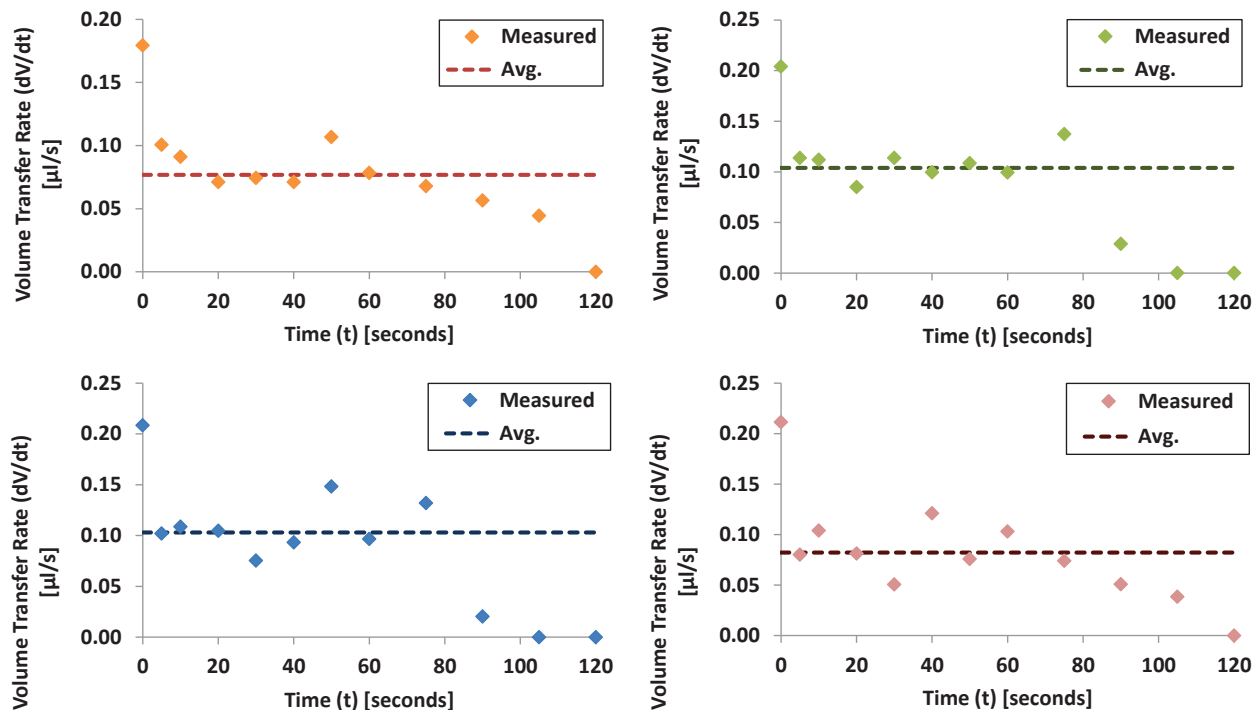


Figure 3-64. Evaporation rates over duration of evaporation tests

The overall time to evaporate the fluid (assumed to be at approximately 75°C) did not exceed two minutes for the tests. The minimum time observed was 105 seconds. A constant evaporation rate model for the given parameters estimated the evaporation time to be between 1.5 and 2 minutes depending on the temperature and humidity of air flowing through the device. The test results show consistent evaporation for the test temperature (75°C). The method of analyzing the images presented in Figure 3-57 through Figure 3-60 was also shown to be effective in determining the total evaporation time and changing evaporation rate.

Evaporation tests were performed with the thin-film heater setup at different temperatures to measure the effects of temperature on evaporation time. To view the cavity during the test, an aluminum spacer with a slot was used as shown in Figure 3-65.

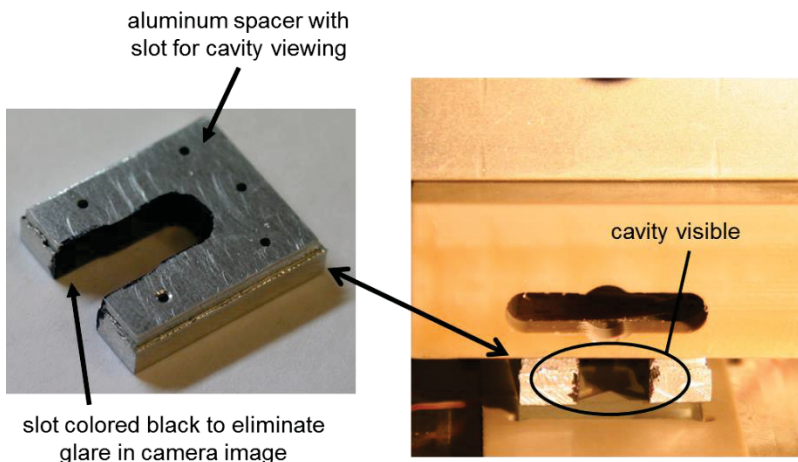


Figure 3-65. Aluminum spacer for cavity viewing

The aluminum spacer is a good conductor and allows heat to be transferred to the glass (See Appendix F.2 for calibration data). A webcam was used to view the cavity during testing as shown in Figure 3-66.



Figure 3-66. Cavity viewing setup

Set temperatures of 40°C, 50°C, 60°C, 70°C, and 80°C were tested. The average temperatures of each test were measured using a K-type thermocouple with a diameter of 0.08 mm (Omega Engineering Inc. part number 5TC-TT-K-40-80) and cRIO data acquisition system (LabView interface). The average temperatures were measured to be 43°C, 53°C, 64°C, 74°C, and 83°C respectively (determined as the average temperature over a cycle – see Appendix F.2 for cycled temperatures with aluminum spacer). Air inlet pressures of 10, 15, and 20 psi were tested for each temperature. The pressures correlate to a total of 460, 690, and 920 $\mu\text{l/s}$ of air flow through the cavity. The total time for evaporation of the solvent was recorded by observing the time from air flow initiation to when the solvent was no longer visible within the cavity. An example of the observed evaporation for 9 μl of solvent at a temperature of 64°C and 15 psi pressure drop across the air inlet tubing is shown in Figure 3-67. At zero seconds, the cavity is full of solvent. At ten seconds the solvent evaporating becomes noticeable, and at 30-90 seconds the fluid body quickly shrinks as evaporated fluid is carried into the air outlet. At 210 seconds, a small amount of fluid remains in the fluid inlet at the rear of the cavity and around the fiber holding post. At 130 seconds, the no fluid is visible in the cavity.

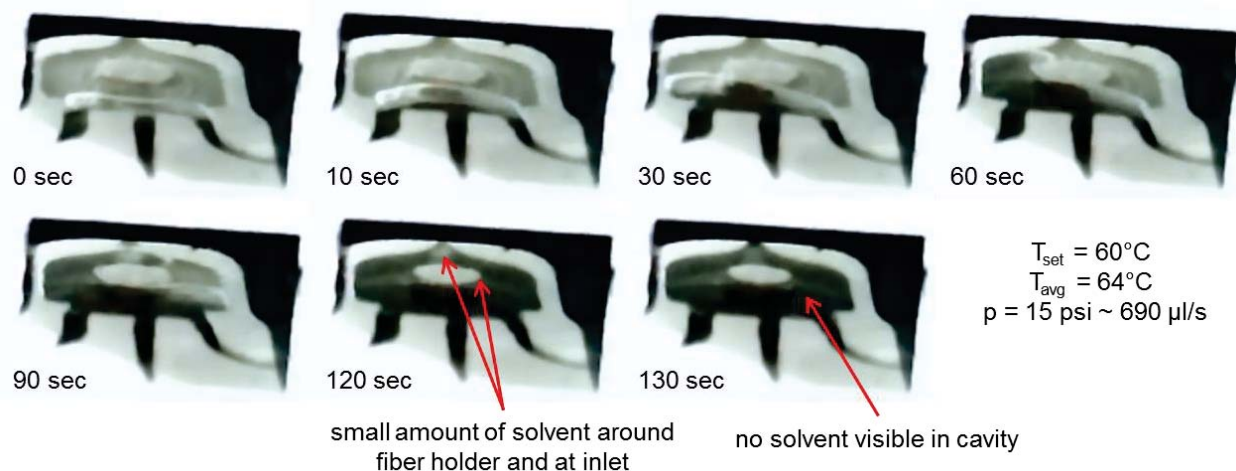


Figure 3-67. Evaporation of solvent at 64°C and 15 psi pressure drop across the air inlet tubing
The data recorded for each test is shown in Table 3-7.

Table 3-7. Evaporation test data for varying temperature and air flow

Air Line Pressure (P_{air}) [psi]	Set Temp (T_{set}) [°C]	Avg. Temp/cycle (T_{cyc}) [°C]	Heating time (t_{heat}) [sec]	Evaporation time (t_{evap}) [sec]	Volume Evaporated (V) [µl]	Evaporation Rate (dV/dt) [µl/s]
10	40	42.9	60	513	9	0.018
10	50	53.5	60	262	9	0.035
10	60	64.0	60	193	9	0.048
10	70	74.3	60	130	9	0.071
10	80	83.0	60	43	9	0.213
15	40	42.9	60	331	9	0.028
15	50	53.5	60	202	9	0.046
15	60	64.0	60	130	9	0.071
15	70	74.3	60	80	9	0.115
15	80	83.0	60	32	9	0.283
20	40	42.9	60	262	9	0.035
20	50	53.5	60	198	9	0.046
20	60	64.0	60	88	9	0.105
20	70	74.3	60	65	9	0.142
20	80	83.0	60	38	9	0.243

The evaporation times and rates from Table 3-7 are plotted in Figure 3-68. It appears the impact of the air velocity is reduced at higher temperatures. The evaporation rate increases almost exponentially as temperature increases, resulting in much shorter evaporation times at high temperatures. At lower temperatures, the time required to evaporate a 9 µL volume of solvent becomes significantly larger for the lower flow rates. This confirms the use of a 20 psi pressure drop for the air inlet tube, should an extraction be performed at low temperature.

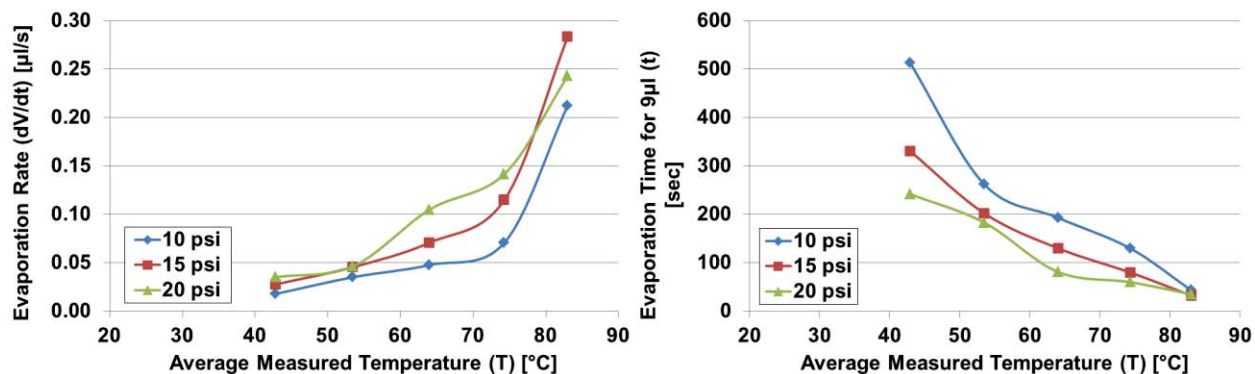


Figure 3-68. Measured solvent evaporation at varying inlet flow and temperature

The temperature dependence of the evaporation was also evaluated with the evaporation model. An estimate of the humidity of the wall air supply was evaluated by measuring its humidity with a Fisher Scientific digital humidity/temperature meter (model number 11-661-8). The humidity was measured to be 10-15%. A value of 15% was used in the model. The local velocity of the air flowing through the device also had to be evaluated. A flow simulation was performed with $460\mu\text{l/s}$ of air flow into the cavity at each air inlet (simulating the 20 psi pressure drop – total of $920\mu\text{l/s}$ of air flow into the cavity). The results of the simulation are shown in Figure 3-69.

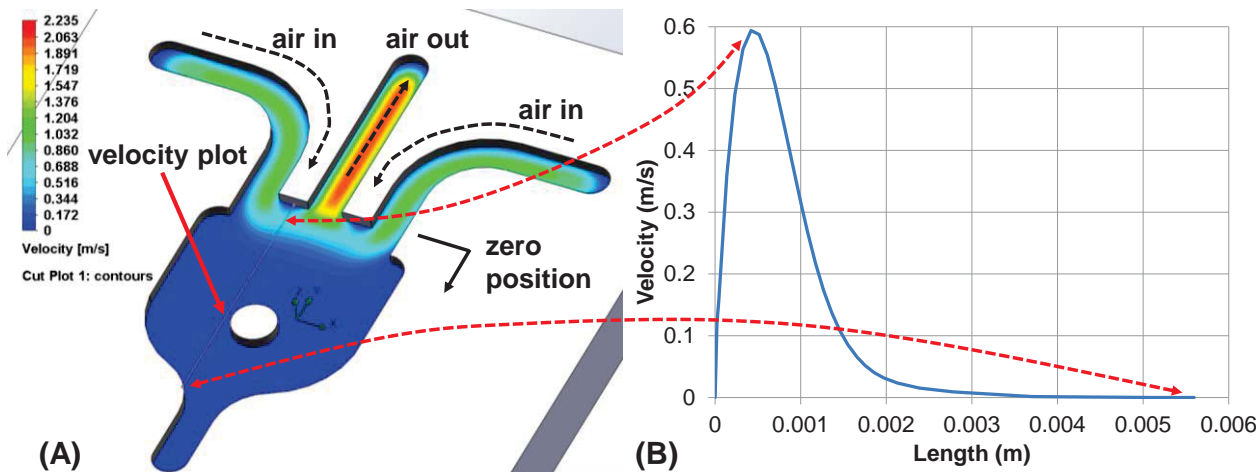


Figure 3-69. (A) Cavity flow simulation results – $920\mu\text{l/s}$ total inlet flow and (B) local velocity along sketch line

A value of $U_{\infty} = 0.6\text{ m/s}$ was put into the evaporation model from the flow simulation results. Similar simulations were performed for total inlet flows of 690 and $460\mu\text{l/s}$. These simulations gave $U_{\infty} \approx 0.45\text{ m/s}$ and 0.3 m/s respectively. All other values used in the model are provided in the MATLAB code in Appendix C.4.

The evaporation model is plotted for a range of 30 - 90°C with the experimentally determined values for a $9\mu\text{l}$ volume in Figure 3-70. The data shows good correlation to the model at the high flow velocity as seen in Figure 3-70(A). The larger discrepancy can be seen at the low pressure setting of 10 psi ($460\mu\text{l/s}$ inlet air flow) in Figure 3-70(B). For the lower flow setting, the difference between the experimental and predicted evaporations could be a result of overestimating air velocity in the model. The smaller surface area of the fluid as it recedes to the inlet could also have a more significant impact on the total evaporation time at the low flow rate. The reduced area

would result in a slower evaporation rate and a greater overall evaporation time than predicted by the constant rate model.

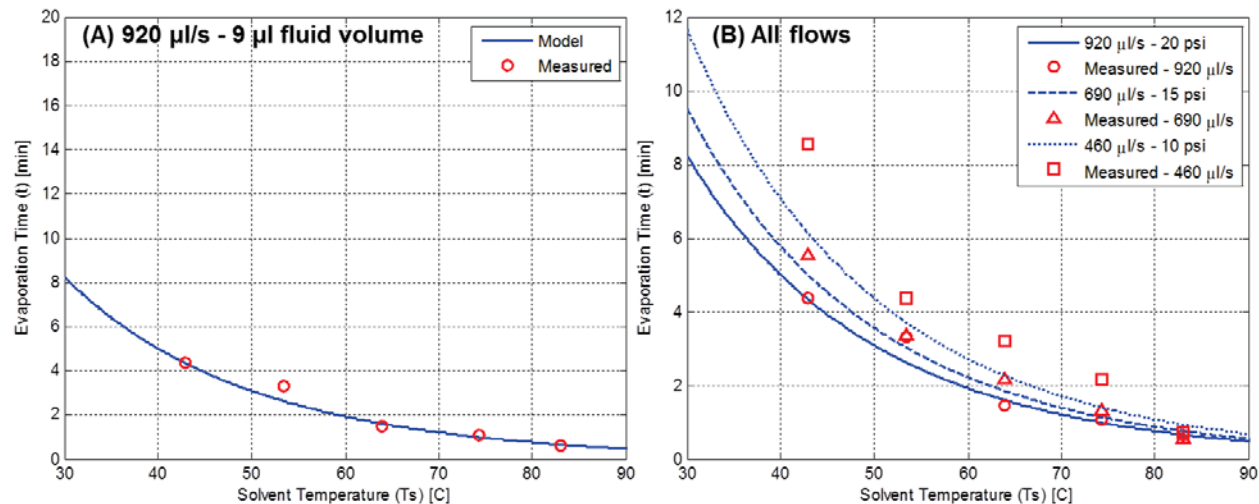


Figure 3-70. Comparison of evaporation model and measured data for (A) the 20 psi air-line pressure only and (B) all three pressure settings tested

3.7 HEAT TRANSFER

3.7.1 INITIAL HEATING SYSTEM AND TEMPERATURE CONSIDERATIONS

The first prototype used two positive temperature coefficient (PTC) heaters to raise the temperature of the cavity. PTC heaters are self-regulating because the resistance of the ceramic heater material increases exponentially with temperature as shown in Figure 3-71.

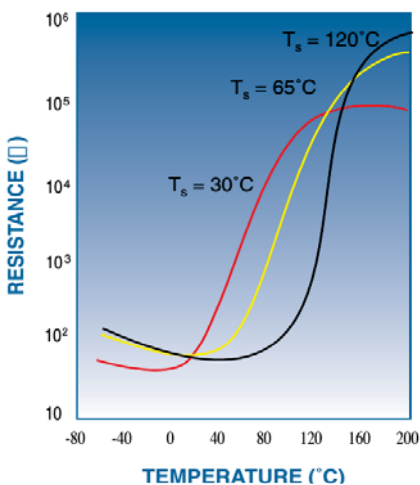


Figure 3-71. PTC heater temperature-dependent resistance curve examples [44]

The electric power consumed by the heater is given in Equation (3.20).

$$P = I^2 R = \frac{E^2}{R} \quad (3.20)$$

where,

I = current
 R = resistance
 E = voltage

At a certain temperature (the set temperature, T_s) the resistance increases asymptotically, and the power consumed by the heater drops off. The power must reach a point of equilibrium with external heat losses so that the temperature remains constant. The block used to heat the microfluidic cavity through the glass cover incorporated the heaters as shown in Figure 3-72.

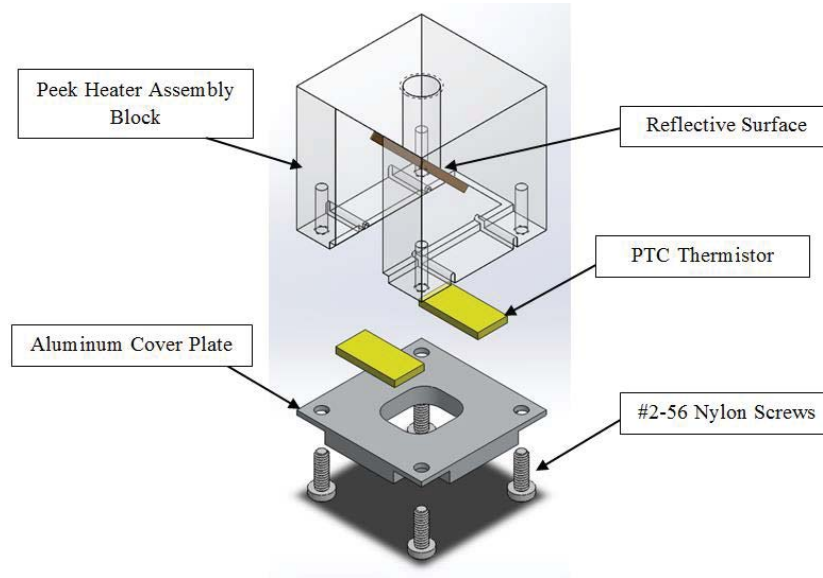


Figure 3-72. Heater setup for prototype 1

The initial heater setup was tested by placing a thermocouple between the cavity and glass as shown in Figure 3-73. Using two PTC thermistors rated for $T_s = 90^\circ\text{C}$ with a 12V power supply, the aluminum cover plate and glass cover were heated. A thermocouple was placed between the glass and FFKM cavity to measure the temperature.

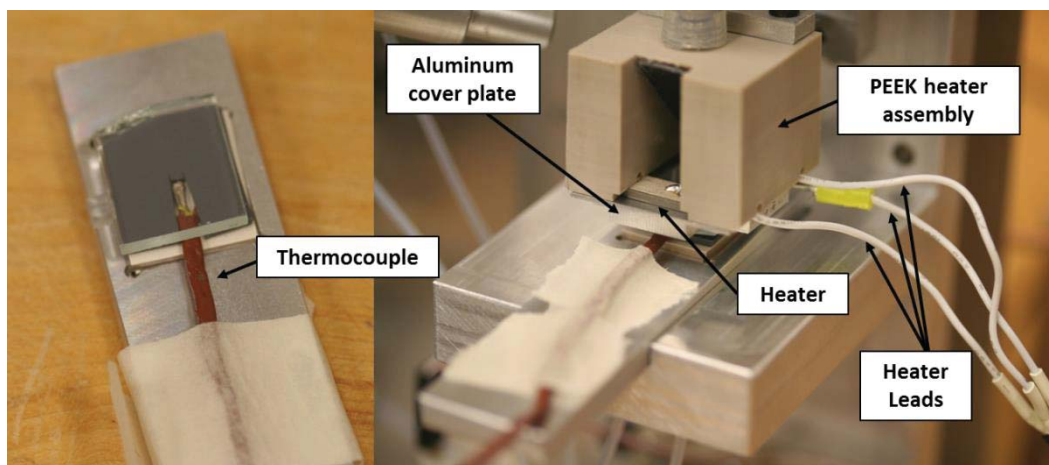


Figure 3-73. Cavity temperature measurement for initial heater setup

The resulting heat curve is shown in Figure 3-74. For this experiment the heaters were able to achieve a temperature of 78°C in the cavity.

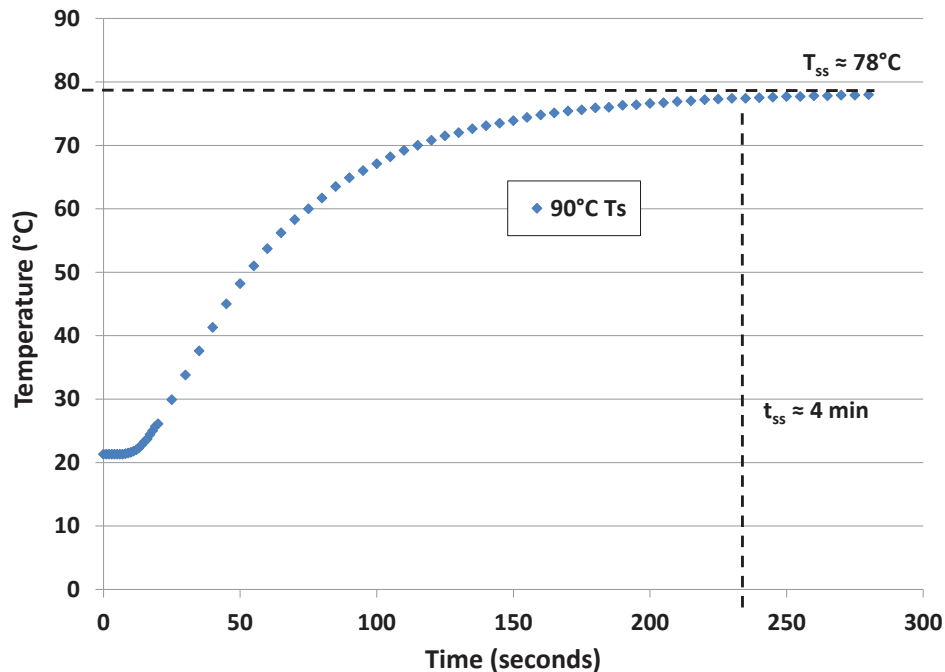


Figure 3-74. Cavity temperature measurements for initial heater setup

A temperature of 78°C is sufficient to extract certain dye types. Direct dyes were successfully extracted at this temperature (see Section 3.8.1). However, the extraction of Acid Yellow 49 dye was unsuccessful at 78°C. An alternative heating solution was developed to improve extraction capability and reduce heating time.

To add the ability to change the set temperature of extraction, thin film resistive heaters were investigated. This type of heater can produce a constant power input with the 12VDC power supply (constant R, see Equation (3.20)). Samples of OhmegaFlex thin film heaters were obtained and tested to determine temperature and control capabilities. The array of standard OhmegaFlex heaters is shown in Figure 3-75.



Figure 3-75. OhmegaFlex thin film heaters [45]

**The resistance of each heater is dependent on the length and width of the resistive material.
Resistance values are provided in**

Table 3-8.

Table 3-8. OhmegaFlex heater resistance values

Heater #	Resistance (R) [Ω]
1	5
2	9
3	26
4	33
5	60
6	65
7	62
8	342
9	435
10	475

3.7.2 HEATING MODEL

To use resistive heaters in the development of the second prototype, a heating model was developed to define the heating characteristics of the system. Initially, only heating of a small piece of aluminum and the glass cover was considered. Other surfaces were treated as insulating (an assumption that can result in a slight overestimation of rate of heating) and only heat loss through natural convection to the surrounding air was considered. This is shown in the model diagram in Figure 3-76.

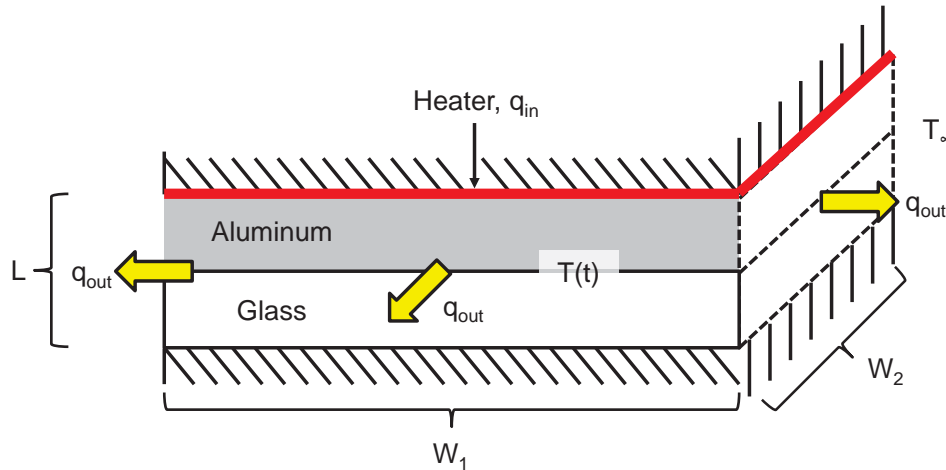


Figure 3-76. Model diagram for aluminum and glass heating analysis

To simplify modelling, the glass and aluminum are combined into one resistance to temperature change as shown in Equation (3.21). In addition, a lumped capacitance approach is considered. With these assumptions, the two bodies are treated as one temperature that has no spatial dependence.

$$m_{tot} c_{p,tot} = (m_g c_{p,g} + m_a c_{p,a}) \quad (3.21)$$

where,

m = mass

c_p = heat capacity

The subscripts g and a denote glass and aluminum respectively. There is a temperature gradient between the heater and the bottom of the glass, but in this model, the difference is assumed to be negligible. The time dependent temperature of the thermal mass is expressed in Equation (3.22).

$$m_{tot}c_{p,tot} \frac{dT}{dt} = q_{in} - q_{out} = \frac{E^2}{R} - hA_s(T - T_{\infty}) \quad (3.22)$$

where,

h = convective heat transfer coefficient

A_s = total surface area

The total surface area is the area around the perimeter of the aluminum and glass as given in Equation (3.23).

$$A_s = 2L(W_1 + W_2) \quad (3.23)$$

The heat loss, Q_{out} , is via natural convection. The natural convection coefficient, h , can be calculated using Equations (3.24)-(3.26) [43,46].

$$h = \frac{Nu \cdot k}{L} \quad (3.24)$$

$$Nu = 0.68 + \frac{0.67Ra^{1/4}}{\left[1 + (.492 / Pr)^{9/16}\right]^{4/9}}, Pr = 0.72 \text{ (for air at } 20^{\circ}\text{C)} \quad (3.25)$$

$$Ra = \frac{g\beta}{\alpha\nu}(T - T_{\infty})L^3 \quad (3.26)$$

where,

Nu = Nusselt number

Pr = Prandtl number

Ra = Rayleigh number

k = thermal conductivity of air

α = thermal diffusivity of air

β = thermal expansion coefficient of air

ν = kinematic viscosity of the air

The temperature is calculated using a simple finite-difference scheme. The solution is given in Equation (3.27).

$$\begin{aligned} \frac{dT}{dt} &= \frac{T_i - T_{i-1}}{\Delta t} = \frac{E^2}{Rm_{tot}c_{p,tot}} - h_iA(T_{i-1} - T_{\infty}) \\ \Rightarrow T_i &= \frac{E^2\Delta t}{Rm_{tot}c_{p,tot}} - h_iA(T_{i-1} - T_{\infty})\Delta t + T_{i-1} \end{aligned} \quad (3.27)$$

Using small time steps (Δt), the temperature at each step, i , can be calculated. A MATLAB program was written to evaluate the temperature and simulate cycling of the heater (see Appendix C.3). A desired high and low temperature are specified for the heater cycle. The heater voltage, E , is set to zero once the high temperature is reached. The only term in the equation is then the natural

convection cooling. When the temperature approaches the low temperature, the voltage is set back to high.

OhmegaFlex heaters 2, 3, and 4 were the best sizes for incorporation into the system. An example plot where $T_{\text{high}} = 100^{\circ}\text{C}$ and $T_{\text{low}} = 95^{\circ}\text{C}$ is shown for heaters 2 and 3 in Figure 3-77. Relevant dimensions and material properties can be found in Appendix C.3.

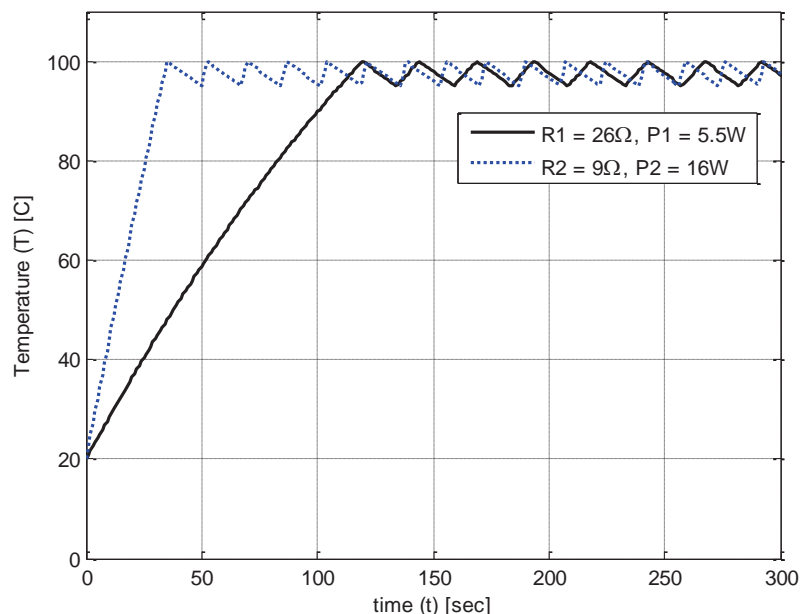


Figure 3-77. Heat cycling prediction

The convection coefficient is also a function of temperature and can be evaluated at each finite step. The model predicts a required heating time of 35 seconds for a 16W power input and 119 seconds for a 5.5W power input.

3.7.3 ANSYS TRANSIENT THERMAL ANALYSIS AND INITIAL HEATING TESTS

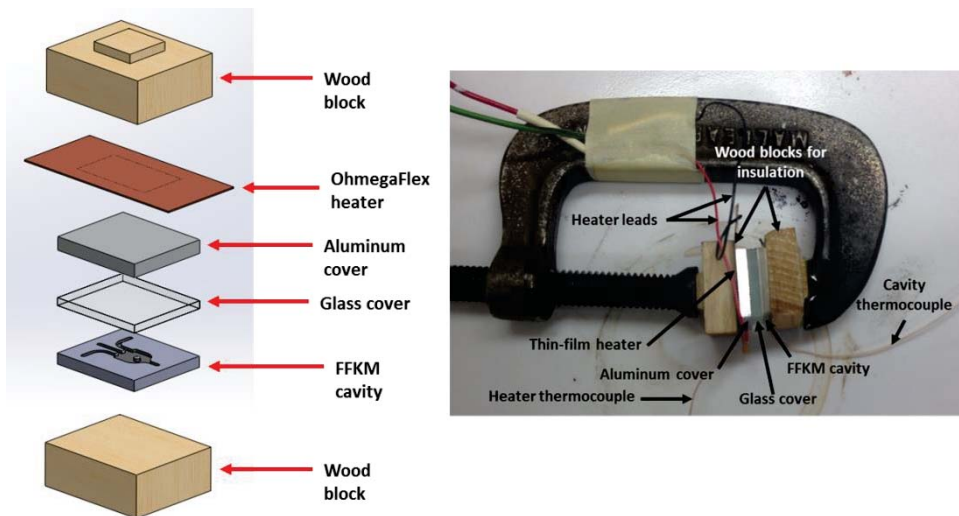


Figure 3-78. OhmegaFlex #4 heater test setup

The model presented for heating a small piece of aluminum with a glass cover predicts heating to 100°C within 90 seconds for a heat input of 6.8W (using the #4 heater with 15V). An ANSYS transient thermal model was examined to verify the time required for the bottom of the glass to reach the desired temperature and to observe the magnitude of the temperature gradient produced between the heater and cavity. A test apparatus was assembled as shown in Figure 3-78 and the temperature simulated using an ANSYS model.

The heater (OhmegaFlex heating element with copper backing) was placed between two wooden blocks, the FFKM cavity, a glass cover, and a piece of aluminum to simulate a well-insulated system. For the ANSYS model, convective boundary conditions were specified at all external surfaces with a convective coefficient of $h = 25 \text{ W/m}^2 \text{ } ^\circ\text{C}$ as shown in Figure 3-79.

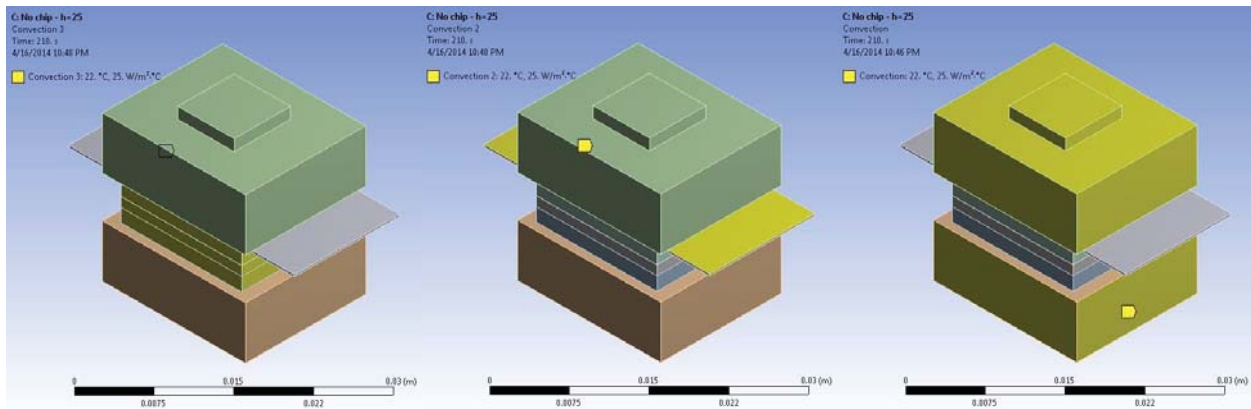


Figure 3-79. ANSYS model – surfaces with convection boundary condition, $h = 25 \text{ W/m}^2 \text{ } ^\circ\text{C}$

The heater and heating element were modelled as shown in Figure 3-80. The heating element has dimensions of 14 mm x 8 mm. A thickness of 0.1 mm was specified in the model. The internal heat generation option was used to create the 6.8 W heat input using a volumetric heat generation of $6.1607 \times 10^8 \text{ W/m}^3$.

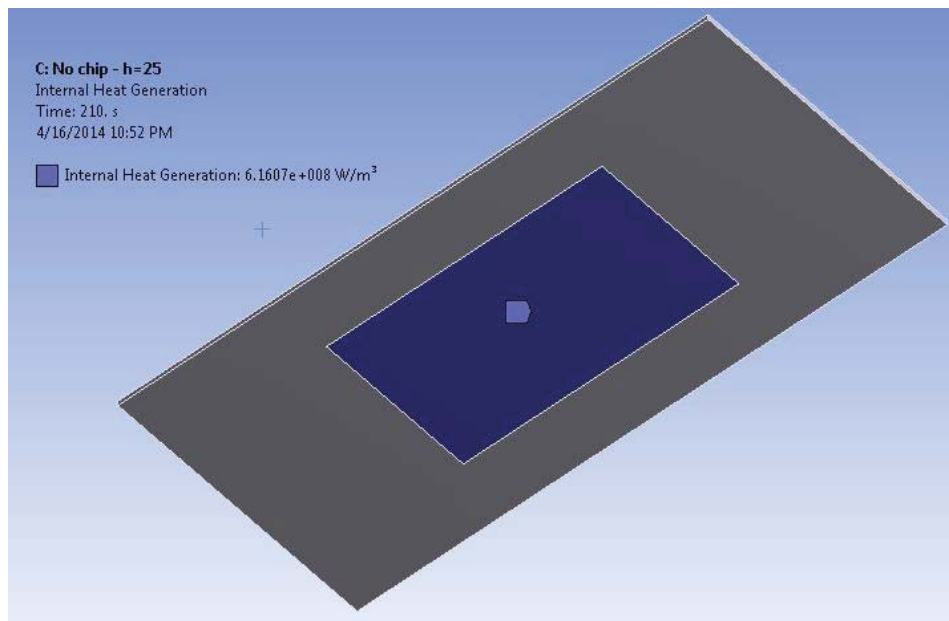


Figure 3-80. ANSYS model – internal heat generation specified for heating element

Temperature probes were placed in the model at the heater element surface and at the fiber holder in the cavity. The fiber holder surface is in contact with the glass and the temperature matches that of the bottom glass surface. The probe placements are shown in Figure 3-81.

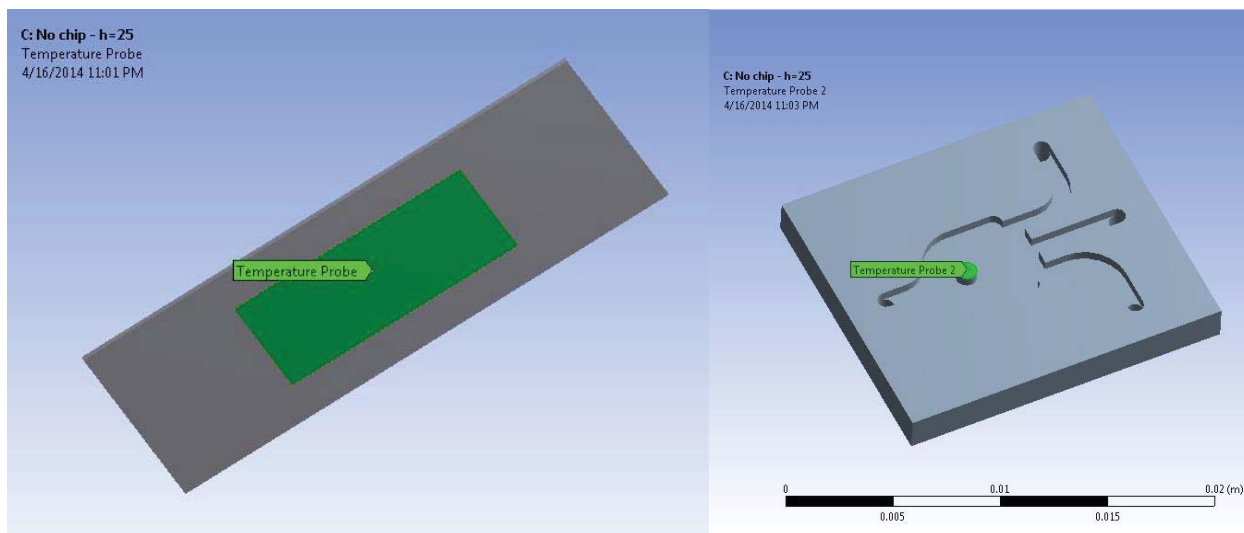


Figure 3-81. ANSYS model – temperature probe placements

The simulation time was set to 210 seconds. The final thermal state of the setup in the simulation is shown in Figure 3-82.

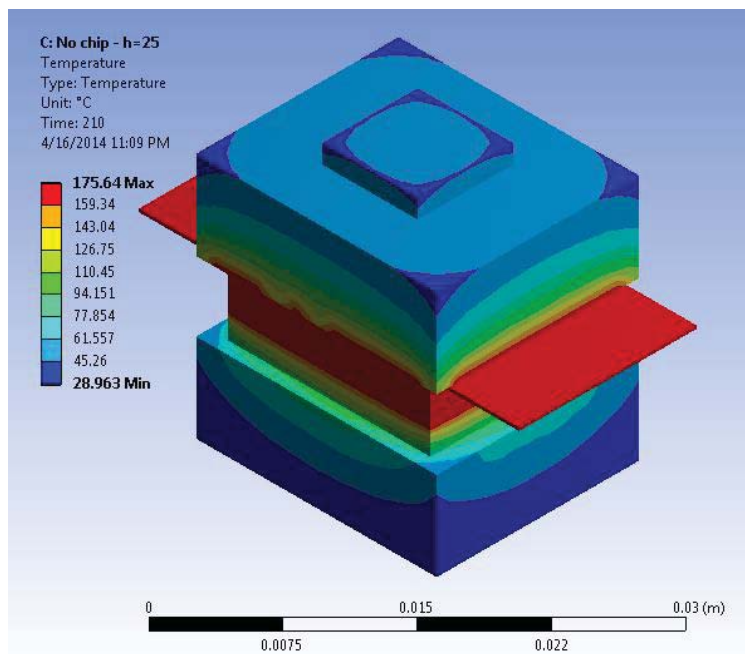


Figure 3-82. ANSYS model – thermal state at 210 seconds

The results of the simulation show good correlation to the test data over the time range of the test. A comparison of the temperature profiles of the heater and the bottom of the glass are shown in Figure 3-83.

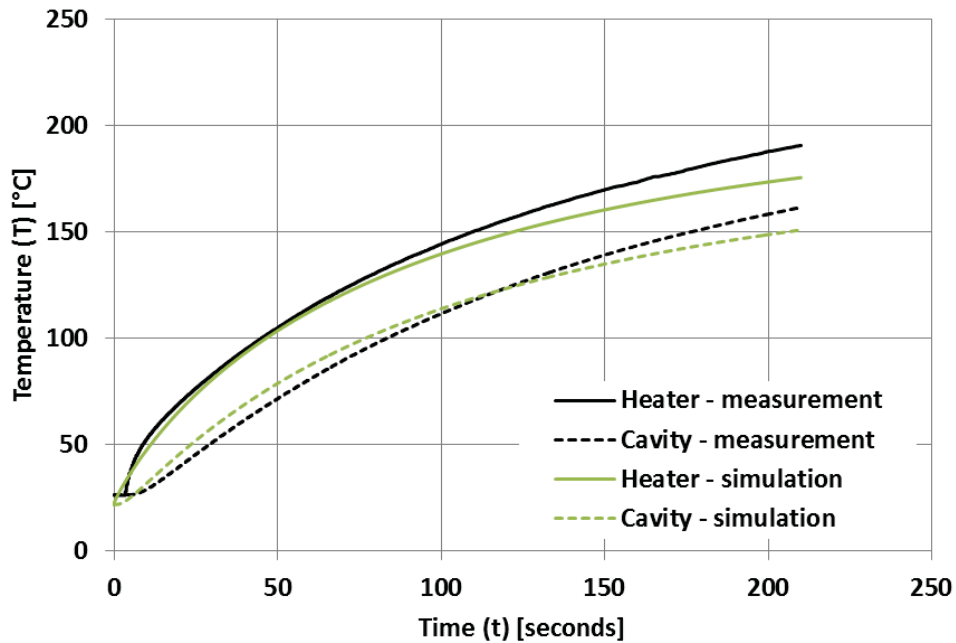


Figure 3-83. OhmegaFlex heater test and ANSYS simulation comparison

For the simulation, it was assumed all heat leaving the system was through convection. Under the conditions of the test, this would be caused by natural convection where the film coefficient (h) changes with the temperature of the components' external surfaces (see Equations (3.24)-(3.26) for temperature dependence of h). For the simulation, a constant film coefficient had to be specified. This could explain the discrepancy between the simulation and test results. In addition, there would be a small amount of conduction to the steel clamp used to hold the test setup together.

A second test was performed to evaluate the effects of the aluminum chip that is used to hold the cavity. The chip acts as an added heat sink, increasing the time required to raise the temperature of the system. The setup is shown in Figure 3-84.

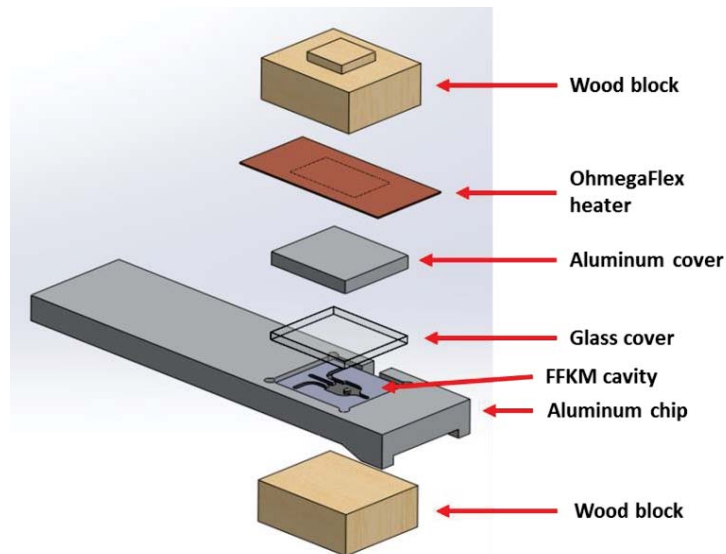


Figure 3-84. Heater test setup with aluminum chip

Using the same power input, test measurements were taken to show the chip's effect on the temperatures. The results are shown in Figure 3-85. The mass of the chip reduces the temperature rise. To improve heating, a chip was machined from PEEK to act as a better insulator ($k_{\text{PEEK}} = 0.4$ W/mK in comparison to $k_{\text{aluminum}} = 238$ W/mK).

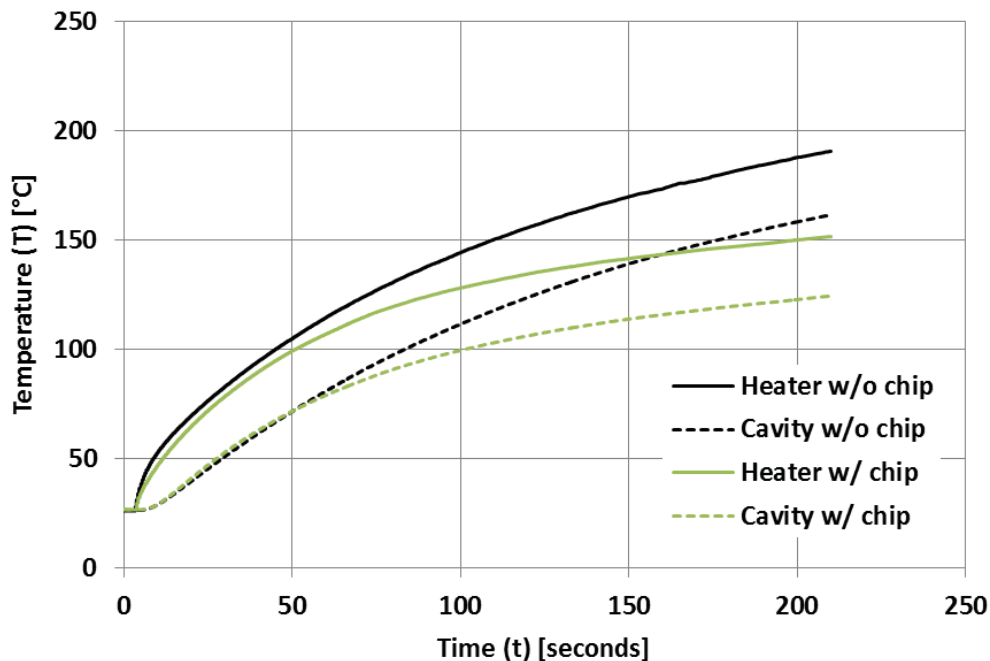


Figure 3-85. Heater test comparison with and without aluminum chip

The heating test results for the PEEK chip are shown in Figure 3-86. The PEEK chip significantly improved the heating results, motivating a change to PEEK material for the chip design.

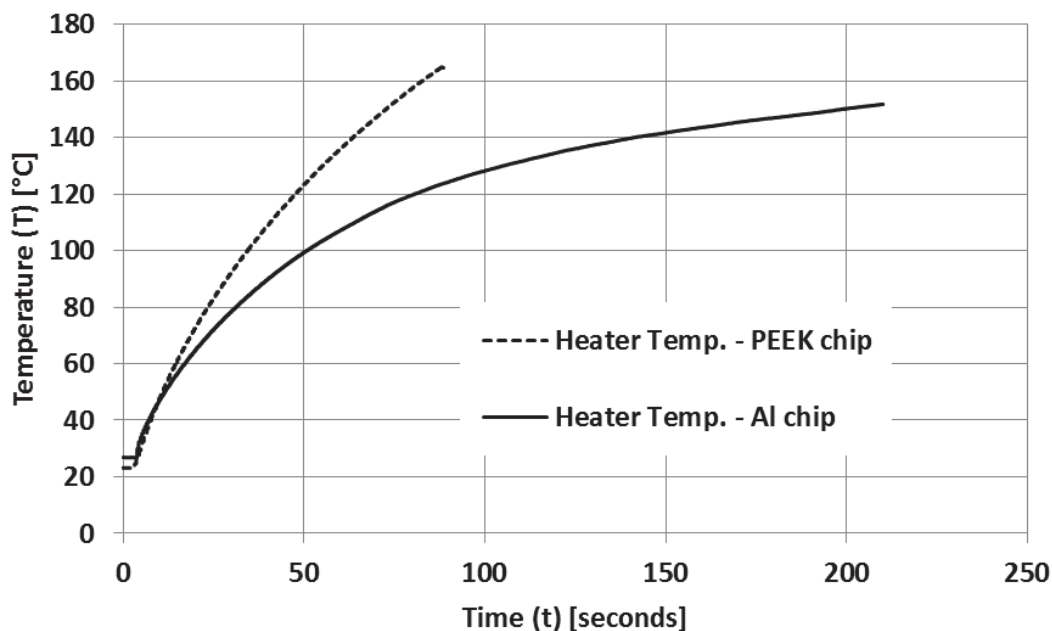


Figure 3-86. Comparison of heater temperatures using PEEK and aluminum chips

3.7.4 HEATER SELECTION

The OhmegaFlex thin-film, resistive heaters were used to determine power and time requirements for cavity heating. Unfortunately, most of the heaters tested failed after several tests. Failures occurred where the resistive material could not withstand the power density (power/area) being applied to the heater. The material burned and separated as shown in Figure 3-87, creating a break in the circuit. In addition, several heater lead connections were melted during heating as the temperatures exceeded 100°C. The manufacturer recommended that the power dissipation not exceed the specifications given in the P3 column of the catalog literature (shown in Figure 3-87 also).

RECTANGULAR HEATERS													
HEATER No.	RESISTANCE (Ω)	APPLIED D.C. CURRENT (Amp)			POWER DISSIPATION (W)			TEMPERATURE RISE (C)			TEMPERATURE RISE TIME (Sec)		
		I1	I2	I3	P1	P2	P3	T1	T2	T3	Time1	Time2	Time3
1	4.5	0.11	0.22	0.67	0.06	0.22	2.00	34	58	230	40	45	60
2	9	0.17	0.33	0.48	0.25	1.00	2.05	56	134	220	35	35	60
3	26	0.12	0.23	0.35	0.35	1.38	3.12	55	125	215	35	50	60
4	33	0.12	0.24	0.36	0.48	1.94	4.36	60	133	210	45	50	45
5	60	0.07	0.22	0.33	0.27	2.82	6.67	40	135	220	45	40	60
6	65	0.08	0.25	0.34	0.38	3.94	7.45	50	122	183	40	50	40
SERPENTINE HEATERS													
7	62	0.03	0.13	0.18	0.06	1.03	1.95	32	135	202	30	30	30
8	342	0.05	0.10	0.13	0.95	3.58	5.66	63	158	225	30	30	50
9	435	0.04	0.10	0.11	0.74	4.06	5.30	52	157	185	30	40	35
10	475	0.05	0.10	0.11	1.42	4.45	6.14	50	107	135	30	45	30

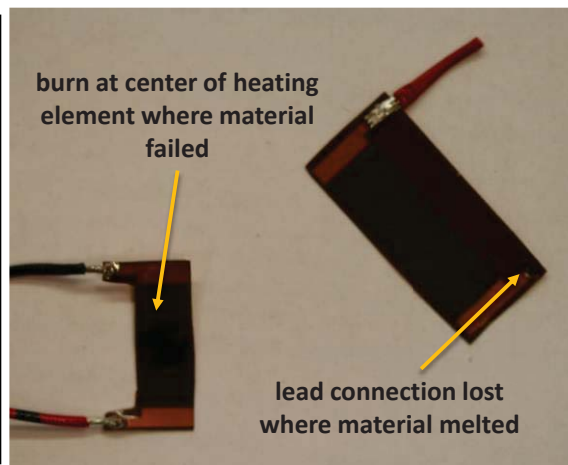


Figure 3-87. OhmegaFlex heater specifications [45] and failed heater samples

A heater with the ability to withstand a higher power density was required. A variety of thin-film heater options are available from Birk Manufacturing, Inc. A 0.5" x 0.5" heater with a resistance of 10.5Ω was selected for the new heater assembly. The selected heater comes with a 0.25" extended tab with built in lead connections as shown in Figure 3-88. With the 12 VDC supply voltage, the heater produces 13.7 W.

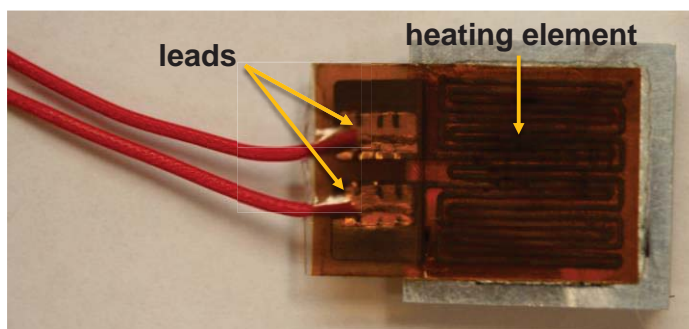


Figure 3-88. Birk heater: BK3546-10.5-L24-01

The Birk heater was placed in a similar test setup to the OhmegaFlex heater shown in Figure 3-84 with a PEEK chip in place of the aluminum chip. The heater was manually cycled on and off between approximately 93°C and 107°C. The results are compared to the analytical model in Figure 3-89. The model frequency matched the measured data and showed good repeatability.

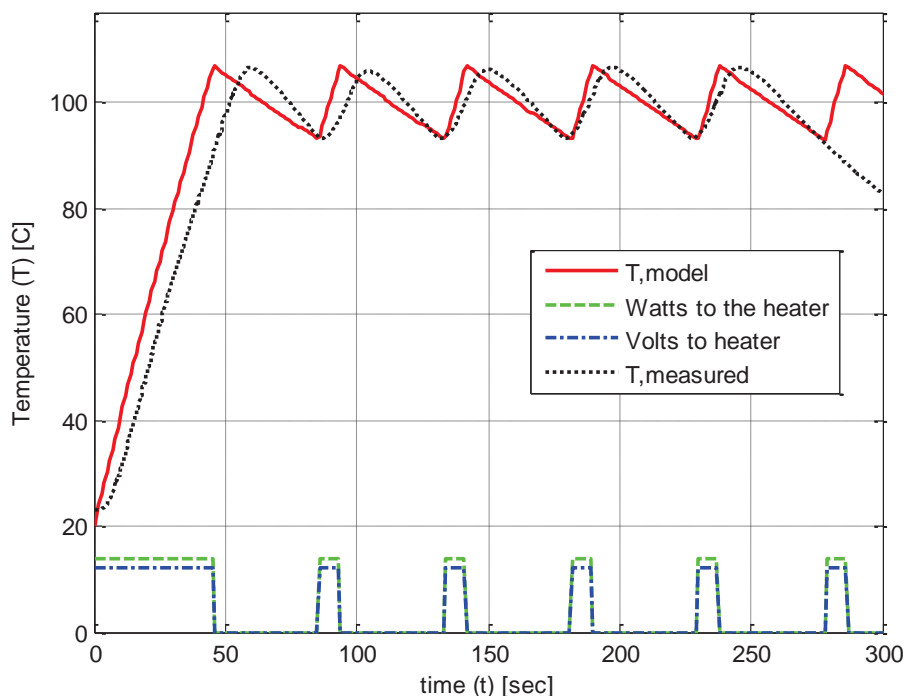


Figure 3-89. Birk heater model and test data comparison

3.7.5 COOLING MODELS

The Textile Chemistry department has shown that acid dyes require higher temperatures to completely remove dye from a fiber for successful detection in a mass spectrometer. Their initial recommendation was to extract at temperatures between 90-115°C for these dyes. The thin film heater had been used effectively to obtain this temperature range in the microfluidic cavity in little more than one minute. However, the high cavity temperature requires too much time to cool before the buffer is injected. The residual heat raises the temperature of the buffer solution, an undesirable side effect.

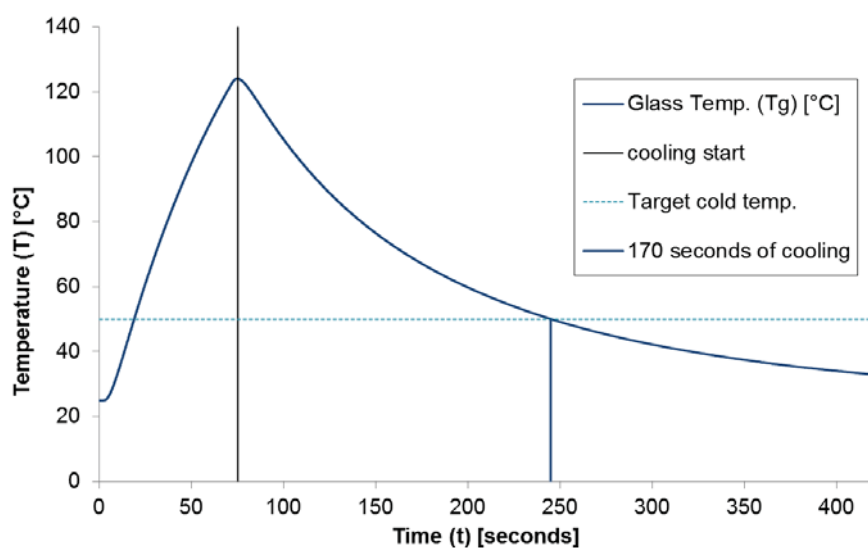


Figure 3-90. Heating and cooling in MFD without air-flow

Heating and cooling of the aluminum and glass cover are shown in Figure 3-90. Cooling of the glass to 50°C is shown to take 170 seconds (~3 minutes). If the buffer filling steps are initiated only after cooling, a significant amount of time is added to the overall process.

To increase cooling efficiency, two cooling methods were tested. A modified heater assembly concept is shown in Figure 3-91 that makes use of compressed air to facilitate cooling. A second system with an axial fan was also tested with the assembly.

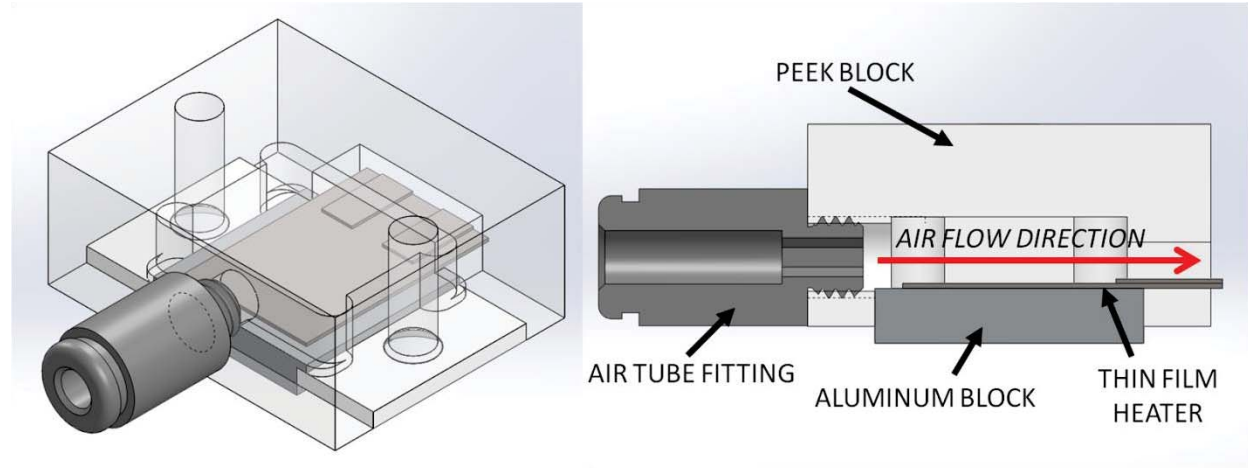


Figure 3-91. Heater assembly modification for compressed air cooling

Air flow can be initiated before the buffer fill step to remove heat directly from the heater and aluminum. As the aluminum cools, heat is also drawn away from the glass cover slip. To estimate the effect of the added cooling capability, the model in Figure 3-92 was created.

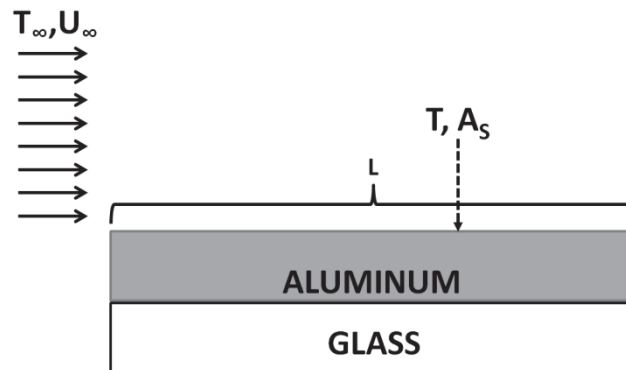


Figure 3-92. Cooling model diagram

By assuming the two masses have a single temperature, the rate of change of temperature is expressed in Equation (3.28).

$$\frac{dT}{dt} = \frac{-hA_s}{m_{tot}c_{p,tot}}(T - T_{\infty}) \quad (3.28)$$

The forced convection heat transfer coefficient can be determined from Equations (3.29)-(3.32).

$$h = \frac{Nu \cdot k}{L} \quad (3.29)$$

$$Nu = 0.664 Pr^{1/3} Re^{1/2} \quad (3.30)$$

$$Pr = \frac{\nu}{\alpha} = 0.72 \text{ (for air at } 20^\circ\text{C)} \quad (3.31)$$

$$Re = \frac{U_\infty L}{\nu_\infty} \quad (3.32)$$

Solving Equation (3.28), the time dependent temperature is given in Equation (3.33).

$$T(t) = T_\infty + (T_i - T_\infty) e^{\frac{-hA_s}{m_{tot}c_{p,tot}}t} \quad (3.33)$$

Assuming a starting temperature of 120°C, the cooling curves are compared to the test data. The compressed air configuration was calculated with $U_\infty = 5$ m/s. The velocity could not be directly measured, so the value was iterated with the model to match the test data. A comparison of the model and test data is shown in Figure 3-93.

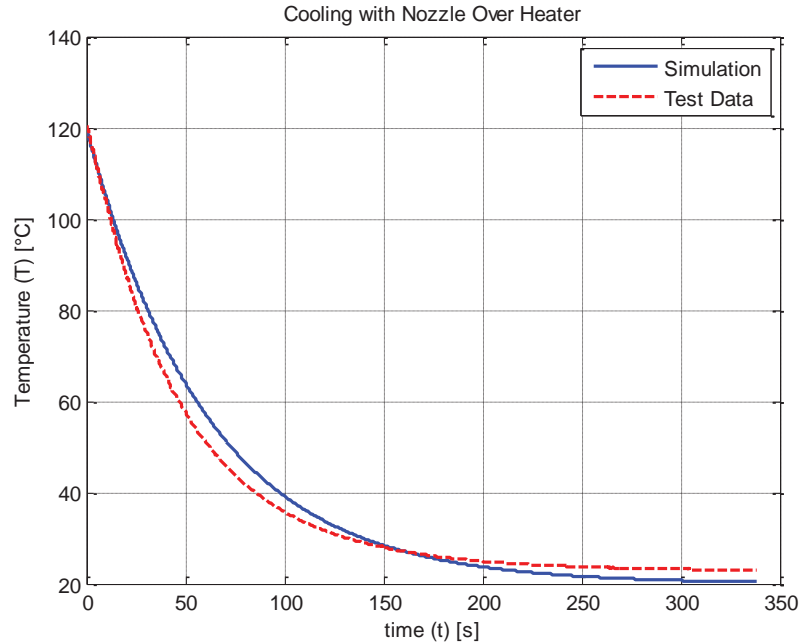


Figure 3-93. Nozzle cooling model vs. test data

The model shows good correlation with the measured data. At a target temperature of 50°C, the model predicts a time of 73 seconds. Measured data shows a cooling time of 69 seconds as shown in Figure 3-94. The addition of the air flow path over the heater and aluminum reduced the time to cool to 50°C by 60%.

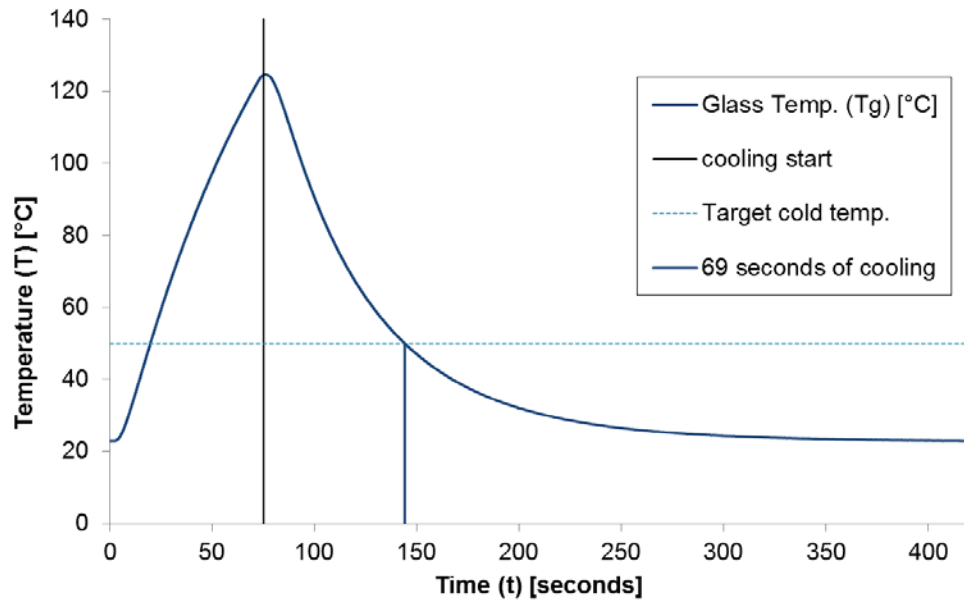


Figure 3-94. Measured glass temperature with nozzle cooling

The second method tested used a computer fan (SUNON KD1208PTB1-6, 2.6 W, 42.5 cfm) to cool the assembly by directing airflow from the side as shown in Figure 3-95.

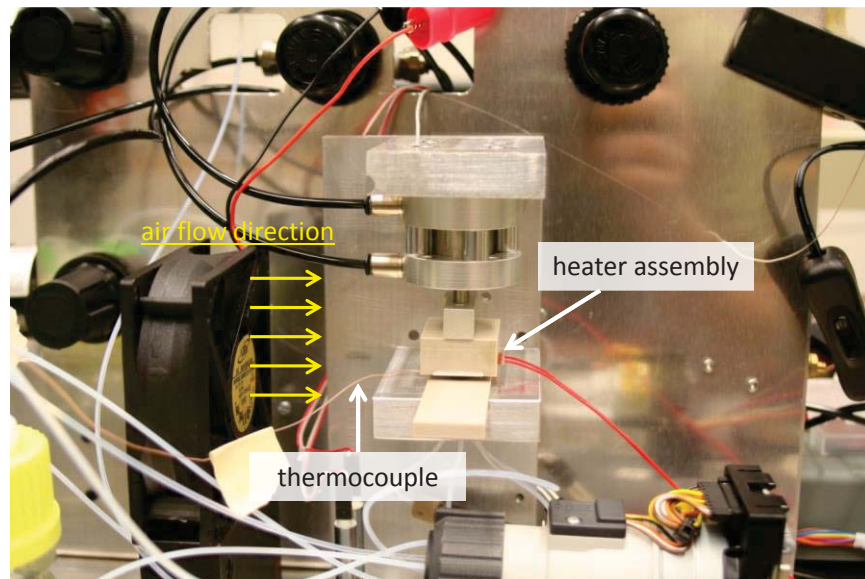


Figure 3-95. Fan cooling setup

Air flows over the bottom of the aluminum surface (between the chip and PEEK block). The length and area are larger for the model. The characteristic length is 30 mm (compare to 16 mm for nozzle cooling) and the area is $\sim 5.1 \text{ mm}^2$ (compare to $\sim 2.6 \text{ mm}^2$ for nozzle cooling). The flow velocity is significantly lower, however, resulting in a net cooling rate slower than that of the nozzle. The air flow velocity was measured near the heater assembly with a Fluke 922 air flow meter. The velocity was between 1.0 and 1.5 m/s. A value of 1.1 m/s was used in the model.

Calculated cooling is compared to test data in Figure 3-96. Again, the model curve matches the test data curve well.

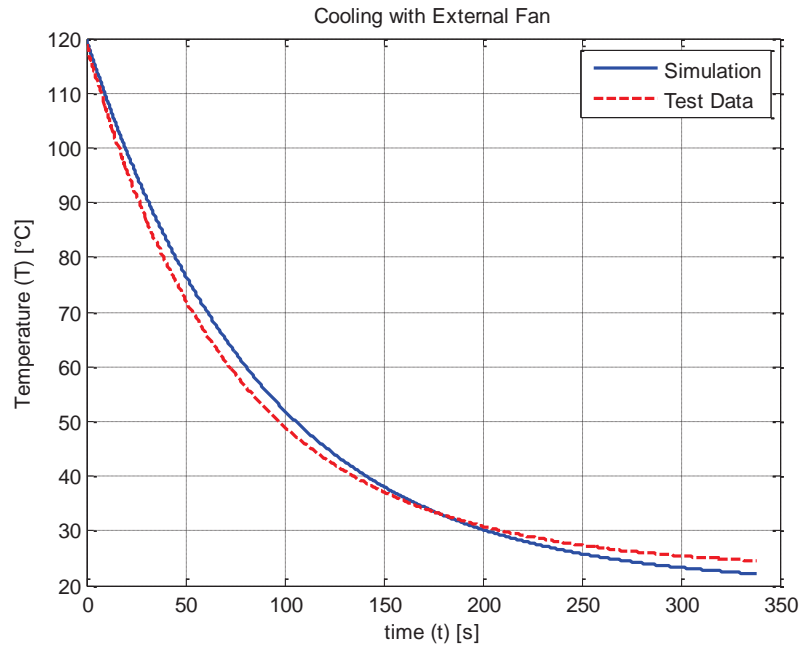


Figure 3-96. Fan cooling model vs. test data

For a target temperature of 50°C, the model predicts a cooling time of 106 seconds. Measured data shows a cool down time of 104 seconds as shown in Figure 3-97.

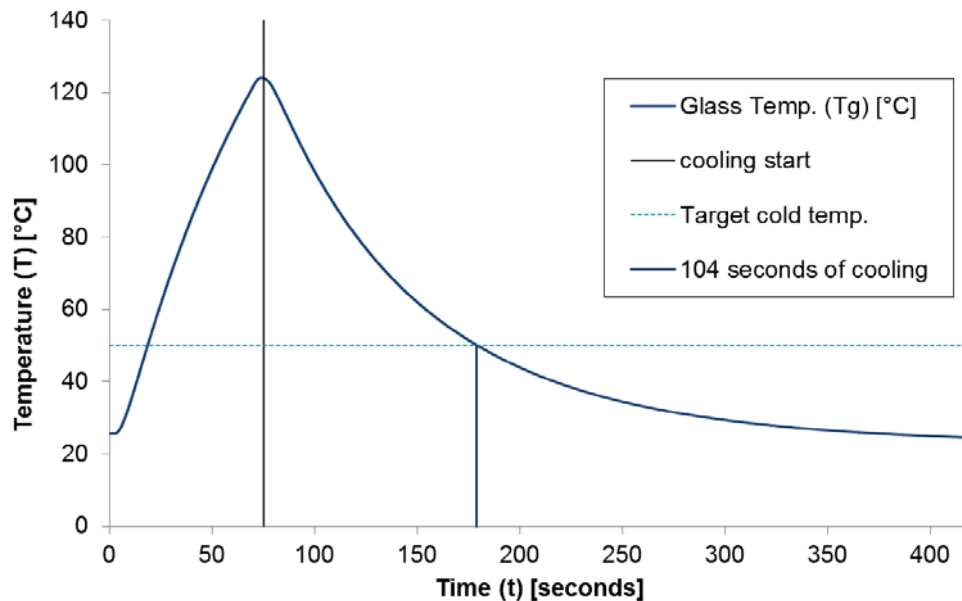


Figure 3-97. Glass temperature with fan cooling

The addition of the fan reduces the time to cool to 50°C by 39% of the no air-flow cooling time. Measured data for each method is displayed in Figure 3-98 with a target cool temperature of 50°C. The time required to cool from 120°C to 50°C is shown for each cooling setup. Without any air flow over the setup, cooling to 50°C took 170 seconds. Cooling with the fan was shown to take 104 seconds and 69 seconds for the compressed air.

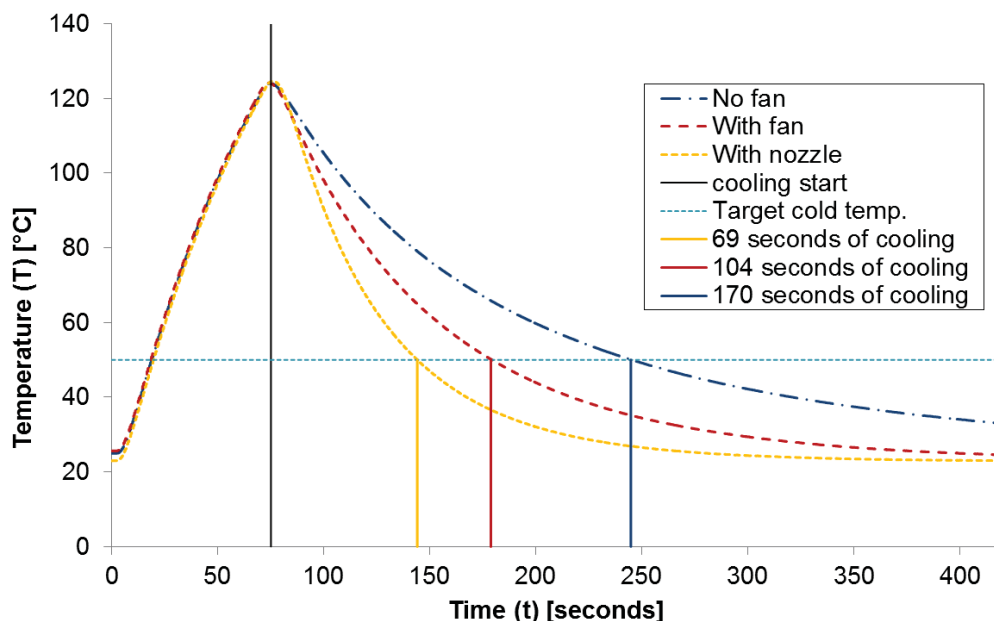


Figure 3-98. Comparison of cooling methods – measured data

3.7.6 HEATER CYCLING

Using the heating and cooling curves of the system, a calibration method was developed to cycle the heaters on and off to maintain a set temperature. Details on the calibration of the system are provided in Appendix F. Because the heating and cooling modes of the system are consistent, open loop control was used to cycle the heaters. Temperature curves for the heater system in a lab room held at 22°C are shown in Figure 3-99. Calibrations were also performed for fume hood testing and the enclosure used in prototype 2.

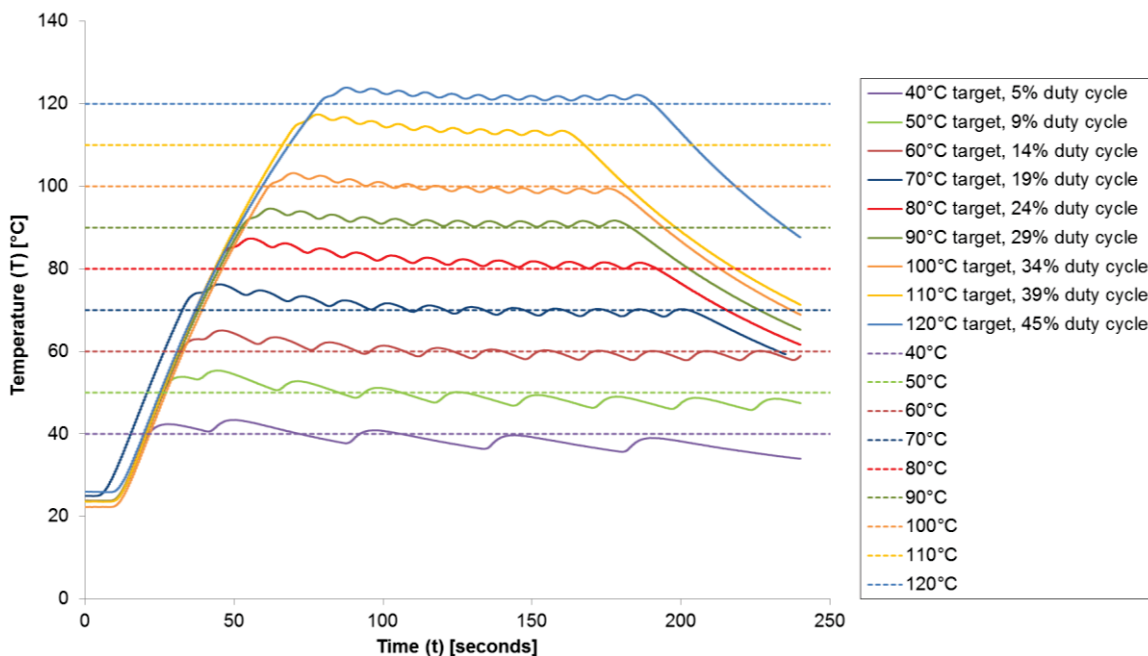


Figure 3-99. Measured cavity temperatures for set values

3.8 EXTRACTION TESTING

Extractions were performed with the first prototype using the PTC and thin-film heater configurations and 20 psi at the air inlet (920 $\mu\text{l/s}$ of total air flow). Initial extractions were performed where the cavity was heated with ceramic PTC heaters (Section 3.8.1). Further extractions were performed with the thin-film heater setup (Sections 3.8.2 and 3.8.4). All extractions were performed with thread less than 5 mm in length. A thread is a strand of natural or synthetic fibers that are twisted together.

3.8.1 EXTRACTIONS WITH PROTOTYPE 1 – PTC HEATERS

The first extraction was performed with Cavity V5. The system layout for the first extraction is shown in Figure 2-8. A thread dyed with Direct Red 81 ($\text{C}_{29}\text{H}_{21}\text{N}_5\text{O}_8\text{S}_2$) dye was placed in the FFKM cavity as shown in Figure 3-100. The thread was approximately 4.5 mm long and held in place by pressing it between the FFKM and glass cover.

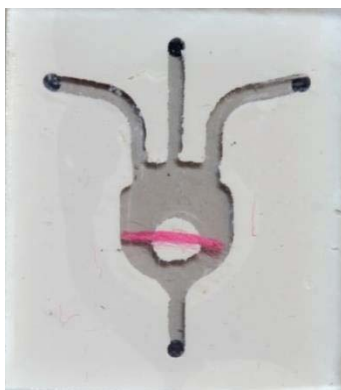


Figure 3-100. Fiber placement in cavity

The chip and cavity were then placed in the extraction device and clamped to the base manifold by a pneumatic cylinder as shown in Figure 3-101.

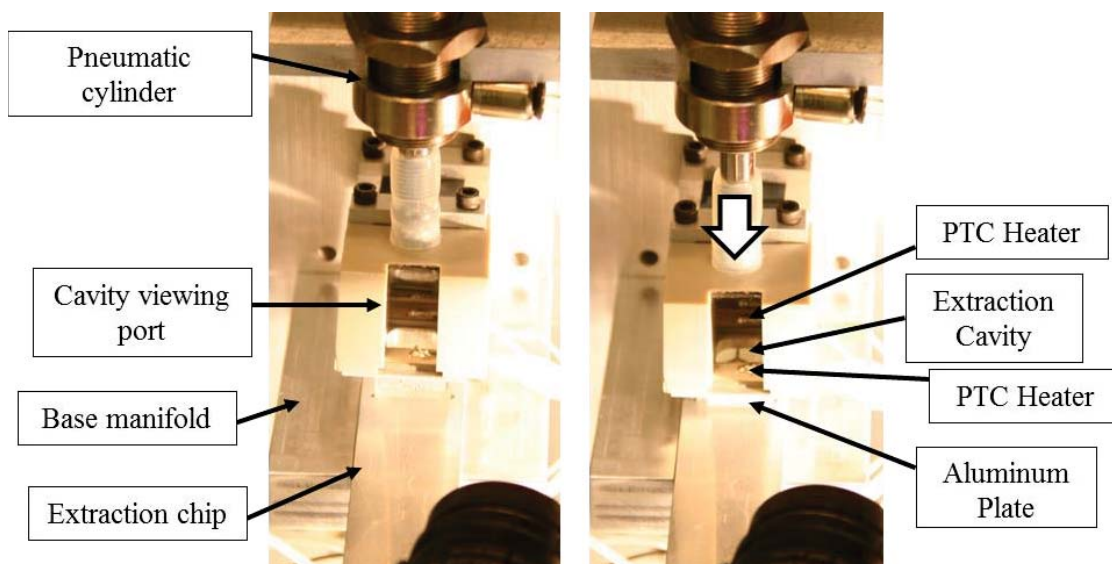


Figure 3-101. Clamping of extraction chip and microfluidic cavity in device for extraction

The extraction sequence was initiated by turning on the two PTC heaters embedded in the clamping fixture at the base of the pneumatic cylinder rod. The heaters heat the aluminum plate at the base of the clamping fixture. Heat is transferred through the glass to the cavity, which reaches a temperature of about 78°C in 4 – 4.5 minutes. The pyridine:water solution (4:3 ratio) was pumped into the cavity during heating. The cavity fill is shown in Figure 3-102.

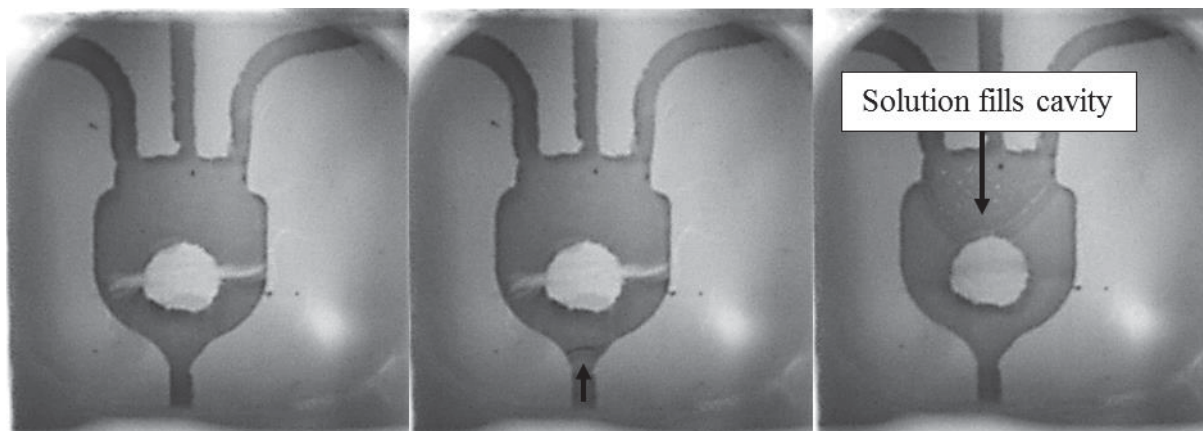


Figure 3-102. Introduction of pyridine:water solution to cavity

The extraction was performed by continuously applying heat through the glass and allowing the fiber to remain in the heated solvent for 10 minutes. Air was then pumped through the device over the fluid surface to evaporate the solvent. Small amounts of dye appeared to be left behind on the glass and FFKM. The evaporation of the fluid can be seen in Figure 3-103.

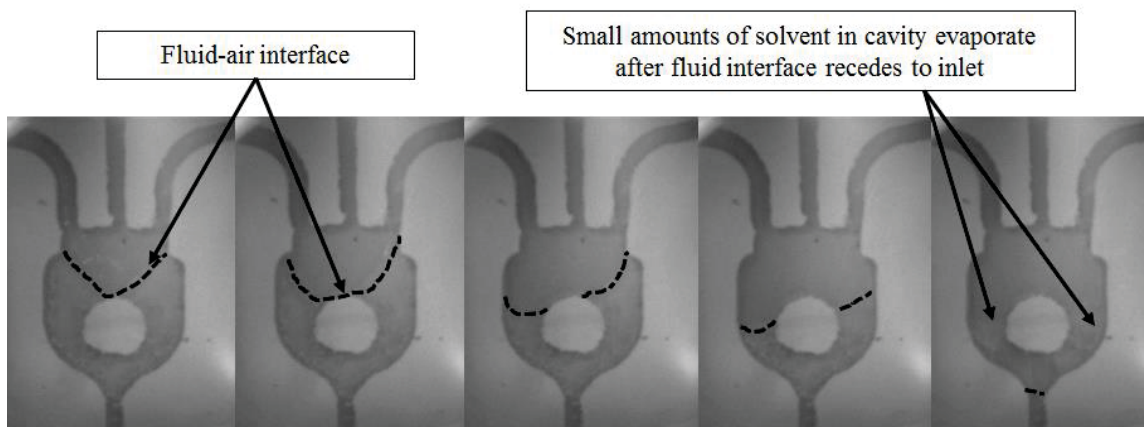


Figure 3-103. Surface profile of fluid during evaporation

The evaporation process was allowed to operate for three minutes to ensure complete evaporation of the solvent. Excess solvent in the tubes was pumped in reverse (i.e. back through the inlet) to a waste container. A buffer solution (97% water, 3% ACN:MeOH) was then pumped into the cavity to dissolve dye stuck to the glass and FFKM surfaces. After five minutes, the solution was then pumped in reverse to a sample container. The total sample volume was approximately 150-200 μL (total volume of the system with directional-control and shut-off valves). This was determined by measuring the volume of fluid pulled out of the sample container with a syringe. Visual inspection shows that the majority of dye was successfully separated from the fiber as shown in Figure 3-104.

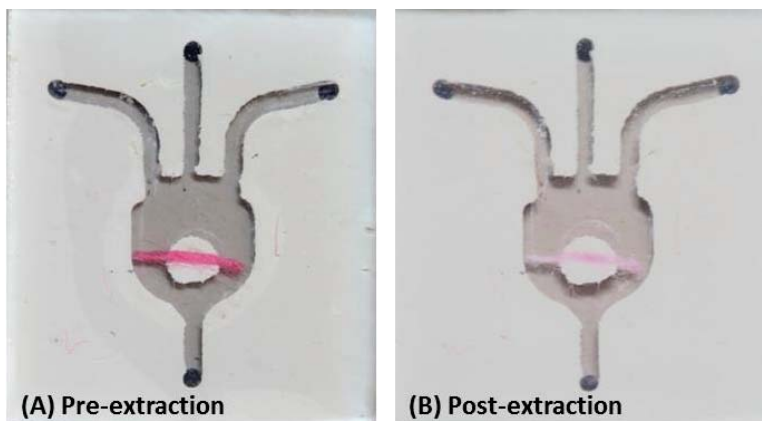


Figure 3-104. Fiber with Direct Red 81 dye (A) before extraction process and (B) after extraction process

Analysis of the sample in the mass spectrometer showed peak detection for the dye. The characteristic ions for the dye have a mass to charge ratio (m/z) of 630.04. The ions were detected as shown in the mass spectrum in Figure 3-105.

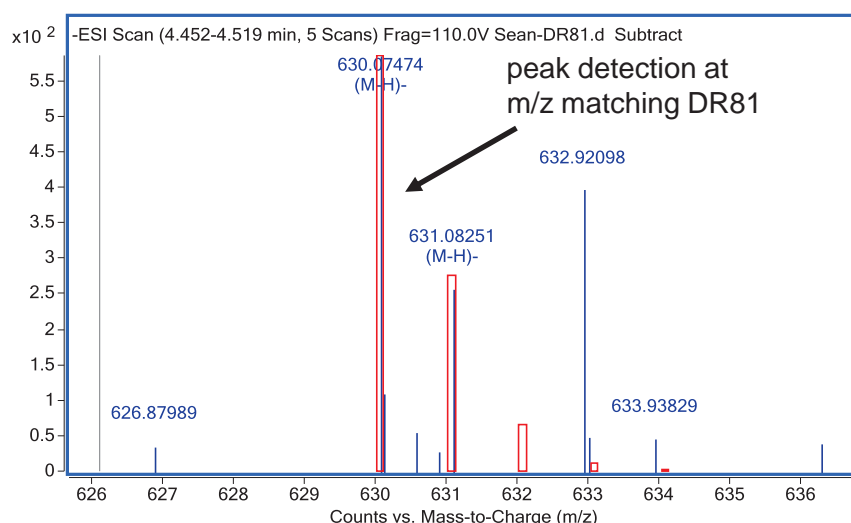


Figure 3-105. Mass spectrum results of Direct Red 81 ($C_{29}H_{21}N_5O_8S_2$) dye extraction

Three extractions were performed using this method. Two threads containing Direct Red 81 and one dyed with Direct Green 26 ($C_{50}H_{33}N_{12}Na_5O_{18}S_4$) were tested. Dye could only be detected in one sample (DR81). The odor of pyridine was noticeable in the samples, indicating possible contamination of the samples with the solvent. The possible causes for this contamination were determined to be related to the directional control valves as discussed in Appendix B.

Cavity V6 was used for further extractions to avoid contamination of the samples by residual solvent. As discussed in Section 3.4, Cavity V6 provides separate inlets for solvent and buffer. The valve array at the inlet is simplified, and the solvent and buffer can be separated to prevent possible contamination. Problems with air expansion during heating prevented the cavity from being a permanent solution (see Section 3.4); however, several extractions were performed with it. A successful extraction of Direct Green 26 was achieved.

A thread of ~2 mm length (dyed with DG26) was used for extraction. The solvent fill, heating for extraction, and evaporation of solvent processes are shown in Figure 3-106. Dye that is separated from the fiber could clearly be seen at the fluid-air interface after heating for 10 minutes. As air flowed into the cavity to evaporate the solvent the dye appeared to be deposited at the base of the fiber holding post and in small amounts on the FFKM and glass. The final image (Figure 3-106(F)) shows a clear removal of dye from the fiber.

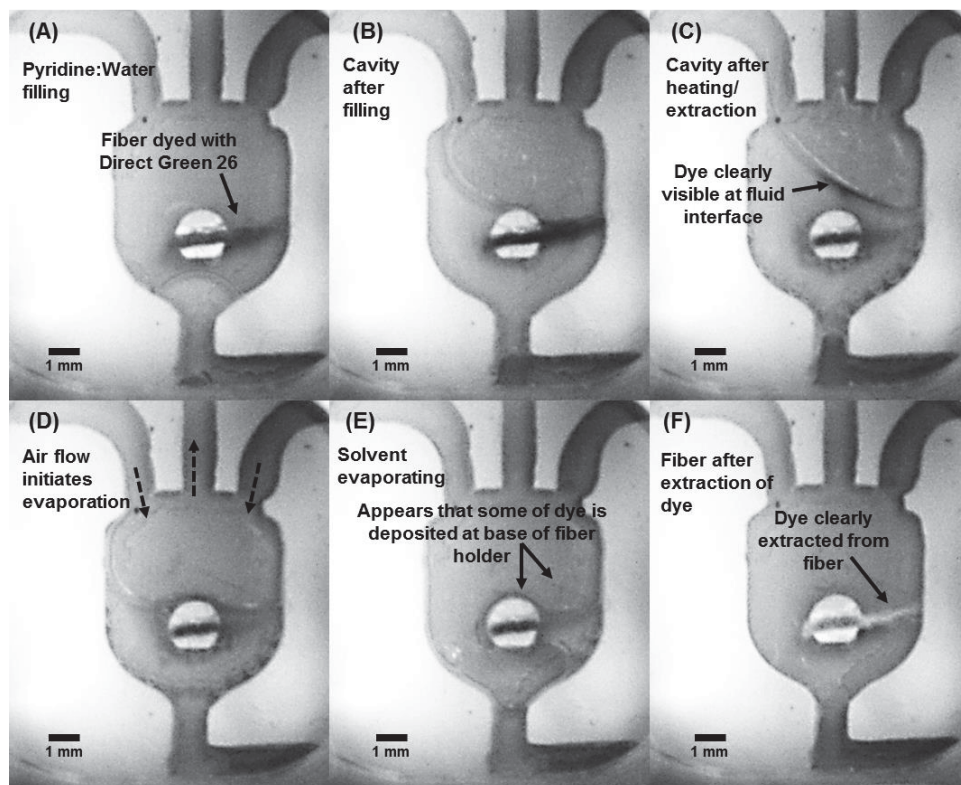


Figure 3-106. Solvent fill, dye extraction, and evaporation for DG26 (cavity V6)

A slight overfill of the cavity during the buffer fill step and expansion of air trapped in the solvent leg forced some of the buffer into the air outlet. This portion of the sample was lost. In addition, a few μ l of sample fluid were trapped in the solvent inlet leg and between the fiber post and cavity wall as shown in Figure 3-107.

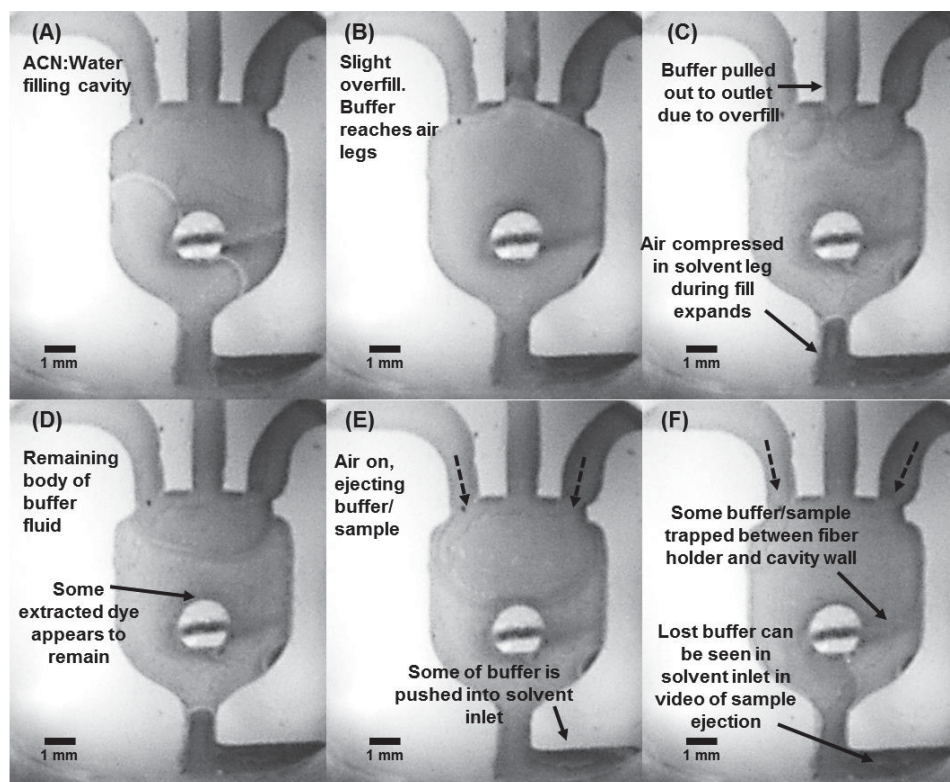


Figure 3-107. Buffer fill, dye pick up, and sample ejection for DG26 (cavity V6)

Upon making contact with the air outlet (top center of the cavity) a portion of the fluid body was pulled out by capillary force (Figure 3-107(C)). Another portion of the buffer in the cavity was trapped in the solvent inlet during sample ejection (Figure 3-107(E)-(F)). In addition, a small amount of buffer was trapped between the fiber holder and the right side of the cavity wall, never making it to the sample container (Figure 3-107(F)).

Examination of the thread clearly shows successful extraction of dye. This is shown in Figure 3-108.

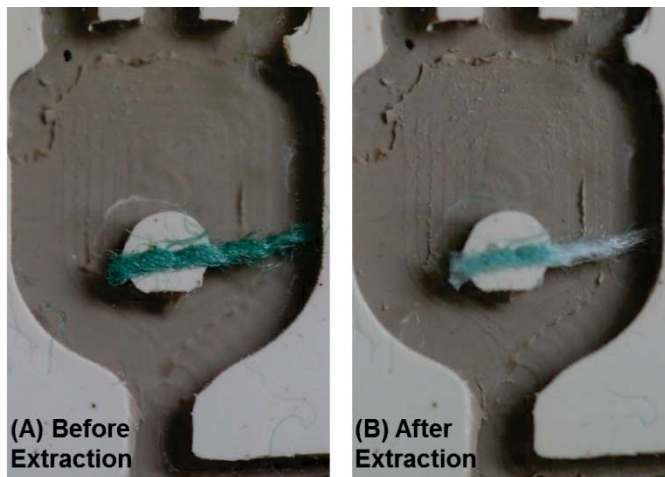


Figure 3-108. Thread dyed with DG26 (A) before and (B) after extraction

Analysis in the mass spectrometer showed peak detection at the characteristic ion of the DG26 dye as well, however, it was not significant. The mass spectrum of the extracted sample is shown in Figure 3-109.

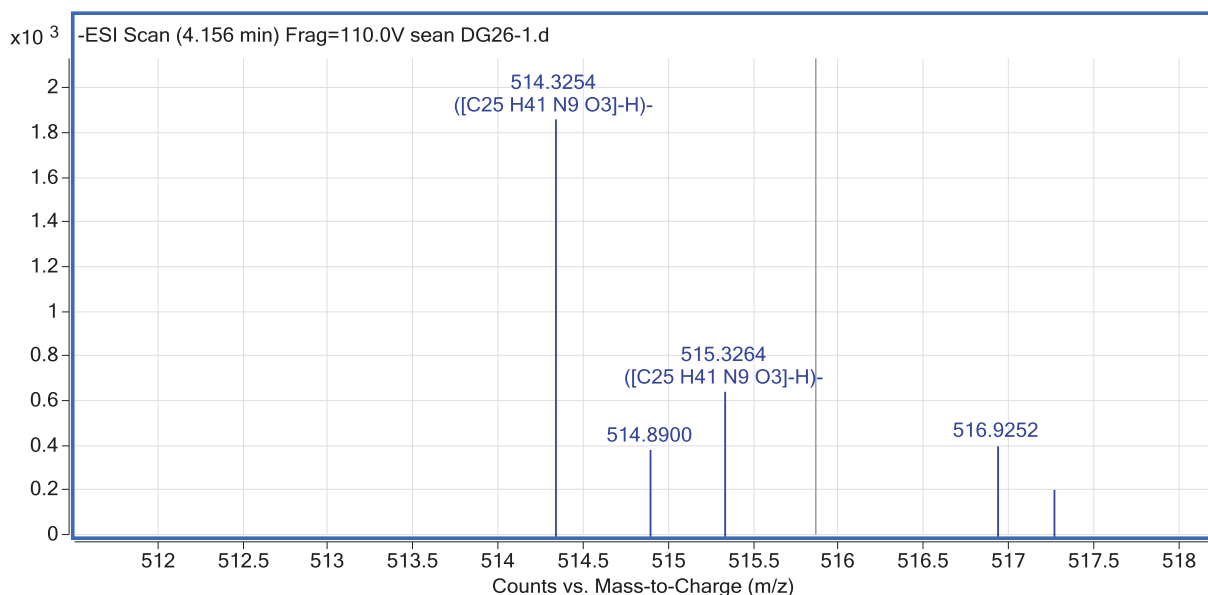


Figure 3-109. Mass spectrum results of Direct Green 26 (C₅₀H₃₃N₁₂Na₅O₁₈S₄) dye extraction

Cavity V6 was used in further extraction tests with Acid Yellow 49 dyed threads ~2 mm long. Inconsistencies in the cavity fill and difficulty with expanding air in the inlet legs resulted in several failed attempts to extract the dye. Two extractions were finally performed, where the process operated as desired. Heating for extraction was performed for 5 and 10 minutes for the tests. Visual inspection of the fibers indicated that most of the dye remained in the fiber for the first extraction (5 min), and much of the dye was extracted in the second (10 min). The fibers used in the tests are shown in Figure 3-110.

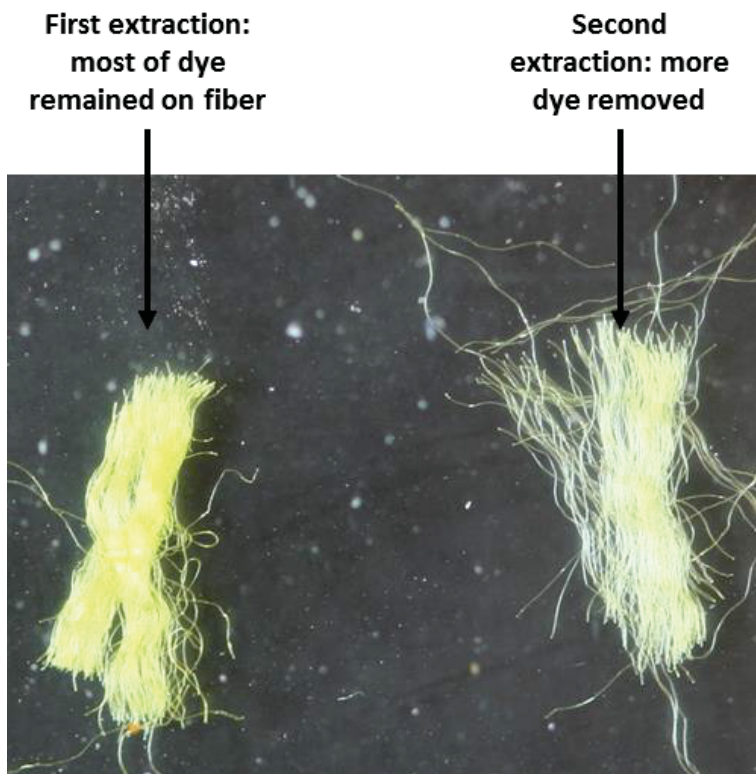


Figure 3-110. Acid Yellow 49 dyed fibers after attempted extractions

The AY49 samples were tested in the mass spectrometer but it showed no detectible dye. To improve extraction, the heating system was redesigned to achieve higher temperatures (see Section 3.7.4).

3.8.2 EXTRACTIONS WITH PROTOTYPE 1 – THIN-FILM HEATERS

Extractions were performed with the thin-film heater system at high temperatures. Initial extractions were attempted between 95 and 120°C based on conditions suggested by the Textile Chemistry Department. No dye was extracted but it was discovered that the solvent was boiling at these temperatures (solvent boiling is discussed in Section 3.8.3). The result was a truncated extraction time because the solvent disappeared. Further tests were performed at lower temperatures. The extraction parameters for these tests are shown in Table 3-9.

Table 3-9. Parameters for dye extraction with thin-film heaters

Dye #	Color Index Name	Approximate Thread Length [mm]	Set Temperature* [°C]	Extraction Time [sec]	Approximate Sample Volume [μl]
1	Acid Blue 25	2	90	300	100
2	Acid Yellow 49	3	90	300	100
3	Acid Red 186	3.5	90	300	100
4	Direct Green 26	3	80	180	100
5	Direct Yellow 106	3.5	80	180	100

* Max temperature in the cavity can exceed set temperature by 3-6°C, indicating the possibility of boiling at Tset = 90°C

Visual inspection of the fibers before and after each test indicated some dye had been removed from the threads for dye numbers 1, 2, 4, and 5. No dye appeared to be removed from the thread

colored with dye number 3 (Acid Red 186). The sample threads for each test are shown in Figure 3-111 through Figure 3-115.

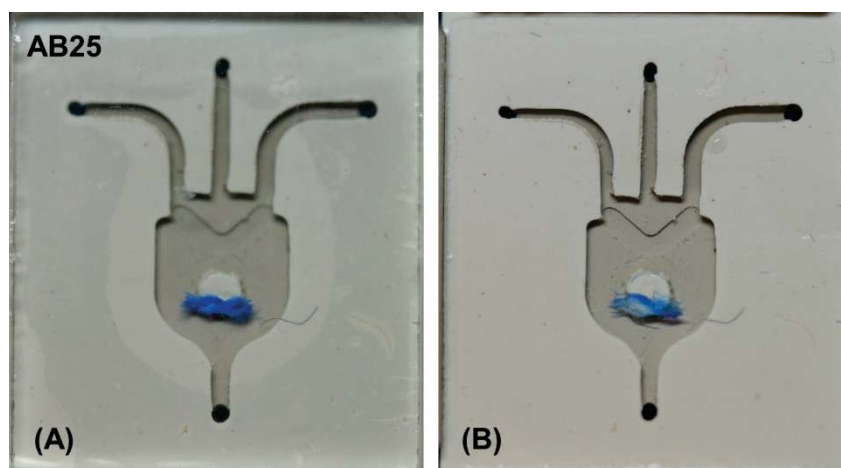


Figure 3-111. Acid Blue 25 (A) before and (B) after extraction

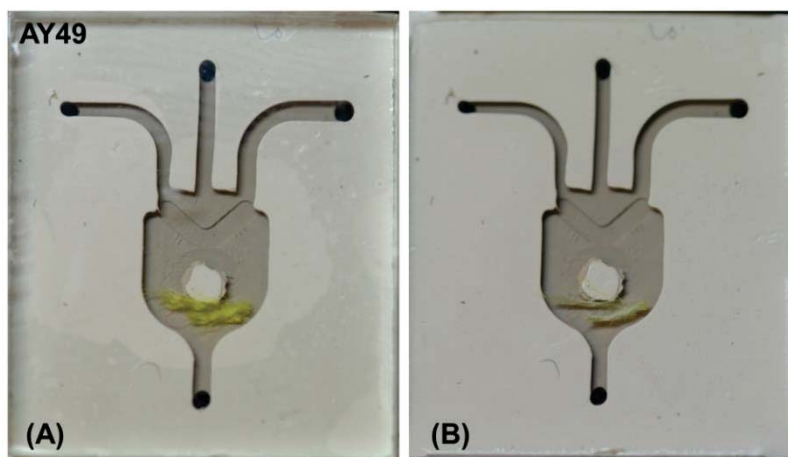


Figure 3-112. Acid Yellow 49 (A) before and (B) after extraction

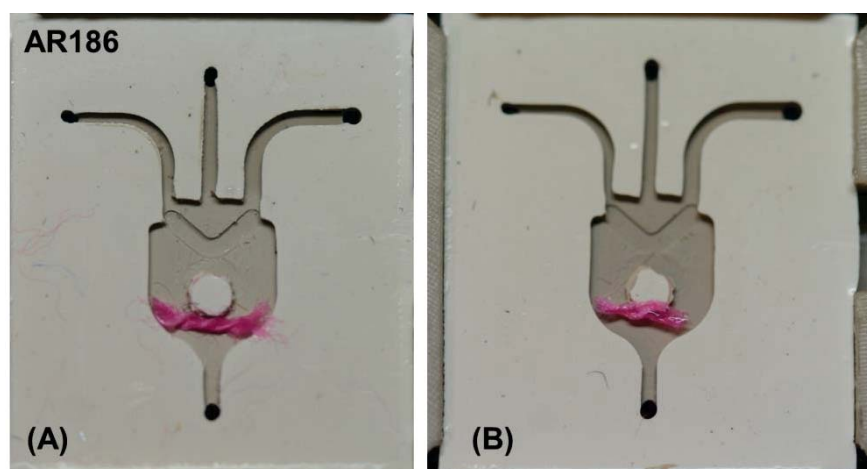


Figure 3-113. Acid Red 186 (A) before and (B) after extraction

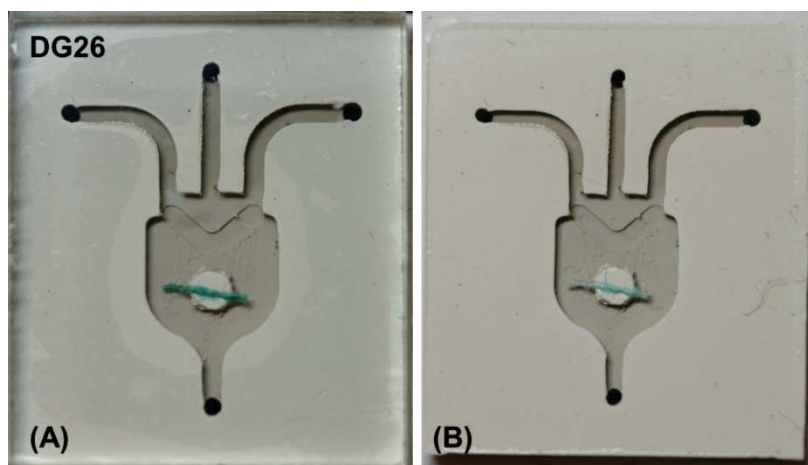


Figure 3-114. Direct Green 26 (A) before and (B) after extraction

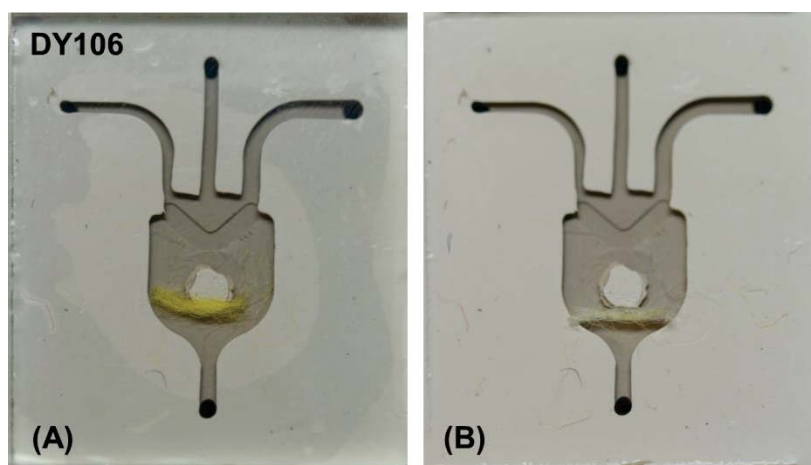


Figure 3-115. Direct Yellow 106 (A) before and (B) after extraction

The results of the test matched expectations from visual inspection of the fibers. Dye numbers 1, 2, 4, and 5 were successfully detected in the mass spectrometer. Dye number 3 was not detected. A summary of the mass spectrum results is provided in Table 3-10.

Table 3-10. Results of extractions with thin film heaters

Dye number	Color Index Name	Chemical Formula	Molecular Ions	Detected with Microfluidic Extraction	Molecular Weight of Deprotonated Ions
1	Acid Blue 25	$C_{20}H_{14}N_2O_5S$	M-H	Y	393.0529
2	Acid Yellow 49	$C_{16}H_{13}N_5O_3SCl_2$	M-H	Y	424.0043
3	Acid Red 186	$C_{40}H_{28}CrN_8O_{16}S_4$	M-H	N	-----
4	Direct Green 26	$C_{50}H_{38}N_{12}O_{18}S_4$	(M-2H)-H	Y	544.0846
5	Direct Yellow 106	$C_{48}H_{18}N_8Na_6O_{18}S_6$	(M-4H)-4H	Y	298.99

Peak detections in the mass spectrums of AY49 and AB25 show the characteristic ions in Figure 3-116.



Figure 3-116. Mass spectrums of (A) AY49 sample and (B) AB25 sample

3.8.3 PYRIDINE-WATER MIXTURE CAVITY BOILING TESTS

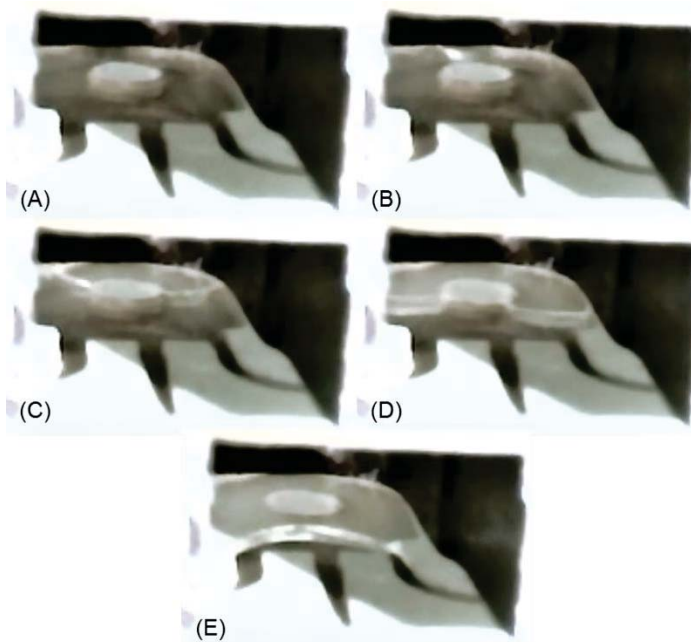


Figure 3-117. Solvent filling cavity

Some extractions were performed with the thin-film heater setup at temperatures in excess of 95°C. Several of the extractions did not result in successful extraction of the dye. The components of the solvent mixture have boiling points of 100°C (water) and 115°C (pyridine). It was assumed that the small volume of solvent was boiling and rapidly evacuating the cavity, thereby leaving the fiber no longer submerged in the solvent. This would cause the unsuccessful extraction of dye. The viewing slot used in the PTC heater design was eliminated from the design for the thin-film heaters to improve heating efficiency. To observe the heating process within the cavity, a slotted aluminum spacer was used as shown in Figure 3-65 (Section 3.6.3). The viewing system shown in Figure 3-66 (webcam and light) was used to observe the cavity. To start the test, the solvent was pumped into the cavity as shown in

Figure 3-117.

The heater was then turned on and video was recorded to observe the fluid in the cavity. No visual change in the fluid body occurred until 63 seconds after heating was initiated as shown in Figure 3-118(A). At 63 seconds, the solvent began to move into the air legs (Figure 3-118(B)). At 70 seconds, bubbling was observed in the rear of the cavity, close to where the aluminum spacer contacted the glass (Figure 3-118(D)). At 73 seconds, large bubbles began to cavitate at this position as the fluid boiled (Figure 3-118(F)). Boiling continued to be observed for 17 seconds. At 90 seconds, all fluid within the cavity had visibly disappeared (Figure 3-118(I)).

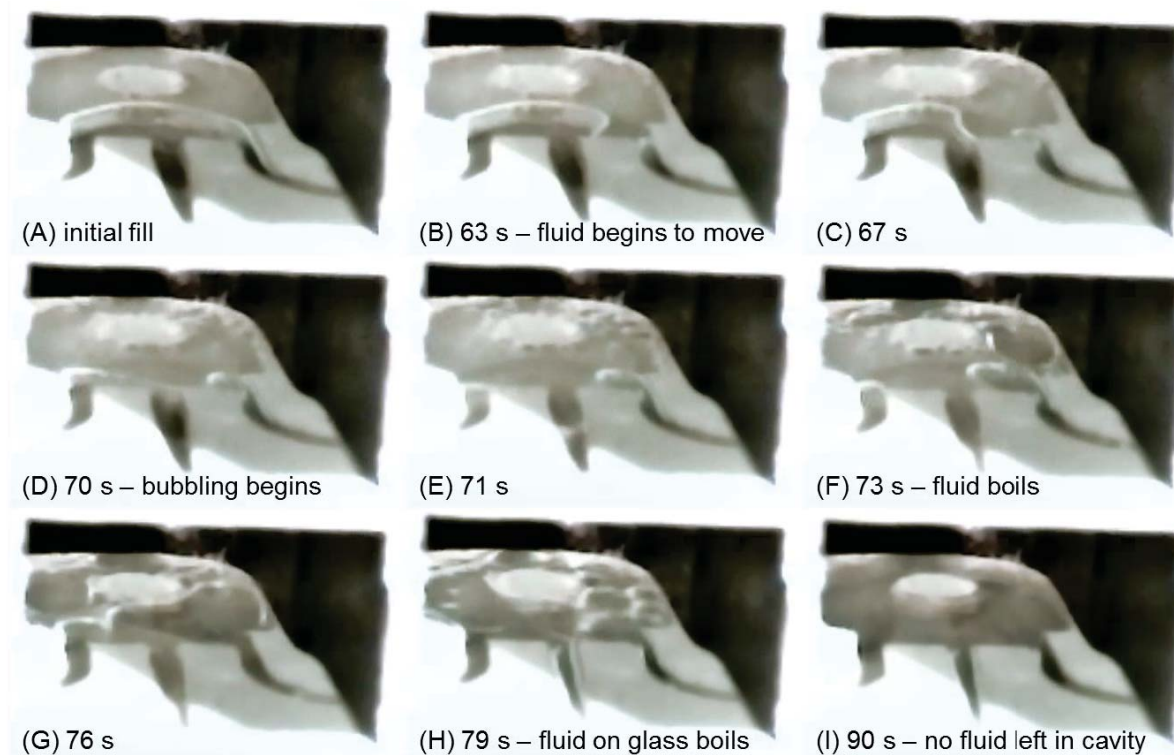


Figure 3-118. Boiling of pyridine:water mixture in cavity

The test verified the predicted boiling. Although high cavity temperatures can improve the extraction of dye, the rapid loss of solvent from boiling leaves the fiber uncovered. The heating system must keep the cavity below the boiling point temperature of the solvent. A thermocouple

was placed between the glass and FFKM to determine the temperature of the cavity at boiling as shown in Figure 3-119. The cavity was heated for 90 s and the temperature recorded.

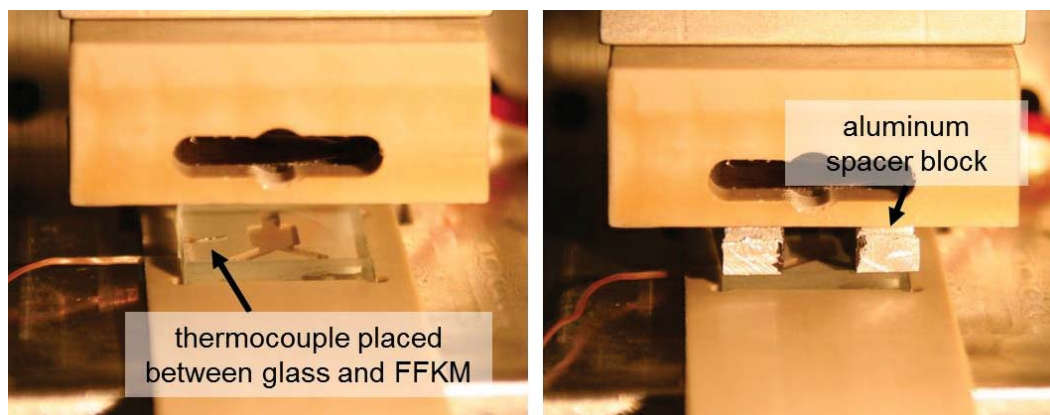


Figure 3-119. Boiling temperature measurement

The temperature of the cavity over the duration of the test is shown in Figure 3-120.

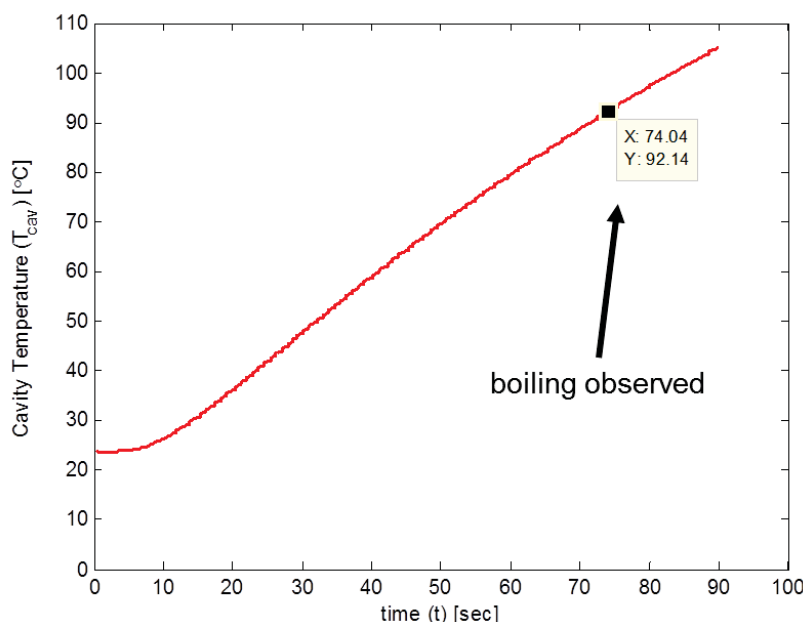


Figure 3-120. Cavity temperature during heating with aluminum spacer present

There was approximately one second of delay after data acquisition was initiated and the heater was turned on. The temperature at 74 seconds was then correlated to the temperature of the cavity when boiling of the fluid was observed. As shown in Figure 3-120, boiling was observed at approximately 92-93°C. A review of literature pertaining to distillation processes showed that the boiling point of a pyridine:water mixture with 57% pyridine by weight (matching the ratio used in the microfluidic system) is 92.6°C [47]. This compares well to the temperature measured in the tests performed.

The (4:3) pyridine:water mixture has a single boiling point which is less than that of its individual components. This is because it is an azeotrope. Azeotropes are mixtures for which the vapor has the same make up as the liquid phase [48]. They also have a single boiling point, and in this case,

it is significantly lower than the individual components. Several extractions were performed with temperatures in excess of the solvent mixture's boiling point because it was erroneously assumed that the boiling point would be no less than the lowest boiling point of the mixture components (i.e. water at 100°C). The failure to extract the Acid Red 186 dye could be the result of the solvent boiling off before the dye could be effectively separated. Although the set temperature was just below the boiling point of the solvent, the system overshoot can result in the temperature exceeding the set temperature by several degrees. The acid dyes typically required a longer time to successfully extract, so the lack of solvent in the chamber after initial heating may have resulted in little or no dye being extracted.

This raises the question of why AB25 and AY49 were successfully detected as they had the same temperature setting. This might be further explained by the specific subclass of each acid dye. The three main subclasses are leveling, milling, and metalized acid dyes. Levelling dyes typically have smaller molecules and are not as washfast as the other classes (meaning they discolor or fade more easily). The metalized acid dyes have the largest molecule and are the most washfast of the three subclasses [49]. The AB25 and AY49 fall into the levelling class of acid dyes. AR186 is a metalized acid dye, which may explain why it did not successfully extract. The molecules of the AR186 dye were not as easily separated from the fiber, requiring the fiber to be immersed in the solvent for a longer period of time. The heater cycling program was adjusted to reduce the temperature “overshoot” of the system and temperature limits were added to prevent the possibility of reaching the boiling point so that the fibers can remain immersed for a longer period of time.

3.8.4 EXTRACTIONS WITH PROTOTYPE 2

The second prototype was calibrated to perform extraction tests. The solvent bottle pressure was set to 9 psi, the buffer bottle to 3 psi, and the cavity air to 20 psi. To calibrate the fill timing, the piston assembly from prototype 1 was used to view the cavity as shown in Figure 3-121.

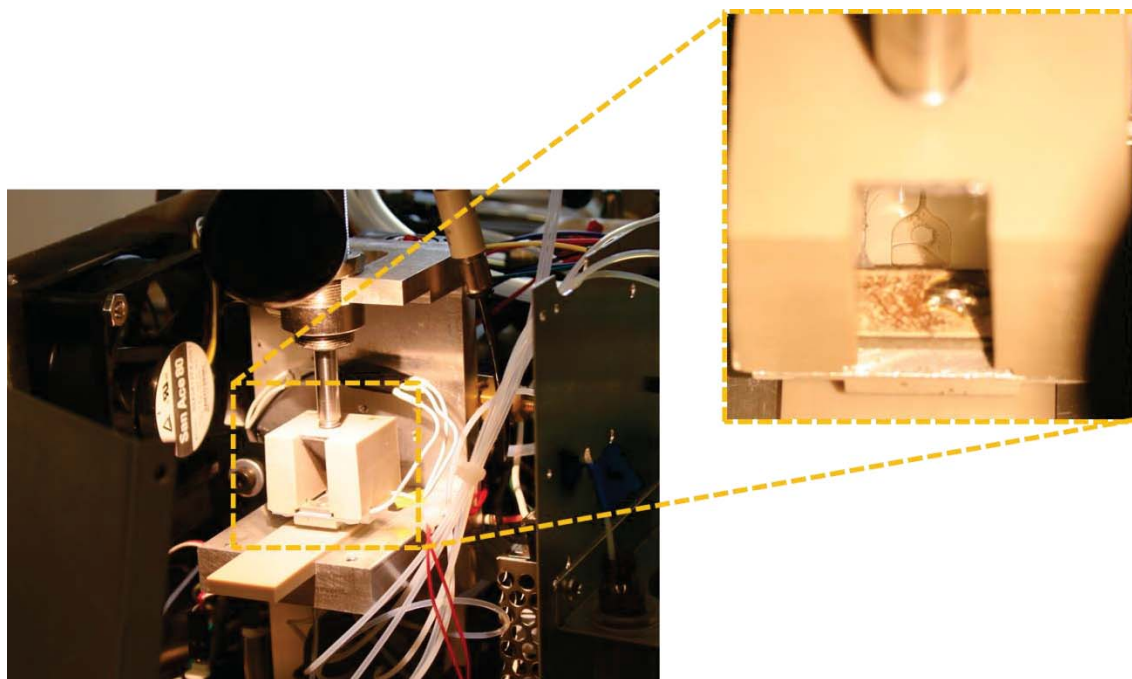


Figure 3-121. Prototype 2 calibration: cavity fill setup

A solvent fill time of 10.5 seconds and a buffer fill time of 7 seconds were determined by filling the cavity with each fluid. The second piston assembly and thin-film heaters were then placed back in the system and the heating system was calibrated in the enclosure. The enclosure heating calibration and equations are provided in Appendix F.3. The cooling of the cavity with the fan was also calibrated. A comparison of natural cooling and cooling with the fan in the device are shown in Figure 3-122.

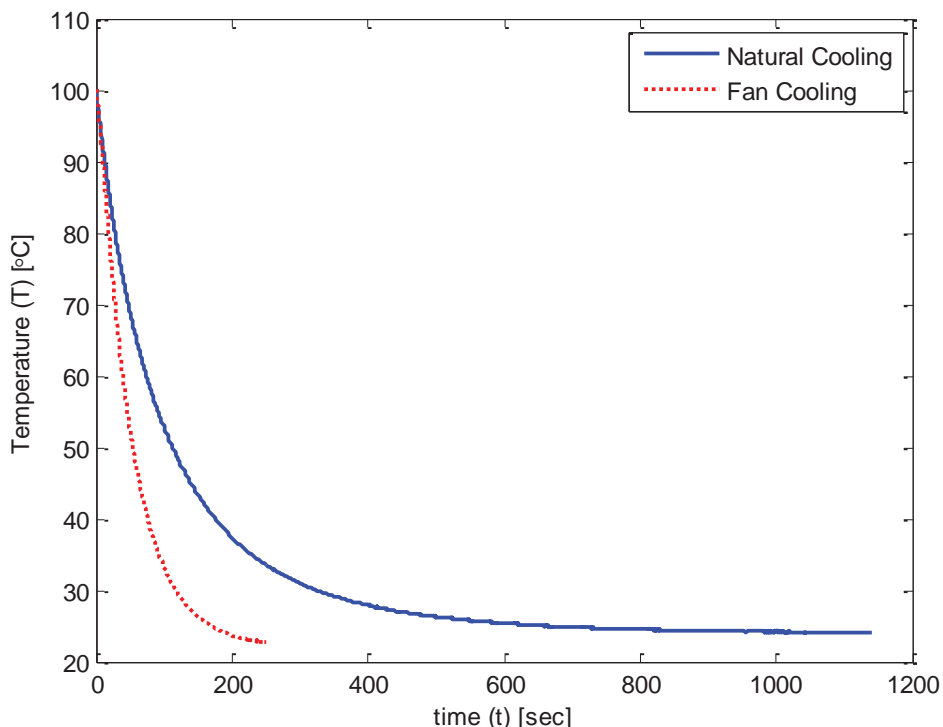


Figure 3-122. Cooling curves comparison in enclosure

A cooling step was added to the dye extraction process after the evaporation of the solvent. The 73 cfm fan was used to cool the cavity to a desired temperature (T_{cool}) before proceeding to the buffer injection step. To allow the user to set a cool temperature, a calibration equation was fit to the fan cooling temperature data as shown in Figure 3-123.

The curve fit was used to determine the time dependence of the temperature as shown in Equation (3.34).

$$T = 82.28e^{-0.01951t} + 21.92 \quad (3.34)$$

From the curve fit, the cooling time for a desired temperature for the buffer fill (T_{cool}) and a set temperature (T_{set}) is given in Equation (3.35).

$$t_{fan} = 51.25 \ln \left(\frac{T_{set} - 21.92}{T_{cool} - 21.92} \right) \quad (3.35)$$

After calibration, 16 dye extraction tests were performed to test the extraction capability of prototype 2. The dye types and extraction parameters are provided in Table 3-11.

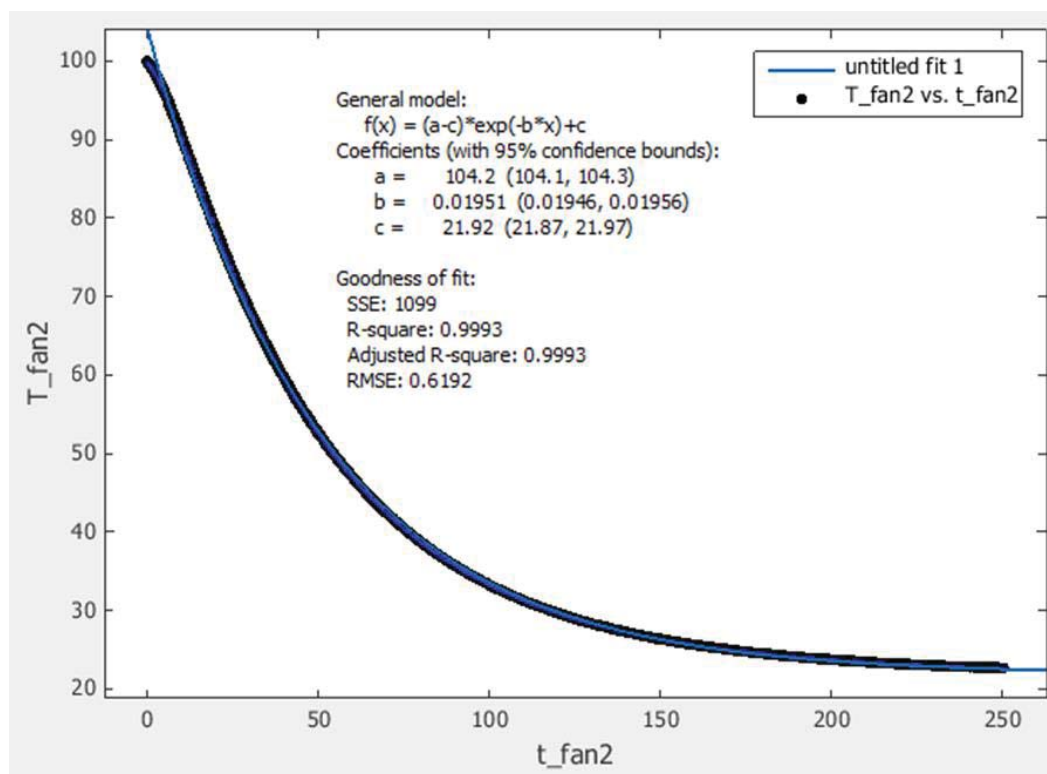


Figure 3-123. Enclosure calibration: fan cooling curve

Table 3-11. Parameters for extractions with prototype 2

Dye #	Color Index Name	Approximate Fiber Length [mm]	Set Temperature [°C]	Extraction Time [sec]	Number of Buffer Fills (~20-25 µl each)	T _{cool} for Buffer Fill [°C]	Total Process Time [sec]
1	Acid Blue 25 (.0625%)	3	88	300	5	70	733
2	Acid Blue 25 (.0625%)	3	88	160	5	70	593
3	Acid Blue 25 (.125%)	3	88	300	5	70	733
4	Acid Blue 25 (.125%)	3	88	160	5	70	593
5	Acid Blue 25 (.250%)	3	88	300	5	70	733
6	Acid Blue 25 (.250%)	3	88	160	5	70	593
7	Direct Green 26	3	75	120	5	60	572
8	Direct Green 26	3	80	180	5	60	640
9	Direct Red 81	3	75	180	5	60	632
10	Acid Red 186	3	88	300	5	70	734
11	Acid Red 114	3	88	180	5	70	614
12	Acid Red 114	3	88	360	5	50	820
13	Acid Orange 67	3	88	180	5	60	626
14	Acid Yellow 151-9 (3%)	3	88	180	5	60	626
15	Acid Yellow 151-9 (2%)	3	88	180	5	60	626
16	Acid Yellow 151-9 (1%)	3	88	180	5	60	626

Six extractions were performed for Acid Blue 25 dyes of three different concentrations. The extractions were performed to test the limits of dye concentration that could be successfully extracted with the device and detected in the HPLC-MS setup. The 160 second extraction time was determined as an optimal extraction time for AB25 by the Textile Chemistry Department (see Section 4.2.4). Extractions of AB25 were also performed for 300 seconds to provide a longer extraction time comparison and to determine if 160 seconds would provide better results within the microfluidic device. Two extractions were performed with AR114 to look at the effect of added extraction time and a lower temperature for the buffer injection step. The fibers for each test are shown in Figure 3-124.

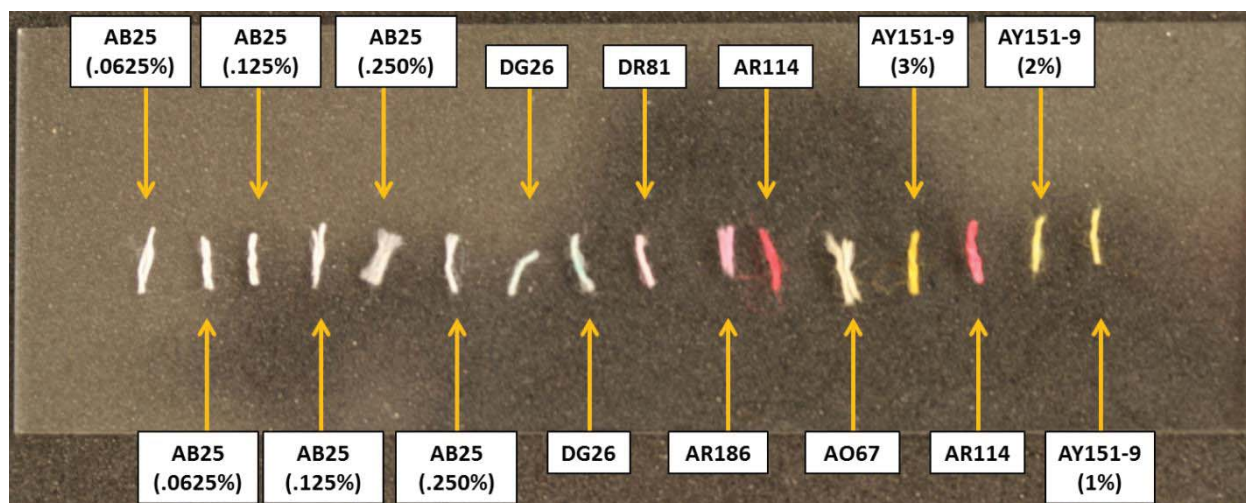


Figure 3-124. Fibers after extraction in prototype 2

Visual inspection of the two AR114 fibers after extraction showed improved dye removal in the fiber with a longer extraction time. Some dye appeared to remain in the fibers dyed with AR186, AR114, and AY151 (individual images of the extracted fibers are provided in Appendix I).

The extracted acid dye subclasses are shown in Table 3-12.

Table 3-12. Extracted acid dye subclasses

Color Index Name	Acid Dye Subclass
Acid Blue 25	Leveling
Acid Red 186	Metalized
Acid Red 114	Milling
Acid Orange 67	Milling
Acid Yellow 151-9	Metalized

4 MACRO EXTRACTION STUDY

4.1 INTRODUCTION

In forensic analysis of fiber evidence, it is not uncommon to have problems while analyzing colorants with different structures and many times the colorants on fiber evidence are blended. The identification of the structures of dyes is important for colorant analysis and requires extracting dyes from fibers using certain solvents. The objective of this study is to develop the most efficient extraction systems for major classes of dyes and fabrics (Cotton, Nylon, Polyester and Acetate) and to extend the growing database that includes extraction conditions, liquid chromatography and mass spectrometry analysis.

Standard methodologies including automatic microfluidic extraction, high performance liquid chromatographic separation, and Electrospray Ionization Quadrupole Ion-Mobility Time-of-Flight Mass Spectrometry (HPLC-ESI-QTOFMS) were developed for analysis of trace fiber containing commercial dyes (direct, acid and disperse dyes). Database containing retention times, and spectra data of 256 commercial dyes (84 acid dyes, 92 disperse dyes, 80 direct dyes) have been established for forensic purposes.

The database of key commercial dyes is growing with samples obtained, fabrics dyed and extractions methods and liquid chromatography–time-of-flight mass spectrometry results identified. Tables 4-1 to 4-3 show a small sample of the database for several dye classes that have been studied to date. T

Table 4-1. Image Capture of Database for Disperse Dyes

Vial Label	Constitution Number	Manufacturer	Trade Name	Lot #	Structure	Molecular Formula	Calculated MI	Molecular Weight	Expected
DB 60 - 001	61104	Huntsman International	Terastop Blue BGE	00001927	Y	C20 H17 N3 O5	379.1168		[M+H]
DB 60 - 002	61104	Crompton & Knowles	Intradil Brill Blue BNS		Y	C20 H17 N3 O5	379.1168		[M+H]
DB 60 - 003	61104	Ciba	Terastil Blue BGE	042D	Y	C20 H17 N3 O5	379.1168		[M+H]
DB 60 - 004	61104	Clariant	Sodyecron Brill Blue SBG 200	19530924156	Y	C20 H17 N3 O5	379.1168		[M+H]
DB 60 - 005	61104	Mobay Chemical Corp	Resolin Brill Blue BGL 200	01-45-589	Y	C20 H17 N3 O5	379.1168		[M+H]
DB 60 - 006	61104	Ciba	Terastil Blue BGE - 01		Y	C20 H17 N3 O5	379.1168		[M+H]
DB 60 - 007	61104	BASF	Palatril Br Blue BG 200%	6-531-070	Y	C20 H17 N3 O5	379.1168		[M+H]
DB 60 - 008	61104	BASF	Palatril Brill Blue BG	P0056300	Y	C20 H17 N3 O5	379.1168		[M+H]
DB 60 - 009	61104	Ciba - Geigy	Terastil Br Blue BG		Y	C20 H17 N3 O5	379.1168		[M+H]
DB 60 - 010	61104	Hoechst	Samaron Brill Blue R-GL	556900	Y	C20 H17 N3 O5	379.1168		[M+H]
DB 60 - 011	61104	Sandoz	Foron Turquoise S-BGL	33/4.100-3	Y	C20 H17 N3 O5	379.1168		[M+H]
DB 60 - 012	61104	Ciba Specialty Chemicals	Terastil Blue BGE - 01 200	349981	Y	C20 H17 N3 O5	379.1168		[M+H]
DB 60 - 013	61104	BASF	Palatril Br Blue BG 200%	8 055 424	Y	C20 H17 N3 O5	379.1168		[M+H]
DB 60 - 014	61104	BASF	Palatril Br Blue BG		Y	C20 H17 N3 O5	379.1168		[M+H]
DB 60 - 015	61104	Ciba - Geigy	Terastil Br Blue BGE 200	162589200	Y	C20 H17 N3 O5	379.1168		[M+H]
DB 27 - 016	60767	Ciba	LF-27N	002	Y	C22 H16 N2 O7	420.0958		[M+H]
DB 27 - 017	60767	Ciba Specialty Chemicals	Terastil Blue GLF	003304MBAA	Y	C22 H16 N2 O7	420.0958		[M+H]
DB 27 - 024	60767	Hoechst	Samaron Pink FRL	90060-SE	Y	C20 H16 N2 O5	355.1420		[M+H]
DB 27 - 025	60767	Ciba	Terastil Blue LF - 27N		Y	C22 H16 N2 O7	420.0958		[M+H]
DB 91 - 026	60767	BASF	Palatril Brill Pink REL	8 054 932	Y	C20 H16 N2 O5	355.1420		[M+H]
DR 86 - 027	62175	Clariant	Foron Red AS-BL	V000944	Y	C22 H16 N2 O5 S	422.0936		[M+H]
DR 86 - 028	62175	Ciba	Terastil Pink 2GLA		Y	C22 H16 N2 O5 S	422.0936		[M+H]
DB 27 - 029	60767	Huntsman International	Terastop Blue GLF	25117EB7	Y	C22 H16 N2 O7	420.0958		[M+H]
DB 27 - 030	60767	Huntsman International	Terastop Blue GLF	22970EB7	Y	C22 H16 N2 O7	420.0958		[M+H]
DB 27 - 031	60767	Ciba	Terastil Blue GLF		Y	C22 H16 N2 O7	420.0958		[M+H]
DB 27 - 032	60767	Ciba	Terastil Blue GLF		Y	C22 H16 N2 O7	420.0958		[M+H]
DB 77 - 033	60766			007	Y	C20 H12 N2 O6	376.0695		[M+H]
DY 163 - 034	111235	Ordered from Classic Dyestuff	Permasil Yellow BRLS	C25142-326871	Y	C18 H14 N6 Cl2 O2	416.0555		[M+H]
DR 86 - 036	62175	DyStar	Dianix Red AM-B8		Y	C22 H16 N2 O5 S	422.0936		[M+H]
DY 42 - 037	10338	Clariant	Foron Yellow AS-FL	CHAA109775	Y	C18 H15 N3 O4 S	369.0783		[M+H]

Table 4-2. Image Capture of Database for Acid Dyes

Database Number	CI Number	Manufacturer	Trade Name	Lot Number	Structure	Chemical Formula	MI	MW
AY7_1-1	56205	Crompton & Knowles	Intracid Flavine B		Y	C19 H14 N2 O5 S	382.0623	382.3999
AB82_2-1	62045	ICI Americas Inc.	Nylomane Blue A-2P	93620	Y	C20 H20 N2 O5 S	400.1093	400.4482
AR27_3-1	16185	DyStar	Isolan Scarlet K-GLS gran 150%		Y	C20 H14 N2 O10 S3	537.9811	538.5276
AR151_4-1	26900	Marlowe-Van Loan Sales Co.	Marvanyl Red HCO		Y	C22 H16 N4 O4 S	432.0892	432.4518
AR186_5-1	18810	BASF	Palatin Fast Pink BNI	P367358	Y	C40 H28 Cr N8 O16 S4	1055.9911	1056.8948
AR337-6-1	17102	Clariant	Nylosan Red E/C2GN P 200	U27CO03001	Y	C17 H12 N3 O4 S F3	411.0501	411.3551
AO67_1_7-1	14172	Huntsman	Erionyl Yellow A-R-01	R10021V8	Y	C26 H22 N4 O8 S2	582.0879	582.6049
AY199_8-1	14205	Dohmen	Dorasyne Yellow A3R 200%	09M52147	Y	C19 H16 N4 O6 S	428.0791	428.4185
AY199_8-2	14205	DyStar	Telon Yellow 4R micro 01	DA 33254	Y	C19 H16 N4 O6 S	428.0791	428.4185
AY199_8-3	14205	M. Dohmen	Dorasyne Yellow A4R 150%	10M52221	Y	C19 H16 N4 O6 S	428.0791	428.4185
AY151_9-1	13908	Dohmen	Dorolan Yellow RTU	11M51567	Y	C32 H28 Co N8 O10 S2	807.0702	807.6755
AY151_9-2	13908	Sandoz Chemical	Lanasyn Yellow LNW 100%	1-5238-0-100	Y	C32 H28 Co N8 O10 S2	807.0702	807.6755
AB92-10-1	13390	D&G Dyes	Doracid Blue RL	2852651	Y	C26 H19 N3 O10 S3	629.0233	629.6382
AB277-11-1	61203	Ciba Geigy	Tectilon Blue 4R		Y	C24 H23 N3 O8 S2	545.0927	545.5847
AB40_12-1	62125	Dohmen	Dorasyne Blue A2G 200 %	10M50629	Y	C22 H17 N3 O6 S	451.0838	451.4519
AB40_12-2	62125	Ciba Geigy	Tectilon Blue 4G		Y	C22 H17 N3 O6 S	451.0838	451.4519
AB25_13-1	62055	Dohmen	Dorasyne Blue AG	10M50593	Y	C20 H14 N2 O5 S	394.0623	394.4006
AB25_13-2	62055	Sandoz Chemical	Nylosan Blue 2AL/C-2AL	1-0260-0-100	Y	C20 H14 N2 O5 S	394.0623	394.4006
AR116-14-1	26660	DyStar	Telon Red 2BN	45797940	Y	C22 H16 N4 O4 S	432.0892	432.4518
AR266_15-1	17101	Dohmen	Dorasyne Red A-2B 200%	06M54845	Y	C17 H11 N3 O4 S F3 Cl	445.0111	445.3160
AR266_15-2	17102	CK Colors	Nylanthrene Red B-2B	03018	Y	C17 H11 N3 O4 S F3 Cl	445.0111	445.3160
ABIK172_16-1	15711	Ciba Specialty Chemical	Lanaset Black B	45808166	Y	C40 H22 Cr N6 O14 S2	926.004078	926.70499
AB113_17-1	26360	Sandoz Chemical	Nylosan Navy N-RBL	PS87-1116	Y	C32 H23 N5 O6 S2	637.1090	637.6849
AR111-18-1	23268	Sandoz Chemical	Nylosan ScarletF-3GL	PS87-1127	Y	C37 H30 N4 O10 S3	786.1124	786.8499
AR128_19-1	24125	Sandoz Chemical	Nylosan F-BRN	PS89-1094	Y	C37 H30 N4 O12 S3	818.1022	818.8487
AY73_20-1	45350	Sigma	Fluorescein (FW 332.3)	89H3616	Y	C20 H12 O5	332.0685	332.3063
AB90_21-1	42655	Sandoz Chemical	Sandolan Cyanine N-G	PS88-1027	Y	C47 H49 N3 O7 S2	831.3012	832.0379
AY42_22-1	22910	D&G Dyes	Doracid Yellow R 200%	2802195	Y	C32 H26 N8 O6 S2	714.1315	714.7276

Direct Dye Master List May 2014 Excel (Product Activation Failed)													
<div> <div>FILE HOME INSERT PAGE LAYOUT FORMULAS DATA REVIEW VIEW ADD-INS JMP</div> <div> </div> <div> <div>Paste Copy Format Painter</div> <div>Clipboard Font Alignment Number Styles Cells</div> <div> <div>Conditional Format as Formatting Table</div> <div>Normal Bad Neutral</div> <div>Insert Delete Format Clear Sort & Find Filter Select</div> </div> </div> </div>													
M38	x	y	z	aa	ab	ac	ad	ae	af	ag	ah	ai	aj
Lot #	C.I. or generic name	CAS Number	Dye Class	Manufacturer	Trade Name	Structure Chemical Formula	MW	MI	Calculated MI				
DIR_DBK22_001	Direct Black 22	6473-13-8	Polyazo	Sandoz	Pyrazol Black G	Y C44H32N13O11Na3S3	1083.9700	C44H35N13O11H3	1016.1668				
DIR_DBK22_002	Direct Black 22	6473-13-8	Polyazo	Atlantic	Alcinate Direct Fast Black Y	C27H17N5Na2O8S2	617.5000	C27H19N5O8S2	572.882				
DIR_DBK80_003	Direct Black 80	8003-69-8	Trisazo	Sandoz	Pyrazol Black BG Conc.	Y C36H23N8Na3O11H3	908.7800	C36H26N8O11H3	841.0810				
DIR_DBK80_004	Direct Black 80	8003-69-8	Trisazo	Ciba-Geigy	Y C36H23N8Na3O11H3	908.7800	C36H26N8O11H3	841.0810					
DIR_DB1_005	Direct Blue 1	2610-05-1 + 3841-14-3	Disazo	Ciba-Geigy	Diphenyl Brill Blue FF Su	Y C34H24N6Na4O16S4	992.8000	C34H28N6O16S4	903.0372				
DIR_DB106_006	Direct Blue 106	6527-70-4	Oxazine	Standard Dyes	Solophenyl BR Blue BL	N C30H16C2N4Na2O8S2		C30H18C2N4O8S2	649.9870				
DIR_DB106_007	Direct Blue 106	6527-70-4	Oxazine	Ciba-Geigy	Solophenyl BR Blue BL	N C30H16C2N4Na2O8S2		C30H18C2N4O8S2	649.9870				
DIR_DB108_007	Direct Blue 108	1324-58-9	Oxazine	Standard Dyestuff	Permalute Blue FFRLL	Y C34H20C2N4Na4O11H3	944.9900	C34H22C2N4O11H3	C34H22C2N4O11H3				
DIR_DB14_008	Direct Blue 14	72-57-1	Disazo	ORCO	Orcomine Blue 3BS	Y C34H24N6Na4O14S4	960.8100	C34H28N6O14S4	C34H28N6O14S4				
DIR_DB15_009	Direct Blue 15	2429-74-5	Disazo	Atlantic	Direct Blue 15	Y C34H24N6Na4O16S4	992.8000	C34H28N6O16S4	C34H28N6O16S4				
DIR_DB15_011	Direct Blue 15	2429-74-5	Disazo										
DIR_DB15_012	Direct Blue 15	2429-74-5	Disazo	Ciba-Geigy									
DIR_DB160_011	Direct Blue 160	12222-02-5	Disazo	C&K (Clompton & Intramet Navy Blue RLL	N Atlantic								
DIR_DB199_013	Direct Blue 199		Disazo	Atlantic									
DIR_DB218_014	Direct Blue 218	28407-37-6	C&K	Ciba-Geigy	Direct Blue 218	Y C32H20C2N4N6Na4O16S4	1091.8429	C32H24C2N6O16S4	1003.9100				
DIR_DB218_015	Direct Blue 218	2598-57-4 + 25180-26-1	Disazo	C&K (Clompton & Azonitrone Jet Black K	N Atlantic	C34H25N5Na2O8S2	741.7005	C34H27N5O8S2	697.7400				
DIR_DB224_016	Direct Blue 224	71838-40-5	Direct	Atlantic	Resin Fast Blue N								
DIR_DB224_017	Direct Blue 224			Sandoz	Pyrrozal Fast Sky Blue 7CN								
DIR_DB229_018	Direct Blue 229												
DIR_DB293_019	Direct Blue 293	142106-29-4	Oxazine	ICI Americas Inc.	Diazol Brilliant Blue GL	N C40H23N7Na4O13S4	1029.8700	C40H27N7O13S4	941.9400				
DIR_DB71_020	Direct Blue 71	4399-55-7 + 87440-96-8	Trisazo	Standard	Solophenylki Blue GL 25CY	Y C42H25N7Na4O13S4	1055.9100	C42H29N7Na4O13S4	941.9400				
DIR_DB75_021	Direct Blue 75	6428-60-0	Trisazo	Atlantic		Y C42H25N7Na4O13S4	1055.9100	C42H29N7Na4O13S4	941.9400				
DIR_DB75_022	Direct Blue 75	6428-60-0	Trisazo	Atlantic	Solophenyl Blue 2GL 20LY	Y C42H25N7Na4O13S4	1055.9100	C42H29N7Na4O13S4	941.9400				
DIR_DB76_023	Direct Blue 76		Disazo	Atlantic									
DIR_DB78_024	Direct Blue 78	2503-73-3 + 25180-10-3	Oxazine	Yorkshire-Americe	Intralute Blue 4GL	Y C42H25N7Na4O13S4	1055.9100	C42H29N7Na4O13S4	1055.9000				
DIR_DB78_025	Direct Blue 78	2503-73-3 + 25180-10-3	Oxazine	Ciba-Geigy	Intralute Blue 4GL	Y C42H25N7Na4O13S4	1055.9100	C42H29N7Na4O13S4	1055.9000				
DIR_DB80_026	Direct Blue 80	12222-00-3	Disazo	Atlantic	Pergalsol Blue 2RL	Y C32H14C2N4Na4O16S4	962.7600	C32H14C2N4Na4O16S4	969.8500				
DIR_DB80_027	Direct Blue 80	12222-00-3	Disazo	Atlantic	Pergalsol Blue 2RL	Y C32H14C2N4Na4O16S4	962.7600	C32H14C2N4Na4O16S4	969.8500				
DIR_DB85_028	Direct Blue 85												

Chemical Separation by High Performance Liquid Chromatography (HPLC) High performance liquid chromatography coupled to a diode array detector (HPLC-DAD) provides better sensitivity and specificity than conventional chromatographic methods used for the analysis of dyes. It discriminates dye component that cannot be detected in the visible range and provides discriminations between dye classes [52]. In this study, a universal HPLC method was used for the analysis of direct, acid and disperse dyes.

Direct Connection from Microfluidic Extraction to the QTOF MS The microfluidic system was also directly connection of microfluidic apparatus to ESI-QTOF mass analyzer. Compared to conventional separate-step fiber analysis, the integrated system has an improved detection limit that minimum lengths of fibers (ng single fibers) can be used as indicated in Section 3.8.4.

4.2 EXPERIMENTAL PROCEDURES

4.2.1 DYEING

Direct Dyeing: Swatches of bleached, desized fabrics (10g, Testfabrics, #400) were dyed at a liquor-to-goods ratio of 20:1 in a dye bath containing 1% owf direct dyes in a DataColor AHIBA dyeing machine in a 150 mL dye bath. The fabrics were rinsed completely and air dried at room temperature.

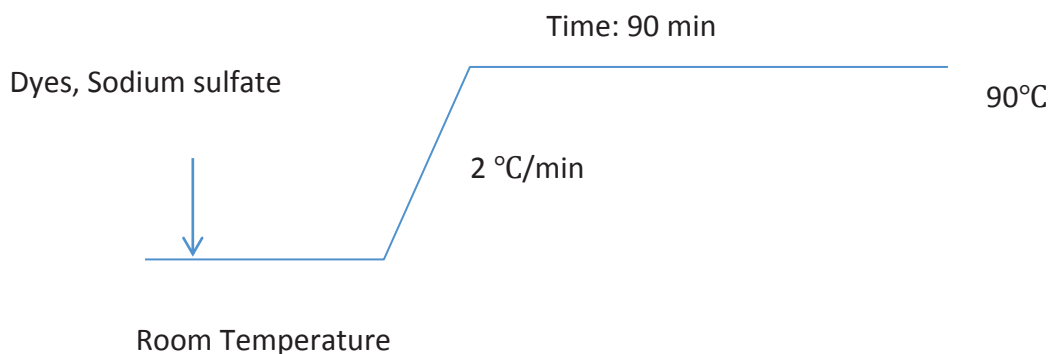


Figure 4-1 Dyeing Procedures of Direct Dyes

Acid Dyes: Stock solutions (1 mg/mL) of commercial dye powder in water were diluted to produce a 300 mL dyebath for a 1% owf dyeing on 5.00 g nylon (Testfabrics, Nylon 6,6,#306) then acidified to pH 4 using glacial acetate acid. The dye bath and fabric were placed into beakers and inserted into the Roaches Pyrotec MB2 dyeing machine with the following heating program: ramp rate of 4 °C from room temperature to 100 °C, then the temperature was held for 60 minutes. Upon completion of dyeing program the samples were allowed to cool and then rinsed using tap water and dried overnight. The dyestuff used in this study are shown in Table 4-1. The dye without chemical formular are confidential and not listed in the Colour Index.

Table 4-4 Information of Acid Dyes

C.I. number.	C.I. Name	Chemical Classes	Manufacturer	Trade Name	Chemical Formula	Molecular weight
1	Acid Blue 25	Anthraquinone	M.Dohmen	Dorasy Blue AG	C ₂₀ H ₁₄ N ₂ O ₅ S	394.0623
2	Acid Blue 45	Anthraquinone	Ciba Geigy	Erio Cyanine S 150%	C ₁₄ H ₁₀ N ₂ O ₁₀ S ₂	429.977
3	Acid Blue 40	Anthraquinone	M.Dohmen	Dorasy Blue A2G 200%	C ₂₂ H ₁₇ N ₃ O ₄ SF ₃ Cl	451.0838
4	Acid Blue 62	Anthraquinone	Classic Dyestuffs	Bernalizarine Blue SRA	C ₂₀ H ₂₀ N ₂ O ₅ S	400.1092
5	Acid Blue 277	Anthraquinone	Ciba Geigy	Tectilon Blue 46	C ₂₄ H ₂₃ N ₃ O ₈ S ₂	545.0927
3	Acid Yellow 49	Monoazo	Mobay Chemical	Telon Yellow FGL 200	C ₁₆ H ₁₃ N ₅ O ₃ SCl ₂	424.0043
4	Acid Yellow 151	Metalized Monoazo	M.Dohmen	Dorolan Yellow RTU	C ₃₂ H ₂₉ CoN ₈ O ₁₀ S ₂	807.0711
5	Acid Orange 67	Monoazo	Huntsman	Erionyl Yellow A-R-01	C ₂₆ H ₂₂ N ₄ O ₈ S ₂	582.0897
7	Acid Red 114	Diazo	Ciba Geigy	Erionyl Red RS	C ₃₇ H ₃₀ N ₄ O ₁₀ S ₃	785.1019
8	Acid Red 186	Metalized Monoazo	BASF	Palatin Fast Pink BNI	C ₂₀ H ₁₆ N ₄ O ₈ S ₂	503.0337

Disperse Dyes: Swathes of prescoured polyester (5 g) were used in the dyeing of samples. The dye bath consisted of deionized water stock solution and glacial acetate acid. The liquor ratio was

maintained at 20:1. The polyester swatches were dyed in a DataColor Ahiba Nuance Top Speed II dyeing machine (Figure 4-2) in a 150-mL dyebath. The dye bath was increased from room temperature to 130°C at a ramp rate of 4°C/min for 30 minutes. The dye bath was held at 130 minutes and allowed to cool for 30 minutes.



Figure 4-2 Ahiba Nuance Top Speed dyeing machine

4.2.2 EXTRACTION PROCEDURE

Extraction Apparatus At Macro-Level Textile fibers (~500 µg) were weighted in Pierce Reacti-Vials. Extracting solvent (200 µL) was added and the vials were heated without lids in a Pierce Reacti-therm module under optimized extraction conditions. Once the fiber become colorless, they were removed from the vials, and the vials are placed back to the heating module and by using nitrogen gas (10 psi) for approximately 5 minutes. An apparatus was constructed to deliver nitrogen gas to the vials is presented in Figure 4-3.



Figure 4-3. Pierce Reative-therm heating module and Nitrogen gas delivery system

Fisherband clear polyvinyl chloride (PVC) tubing (0.312 inch internal diameter (I.D.) x 0.625 inch wall thickness) was connected to the nitrogen tank regulator. A smaller diameter clear PVC tubing are connected to the 0.312 inch I.D x 0.0625 inch wall thickness tubing via screw band metal clamps. Five tubes of the same diameter and wall thickness were connected. At the end of five tubes, metal needles are attached. The needles, which were delivered nitrogen gas to the vials, were guided by a wood panel. Two lab stands with clamps holding tubes in place.

Macro-Level Extraction Procedure Dyed yarns or single fibers were immersed into 200 μL of certain solvent solution in a sealed glass reactive vial with cone bottom for 20 min under different temperatures. After extraction, the fibers were kept in the vial and cap of the vial was removed to let the extractant solvent evaporate completely under nitrogen gas (10 psi). Dye extract after evaporation was recovered with 100 μL buffer. The mixture was extracted with Hamilton needles connected to the National Scientific Company disposable syringes (1 mL) and filtered into Agilent LC vials using Millex-GV 13 mm, 0.22 μm PVDF filters (Milli water).

Preliminary Selection of Solvent System Fabrics samples were cut into small squares (0.5 x 0.5 cm, ~ 5 mg). Extracting solvent was made from organic solvent and water with certain ratio. [57] The formula and conditions of extraction are shown in the Table. 200 μL extracting solvent was added for a certain period of time. The recipes for extraction are shown in Table 4-5.

Table 4-5. Preliminary Screening of Extracting Solvent

Extracting solvent (2ml)	Time (min)	Temperature ($^{\circ}\text{C}$)
Methanol/H ₂ O 4:3	20	25-50
Acetone/H ₂ O 4:3	20	25-50
Ethanol/H ₂ O 4:3	20	25-50
Pyridine/H ₂ O 4:3	30	25-90
Pyridine/H ₂ O 2:1	15	80
Pyridine/H ₂ O 35:65	15	80
Formic acid/ H ₂ O 88:12	15	80

4.2.3 DYE MEASUREMENT

Vis-Spectrometry Concentrations of dye solutions were measured by vis-spectrometer. The basic principle of this method is Beer's law shown in Equation 4-1 and the concentrations can be calculated from light absorbance when the light pass through the dye solutions. The measured absorbance of a solution to light, A

$$A = \log_{10} \frac{I_0}{I} = \epsilon c L \quad (4-1)$$

where;

I_0 is the intensity of incident light at a given wavelength

I is the transmitted intensity,

L is the path length through the vials, and

c is the the concentration of the solution.

ϵ is a constant known as molar absorptivity coefficient, which is a measure of how strong a chemical species absorbs light at a given wavelength that should be determined before testing. The scan range of the spectrometer was set from 360 nm to 660 nm.

Color Measurement of Fabrics The color difference between the fabric before and after extraction provides an estimate of extraction effects. A large color difference value indicates a good extraction property. Color difference (ΔE_{cmc}) is measured by Datacolor Check Pro (Datacolor, USA) and is obtained by means of the chromatic coordinates: L, C, h, which correspond respectively to luminosity, chroma, and hue. ΔL , ΔC and Δh are defined as the

differences of each parameter with respect to the reference. The references are the dyed fabrics before-extraction, and the test samples are fabrics after-extraction. The basic setting of color measurements are as follows: D65 illuminant and 10°observer, UV included, and specular component included. The fabrics were measured at three locations and the results are averaged for comparisons.

4.2.4 STATISTIC OPTIMIZATION OF EXTRACTION

D-Optimal Screening Experiment of Extraction The D-Optimal screening experiments were designed statistically to determine the main factors affecting the extraction performance of the pyridine/water system under certain conditions, and to discover the interactions between all the factors in the extraction system. Three factors namely temperature, time, and extracting solvent volume were taken as the factors and the concentration of extracted dye solution was the response. The statistic software employed was JMP 9.0 and Design of Experiment 7.2. The list of conditions for the screening experiment is listed in Table 4-6.

Table 4-6 Design of D-Optimal screening experiment for direct dye extraction

	Pattern	Block	Temperature/ °C	Time (min)	Volume (μL)	Concentration (mg/L)
1	--++	1	25	20	800	6.373
2	++--	1	80	20	250	9.089
3	+--+	1	80	2	800	9.377
4	000	1	52.5	11	525	8.649
5	----	1	25	2	250	9.342
6	---+	2	25	2	800	5.883
7	--+-	2	25	20	250	3.876
8	+---	2	80	2	250	5.147
9	++++	2	80	20	800	8.833
10	000	2	52.5	11	525	7.056

The concentrations of dye solutions were employed to fit a statistic model and an estimate of factors affecting the extraction are listed in Figure 4-6. The statistic value P of factors indicates how significant are the factors affecting the response. If the P value is lower than 0.05, the corresponding factor is significant in the statistic model. According to the results, the P value of time is smallest among all the factors, which is only 0.0198, indicating extraction time plays the most important role, followed by temperature and the volume of extracting solvent. The trends of how the extracted dye percentage goes with the increase the three factors are shown in Figure 4-4. It is clear that as the extraction time and temperature increase, the extraction performance goes up, but the extraction volume has a P value of higher than 0.05, indicating it didn't affect extraction performance very much.

Table 4-7. Statistic Estimate of Effect of Factors

Term	Estimate	STD Error	t Ratio	Prob> t
Time/min(2-16)	1.630	0.517	3.15	0.0198
Temperature / ° C (25-50)	0.773	1.13	0.68	0.5224
Volume (μ L) (250-800)	0.026	0.51	0.06	0.9562

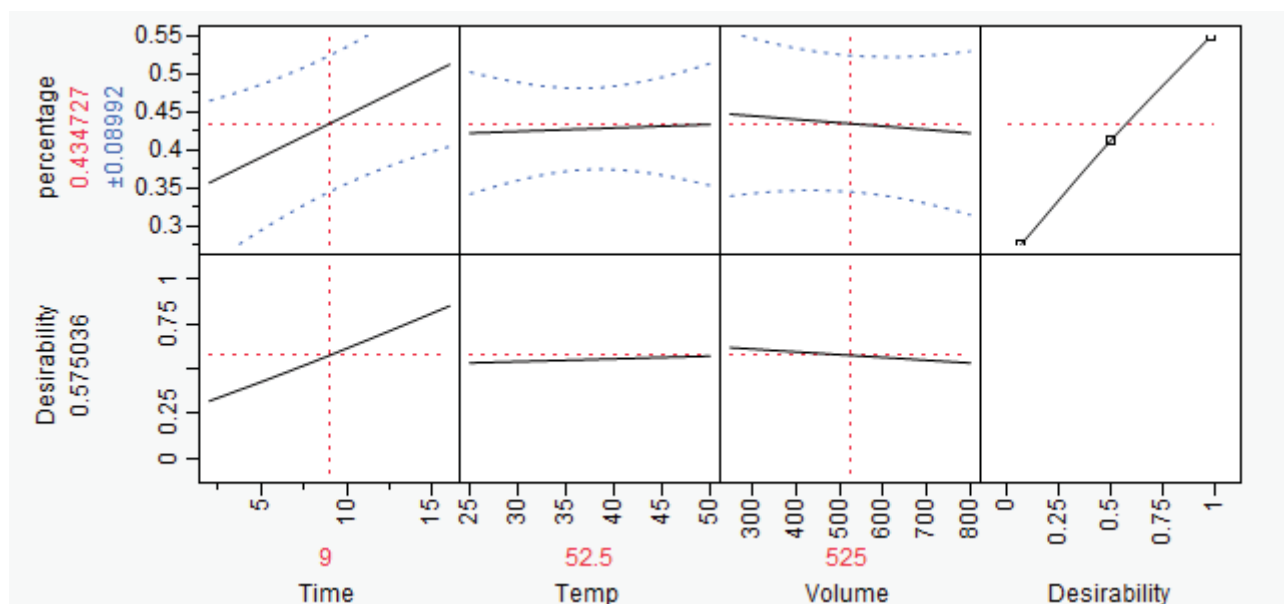


Figure 4-4. Influence of Factors on Extraction Performance of Pyridine/Water (4:3)

A further analysis by a screening model in Figure 4-5 shows the extracted dye percentage versus time follows a quadratic model in the studied time periods. The maximum extraction percentage of C.I. Direct Yellow 86 reaches to about 52.5% when the extraction time is 11.68 min.

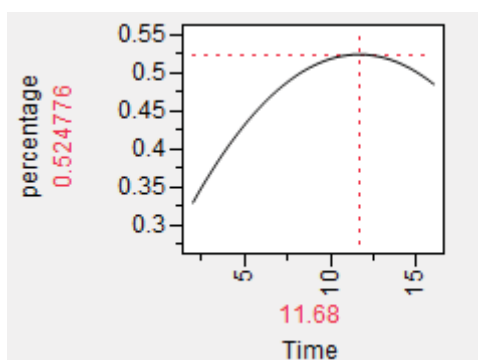


Figure 4-5. Statistical Model of Dye Extraction Percentage vs. Time

Central Composite Design of Extraction A central composite design (CCD) of experiment allows for systematic examinations of multiple factors and interactions simultaneously in order to determine their degree of significance, predict responses by prediction profilers. Table 4-8 illustrates the four independent variables and levels of CCD experimental design. Two levels are

chosen for each factor, a maximum and minimum, which reflect the practical ranges of it. Design resolution represents the degree of aliasing that will be allowed. A resolution V design has main factors and interactions from themselves and each other.

Table 4-8 Experiment Design of Dye Extraction

Factor	High	Low	1 Center point	Response
Time (second)	300	30	165	Peak Intensity of QTOF MS
Temperature (°C)	80	120	100	
Thread length (μm)	200	2000	600	
Dye concentration (owf %)	0.5	2	1.25	

Optimization of Macro Level Evaporation Solvent evaporation is designed to evaporate extracting solvent containing pyridine before HPLC MS analysis. Evaporation of solvent is carried out after dyes have been extracted from fiber and the fibers have been taken out after extraction. The main substance present in solvent, pyridine, has unpleasant smells and too much pyridine cause interferences in the mass spectra. Therefore, pyridine should be removed before mass spectrometric analysis. In order to shorten the whole process, the evaporation process of solvent has the same temperature with that of extraction. A prediction profiler was designed using JMP Pro. 9.0 to predict of the minimum evaporation time, so that pyridine could be removed completely when temperature and buffer solution of extraction are optimized. In this experiment, a full factorial experiment was designed to construct a statistic model for both optimization and prediction of evaporation time. Temperature, extraction volume and nitrogen flow speed were taken as factors and the time required for complete evaporation was the response. The solvent for study contains 4:3 pyridine/water. The experiments are performed in two different days, and the design of experiment and results is listed in Table 4-9.

Table 4-9 DOE of Evaporation and Results

Pattern	Block	Temperature (°C)	Extracting Volume (μl)	Nitrogen (Psi)	Time (second)
+-+	1	120	20	15	30.64
000	1	90	60	10	144.74
---	1	60	20	5	162.64
++-	1	120	100	5	145.82
-++	1	60	100	15	264.34
000	2	90	60	10	79.66
---+	2	60	20	15	76.24
+++	2	120	100	15	60.94
-+-	2	60	100	5	213.69
+--	2	120	20	5	46.22

4.3 OPTIMIZED EXTRACTION AT MACRO-LEVEL

4.3.1 EXTRACTION PERFORMANCE OF EXTRACTING SOLVENT

Evaluation of Extraction The color differences of fabrics before and after preliminary extraction shown in Table 4-9, and Figure 4-6 in which the color difference was used as a quantitative method to compare the dye extracted from fabrics. A larger color difference indicates a better extraction effect. Also, the extraction performance was evaluated when the dye concentration on fabrics differs.

The results indicate that pyridine/water 4:3 is the best among all extracting solvent, followed by acetone and methanol, ethanol. Moreover, there are not significant color differences observed when the dye concentration is lower, indicating the extraction performance wasn't affected much by the concentration of dyes in the investigated range.

Table 4-9. Concentration Effect on Extraction

Dye	Concentration (owf %)	Methanol: H ₂ O ₂ =4:3, RT		Acetone: H ₂ O ₂ 4: 3, RT		Ethanol: H ₂ O ₂ 4:3, RT		Pyridine: H ₂ O ₂ 4:3 (60 °C)	
		ΔL	ΔEcmc	ΔL	ΔEcmc	ΔL	ΔEcmc	ΔL	ΔEcmc
Direct Red 81	0.5	3.43	4.66	4.62	5.80	3.39	4.25	16.8	24.26
	1	2.65	3.74	4.79	6.50	2.4	3.42	19.25	26.18
	2	2.95	3.80	4.88	6.25	2.64	3.64	20.76	26.23
	3	3.14	4.00	5.49	6.97	3.62	4.76	23.63	29.06
Direct Yellow 44	0.5	0.34	4.15	0.67	6.94	0.62	4.90	1.67	20.96
	1	0.57	3.94	1.06	6.94	6.54	4.47	1.82	21.58
	2	0.61	3.72	1.06	6.63	0.34	3.77	2.78	21.66
	3	0.4	3.19	1.08	6.72	0.46	4.08	3.4	23.28
Direct Violet 55	0.5	3.35	3.87	5.28	6.07	3.74	4.38	16.39	21.16
	1	4.32	4.82	4.29	4.67	6.87	7.69	21.07	24.75
	2	2.79	3.04	5.23	5.79	2.84	3.26	23.81	21.1
	3	4.5	4.93	7.38	7.93	5.35	5.88	26.91	29.20
Direct Black 22	0.5	0.58	1.29	0.23	1.42	0.78	1.31	17.92	18.00
	1	0.8	0.84	0.75	1.44	0.98	1.41	21.01	21.02
	2	0.31	1.23	0.01	1.13	0.64	1.29	18.43	18.62
	3	0.18	0.98	7.76	8.05	0.41	1.12	29.93	30.01

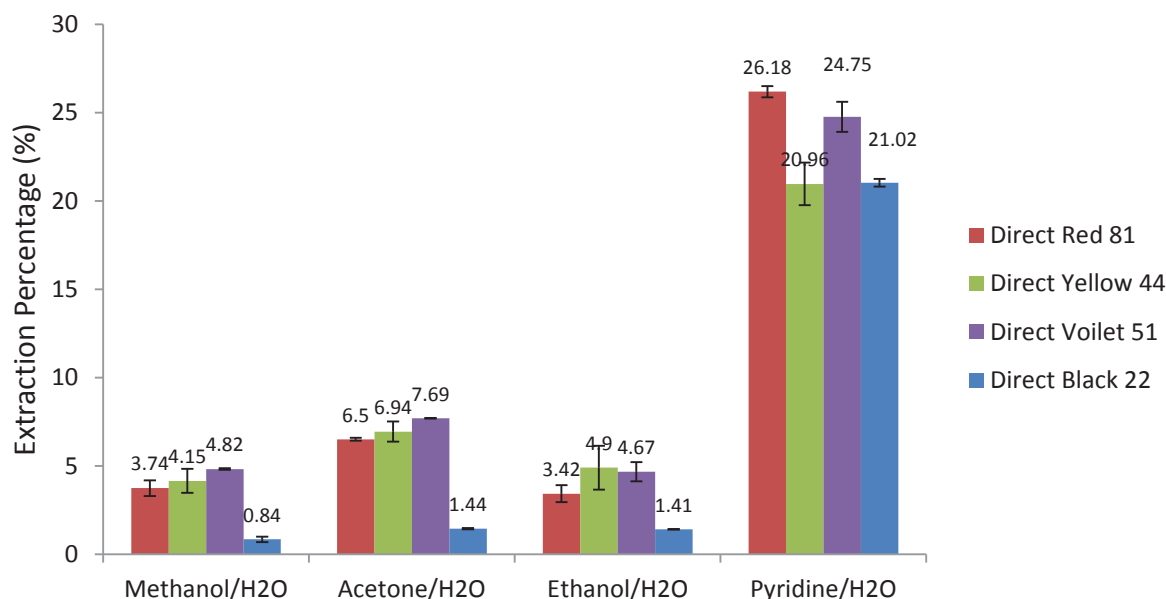


Figure 4-6. Extraction Percentage of Different Solvent System (Solvent/Water 4:3 v/v) Calculated from Vis-Spectrometer measurement of the solvent system before and after extraction (1%owf dye concentration)

Four optimized extraction condition from previous research was investigated. Preliminary extraction shows the pyridine/water 4:3 were the most efficient extraction, followed by acetone/water 4:3, for acid dyes. In case of disperse dyes, dichlorobenzene gave the best performance, followed by pyridine/water and methanol/water. Especially, the acetate fibers are easy to be dissolved in the formic acid/water solvent. A comparison was performed with the optimized conditions performed in previous research. Formic acid/water 88:12 melt the acetate and nylon fibers in less than 5 minutes, and gave inferior extraction performance than pyridine/water. Pyridine/water 4:3 can give satisfactory extraction performance in cases of direct dyes on cotton, acid dyes on nylon, however, it is less efficient for disperse dyes on nylon fibers, and it also melt the acetate fibers in less than 10 minutes. Further optimization of pyridine/water ratio demonstrated that a ratio of 1:2 can extract disperse dyes without melting acetate fibers. Furthermore, in the case of polyester, dichlorobenzene can give a satisfactory results when the extraction temperature is as high as 120 °C. The optimized extraction conditions for the major dyes are summarized in Table 4-11.

Table 4-10 Comparison of Extraction Performance of Three Optimized Extraction Solvent

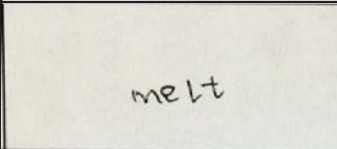
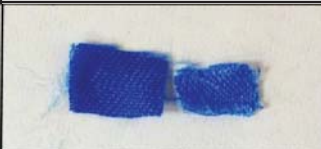
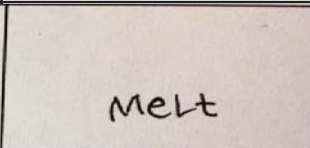





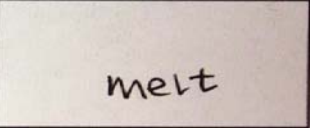



Temp: 80 °C Time 10 min	Pyridine/water 4:3	Pyridine/water 35:65	Formic Acid/Water: 88:12
Disperse Blue 73 (Acetate Fibers)			
Direct Green 26 (Cotton)			
Acid Blue 25 (Nylon 6,6)			
Disperse Red 1 (Polyester)			

Table 4-11 Optimized Extraction Solvent for Dyes in Different Fibers.

Dye	Fabrics	Solvent	Time (min)	Temp (°C)
Direct Dye	Cotton	Pyridine/water (4:3)	10-15	85-90
Acid Dye	Nylon	Pyridine/water (4:3)	10-15	85-90
Disperse Dye	Polyester	Dichlorobenzene	25-30	120
	Acetate	Pyridine/water (1:2)	10-15	80

4.3.2 QUANTIFICATION OF DYE EXTRACTS IN MACRO EXTRACTION

C.I. Acid Blue 25 extract was quantified and is marked with a yellow dot on the curve shown in Figure 4-7. The estimated concentration was approximately 1.319 µg/L. Quantification of acid dye extracts from single fibers is currently being investigated, and the main problem for quantification is lack of reproducibility for a small amount of fibers.

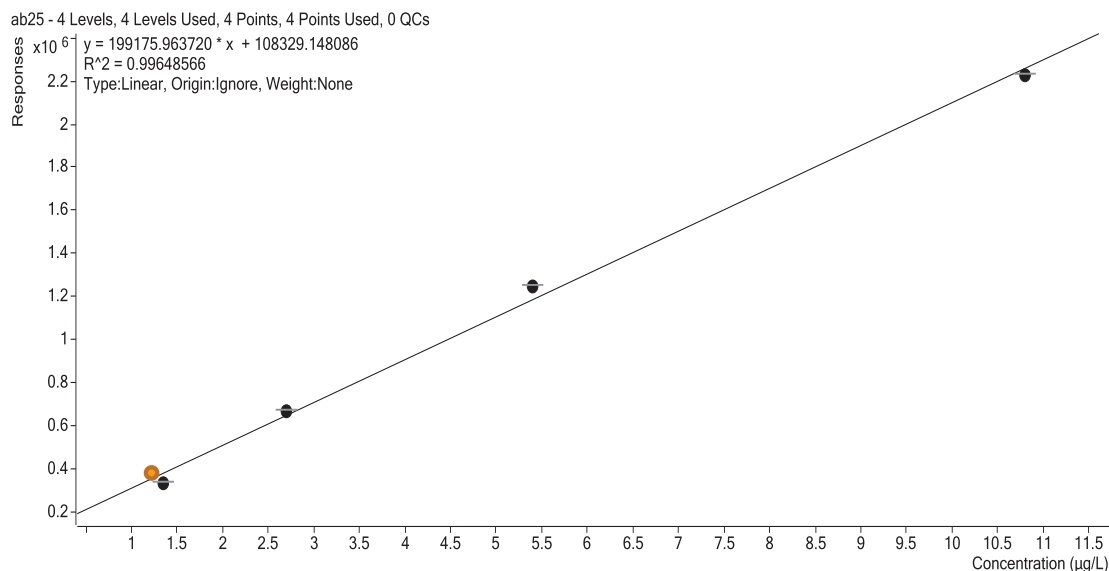


Figure 4-7 Quantification of C.I. Acid Blue 25 Extract from Fiber Yarns

4.4 OPTIMIZATION OF EVAPORATION AT MACRO-LEVEL

4.4.1 STATISTICAL ANALYSIS OF MACRO-LEVEL EVAPORATION

A full factorial design of experiment allows for systematic examinations of multiple factors and interactions simultaneously in order to determine their degree of significance and predict responses by prediction profilers. In a full factorial DOE two levels are chosen for each factor, a maximum and minimum, which reflect its practical range. Here center points (0) are also included for each factor to account for middle values. Design resolution represents what degree of aliasing will be allowed. A resolution V design has main factors and their interactions. The results for DOE of evaporation are shown in Fig 12. A full list containing all of the main factors and interactions is shown in Fig 12. The significant variables along with their corresponding contrasts, t-ratio, and p-values can be found. A parameter is considered to be significant if its p-value is smaller than 0.1 (90% confidence). Those which have p-values marked with an asterisk represents the variance in the data with 95% confidence (p-value smaller than 0.05). The contrasts which are listed give an indication as to which influence the response. The sign of contrast (+/-) provides the some indication as to whether the maximum or minimum setting provided the best response. Two of the three factors were found to be significant: Temperature and volume of solvent. The reason is that a higher temperature increases kinetics of evaporation and a larger volume of solvent needs longer time to evaporate completely.

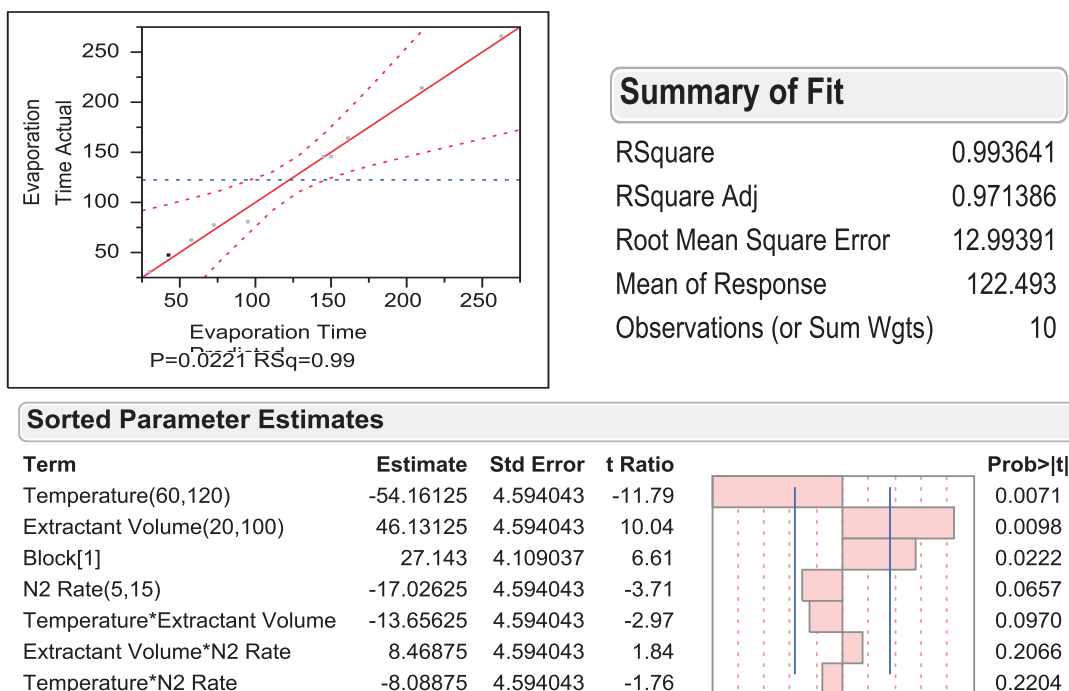


Figure 1254-7. Statistic Model for Evaporation

4.4.2 THE PROFILER TRACE OF EVAPORATION

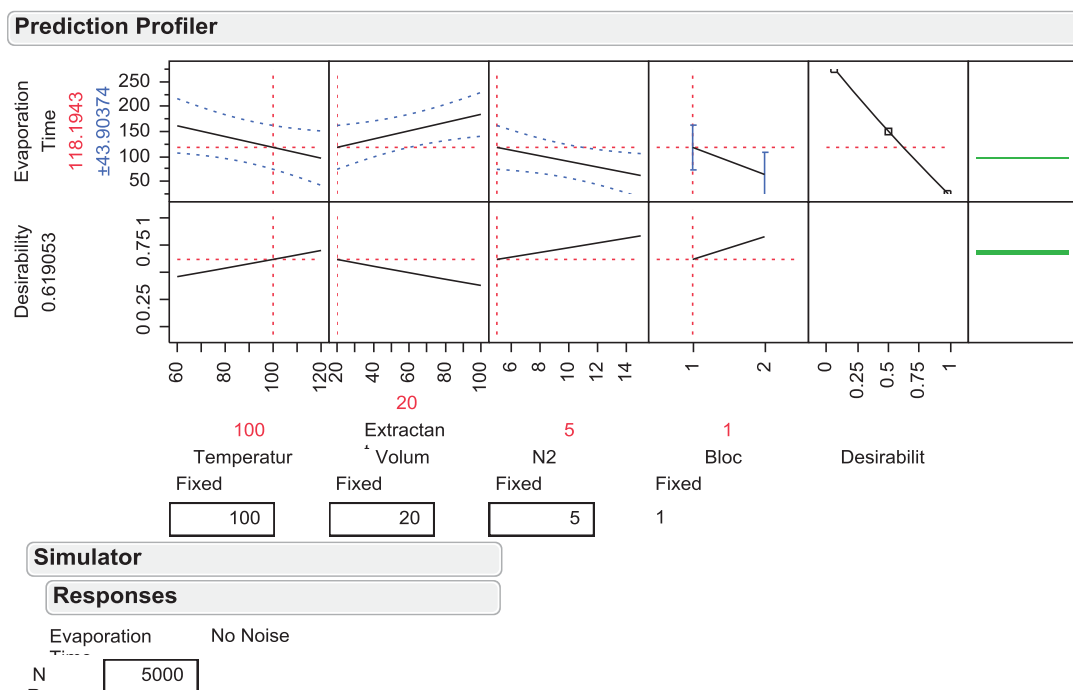


Figure 126 Prediction Profiler Based on Statistical Model Fitting

The function of profiler displays profile traces for each variable in the model. The profilers recomputed the profiles and predicted responses in real time as the values of variables were changed. The vertical dotted line for variables shows its current value: the temperature was set as

100°C, extracting solvent volume 20 μ L, 5 psi Nitrogen gas flow rate. The horizontal dotted line shows the current predicted evaporation time: 118.1 ± 43.9 seconds. The black lines within the plots show how the predicted values changes as the current variables change. In fitting platforms, a dotted blue curve surrounding the prediction trace shows the 95% interval for predicted values. This method could also be applied for profiler trace of the extraction process, to predict dye extraction percentage changes with variables like temperature, and extraction time. The optimization of acid dye extraction is currently being studied.

5 MICROFLUIDIC EXTRACTION STUDY

5.1 MICROFLUIDIC EXTRACTION CONDITIONS

Direct Dyes: 3 mm cotton fibers dyed with direct dyes was extracted in the automatic extraction microfluidic apparatus with 8 μ L extraction solvent at 70 °C for 10 min in a sample holder, as is shown in Fig 6. Then the solvent was evaporated by nitrogen gas flow for 2.5 min. 100 μ L buffer flows into the sample holder to dissolve dyes extracted from the fibers. The buffer was then collected and filtered for LC-QTOF-MS analysis.



Figure 5-1 Dye Threads in a Microfluidic Cavity

Acid Dyes: 3mm nylon threads with 1% owf (weight of dye on fabrics) were put into the microchips. 9 μ L extracting solvent (pyridine: water 4:3) was injected into the sample holder. After 300 second extraction at a temperature of 90 °C, extracted dye was diluted by buffer for four times. The buffer stays in the sample holders for 20 s after extraction (stay time), allowing dye extract to be completely dissolved in buffer. Pyridine/water extracting solvent was evaporated for 150 s, followed by a cooling process to prevent the dyes extracted to be absorbed by the fibers again. The total extraction time required by three typical acid dyes are illustrated in Table 5-1. As the leveling dyes comes off easily, the extraction time was set as 5 min. The microfluidic extraction conditions are illustrated in Table 5-1 (repeat of Table 3-11 with different properties).

Table 5-1 Microfluidic Extraction of Typical Acid Dyes

Dye #	Color Index Name	Extraction Time [sec]	Chemical Formula	Molecular Weight of Ions	Molecular Ion
1	Acid Blue 25 (.0625%)	300	C20H14N2O5S	393.05	M-H
2	Acid Blue 25 (.0625%)	160	C20H14N2O5S	393.05	M-H
3	Acid Blue 25 (.125%)	300	C20H14N2O5S	393.05	M-H
4	Acid Blue 25 (.125%)	160	C20H14N2O5S	393.05	M-H
5	Acid Blue 25 (.250%)	300	C20H14N2O5S	393.05	M-H
6	Acid Blue 25 (.250%)	160	C20H14N2O5S	393.05	M-H
9	Direct Red 81(1%)	180	C29H19N5Na2O8S2	314.53	(M-2H)-4
10	Acid Red 186 (1%)	300	C20H14N4Na2O8S2	514.33	-----
11	Acid Red 114 (1%)	180	C37H28N4Na2O10S3	785.1	M-H
12	Acid Red 114 (1%)	360	C37H28N4Na2O10S3	785.1	M-H
14	Acid Yellow 151-9 (3%)	180	C32H28CoN8O10S2.2H	807.07	M-H
15	Acid Yellow 151-9 (2%)	180	C32H28CoN8O10S2.2H	807.07	M-H
16	Acid Yellow 151-9 (1%)	180	C32H28CoN8O10S2.2H	807.07	M-H

5.2 ANALYSIS OF DYES WITH HIGH PERFORMANCE LIQUID CHROMATOGRAPHY

5.2.1 SAMPLE PREPARATIONS FOR Q-TOF LC/MS ANALYSIS

1mg dye powders were made into dye stock solutions by being diluted in 30 μ L organic solvent (Methanol/Acetonitrile 7: 3) and 970 μ L HPLC-grade water. 0.5 mg uracil was also diluted with the same solvents as the dye stock. Then 30 μ L dye solution and 10 μ L uracil solution was added into 930 μ L HPLC-grade water and 30 μ L organic solvents (Methanol/Acetonitrile 7: 3). The new solutions made were filtered and put into glass vial for LC/MS analysis. In case of disperse dye, the buffer was replaced by buffer containing (Acetonitrile/Water 48: 52).

5.2.2 OPTIMIZED CHROMATOGRAPHY FOR HPLC

High performance liquid chromatography (HPLC) is a separation technique involves mobile phase and stationary phase. In reverse phase HPLC, the sample is injected via an auto sampler into a column along with a constant flow of solvent controlled by a binary, while the analyte of interest undergoing separation between the mobile phase and stationary phase undergoing separation. The detector plots out the UV-Vis absorption as a function of time. Figure 5-2 shows a schematic of the HPLC system used for the research. The flow of solvent through the system is marked with the black arrow.

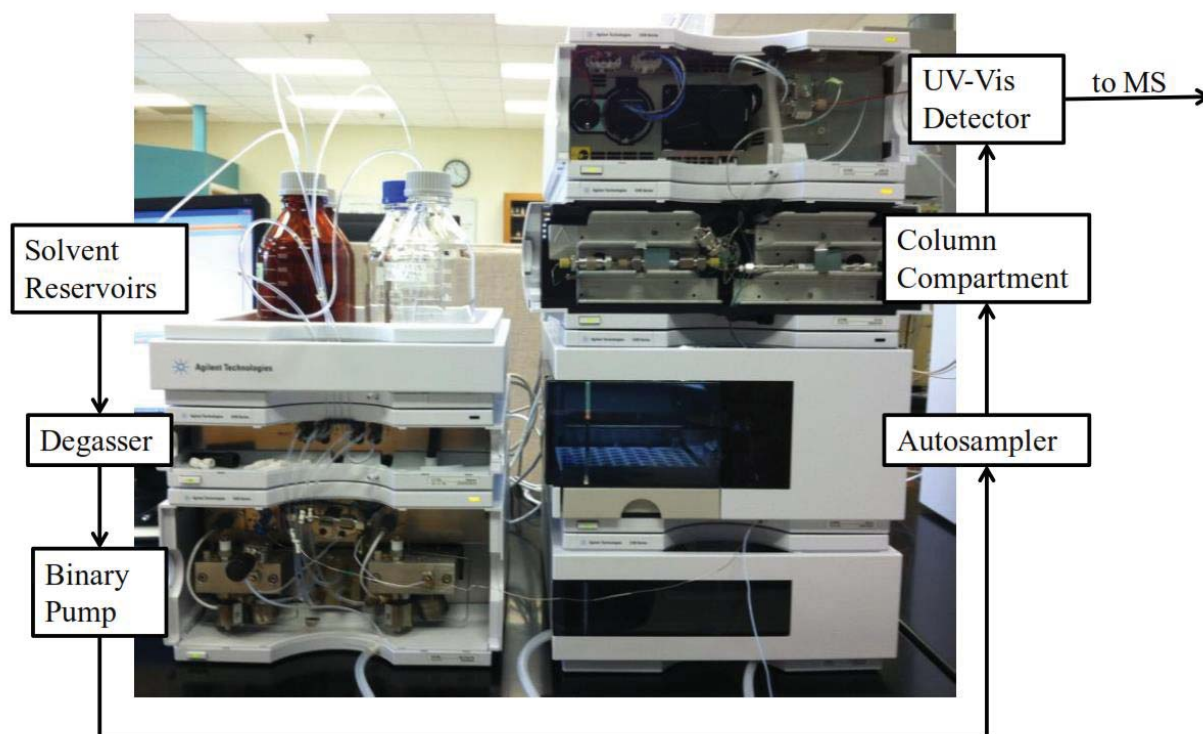


Figure 5-2. HPLC System

5.2.3 MOBILE PHASE PREPARATION

Disperse dye: Solvents for LC/MS analysis consisted of acetonitrile as the organic phase (phase B) and water as the aqueous phase (phase A). Mobile phase was prepared based on the number of samples analyzed. A total of 19.5 min at a flow rate of 0.5 mL/min requires at least 195 ml for 20 samples. Both aqueous and organic phases would be pre-organic phase was placed in reservoir B and the aqueous phase was placed in reservoir A. Formic acid (0.1%) was added to both reservoirs and mixed.

Direct dye/acid dyes: Solvents for direct dye/acid dye separation consisted of acetonitrile/methanol 3:7 as the organic phase (phase B), and water as the aqueous phase (Phase A). 20 Mm Ammonium acetate (ammonium formate for acid dyes) and Formic acid (0.01%) was added to reservoir A and mixed.

5.2.4 OPTIMIZED CHROMATOGRAPHY FOR DIFFERENT DYE CLASSES

Disperse Dyes: Dye analysis was performed on an Agilent Technologies 1260 SL liquid chromatograph equipped with a photodiode array detector (DAD). The DAD was used on a 380 – 780 nm wavelength scan. Chromatographic separation was performed at 45Agilent Poroshell™ 120 EC – C18, 2.7 μ m, 3.0 x 100 mm reverse-phase column. The gradient used is presented in Table 2. The flow rate was 0.5 mL/min, the total run time was 12.5 minutes, and the equilibration time between samples was 7 minutes. The injection volume of each sample was 2 μ L.

Acid Dyes: Chromatographic separation was performed at 45 °C with an Agilent ZORBAX 2.1mm x 50 mm narrow bore column C18 Reverse phase. Dye samples were analyzed with a mobile phase

consisting of (A) 20 mM ammonium formate with 0.01% formic acid and (B) aqueous MeOH/Acetonitrile (7:3) at 0.5 mL/min. The gradient shown in Table 1 was demonstrated to be the most efficient chromatograph in analysis of dye standards: the elution started 3% B for 1 min and then it was linearly increased to 60% of B in 0.5 min, further increased to 90% of B in the next 6.5 min, and B% was kept for another 2 min at 90%, and then returned to initial conditions. The post time for flushing the column is 4 min. The injection volume of the sample was 3 μ L for dye powder samples and 5 μ L for quantitative analysis. The gradient is shown in Table 5-2.

Table 5-2 Time Table of B% for Optimized Chromatography for Acid Dyes

Time	Flow	Pressure	Mobile Phase B%
0	0.5	400	3
1	0.5	400	3
1.5	0.5	400	60
7	0.5	400	90
9	0.5	400	90
9.5	0.5	400	3

Uracil as a Standard Uracil is the fourth nucleobases in the nucleic acid of RNA that are represented by the letters A, G, C and U. The others are adenine, cytosine, and guanine. In RNA, uracil binds to adenine via two hydrogen bonds. In reverse phase chromatography, uracil can be used as an unretained void volume indicator. The addition of uracil can also be used to calculate retention factor k' , which is used to monitor column performance.

Four direct dyes with similar color were mixed and analyzed by HPLC-DAD. The most important aspect of HPLC analysis is optimization of chromatography of HPLC by adjusting mobile phase B's content. This gradient shown in Table 5-3 was used as a start point for optimization of chromatography for dye mixtures. Modifications were made trial by trial until good chromatography was developed. Four yellow direct dyes with similar UV-spectra were chosen for gradient optimization.

Table 5-3 Information of Direct Dye Mixtures

Colour Index Name	Max absorption wavelength (nm)
C.I. Direct Yellow 106	420
C.I. Direct Yellow 27	400
C.I. Direct Yellow 6	420
C.I. Direct Yellow 44	400

5.2.5 HPLC COUPLED TO ELECTRO SPRAY IONIZATION QUADROPLE TOF-MS

Accurate mass MS analysis of commercial dyes/dye extracts was performed using a Agilent Technologies 1260 SL liquid chromatograph (HPLC) coupled to an Agilent Technologies 6520 Accurate-Mass Quadrupole Time-of-Flight mass spectrometer (QTOF-MS) equipped with an electrospray ionization (ESI) source (Figure 5-3). Ionization was carried out in negative ionization mode (Figure 5-4) with the following setting: nebulizer pressure (35 psig), capillary voltage (4000

V), drying gas flow (12 L/min at 350° C), and fragmentor voltage (90 V). Calibration of the mass spectrometer was performed per manufacturer settings. Data collection and analysis were performed using Agilent MassHunter Workstation Acquisition and Agilent MassHunter Quantitative Analysis B.04.00, as well as Quantitative Analysis TOF, respectively.



Figure 5-3 Agilent Technologies 6520 Accurate-Mass Quadrupole Time-of-Flight Mass Spectrometer (QTOF-MS)

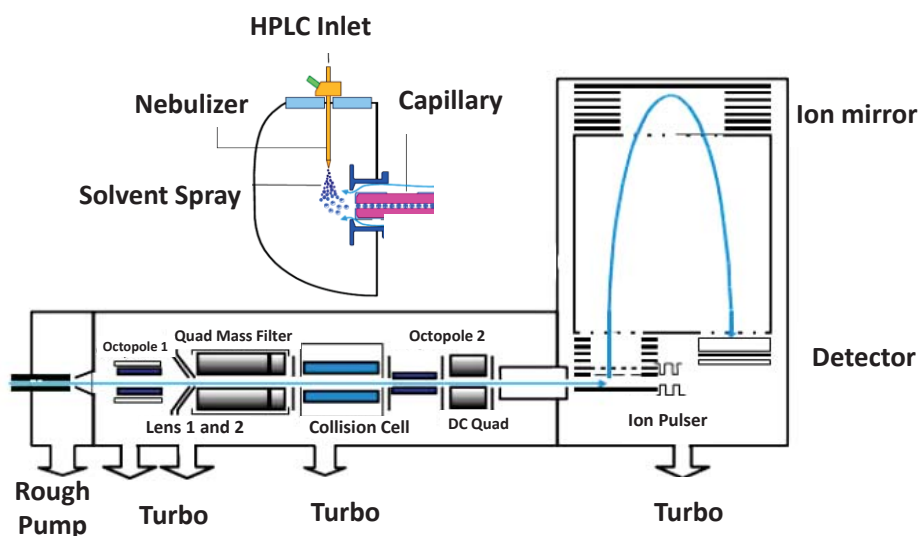


Figure 5-4 Schematic of Negative Mode LC-ESI-QTOF-MS

5.2.6 MICROFLUIDIC EXTRACTION-ESI QTOF MS

An integrated system was built by connecting microfluidic apparatus to ESI QTOF MS. 3 mm nylon threads with 1% owf (weight of dye on fabrics) were put into the microfluidic sample holder. Press the button on the microfluidic extraction control software, 9 μ L extracting solvent (pyridine/water 4:3) was automatically injected into the holder. After 300 second at a temperature of 85 °C, extracting solvent was evaporated for 150 s, followed by a cooling process at a temperature of 60 °C to prevent the dyes extracted to be absorbed by the fibers again. Then

appropriate buffer was flush into the sample holder to dissolve dyes for 20 second (stay time), allowing dye extract to be completely dissolved in buffer. 4 extra 20 μ L-volume buffer was flushed to completely flush dye residue present in sample holders and tubes. At the same time, Agilent Mass Hunter Data Acquisition started to collect data when the buffer flush into the mass spectrometer. The mass analyzer plots out the ion peaks when the dye extract reach to the QTOF detector. The operation time including heating, extraction, evaporation, cooling and mass analysis is 500~700 second.

5.2.7 LC/MS ANALYSIS OF DYE EXTRACT FROM MICROFLUIDIC EXTRACTION

Direct Dyes: C.I. Direct Red 81 was extracted from cotton fibers via microfluidic extraction system. The extracted ion current for m/z 314.53 revealed a peak in the DAD chromatogram at a retention time of 4.447 min, corresponding to the elution of C.I. Direct Red 81. The mass spectrum associated with the structure of the analyte peaks, along with the major ion structure is shown in Figure 5-5.

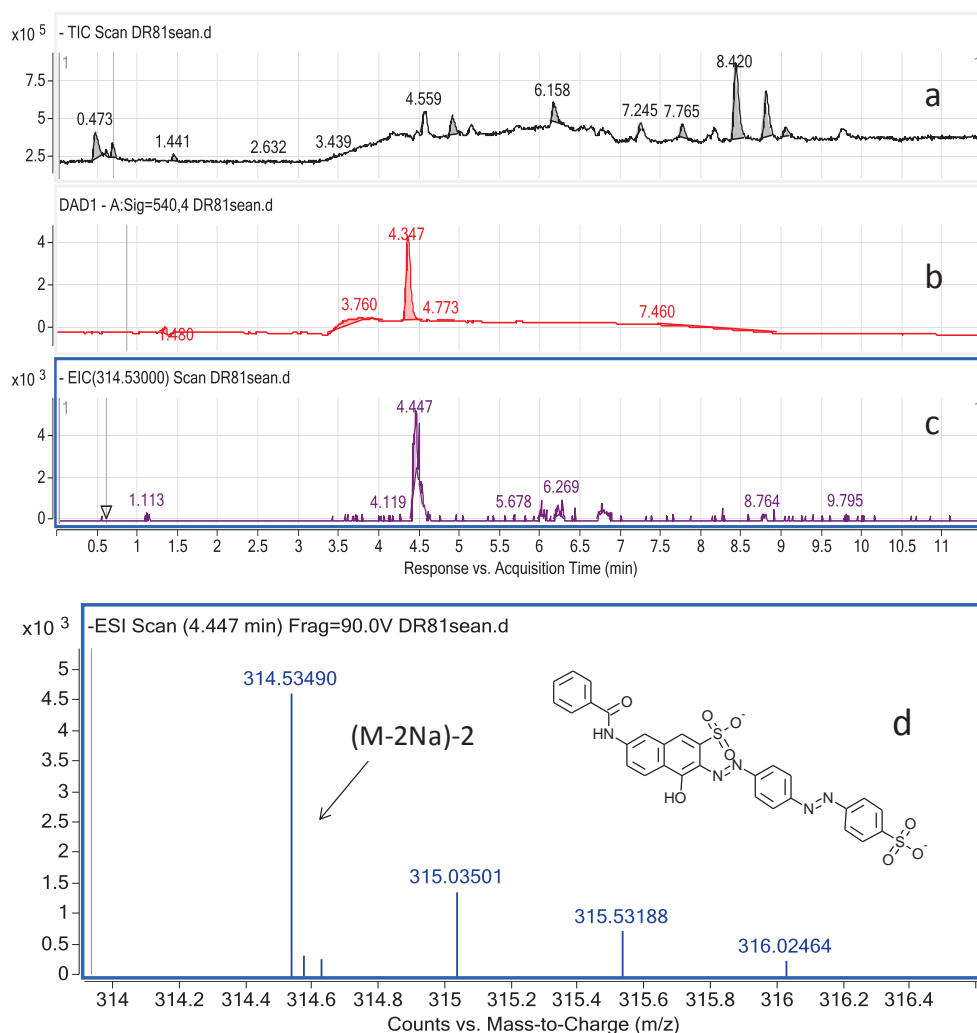


Figure 5-5. LC-QTOF-MS data for C.I. Direct Red 81 extracted from a cotton fiber in microfluidic extraction system. (a) Total ion chromatogram, (b) DAD chromatogram at 540 nm, (c) Extracted ion current for m/z 314.53, (d) mass spectrum corresponding to the peak observed in the m/z 314.53 extracted ion current.

Acid Dyes: Dye extracts from microfluidic extraction after a period of 5-15 minutes extraction showed that acid leveling dyes and milling dyes can be successfully detected (Figure 5-7).

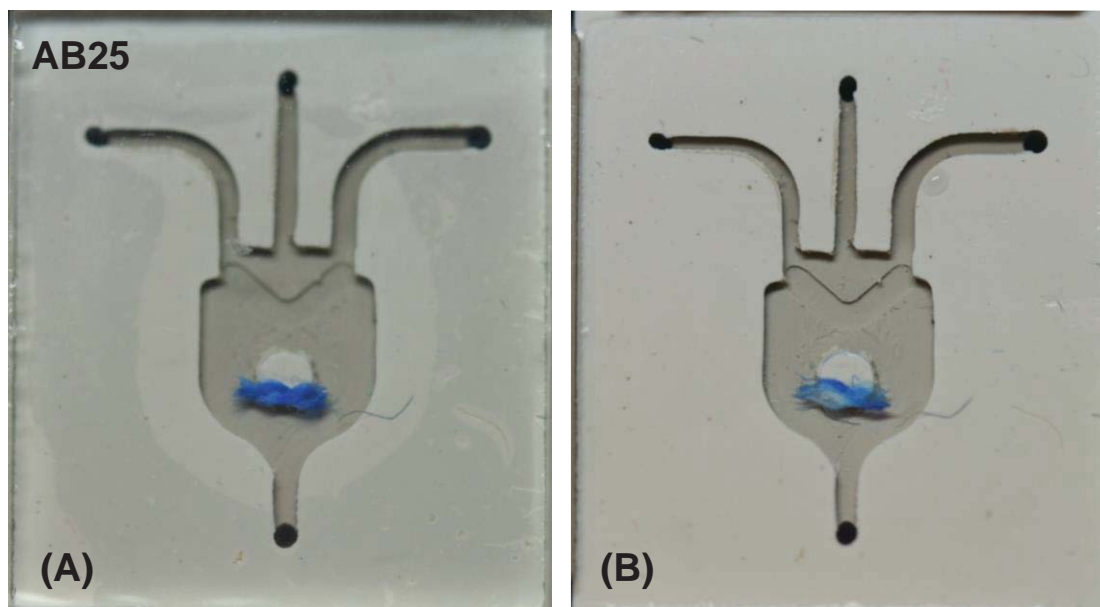


Figure 5-6 Microfluidic Extraction of C.I. Acid Blue 25 (A: Before Extraction, B: After Extraction, Condition: 3mm, T = 90 °C, Ext time = 300 s, Buff 1 = 20 s, X Buff = 4, EB time = 10 s, Evap time = 150 s, Tem. cool = 75°C, total time = 779 s)

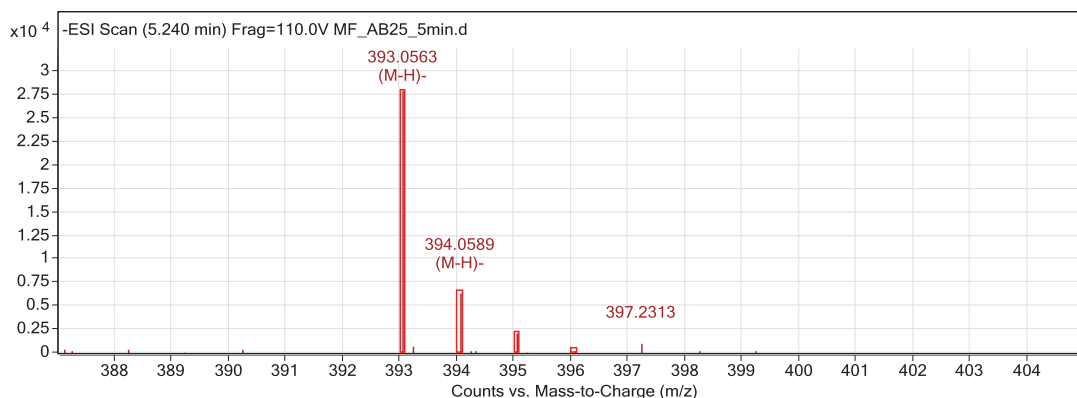


Figure 5-7 LC-MS Mass Spectra of C.I. Acid Blue 25 from Microfluidic Extraction

The microfluidic-extraction coupled to LC-MS can successfully separate dye impurities and detect the colorant with high sensitivity. As is illustrated in Figure. 23, the main component of C.I. Acid Red 114 has a retention time of 6.113 min in the HPLC-DAD chromatograph (540 nm), two smaller peaks at retention time 4.37 and 5.07 min corresponds to two different red components present in the dye extracts. Therefore, the microfluidic extraction can be coupled with LC-MS for analyzing components in single commercial dye as well as dye mixtures.

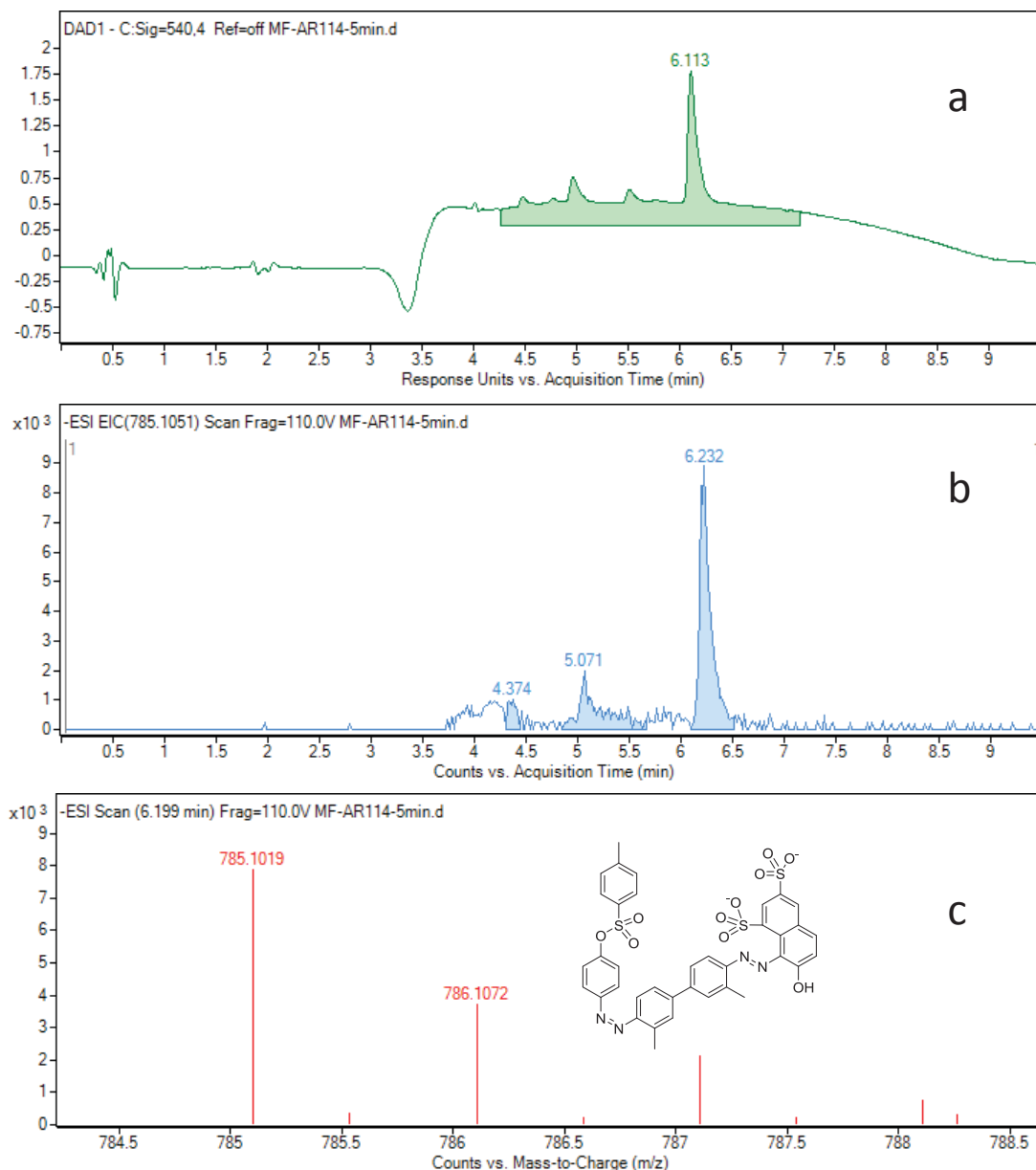


Figure 5-8 LC-QTOF-MS data for C.I. Acid Red 114 (Acid Milling Dye) out of microfluidic extraction system. (a) DAD chromatogram at 540 nm, (b) Extracted ion current for m/z 718.10, (c) mass spectrum corresponding to the peak observed in the m/z 718.10 extracted ion current.

5.2.8 DETECTION LIMIT OF STANDARD SOLUTION BY LC-QTOF-MS

Quantification Of Extraction Of C.I. Direct Yellow 106 Via LCMS Analysis Dye extract concentration was estimated by building up a calibration curve with Agilent TOF quantitative analysis software to measure standard dye solution in a range from 0.3 ~10 µg/ ml (ppm). A calibration curve for quantitative analysis was fitted by integrating the ion abundance detected by mass spectrometer versus known dye concentrations. Triplicate sets of standard dye stock was prepared by purified C.I. Direct Yellow 106 with concentration ranging from 0.315 µg/ ml to 125 µg/ ml. The mass to charge ratio of the target was set as 298.99, which is doubly charged characteristic ions of dye molecule. Calibration curve was then fitted by plotting integrated ion

abundance as a function of dye concentration. The linear regression parameters (y-intercept, slope, R^2) were analyzed. Limit of detection was defined as the minimum amount of an analyte that can be detected, where the signal to noise ratio of the integrated EIC should be higher than 10:1.

5.3 MICROFLUIDIC EXTRACTION COUPLED TO DIRECT INJECTION MASS SPECTROMETRY (DIMS)

Dye extract from microfluidic extraction was further detected by Direct Injection Mass Spectrometry (DIMS) through manually inject the dye extract to the QTOF mass analyzer through a metal syringe. Direct injection mass spectrometry skips the LC-separation step to rapidly detect dye extracts with high sensitivity and robustness: As the syringe as a dead volume of around 50 μL , the dye extract was diluted by three times (from less than 100 μL to 300 μL) prior to direct injection analysis. The mass spectra obtained by direct injection is shown in Figure 5-9, indicating that the diluted acid leveling dye extract can still be successfully detected.

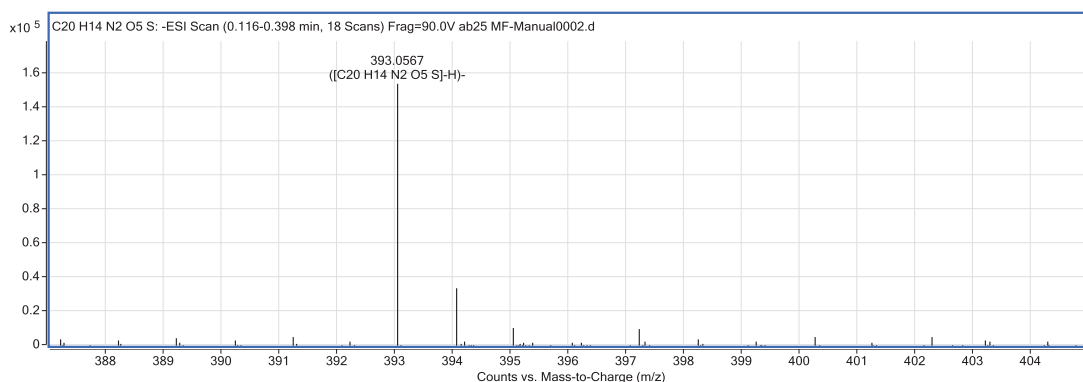


Figure 5-9 Mass Spectra of C.I. Acid 25 from Microfluidic Extraction Coupled to Direct Injection Mass Spectrometry

5.4 QUANTIFICATION OF EXTRACTION AND TEST OF LIMIT OF DETECTION

5.4.1 QUANTITATIVE ANALYSIS OF C.I. DIRECT YELLOW 106 EXTRACT

Calibration Curve The software Mass Hunter Quantitative TOF integrated the ion abundance of the molecular ions at a mass to charge ratio of 298.99. Quantification was based on the external standard method and the concentrations of Direct Yellow 106 were 0.3125, 0.625, 1.25, 2.5, 5, 7.5, 10 $\mu\text{g}/\text{ml}$. The best fit standard curve was prepared by linear regression of integrated ion abundance and the concentration, as is shown in the Figure 5-10. The coefficient obtained for C.I. Direct yellow 106 is 0.9820. The standard curve can be expressed as $y = 5.011041x + 794.764056$. The fitted calibration curve can be used to quantitatively measure the amount of samples of unknown concentration.

Quantification and detection of limit test LC-Q-TOF MS analysis of standard dye solution revealed that the minimal concentration of the C.I. Direct Yellow 106 is as low as 0.625 mg/ml when extraction volume is 5 μL , namely 3.125 ng purified C.I. Direct Yellow 106 can be detected. Assuming the 20% loss of dyes extracted from 1% owf dyed fibers, about 7.8 μg fibers can be detected under studied conditions. Detailed quantitative analysis of C.I. Direct Yellow 106 is shown in Table 2, including calibrated concentration, accuracy and signal to noise ratio.

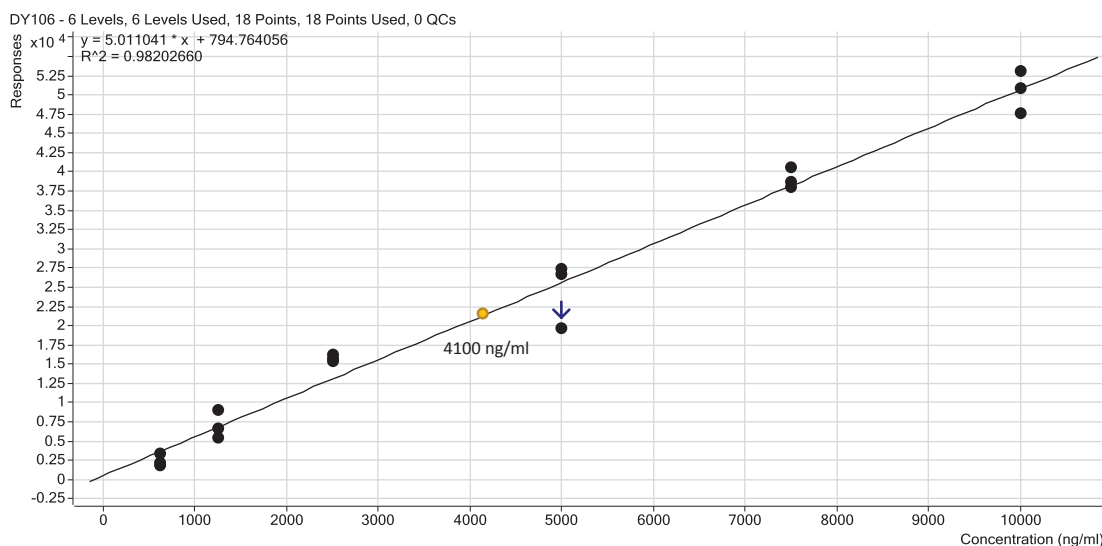


Figure 5-10 Integrated Ion Abundance at $m/z = 298.99$ vs. Dye Concentration of C.I. Direct Yellow 106

The minimal weight of dyed fiber, namely 100 μg dyed C.I. Direct Yellow 106 with 1% owf has around 410 ng (4100 ng/ml \times 100 μL = 410 ng) dye has been extracted. The extraction efficiency can be around 80 % (4.1 ng/100 μg \times 1000 \times 0.01 \times 0.6) according to the following equation, assuming only 60% dye has been absorbed by cotton fibers after dyeing procedures. The loss of extraction can either happen during operation or sample handling at macro-level extraction.

$$\text{Extraction efficiency} = \text{Actual dye detected} / \text{theoretical dye}$$

5.4.2 DETECTION OF LIMIT TEST OF LC/MS ANALYSIS OF ACID DYE STANDARDS

In the same method done as the above, two acid dyes C.I. Acid Blue 40 (MI = 450.27) and C.I. Acid yellow 36 (MW = 352.07) were analyzed and turned out to have much smaller limits of detection, which are 0.1175 ng/ml and 0.095 ng/ml, respectively. This is because they have much less molecular weight, and higher sensitivity to the mass analyzer, thereby more easily detected by the detector.

Previous study found that the amount of dye in a single fiber length of 2-10 mm is about 2-200 ng, and the value of which varies with different dyes. [55] Single cotton fiber of 8 mm analyzed through the optimized extraction procedures was successfully detected by QTOF mass analysis.

5.4.3 DETECTION OF LIMITATION-LC/MS

Acid Leveling Dyes: The information obtained through microfluidic extraction-LC/MS demonstrates that C.I. Acid blue 25 can be detected by both HPLC- Diode-Array Detection and QTOF mass analyzer 0.125% owf of 3 mm nylon threads under the studied conditions. Furthermore, both acid milling dyes and metal complexes can be detected with 1% dye in the threads can be identified via diode-array detection and QTOF mass analyzer.

In the same method done as the above, two acid leveling dyes C.I. Acid Blue 40 (MI = 450.27) and C.I. Acid yellow 36 (MW = 352.07) were analyzed and turned out to have much lower limits of detection than direct dyes, which are 0.1175 ng/ml and 0.095 ng/ml, respectively.

Acid blue 25 with a detection of limit of HPLC-DAD with 1% owf. However, QTOF mass analyzer has a much higher detection of limit when the dye concentration is 0.0625%, which is

equal to 12.5 ng/ml in the recovered samples, which is higher than the detection of limit of LC-MS (Table 5-4).

Table 5-4 LC/MS Analysis of Acid dye Extract from Microfluidic Extraction

Dye #	Color Index Name	Extraction Time [sec]	Chemical Formula	HPLC-DAD	MS	Molecular Weight of Ions	Molecular Ion
1	Acid Blue 25 (.0625%)	300	C ₂₀ H ₁₄ N ₂ O ₅ S	N	Y	393.05	M-H
2	Acid Blue 25 (.0625%)	160	C ₂₀ H ₁₄ N ₂ O ₅ S	N	Y	393.05	M-H
3	Acid Blue 25 (.125%)	300	C ₂₀ H ₁₄ N ₂ O ₅ S	Y	Y	393.05	M-H
4	Acid Blue 25 (.125%)	160	C ₂₀ H ₁₄ N ₂ O ₅ S	Y	Y	393.05	M-H
5	Acid Blue 25 (.250%)	300	C ₂₀ H ₁₄ N ₂ O ₅ S	Y	Y	393.05	M-H
6	Acid Blue 25 (.250%)	160	C ₂₀ H ₁₄ N ₂ O ₅ S	Y	Y	393.05	M-H
9	Direct Red 81(1%)	180	C ₂₉ H ₁₉ N ₅ Na ₂ O ₈ S ₂	Y	Y	314.53	(M-2H)-4
10	Acid Red 186 (1%)	300	C ₂₀ H ₁₄ N ₄ Na ₂ O ₈ S ₂	Y	Y	514.33	-----
11	Acid Red 114 (1%)	180	C ₃₇ H ₂₈ N ₄ Na ₂ O ₁₀ S ₃	Y	Y	785.1	M-H
12	Acid Red 114 (1%)	360	C ₃₇ H ₂₈ N ₄ Na ₂ O ₁₀ S ₃	Y	Y	785.1	M-H
14	Acid Yellow 151-9 (3%)	180	C ₃₂ H ₂₈ CoN ₈ O ₁₀ S ₂ .2H	Y	Y	807.07	M-H
15	Acid Yellow 151-9 (2%)	180	C ₃₂ H ₂₈ CoN ₈ O ₁₀ S ₂ .2H	Y	Y	807.07	M-H
16	Acid Yellow 151-9 (1%)	180	C ₃₂ H ₂₈ CoN ₈ O ₁₀ S ₂ .2H	Y	Y	807.07	M-H

5.5 ANALYSIS - MICROFLUIDIC EXTRACTION DIRECT TO THE QTOF MS.

5.5.1 ANALYSIS OF SINGLE FIBERS

Single nylon fibers (< 1 ng) dyed with C.I. Acid Blue 25 can be successfully detected with the integrated system as shown in Figure 5-11. The ion abundance of mass spectra were significantly improved by 10³ than the separate step analysis. The automatic extraction can be finished within 700 second before the molecular information was obtained by mass analyzer. This process can produce a highly reproducible and productive standard methodology for trace fiber analysis.

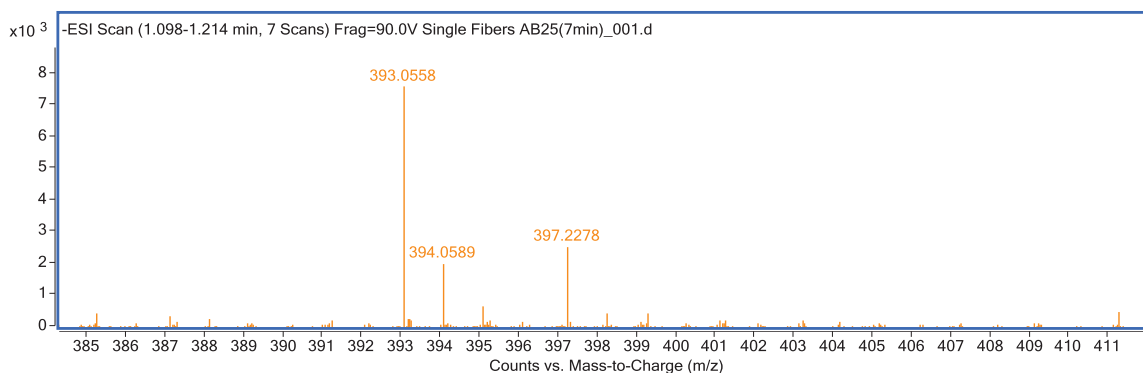


Figure 5-11 MS Spectra of C.I. Acid Blue 25 from Single Fiber (5-10 mm) with Automatic Microfluidic Extraction-MS

5.5.2 ANALYSIS OF FIBERS CONTAINING MIXED DYES

Mixed nylon fibers with C.I. Acid Blue 25 and C.I. Acid Yellow 49 in the microfluidic context can be successfully detected without interaction, as are shown in Figure 5-12.

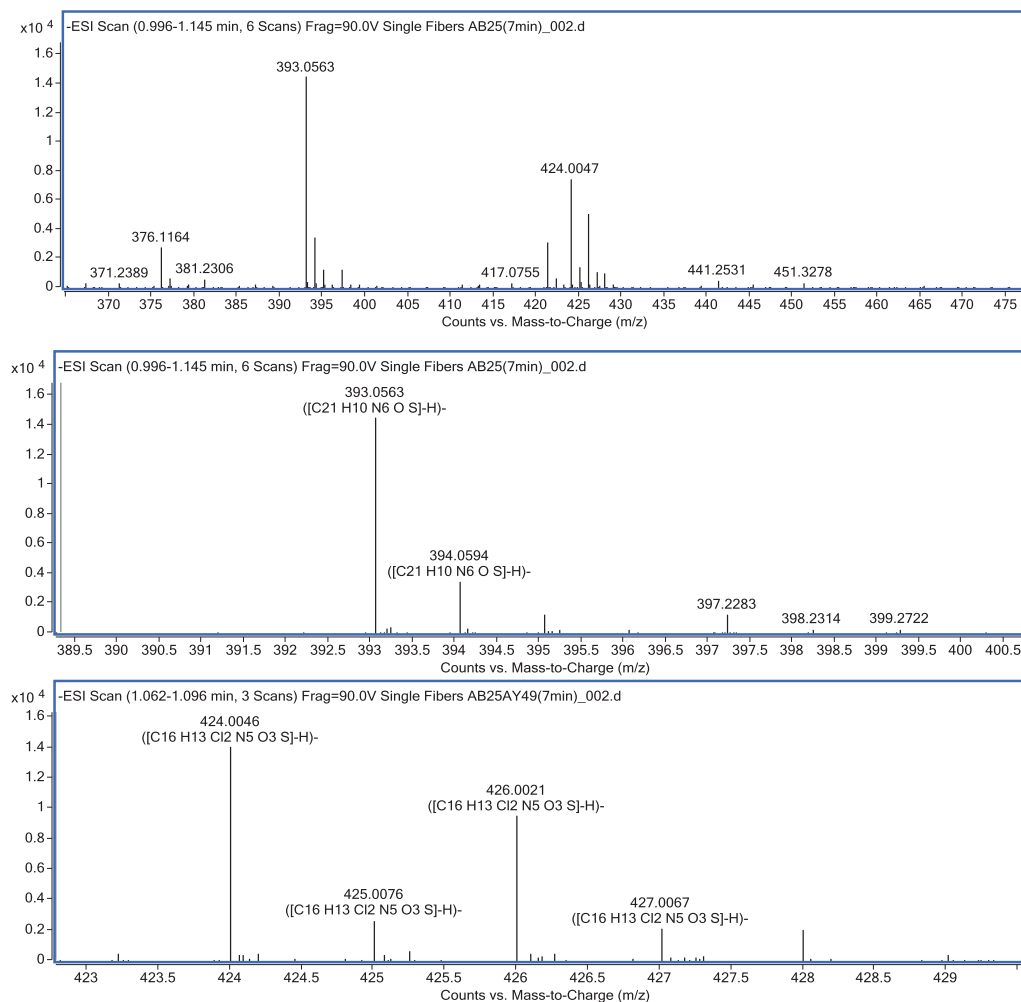


Figure 5-12. MS Spectra of mixed fibers (C.I. Acid Blue 25 and C.I. Acid Yellow 49) (5-10 mm) with Automatic Microfluidic Extraction-MS (top: Full mass spectra of dye extract, middle: Mass spectra of C.I. Acid Blue 25, bottom: Mass Spectra of C.I. Acid Yellow 49)

6 CONCLUSIONS

The two major goals of this project were to produce a microfluidic device capable of automated extraction of dye from fibers and to design the components to provide optimum performance. Design optimization was achieved by using models of the processes in the device (i.e. fluid flow, heat transfer, evaporation). The following list describes the accomplishment of objectives defined for the project:

6.1 DEVICE DESIGN OBJECTIVES:

- ***Automation: The user will place a fiber in the device and initiate the extraction sequence.***
The operation of the extraction device was successfully automated using the Tern controller. A microfluidic rotary valve was incorporated and provides fluid selection capabilities and consistent fill of a 9 μl cavity through timed operation. The required extraction steps of cavity filling (with solvent and buffer), heating, and evaporation of solvent were shown to be repeatable and controllable with timed operation of valves and heaters. In addition, a microfluidic cavity capable of controlling fluid fill was successfully designed and fabricated.
- ***Repeatability: The device must be able to extract dye from multiple samples in succession and produce useful results.***
Multiple extractions were performed with the device and produced samples of good quality (where quality refers to detectability of extracted dye). By including a system cleaning function to be used between each extraction test, residual solvent and/or dye within tubes and manifolds is removed. This should be verified in future testing with production of null samples between extractions that are analyzed in a mass spectrometer.
- ***Reliability: Dye samples produced must be of useable quality, i.e. they must be equivalent to those of laboratory extraction procedures.***
The samples that were successfully extracted in tests with the thin-film heaters in prototype 1 and prototype 2 were detected in the mass spectrometer. Due to limitations of time and the number of samples that could be tested in the HPLC-MS setup, a statistically relevant number of extraction tests for each dye type has yet to be performed to verify repeatable results. The device should be used by the Textile Chemistry Department to optimize extraction conditions and to establish its rate of successful extraction.
- ***Fulfill the needs of forensic scientists: It should be ergonomic, easy to use, and reduce the amount of interaction and time required to extract dye samples.***
The initial idea for the chip design was to incorporate the extraction chip and glass cover into a single piece mechanical design. After discussion with the forensic scientist at the North Carolina State Crime Laboratory, it was determined that a chip design with a non-connected glass cover was preferable. The extraction chip that was designed provides easy manipulation of the fiber within an extraction cavity and placement of a sealing glass cover. The user can then view the fiber through the cover for proper placement and to examine the post-extraction appearance of the fiber. The design of the MFD and enclosure allows for easy insertion of the chip. A user interface was also developed to provide control over key extraction parameters including extraction temperature, extraction time, buffer hold time, and rough sample volume. The total extraction process can be performed in less than ten minutes depending on the desired extraction time.
- ***Fabrication and testing: The design will be fabricated and tested to verify dye extraction capability.***

Two prototypes were fabricated. The first prototype was used to identify the proper configuration of components (valves, heaters, reservoirs, regulators, etc.) required to produce a consistent automated process and to verify the dye extraction capabilities of the device. The second prototype reduced the overall footprint of the device from 12" long and 24" wide to 10" long and 6" wide. Pressure measurement capabilities and a cooling fan were incorporated in the design. Both prototypes were used to perform successful dye extractions.

6.2 MODELING PROCESSES OF INTEREST:

- ***Predict fluid flow, heating, and evaporation so that extraction sequence steps can be timed.***

Models of key processes within the device were examined and used to predict behavior of those processes. Analytical equations were used to accurately predict flow rates. By understanding the effects of tube dimensions and surface properties on flow, appropriate tube inner diameters and lengths were selected for fluid and air inlets and outlets to the cavity. Computational fluid dynamic models were also examined and used to select proper air flow conditions, predict evaporation times, and to optimize the design of the microfluidic cavity. An analytical heating model and transient thermal FEA (finite element analysis) were used to estimate the power required to produce high temperatures within the cavity in a relatively short amount of time. Using the models a heater was selected to produce adequate heat input to the system to achieve temperatures in excess of 100°C in less than two minutes. In addition, an analytical cooling model was used to show the cooling mode of the heater setup. Finally, a simplified analytical model of the convective evaporation of solvent was established. Through literature review, proper fluid properties of the solvent mixture were determined and used as inputs to the model. With these values and predicted air velocities from FEA simulations, evaporation rates and times were predicted. The model showed that the solvent should evaporate within five minutes for a 9 μl volume, $\sim 920 \mu\text{l/s}$ of total air flow (using 20 psi pressure drop on air line), and fluid temperatures in excess of 40°C.

- ***Verify process models with experimental data.***

Experimental setups were designed and used to examine flow predictions. Results from flow tests prompted the development of a simple slip flow model for the prediction of flow in the PTFE tubing. The model matched test results for an empirically determined slip length within an average of $\sim 6\%$. The slip model has the added advantage that any uncertainty in the inner diameter of the tube is essentially covered in the slip length (for very small difference from nominal dimension). Heating tests showed general agreement with the heating model and simulations in regards to time. Temperature "overshoot" observed within the device verified the existence of a temperature gradient that had to be taken into account in calibration of the device. Cooling tests were also performed and showed the cavity temperature to follow the general cooling mode predicted. Finally, the evaporation model was verified for different temperatures and approximate air flows. Test data points were accurately predicted by the model at the highest air flow setting (20 psi $\sim 920 \mu\text{l/s}$). The average difference between the model and test data was ~ 0.2 minutes.

- ***Use process modelling to calibrate the device.***

Process models were mainly used to optimize the design of the system and components. The flow model was used to select tubing diameter and length and to estimate required fill

times. The flow was calibrated by setting the pressure and observing the time required to fill the cavity. Consistent fill with the system for set conditions was verified through simple automation testing. The heating model was used in the selection of heaters and to predict general heating requirements. It was not used for system calibration because it did not accurately capture the temperature gradient between the heater and cavity (therefore it did not capture the temperature “overshoot”). The cooling model was used to produce a proper curve fit in the cooling calibration. By combining experimental heating and cooling data, a proper calibration and heater control method was developed and successfully tested. The evaporation model was used to set a minimum evaporation time for a given solvent temperature (at 20 psi inlet setting). A fixed amount of time was then added in the program code to the baseline value to ensure complete evaporation.

6.3 DEVELOP DATABASE OF DYE INFORMATION

- The extraction, chemical separation, and mass spectrometry for the major synthetic dyes were optimized for an integrated system coupling automatic microfluidic extraction to high resolution mass spectrometry analysis. Compared to macro-fiber examine procedures, the integrated system uses minimum lengths of fibers (ng single fibers) and permits minimal volumes of solvent (<10 μ L) to be prepared for mass spectrometry analysis. It shortens analysis time with high reproducibility and productivity, and improves fiber analysis repeatability with minimal operator input, thereby reducing contamination potential.
- A universal HPLC-ESI-QTOF MS methodology was developed for the analysis of direct, acid and disperse dyes, and a database containing retention times and spectra data of 256 commercial dyes (84 acid dyes, 92 disperse dyes, 80 direct dyes) have been developed, providing reliable references for forensic trace fiber analysis.

7 FUTURE WORK

Future work will focus on the optimization of extraction conditions for different dyes and fiber types. As the database being produced by the Textile Chemistry Department expands, the microfluidic device can be used to increase throughput of fiber samples.

- a) A comprehensive discriminating power assessment of the developed methods compared to select traditional methods (especially microscopy, microspectrophotometry, FT-IR, and Raman) using representative dyed fiber samples.
- b) A real-world assessment of the analytical method and current standard methods to determine the potential for a coincidental match.
- c) Optimization of extraction conditions with the device will focus on the following parameters:
 1. Extraction temperature.
 2. Extraction time.
 3. Buffer hold time.
 4. Sample volume (total buffer volume).
 5. Limits of detection (LOD) – determination of the minimal fiber size and dye concentration that can be successfully extracted and tested with an HPLC-MS system.

The second prototype design of the device was produced with the aim of minimizing its footprint. Although this was achieved, development of a third prototype might seek to incorporate some or all of the following additions:

1. Temperature measurement – The Tern controller provides only four analog inputs, each of which is assigned to a pressure transducer. Another design iteration of the device might seek to incorporate thermal feedback from the heater via a resistance temperature detector (RTD) or thermocouple. Temperature measurement can be used to detect the failure or deterioration of the heating element. In addition, it can be used to control the temperature, thereby eliminating the need for calibration or environmental control. The current heating system relies on a relatively consistent initial temperature and atmospheric temperature to operate at the set temperature properly. The addition of temperature measurement would require additional data input capabilities and possibly a different controller.
2. Electronic pressure regulators – The use of electronic pressure regulators would serve to further automate the system. The current system requires manual setting of four regulators to the proper pressure. However, it should be taken into account that incorporation of electronic regulators would likely add to the cost, size, and control complexity of the system.
3. Fixed volume pumping – Timed filling with pressurized reservoirs was done successfully with the first prototype designs. This technique can be extended to various liquids, but it requires some consistency in the temperature of the fluid (for constant viscosity) and a consistent reservoir pressure. Fixed displacement pumping technologies exist and provide the ability to achieve consistent pumped volume regardless of fluid temperature or reservoir pressure. A simple concept is shown in Figure 7-1, where a piston with a fixed stroke is used as a pumping mechanism. The Lee Company makes two fixed pump lines for example. Their LPL series comes with standard dispense volumes of 25 and 50 μl . For more precise pumping, their LPV series offers standard dispense volumes ranging from 0.04 to 1.5 μl .

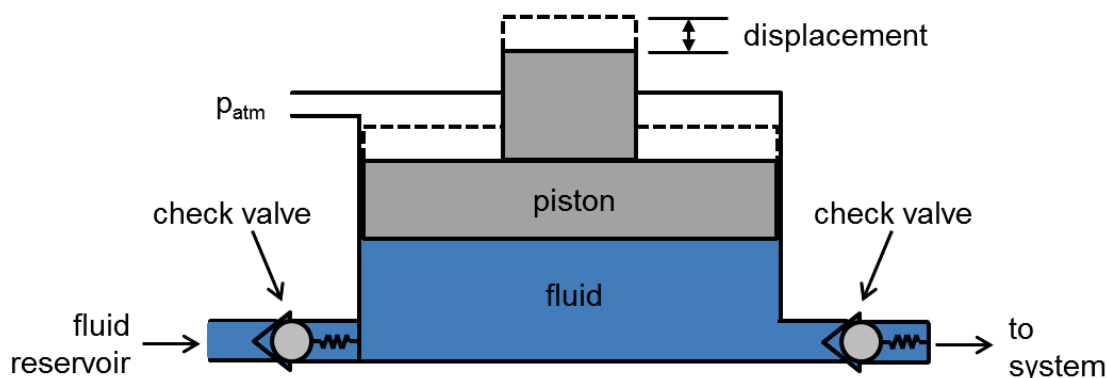


Figure 7-1. Fixed volume pump concept

One conclusion that can be taken from this project is that automated lab on a chip devices using timed flow control, heating, and convective evaporation on a microliter scale can operate successfully and consistently (in regards to the individual processes). It has also been shown that these automated systems can be used for trace sample detection purposes. The following is a short list of potential applications for the technology that was compiled by the Textile Chemistry Department:

1. Drug testing – extractions on human hair
2. General drug monitoring
3. Identification of banned, carcinogenic and mutagenic colorants
4. Fermentation process monitoring
5. DNA analysis

6. Dioxin contamination in food
7. Elementary analysis of semi-conductor materials

More generally, the technology has potential for use in any process that requires small scale extraction of molecules from solid materials. To provide a more general use, the capabilities of the system can be expanded to provide multiple solvents. This can be easily done with the rotary valve coupled with individual shut-off valves as depicted in Figure 6-2.

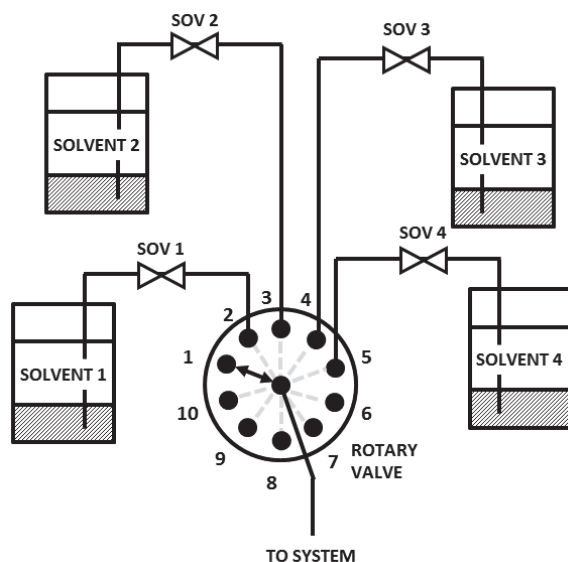


Figure 6-2. Multiple solvent concept with rotary valve

By providing the microfluidic cavity as a separate and unique piece to the chip and fluid system, a large variety of individualized cavity shapes, sizes, and materials can be designed and used as well. In theory, the system can be extended for broader use in any applications where small volumes of fluid and heat application are required.

8 REFERENCES

- 1 A Embar-Seddon, AD Pass. The Training of Medical Examiners The only general requirement for becoming, *Crim.Justice.* 2 (2006) 671.
- 2 W Hunter 1971-, Mark and trace analysis electronic resource], Mason Crest Publishers, Philadelphia, 2006.
- 3 Image courtesy of Alexander Sohn, Guillaume Robichaud, and Thomas Dow.
- 4 JV Goodpaster, EA Liszewski. Forensic analysis of dyed textile fibers, *Analytical and bioanalytical chemistry.* 394 (2009) 2009-2018.
- 5 EG Bartick, *Criminal Forensic Analysis, Infrared and Raman Spectroscopy in Forensic Science*, John Wiley & Sons, Ltd, 2012, pp. 87-109.
- 6 PM Fredericks, *Forensic Analysis of Fibres by Vibrational Spectroscopy, Infrared and Raman Spectroscopy in Forensic Science*, John Wiley & Sons, Ltd, 2012, pp. 153-169.
- 7 L Kobilinsky, *Forensic Chemistry Handbook*, John Wiley & Sons 2011.
- 8 J Kieser, *Forensic biomechanics electronic resource]*, Wiley-Blackwell, Chichester, West Sussex, UK ; Hoboken, NJ, 2013.
- 9 R Saferstein. *Forensic science handbook*, (1993).
- 10 KG Wiggins. Thin layer chromatographic analysis for fibre dyes, *Forensic Examination of Fibres*, 2nd edition, Eds: Robertson, J.& Grieve, M. (1999) 291-310.
- 11 Wiley Series on Pharmaceutical Science and Biotechnology : Practices, Applications and Methods : *Mass Spectrometry Handbook*, Wiley, Somerset, NJ, USA, 2012.
- 12 PS Dittrich, A Manz. Lab-on-a-chip: microfluidics in drug discovery, *Nature Reviews Drug Discovery.* 5 (2006) 210-218.
- 13 S Haeberle, R Zengerle. Microfluidic platforms for lab-on-a-chip applications, *Lab on a Chip.* 7 (2007) 1094-1110.
- 14 GM Whitesides. The origins and the future of microfluidics, *Nature.* 442 (2006) 368-373.
- 15 JR Anderson, DT Chiu, H Wu, OJ Schueller, GM Whitesides. Fabrication of microfluidic systems in poly (dimethylsiloxane), *Electrophoresis.* 21 (2000) 27-40.
- 16 GS Fiorini, DT Chiu. Disposable microfluidic devices: fabrication, function, and application, *BioTechniques.* 38 (2005) 429-446.
- 17 DJ Beebe, GA Mensing, GM Walker. Physics and applications of microfluidics in biology, *Annu.Rev.Biomed.Eng.* 4 (2002) 261-286.
- 18 T Masuzawa. State of the Art of Micromachining, *CIRP Ann.Manuf.Technol.* 49 (2000) 473-488.
- 19 J Khandurina, TE McKnight, SC Jacobson, LC Waters, RS Foote, JM Ramsey. Integrated system for rapid PCR-based DNA analysis in microfluidic devices, *Anal.Chem.* 72 (2000) 2995-3000.
- 20 D Erickson, D Li. Integrated microfluidic devices, *Anal.Chim.Acta.* 507 (2004) 11-26.

- 21 JY Zhang, M Mahalanabis, L Liu, J Chang, NR Pollock, CM Klapperich. A disposable microfluidic virus concentration device based on evaporation and interfacial tension, *Diagnostics*. 3 (2013) 155-169.
- 22 H Yin, K Killeen, R Brennen, D Sobek, M Werlich, T van de Goor. Microfluidic chip for peptide analysis with an integrated HPLC column, sample enrichment column, and nanoelectrospray tip, *Anal.Chem.* 77 (2005) 527-533.
- 23 PB Lillehoj, F Wei, C Ho. A self-pumping lab-on-a-chip for rapid detection of botulinum toxin, *Lab on a Chip*. 10 (2010) 2265-2270.
- 24 <http://www.coleparmer.com/Chemical-Resistance>, 2013.
- 25 <http://www.theleeco.com/>, 2014 (2013).
- 26 PM Eller, ME Cassinelli, NIOSH manual of analytical methods, DIANE Publishing 1994.
- 27 Bottom-of-the-Bottle™ Filters. <http://webstore.idx-hs.com/Products/specsheet.asp?vSpecSheet=117>., 2014 (2010).
- 28 586-Engine-P. <http://www.tern.com/portal/>, 2014 (2012).
- 29 H Hartley, NG Thomas, MP Applebey. L.—Some physico-chemical properties of mixtures of pyridine and water, *Journal of the Chemical Society, Transactions*. 93 (1908) 538-560.
- 30 I Kul, T Lieu. Thermodynamic properties of aqueous solutions of pyridine and piperidine, *Fluid Phase Equilib.* 290 (2010) 95-102.
- 31 PK Kundu, IM Cohen, H Hu. *Fluid mechanics*. 3rd, (2004).
- 32 AE Dunstan, FBT Thole, JS Hunt. CLXIII.—The relation between viscosity and chemical constitution. Part I. The viscosity of pyridine solutions, *Journal of the Chemical Society, Transactions*. 91 (1907) 1728-1736.
- 33 J Abe, K Nakanishi, H Touhara. Thermodynamic properties of aqueous solutions of hydrophilic compounds 1. Pyridine and methylpyridines, *The Journal of Chemical Thermodynamics*. 10 (1978) 483-494.
- 34 R Andon, J Cox, E Herington. Phase relationships in the pyridine series. Part 6. The thermodynamic properties of mixtures of pyridine, and of three of its homologues, with water, *Transactions of the Faraday Society*. 53 (1957) 410-426.
- 35 RC Weast. *Handbook of chemistry and physics*, Am.J.Med.Sci. 257 (1969) 423.
- 36 C Kleinstreuer, *Modern fluid dynamics : basic theory and selected applications in macro- and micro-fluidics*, Springer, Dordrecht ; New York, 2010.
- 37 AP PUNTAMBEKAR, MICROFLUIDIC DISPENSERS BASED ON STRUCTURALLY PROGRAMMABLE MICROFLUIDIC SYSTEMS (sPROMs) AND THEIR APPLICATIONS FOR μ TAS, (2004).
- 38 I Rao, K Rajagopal. The effect of the slip boundary condition on the flow of fluids in a channel, *Acta Mech.* 135 (1999) 113-126.
- 39 C Navier. Mémoire sur les lois du mouvement des fluides, *Mémoires de l'Académie Royale des Sciences de l'Institut de France*. 6 (1823) 389-440.

- 40 H Liu, H Gong, N Ramalingam, Y Jiang, C Dai, KM Hui. Micro air bubble formation and its control during polymerase chain reaction (PCR) in polydimethylsiloxane (PDMS) microreactors, *J Micromech Microengineering*. 17 (2007) 2055.
- 41 DS Kim, K Lee, TH Kwon, SS Lee. Micro-channel filling flow considering surface tension effect, *J Micromech Microengineering*. 12 (2002) 236.
- 42 MY Okiishi, B MUNSON, D YOUNG. *Fundamentals of Fluid Mechanics*, John Wiley & Sons, Inc. (2006).
- 43 F Ineropera, D DeWitt, T Bergman. *Fundamentals of Heat and Mass Transfer (The 6th Edition)*, (2007).
- 44 PTC Thermistor Engineering Notes. <http://www.meas-spec.com/>, 2014.
- 45 OhmegaFlex™ Heaters. <http://brigitflex.com/document/heaters.pdf>, 2014.
- 46 A Bejan, *Heat transfer*, John Wiley & Sons, Inc., New York, 1993.
- 47 S Young 1857-1937., *Distillation principles and processes*, Macmillan, London, 1922.
- 48 E Hilmen. *Separation of azeotropic mixtures: tools for analysis and studies on batch distillation operation*, (2000).
- 49 JA Kent, *Handbook of Industrial Chemistry and Biotechnology: Volume 1 and 2*, Springer 2013.
50. EB Arkilic, MA Schmidt, KS Breuer. *Slip Flow in MicroChannel*, (1995).
51. Zhang, X., et al., *Extraction optimization of the polysaccharide from Adenophorae Radix by central composite design*. *International Journal of Biological Macromolecules*, 2014. **67**(0): p. 318-322.
52. Stefan, A., et al., *Microextraction, capillary electrophoresis, and mass spectrometry for forensic analysis of azo and methine basic dyes from acrylic fibers*. *Analytical and Bioanalytical Chemistry*, 2009. **394**(8): p. 2087-2094.
53. Holčápek, M., K. Volná, and D. Vaněrková, *Effects of functional groups on the fragmentation of dyes in electrospray and atmospheric pressure chemical ionization mass spectra*. *Dyes and Pigments*, 2007. **75**(1): p. 156-165.
54. Lech, K., et al., *Early synthetic dyes – a challenge for tandem mass spectrometry*. *Journal of Mass Spectrometry*, 2013. **48**(2): p. 141-147.
55. Petrick, L.M., T.A. Wilson, and W. Ronald Fawcett, *High-Performance Liquid Chromatography–Ultraviolet–Visible Spectroscopy–Electrospray Ionization Mass Spectrometry Method for Acrylic and Polyester Forensic Fiber Dye Analysis**. *Journal of Forensic Sciences*, 2006. **51**(4): p. 771-779.
56. Rafaëly, L., et al., *Optimisation of ESI-MS detection for the HPLC of anthraquinone dyes*. *Dyes and Pigments*, 2008. **77**(1): p. 191-203.
57. Albert A. Tuinman, L.A.L., and Samuel A. Lewis, Sr., *Trace Fiber Color Discrimination by Electrospray Ionization Mass Spectrometry: A Tool for the Analysis of Dyes Extracted from Submillimeter Nylon Fibers*. *Analytical Chemistry*, 2003. **73**: p. 2753-2760.

9 DISSEMINATION OF RESEARCH FINDINGS

Papers are being prepared based on the microfluidic design, operation and the additions to the textile dye database. These will be submitted in the Fall of 2014.